MULTINUCLEAR SOLID-STATE NMR STUDIES OF POLYMERS AND IMMOBILIZED SONOGASHIRA CATALYSTS FOR CROSS-COUPLING REACTIONS

A Dissertation

by

JACQUELINE CHRISTINE POPE

Submitted to the Office of Graduate and Professional Studies of
Texas A&M University
in partial fulfillment of the requirements for the degree of

DOCTOR OF PHILOSOPHY

Chair of Committee,	Janet Bluemel
Committee Members,	Abraham Clearfield
	Donald Darensbourg
	Hae-Kwon Jeong
Head of Department,	David Russell

December 2014

Major Subject: Chemistry

ABSTRACT

The major directions of this thesis involve (1) the study of performance polymers with solid-state NMR techniques, (2) the synthesis, immobilization, and characterization of phosphine linkers on silica for immobilizing Sonogashira cross-coupling catalysts, and (3) the investigation of the coordinating strengths of phosphine linkers at Pd centers.

Solid-state NMR spectroscopy, a very versatile and comprehensive tool for the study of a wide range of materials, is at the center of this research. First, the treatment and characterization of high performance polymers for the oil and gas industry will be discussed. Performance polymers like *p*oly*a*ryl*e*ther*k*etones (PAEK) are immensely important in energy applications due to their lower weight and superior corrosion resistance under demanding conditions. Blends of PAEK polymers, such as *p*oly*e*ther*e*ther*k*etones (PEEK) and *p*oly*e*ther*k*etone*k*etones (PEKK), with *p*oly*b*enz*i*midazole (PBI) are of commercial interest due to their improved high-temperature stability and their superior wear characteristics.

However, regarding the PBI component, the origins of the properties that are disadvantageous in thermally or chemically aggressive environments are not well understood. The focal point of this research is the morphological and molecular changes of PEEK-PBI and PEKK-PBI blends after stirring them in liquid water and steam-treating them at high temperatures and pressures. The pure polymer components and the PAEK-PBI (50:50 wt%) blends are steam-treated at 150 °C (ca. 300 °F) and 315 °C (ca. 600 °F). Interactions and reactions of H_2O with the functional groups of the polymers are studied

using D_2O in combination with IR, ^2H MAS, and ^1H wideline solid-state NMR. Three different processes taking place during high-temperature steam-treatment are identified.

In a parallel project the synthesis and characterization of chelating phosphine linkers, which are bound to silica via ethoxysilane groups will be described. These readily coordinate to the Pd and Cu complexes used for the Sonogashira reaction. This research brings forth new insights concerning the synthesis, immobilization and characterization of Pd(0)/Cu(I) Sonogashira catalyst systems as well as the optimization of the reaction conditions for the catalysis. Under the optimized conditions, and taking the coordinating strengths of the phosphine ligands, as determined by ^{31}P HRMAS competition experiments, into account, catalysts that exhibit unprecedented activities and lifetimes are obtained.

DEDICATION

For my parents,

for all the support and love throughout everything

ACKNOWLEDGEMENTS

I would like to start off by thanking my parents, without whom I wouldn't have been able to accomplish my goals. Thank you for always pushing me to do my best in everything. Thank you for teaching me that even when times get tough, you have to push forward to succeed. I would also like to thank my fiancé Griffin, who has supported me through thick and thin. It was your love and guidance that helped me also achieve my goal.

I would like to thank my committee chair and research advisor, Dr. Janet Bluemel for her guidance and support over the past five years. I appreciate her time and direction as well as always pushing me to do my best in everything. It has helped tremendously in my development in becoming a successful chemist.

Thank you also to Dr. Tim Bremner and Dr. Hung-Jue Sue for giving me the opportunity to participate in the APPEAL Consortium. I learned a great deal from both of you about polymers and life in industry. Thank you also to Dr. Vladimir Bakhmoutov for his countless help with the solid-state NMR, whether it be setting up a new pulse program with me or helping me implement the new instrumentation.

I would also like to thank my committee members, Dr. Abraham Clearfield, Dr. Donald Darensbourg, and Dr. Hae-Kwon Jeong. Thank you for attending my seminars and allowing me the time to present my research to you. You also have provided insightful questions and valuable input about what directions my research should go. Also, thank you to Dr. Gyula Vigh for supporting me as a committee member during the beginning of my Ph.D. and my preliminary exam.

I would like to thank my coworkers in the Bluemel research group. Thank you to Casie and Johannes for their direction and insight with my research. You were both always there for me whenever I needed a helping hand. I especially would like to thank Kyle for his help with ^{2}H simulation and crystal structures. Thank you to the rest of the group for always listening to my practice talks and for providing valuable insight and criticism to help me improve.

Last but not least, I would like to acknowledge and thank my friends both here in College Station, across Texas and the United States. Thank you for always being there for me and being a shoulder to lean on. Thanks for helping me through the tough times as well as being there with me to celebrate the great times. I love you all and appreciate you more than you know. Thank you!!!

NOMENCLATURE

δ	chemical shift in ppm
λ	wavelength
^{79}Br	bromine nucleus (NMR)
^{13}C	carbon nucleus (NMR)
^{2}H	deuterium nucleus (NMR)
^{7}Li	lithium nucleus (NMR)
^{15}N	nitrogen nucleus (NMR)
^{1}H	proton nucleus (NMR)
^{31}P	phosphorus nucleus (NMR)
{^{1}H}	proton decoupled
{^{31}P}	phosphorus decoupled
Å	Ångstrom
AIBN	azabisisobutyronitrile
BET	Brunauer Emmett Teller
br	broad
Bu	butyl
COSY	COrrelation SpectroscopY (2D NMR)
CP	cross-polarization
CP/MAS	cross-polarization/magic angle spinning
CSA	chemical shift anisotropy
Cy	cyclohexyl
d	doublet (NMR), days

DABCO	1,4-diazabicyclo[2.2.2]octane
DD	dipolar dephasing
DMSO	dimethylsulfoxide
D_2O	deuterium oxide
eq	equivalents, equatorial (NMR)
FID	free induction decay (NMR), flame ionization detector
FT	Fourier Transformation
GC	gas chromatography
h	hours
HRMAS	high-resolution magic angle spinning
Hz	Hertz
i	ipso
J	scalar coupling constant
IR	infrared
m	multiplet (NMR), medium (IR)
m	meta
MAS	magic angle spinning
Me	methyl
NCPh	benzonitrile
NMR	nuclear magnetic resonance
NOESY	Nuclear Overhauser Effect SpectroscopY (2D NMR)
o	ortho
p	para
PAEK	polyaryletherketones
PBI	polybenzimidazole

PEEK	polyetheretherketone
PEKK	polyetherketoneketone
Ph	phenyl
ppm	parts per million
py	pyridine
R	alkyl group
RT	RT
s	singlet (NMR), strong (IR)
sept	septet (NMR)
t	triplet (NMR)
t	tertiary
TEM	transmission electron microscopy
THF	tetrahydrofurane
TMEDA	tetramethylethylenediamine
T_g	glass transition temperature
UV	ultraviolet
$\Delta\nu_{1/2}$	signal width at half height
Vis	visible
vs	very strong (IR)
VT	variable temperature
w	weak (IR)

TABLE OF CONTENTS

Page

CHAPTER Page

LIST OF FIGURES

LIST OF SCHEMES

SCHEME Page

LIST OF TABLES

CHAPTER I

INTRODUCTION

Chemists are concerning themselves with a variety of problems at the beginning of the 21st century. These require, due to their complexity, an increasingly comprehensive approach involving synthesis, spectroscopic methods, as well as theoretical approaches. This holds true for many if not all areas of chemistry, such as materials sciences, life sciences, or catalysis.

The main focus of this thesis is the application of solid-state NMR techniques in different areas of chemical research. NMR provides information on the molecular nature of both crystalline and amorphous, insoluble materials which is not easily accessible by other methods. Certain NMR parameters are sensitive to molecular motion over a wide frequency range. This makes solid-state NMR a popular tool in polymer and materials sciences.

The chapters of this dissertation span a wide range from research in polymer treatment and characterization in chapters II and III, to coordination chemistry and catalysis in chapter IV.

Chapters II and III focus on the study of performance polymers with solid-state NMR techniques. Performance polymers like ***p***oly***a***ryl***e***ther***k***etones (PAEK) are immensely important in energy applications due to their lower weight as compared to metals, and their superior corrosion resistance under demanding conditions, e.g. off-shore drilling or fracking operations. Blends of PAEK polymers, such as ***p***oly***e***ther***e***ther***k***etones

(PEEK) and ***p***oly***e***ther***k***etone***k***etones (PEKK), with ***p***oly***b***enz***i***midazole (PBI) are of commercial interest for the oil and gas industry due to their improved high-temperature stability and their superior wear characteristics. However, regarding the PBI component, the origins of the properties that are disadvantageous in thermally or chemically aggressive environments are not well understood. The same accounts for the specifics of the interactions between the PBI and PAEK components in melt or dry blend systems.

We focus on the morphological and molecular changes of the pure components as well as the blends after treating them with liquid water and steam at high temperatures and pressures. The polymers are steam-treated at 149 °C (300 °F) and 316 °C (600 °F). The goal is to understand the chemical changes on the molecular level that take place upon high-temperature steam-treatment and to examine the reversibility of the moisture uptake of this material. IR and solid-state NMR spectroscopy are used to study chemical or morphological transformations of the polymers. Interactions and reactions of H_2O with the functional groups of the polymers are studied using D_2O in combination with IR, ^2H MAS, and ^1H wideline solid-state NMR.

Chapter IV will focus on the synthesis, immobilization, and characterization of catalysts on silica supports for Sonogashira cross-coupling reactions, as well as the coordinating strengths of phosphine linkers at Pd centers. Molecular catalysts immobilized on oxide supports are easy to design and they are as selective and active as their homogeneous analogues. Furthermore, they take on the properties of heterogeneous catalysts because they can easily be separated from the reaction mixtures and recycled many times. Homogeneous catalysts can be bound to oxide supports by phosphine linkers,

with silica being the most favorable support. For the analysis of the resulting amorphous solid materials we applied classical solid-state (CP/MAS) NMR and high-resolution (HRMAS) NMR spectroscopy of slurries. Both can be employed for probing the nature and mobility of surface-bound species.

Chelating phosphine linkers, which can be bound to oxide supports via ethoxysilyl groups, have been synthesized and characterized. These linkers readily bind to Pd and Cu complexes, which have been used in the Sonogashira cross-coupling reaction of aryl halides with terminal acetylenes. Here, we will focus on new insights concerning the synthesis, immobilization, and characterization, as well as activities and lifetimes of Pd(0)/Cu(I) Sonogashira catalyst systems. The conditions for the catalyst systems with respect to solvent and base amounts have been probed, and optimal ratios of the catalyst components have been determined.

This chapter will also describe the coordinating strength of the phosphines used as ligands for the immobilized catalyst systems for Sonogashira C-C bond forming reactions. These ligands represent both monodentate as well as chelating phosphines. HRMAS techniques have been applied to gain a better understanding of the coordinating strengths of these ligands, and this will give a better insight into how this parameter affects the catalytic activities.

CHAPTER II

MULTINUCLEAR SOLID-STATE NMR STUDY OF THE MOISTURE DISTRIBUTION IN PEEK-PBI AND PEKK-PBI BLENDS

INTRODUCTION

The group of polyaryletherketones (PAEK) within thermoplastic polymers,[1] including PEEK (polyetheretherketone) and PEKK (polyetherketoneketone) polymers (Scheme 2.1), is of growing interest in a wide range of applications that demand superior mechanical strength, corrosion resistance and retention of dimensional and physical properties at high temperatures and pressures. One important example would be low-weight downhole materials in oil and gas drilling and fracturing processes. While the different commercially available PAEK grades are already of benefit to the end users, the demand for even higher temperature applications continues to grow, and along with it the quest for improved tribological performance.

One way to meet these demands is to provide blends of polyaryletherketone polymers with PBI (polybenzimidazole) resins (Scheme 2.1). This strategy takes advantage of the increased service temperatures and some improvement in the wear properties afforded by the PBI component. For example, PEKK-PBI blends are manufactured primarily to elevate the service temperature of the PEKK polymer, and to improve its wear performance. A potential drawback of PBI blends is the comparatively poor chemical stability associated with this component. Most importantly, in contrast to

the pure PAEK components, the PBI addition leads to a more complex interaction of the blend with aqueous systems, such as water and steam,[2] as well as salt solutions.

Therefore, a better understanding of the interactions of water with the functional groups of the PBI component at the molecular level is indispensable. Furthermore, a deeper insight into how the water affinity of PBI translates into the characteristics of its blends with PEEK and PEKK is sought. In this study, the traditional celazole-type PBI (poly[2,2'-(*m*-phenylene)-5,5'-bibenzimidazole]), and its 50:50 wt% PEEK- and PEKK-PBI blends are exposed to liquid D_2O at ambient temperature. Additionally, PBI and the PEEK- and PEKK-PBI blends are exposed to H_2O and D_2O steam at 150 °C (ca. 300 °F) and 315 °C (ca. 600 °F) for prolonged times to simulate real-life conditions, as they might, for example, be applied in oil and gas drilling and fracturing processes.

The impact of water or steam on PEEK and PEKK polymers and their PBI blends has not been described extensively by other groups, but using a molecular model compound mimicking PBI, one report discusses two ways in which water could reside in PBI.[3] It can either be present in larger aqueous domains nestled between the PBI polymer strands, or it can be bound to the N-H groups in the PBI backbone by hydrogen bridges. Hereby, on average one H_2O molecule is bound per N-H group.[3]

PAEK and PBI polymers and their incorporation of water are in general amenable to investigation by IR spectroscopy.[2,4,5] Changes of the carbonyl stretching band and modifications in the fingerprint area, for example, are indicators for both chemical and morphological transformations.[4]

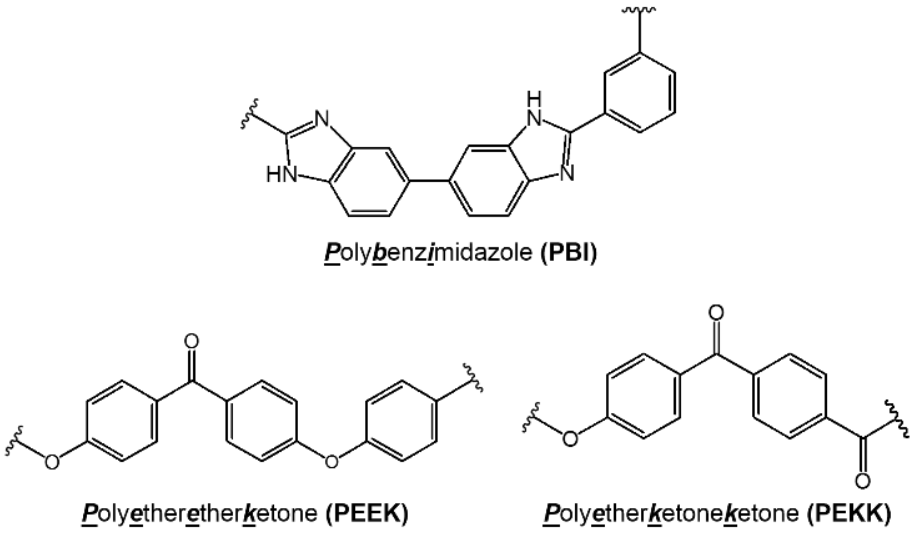

Scheme 2.1. Structures of Polybenzimidazole (PBI), Polyetheretherketone (PEEK), and Polyetherketoneketone (PEKK).

However, solid-state NMR spectroscopy is a more powerful method for studying polymers on a molecular level and providing detailed structural and dynamic information.[2,5-6] Chemical changes during the exposure to adverse conditions can be studied by ^{13}C CP/MAS NMR, [2,5-6] while morphological changes, involving the ratio of rigid versus mobile domains in the polymer, can be investigated by the ^{13}C T_1 relaxation time characteristics.[2] The prerequisite for any chemical change of the polymer due to the exposure to water at RT or steam at elevated temperatures is that water penetrates into the polymer network.[7] Especially for mostly amorphous materials like PBI[8] this scenario can be studied by ^{1}H wideline NMR, where proton measurements of the solid samples are recorded without sample spinning.[9-10]

In the following, solid-state NMR spectroscopy is employed to probe the interactions of H_2O and D_2O with PBI and its blends. For ^{13}C[2,5-6]and ^{15}N[11] cross polarization (CP) of magnetization from the abundant protons in the polymer sample to the measured nuclei improves the obtained signal to noise ratio.[12,6] Additionally, it will be demonstrated in the following that ^{1}H wideline,[9-10] and ^{2}H,[10a,13] ^{7}Li,[14] and ^{79}Br MAS NMR can give valuable complementary insights into the polymer systems on the molecular level as well. Different locations and types of water and protons in PBI and in the PEEK-PBI and PEKK-PBI blends are described in the following and it will be proven that the PBI component is mainly responsible for the water and salt uptake into the blends.

RESULTS AND DISCUSSION

Characterization of PBI and its PEEK and PEKK blends with ^{13}C and ^{15}N CP/MAS NMR

In order to characterize the pure polymer components and the PEEK- and PEKK-PBI blends the ^{13}C CP/MAS NMR spectra shown in Figures 2.1 and 2.2 have been recorded. Most of the signals are resolved and only two signal groups overlap. All resonances can be assigned unequivocally to the corresponding carbon positions in the structure, in accordance with the literature.[15-16]

The melt-blended PEEK-PBI (Figure 2.1c) results in a ^{13}C CP/MAS spectrum that shows both components in the anticipated 50:50 ratio. This is best visible in the approximate 1:1 intensity ratio of the signals b of the PEEK and 2 of the PBI components, which do not overlap.

In order to test whether melt-blending leads to interactions of the PEEK and PBI components on a molecular level, which might be seen in the ^{13}C CP/MAS spectra, a physical mixture of PEEK with PBI powder has been measured (Figure 2.1d). The spectrum of this mixture is practically identical with the spectrum of the melt-blended sample (Figure 2.1c). In particular, the signal a of the carbonyl carbon at 194 ppm retains the same chemical shift. In the case of strong N-H···O=C hydrogen bridge formation of the PBI and PEEK strands on the molecular level a shift of the carbonyl carbon resonance would have been expected.

Next, the ^{13}C CP/MAS NMR spectra of the pure components PBI and PEKK (Figure 2.2a and 2.2b), as well as the melt-blended polymer (Figure 2.2c) and a physical mixture of PBI and PEKK powder in a 50:50 wt% ratio (Figure 2.2d) have been recorded. Again, the signal assignments for PEKK are in agreement with the literature[15-16] and the amounts of the components are confirmed by the approximate 1:1 intensity ratio of the signals b of the PEKK and 1 of the PBI component. No obvious changes can be detected in the spectra of the melt-blended versus physically mixed samples (Figures 2.2c and 2.2d). In particular, the carbonyl carbon resonance at ca. 180 ppm retains its chemical shift after the melt-blending process.

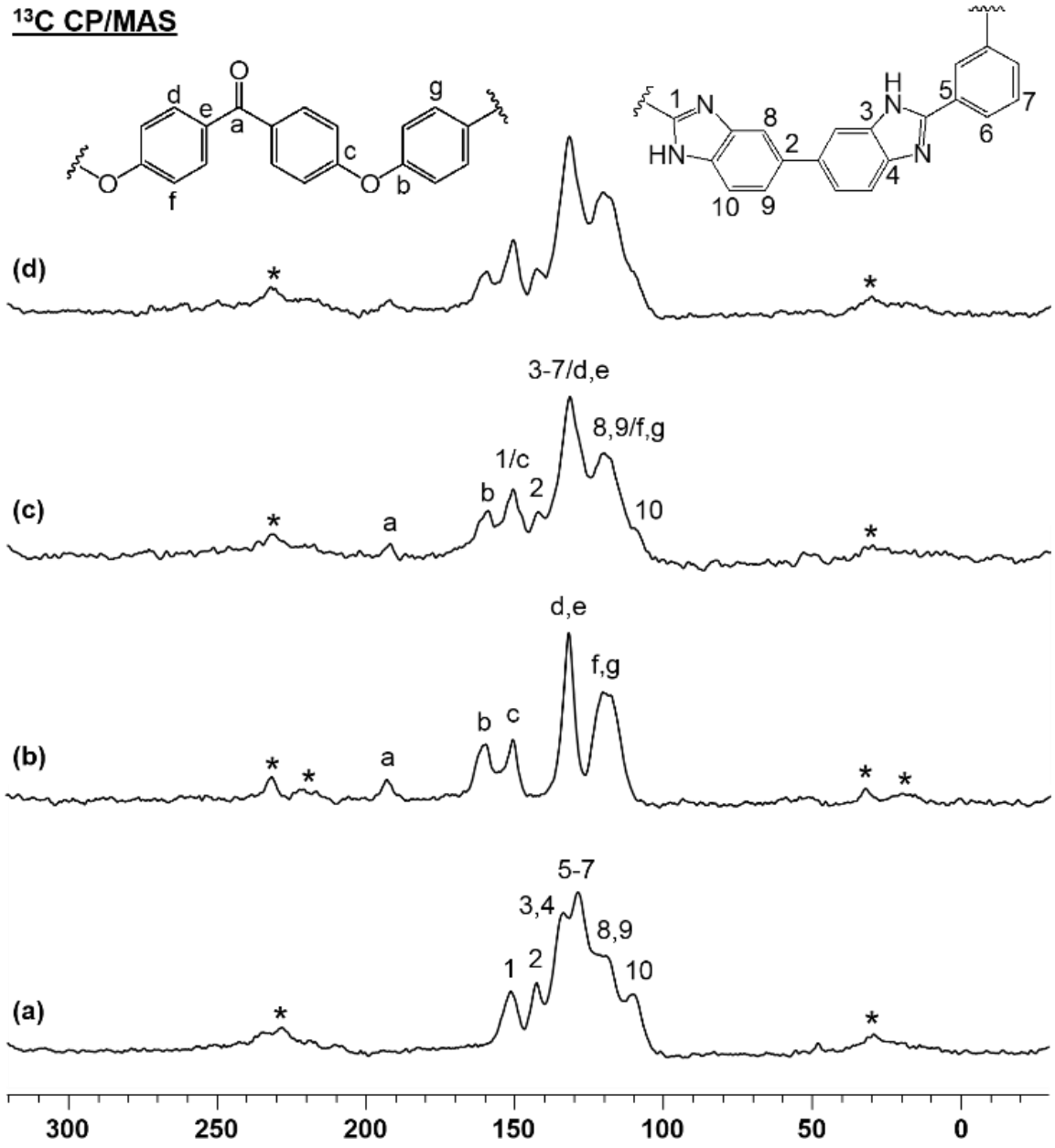

Figure 2.1. ^{13}C CP/MAS NMR spectra of PBI (a), PEEK (b), melt-blended PEEK-PBI (c), and a physical mixture of powdered PEEK and PBI (50:50 wt%) (d). The spinning speed is 10 kHz for all spectra, and the asterisks denote rotational sidebands.

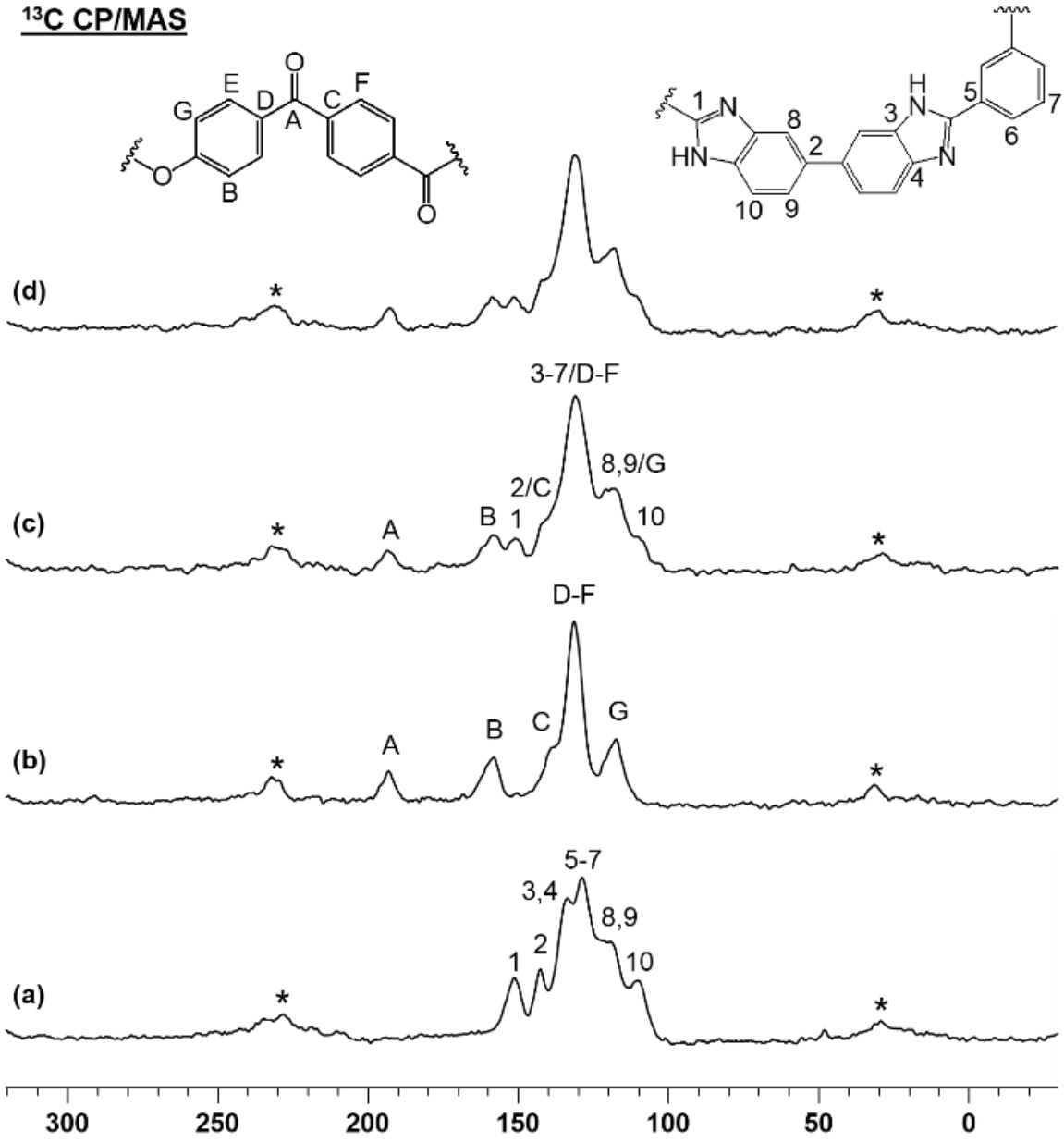

Figure 2.2. ^{13}C CP/MAS NMR spectra of PBI (a), PEKK (b), melt-blended PEKK-PBI (c), and a physical mixture of powdered PEKK and PBI (50:50 wt%) (d). The spinning speed is 10 kHz for all spectra, and the asterisks denote rotational sidebands.

However, when IR spectroscopy is employed as another powerful tool,[4,5] a change becomes visible. The IR spectra of a physical mixture and the melt-blended sample differ slightly (Figure 2.3). The C=O stretching band in the physical mixture is found at 1653 cm^{-1}, while the wavenumber and therewith frequency are lower in the spectrum of the melt-blended sample. This indicates that some hydrogen bridges between C=O and N-H groups of different polymer strands occur after the melt-blending process. The hydrogen bridges lead to a weakening of the C=O bond and therefore a lower wavenumber of 1651 cm^{-1} for its stretching band.

In order to further investigate whether hydrogen bonding interactions between the N-H groups of the PBI and the C=O groups of PEEK and PEKK are visible in the chemical shift of the nitrogen nucleus, the ^{15}N CP/MAS spectra[11] shown in Figure 2.4 have been recorded. Due to the low natural abundance and long relaxation time of ^{15}N in the solid state[11] the signal to noise ratio of the spectra obtained is comparatively low. The fact that in the blends only 50% of the sample contains nitrogen nuclei from the PBI adds to this disadvantage. Together with the large linewidths of the signals and the obvious presence of more than one ^{15}N resonance in each spectrum, this renders an unequivocal interpretation of any chemical shift trend difficult. However, a cautious preliminary evaluation of the spectra can be undertaken.

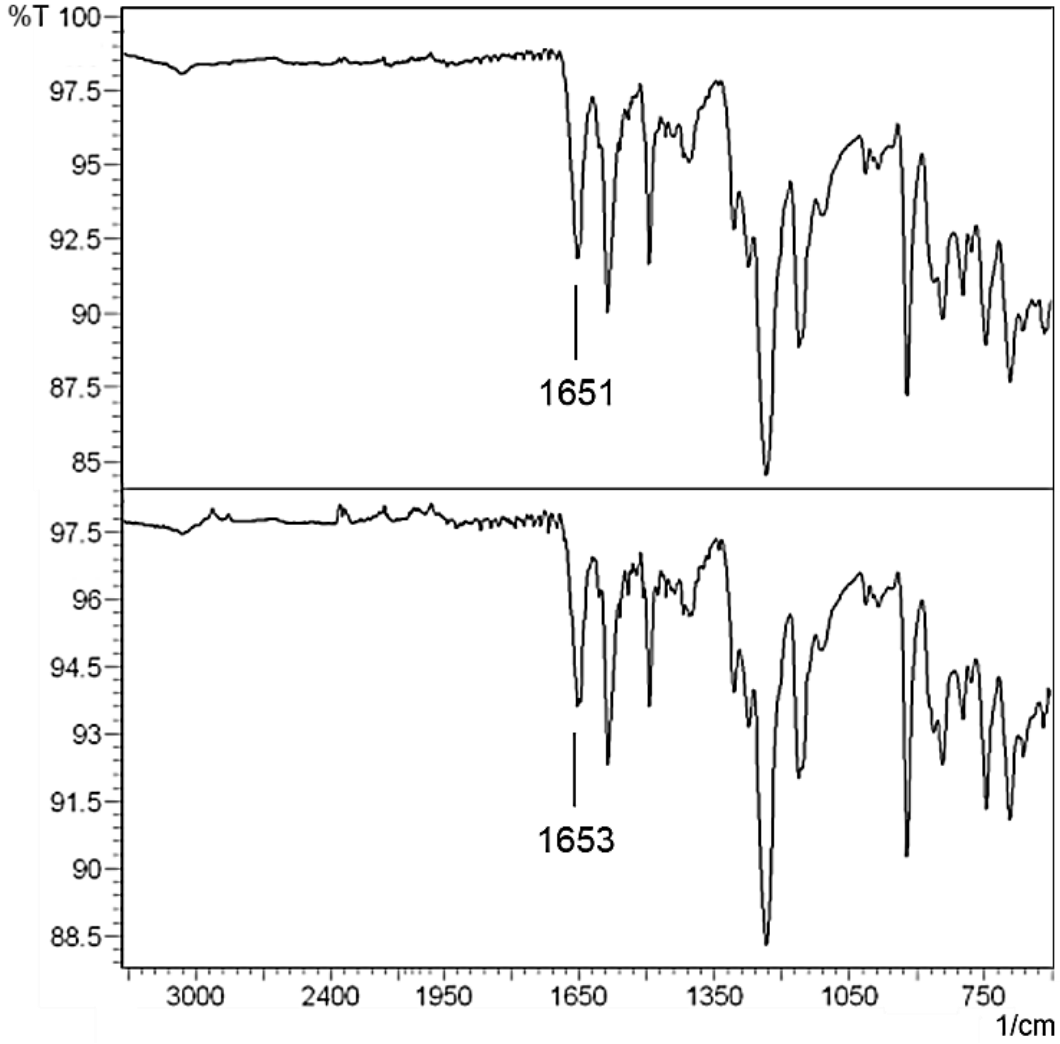

Figure 2.3. IR Spectra of melt-blended PEKK-PBI (top), and a physical mixture of PEKK and PBI (bottom).

As discussed in more detail below, the most striking change is visible in the chemical shift of the thoroughly dried PBI, 113.2 ppm, (Figure 2.4b) and PBI steam-treated with H_2O at 150 °C, 120.6 ppm (not shown). When deuterated water, D_2O, is used for the steam-treatment, the ^{15}N NMR signal appears at 118.0 ppm (Figure 2.4a), which might be due to the secondary isotope effect the directly bound ^{2}H exerts on ^{15}N. This means that the N nuclei in the PBI are affected by the steam-treatment reagent at 150 °C, supporting our later hypothesis that N-H protons are exchanged by deuterium in the course of the steam-treatment.

Furthermore, there are chemical shift changes between the thoroughly dried PBI, 113.2 ppm (Figure 2.4b), the melt-blended PEEK-PBI, 110.4 ppm (Figure 2.4c), and the melt-blended PEKK-PBI, 116.3 ppm (Figure 2.4d). One might cautiously interpret this as reflecting an increased potential for N-H···O=C hydrogen-bonding between the PEKK and PBI components, as compared to PEEK-PBI. Overall, we conclude that the N-H groups of the benzimidazole unit of PBI are in the "center of the action" when steam-treatment is performed, and the ^{15}N resonance is sensitive to the second component in PBI blends and "sees" the difference between PEEK and PEKK.

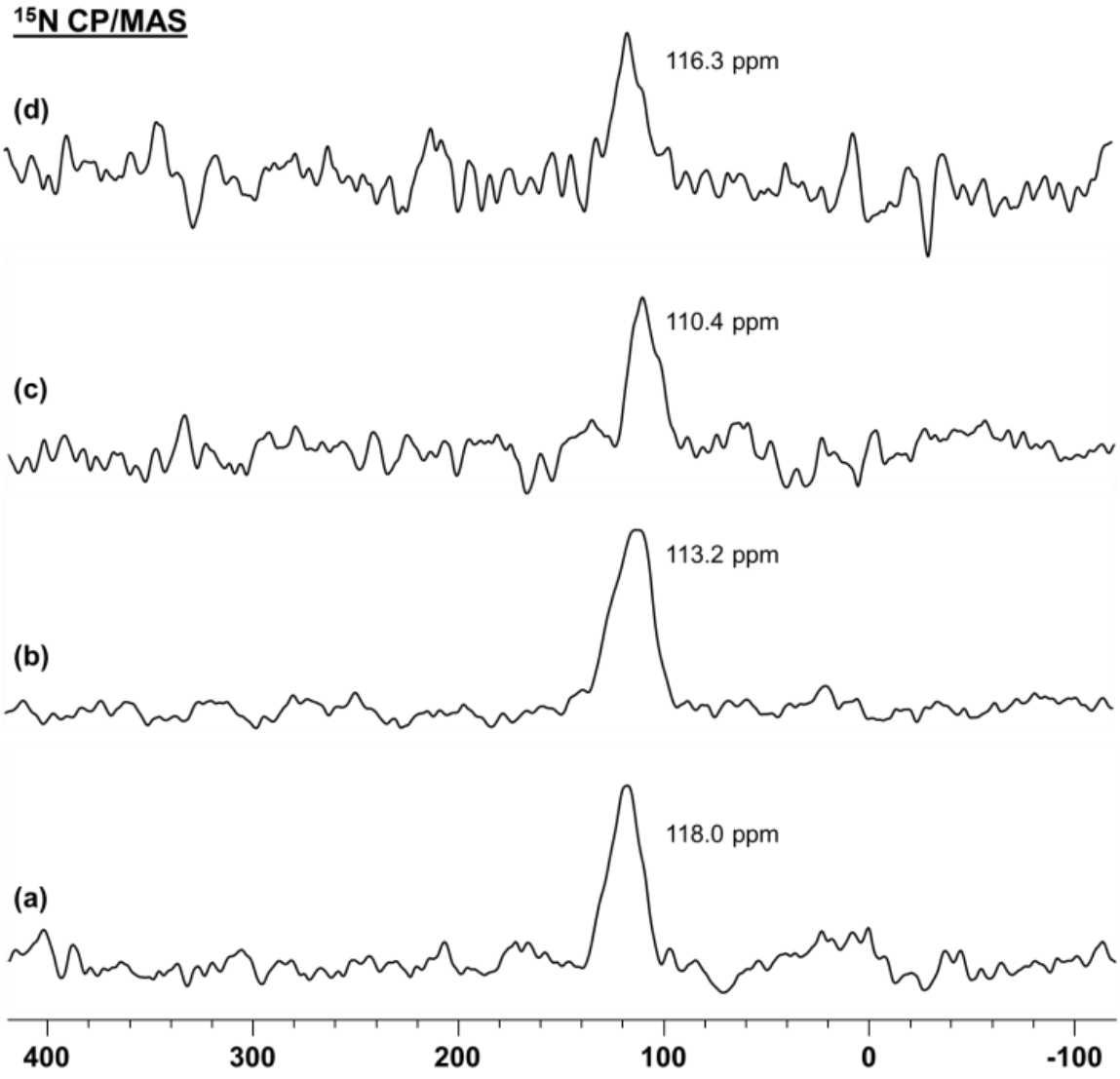

Figure 2.4. ^{15}N CP/MAS NMR spectra of PBI, steam-treated with D_2O at 150 °C (6 kHz) (a), dried PBI (6 kHz) (b), melt-blended PEEK-PBI (10 kHz) (c), and melt-blended PEKK-PBI (10 kHz) (d).

Macroscopic water removal and rehydration of PBI, PEEK-PBI and PEKK-PBI at moderate temperatures

As described qualitatively in previous work,[2] PBI is hydrophilic and prone to taking up water readily from the atmosphere. In order to obtain a more quantitative estimate of this characteristic, PBI powder and melt-molded samples have been dried under vacuum (0.1 torr) at 110 °C for 144 h (6 days) and 600 h (25 days), respectively. This process is monitored in a straightforward manner by weighing the samples at given time intervals. The drying curves are displayed in Figures 2.5 and 2.6. The PBI powder shows no more weight loss after about 4 days while the melt-molded samples still retain residual moisture after 25 days. This result demonstrates that whenever rigorously dried PBI is needed, a powder should be used. Due to its larger specific surface area it allows the absorbed water to leave the sample more quickly.

The slightly different curves obtained for the three melt-molded tensile specimens (Figure 2.6) corroborate the assumption that the surface area of the samples is crucial for the drying rate. Since constant weight is achieved after drying the PBI powder we assume that the moisture content of this particular sample amounts to about 9% of its weight. This value is in the same range (5-11%) as the moisture contents found by TGA for PBI tensile specimens treated with water and steam under different conditions.[17]

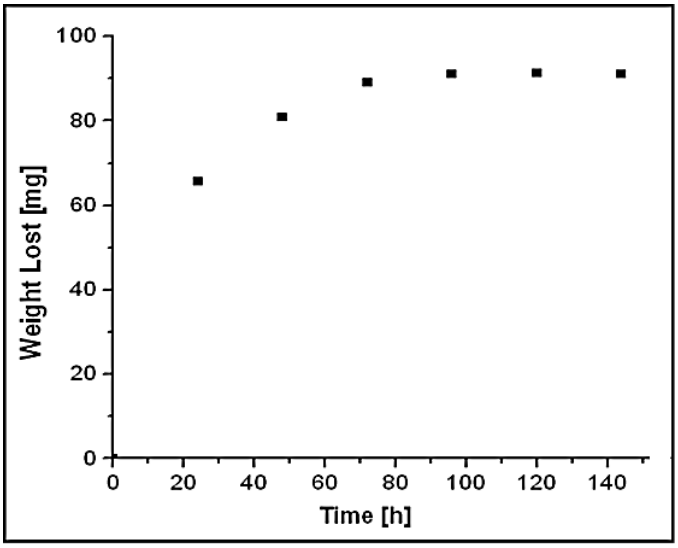

Figure 2.5. Weight loss of 1 g of PBI powder during drying *in vacuo* at 110 °C over the course of 6 days.

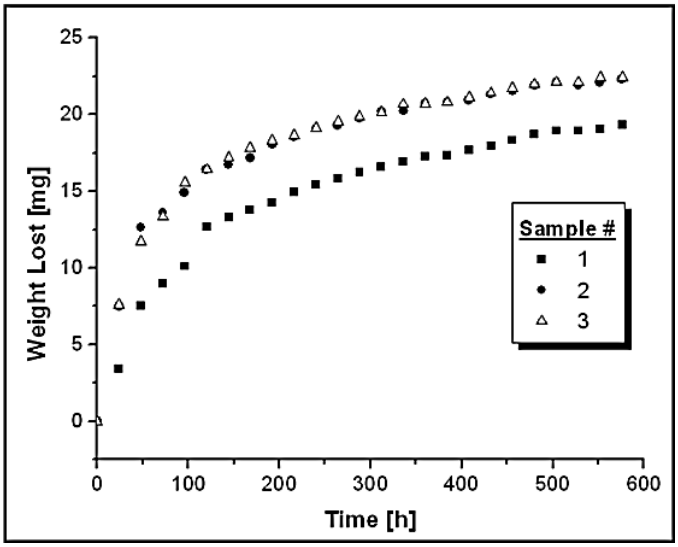

Figure 2.6. Weight loss of 1 g of melt-molded PBI during drying *in vacuo* at 110 °C for 25 days. The curves for three melt-molded tensile specimens of slightly different size and surface area are displayed.

For PEEK and PEKK blends of PBI, it is generally assumed that the PBI component is mainly responsible for the water uptake. In order to quantify this effect, the weight loss of the blends has been recorded over time. When PEEK-PBI and PEKK-PBI (50:50 wt%), as received, are dried *in vacuo* at elevated temperatures, the curves displayed in Figures 2.7 to 2.10 are obtained.

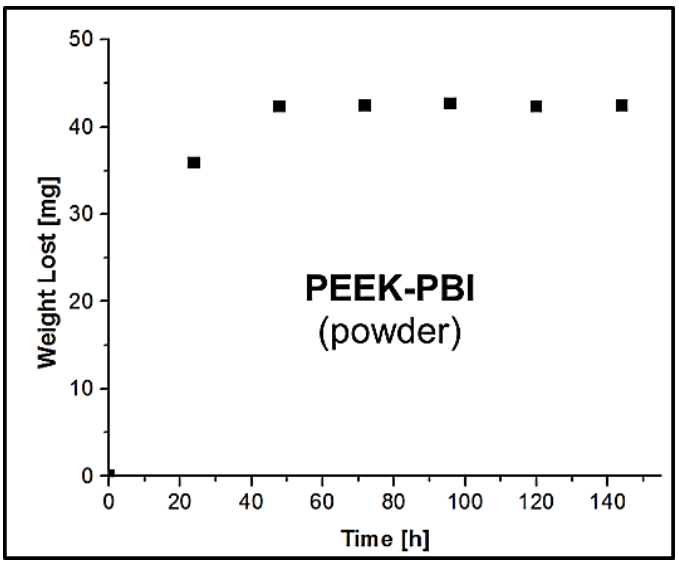

Figure 2.7. Weight loss of 1 g of PEEK-PBI powder when dried *in vacuo* at 110 °C.

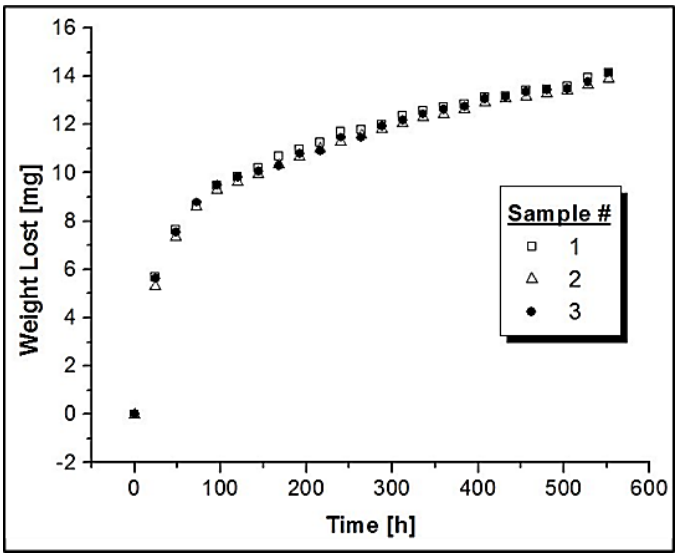

Figure 2.8. Weight loss of 1 g of PEEK-PBI when treated *in vacuo* at 110 °C. The curves for three melt-blended tensile specimens are displayed.

The PEEK-PBI powder reaches constant weight after about 50 h (Figure 2.7), while PEKK-PBI initially loses the moisture much faster and is completely dry after roughly 45 h (Figure 2.9). This result nicely confirms earlier assumptions that PEEK is slightly more prone to take up and retain moisture from the environment than PEKK. The total amount of weight loss, however, is about the same for both blends with ca. 4.3% (Figures 2.7 and 2.9). This is nearly half the amount of water found for PBI, which indicates that practically all the water of the 50:50 wt% PEEK-PBI and PEKK-PBI blends is residing in the PBI component.

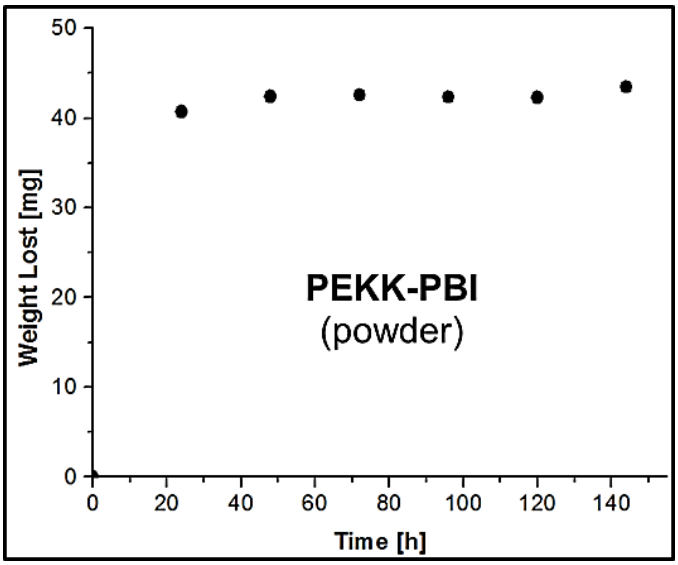

Figure 2.9. Weight loss of 1 g of PEKK-PBI powder when treated *in vacuo* at 110 °C for 6 days.

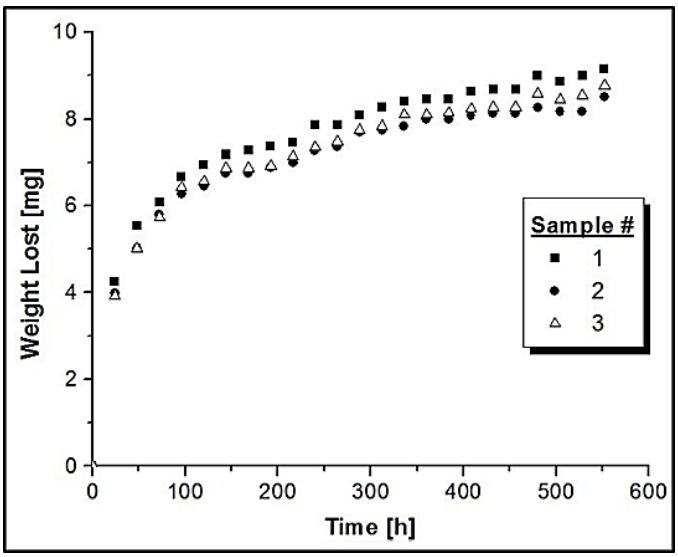

Figure 2.10. Weight loss of 1 g of PEKK-PBI when treated *in vacuo* at 110 °C. The curves for three melt-blended tensile specimens are displayed.

As in the case of PBI, and in order to test the reproducibility, three f tensile specimens have been submitted to the drying procedure for both the PEEK-PBI and the PEKK-PBI blends. As the curves in the Figures 2.8 and 2.10 show, there is only a minimal difference between the drying progress of the three samples of each material, which might again be attributed to slightly different sizes and surface areas of the specimens. The PEEK-PBI starting material releases more moisture than the PEKK-PBI blend within the given time frame. After 25 days of drying *in vacuo* about 14 mg of water per 1 g of PEEK-PBI is lost (Figure 2.8), but only ca. 9 mg per g of PEKK-PBI (Figure 2.10).

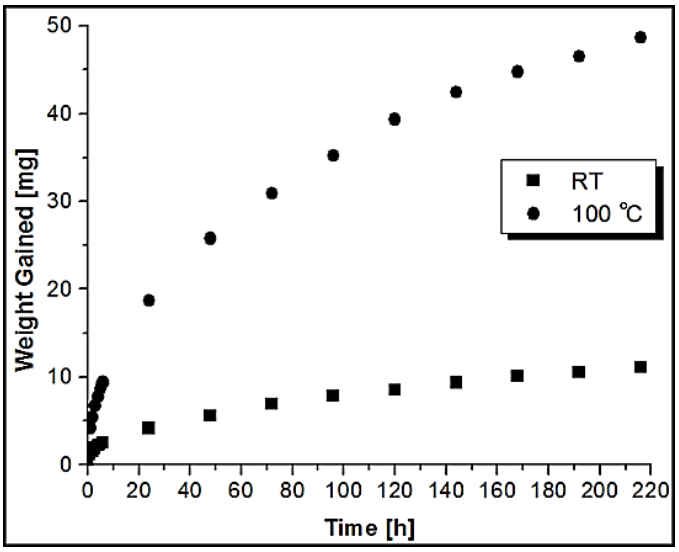

Figure 2.11. Weight gain of 1 g of PEEK-PBI melt-blended tensile specimens when stirred in water at RT and at 100 °C.

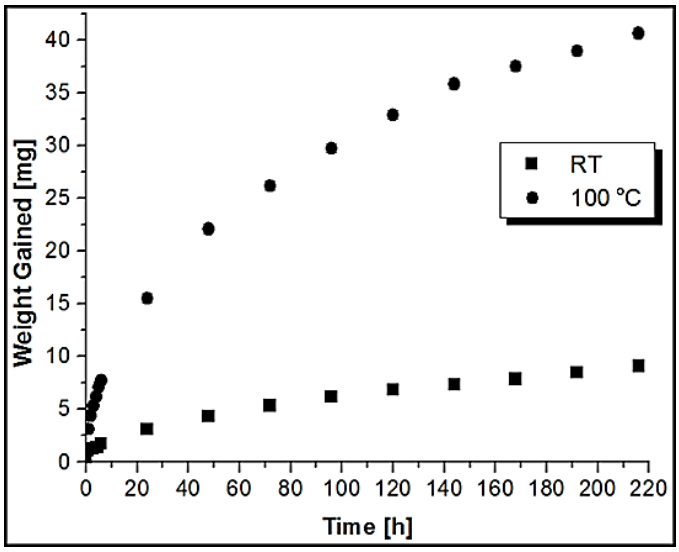

Figure 2.12. Weight gain of 1 g of PEKK-PBI melt-blended tensile specimens when stirred in water at RT and at 100 °C.

It has been demonstrated earlier by ^{13}C T_1 relaxation time measurements that the uptake of water in PBI blends is reversible as long as the conditions are relatively mild.[2] In order to quantify this effect the dried PEEK-PBI and PEKK-PBI tensile specimens have been exposed to water at ambient and elevated temperatures. As Figures 2.11 and 2.12 show, both PEEK-PBI and PEKK-PBI samples take up moisture readily, but at RT only about 10 mg of H_2O have been absorbed per g of material within 220 h. However, at 100 °C both blends take up moisture vigorously and in excess of what the samples contained when received. Again, PEEK-PBI has a stronger affinity to H_2O than PEKK-PBI, as it takes up 50 mg per 1 g of material within 220 h, versus only about 40 mg in the latter case.

Steam-treatment of PBI and its PEEK and PEKK blends with H_2O and D_2O

All samples have been stirred in liquid water for the above indicated amounts of time. In order to mimic more realistic conditions of exposure to fluids, powdered PBI and melt-blended tensile specimens of PEEK-PBI and PEKK-PBI have also been subjected to steam-treatment with H_2O. For this purpose, the samples are placed into stainless steel pressure vessels which are filled with 150 mL of liquid water to the height of about 1.5 cm, then sealed and heated.

The pressures reached in the closed vessels are 5 bar (72 psi) at 150 °C and 110 bar (1600 psi) at 315 °C. The exposure of the samples to water at RT and 150 °C has been maintained for 48 h, and at 315 °C for 72 h. Interestingly, the initially used stainless steel grids holding the samples in place above the liquid phase in the reactor corrode significantly where they are exposed to steam, while they stay intact in the liquid phase (Figure 2.13, left). Therefore, special glass sample holders with longer lifetimes have been designed and manufactured (Figure 2.13, right).

Figure 2.13. Stainless steel (left) and especially designed glass sample holders (middle and top view right) for positioning samples above the liquid phase in the pressure vessels.

When melt-molded PBI samples are exposed to water at RT, and steam at 150 °C and 315 °C, and subsequently subjected to TGA analysis, 5%, 11%, and 9% of moisture are released, respectively.[17] So, the highest water content in the PBI samples is achieved after steam-treatment at 150 °C, in accordance with the findings after complementary analyses.[2]

The TGA results after exposing PEEK-PBI and PEKK-PBI to water at RT, 150 °C, and 315 °C. For both blends the highest moisture contents of 6% and 7% are found after steam-treatment at 150 and 315 °C. A slight difference of about 1% favors moisture in the PEEK-PBI blend (4%, Figure 2.14) after exposure to liquid water at ambient temperature as compared to the PEKK-PBI (3%, Figure 2.15). These data show that

especially at higher temperatures the PEEK and PEKK components of the blends reduce the amount of water that pure PBI would incorporate.

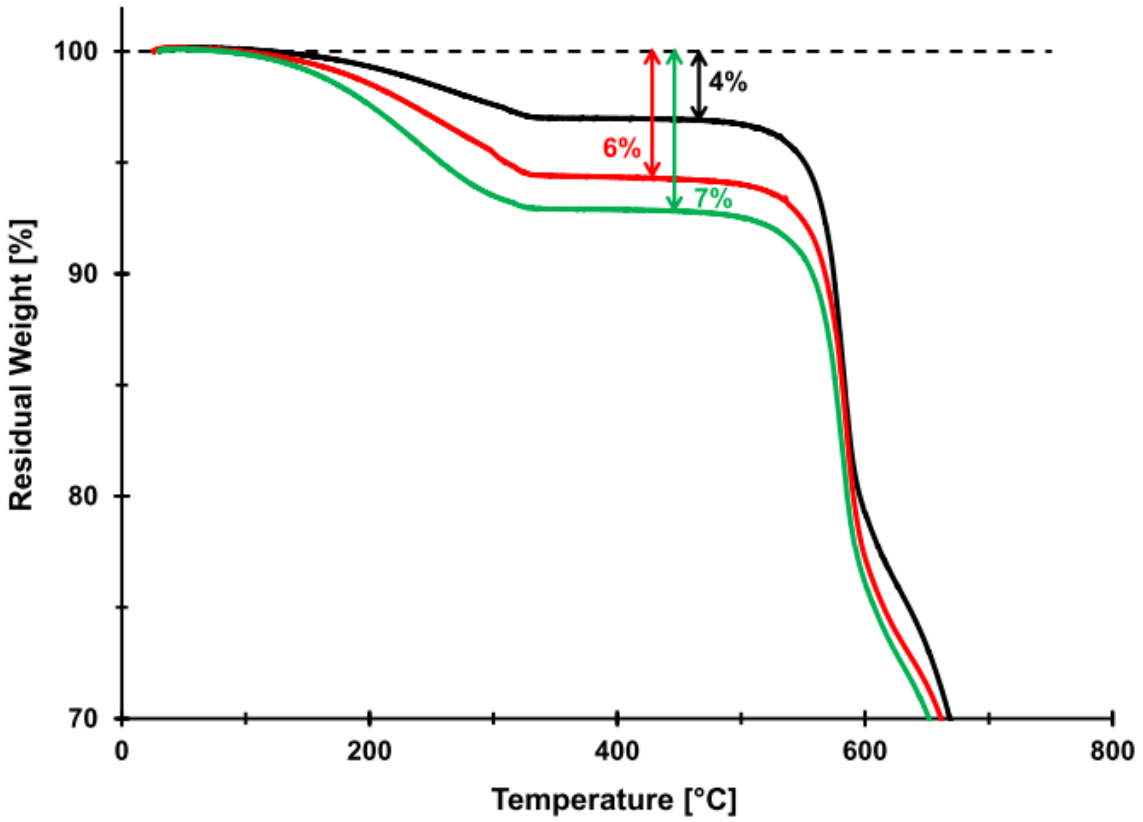

Figure 2.14. TGA of melt-blended PEEK-PBI melt-blended tensile specimens after treatment with liquid H_2O and steam-treatment at 150 °C and 315 °C.

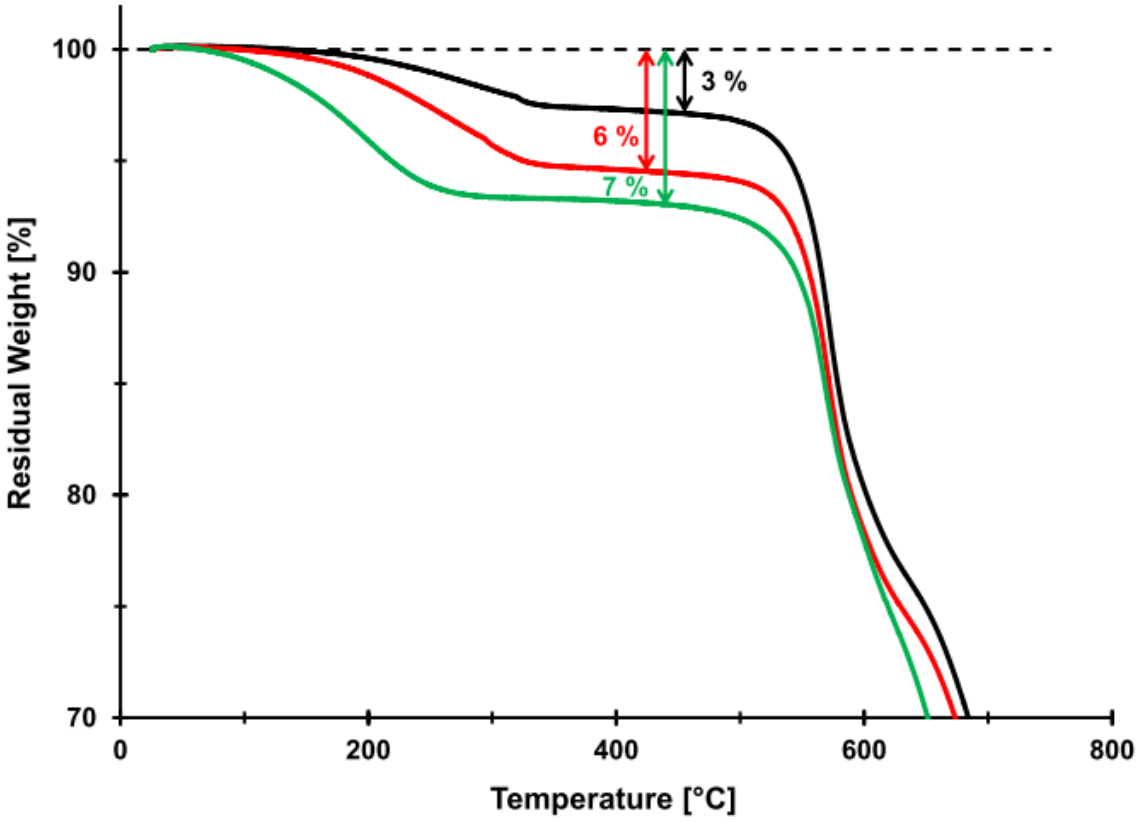

Figure 2.15. TGA of melt-blended PEKK-PBI tensile specimens after treatment with liquid H_2O and steam-treatment at the indicated temperatures.

^{13}C, ^{2}H, and ^{1}H NMR spectroscopy for probing different H_2O sites in PBI, PEEK-PBI, and PEKK-PBI

Following this global assessment of water incorporated into PBI and its blends, a more differentiated picture is sought. For this purpose, besides ^{13}C solid-state analysis, ^{1}H and ^{2}H MAS spectroscopy will be applied. In the latter case the samples have been treated with D_2O instead of H_2O. Since the largest amount of moisture obviously resides in the PBI it will be discussed next.

Analysis of PBI after exposure to D_2O as liquid and steam: It is obvious from the darkening color of PBI powder after stirring it in water at ambient temperatures that there are changes in the appearance of the material occurring already under these mild conditions (Figure 2.16). Steam-treatment of the PBI powder at 150 °C leads to a further deepening of the color and visible morphological changes. After steam-treatment of the sample at 315 °C with D_2O the powder makes a "baked" black and charcoal-type impression (Figure 2.16, right). It should be pointed out that D_2O practically does not differ in its reactivity from H_2O, and the same observations are made using the latter for steam-treatment.

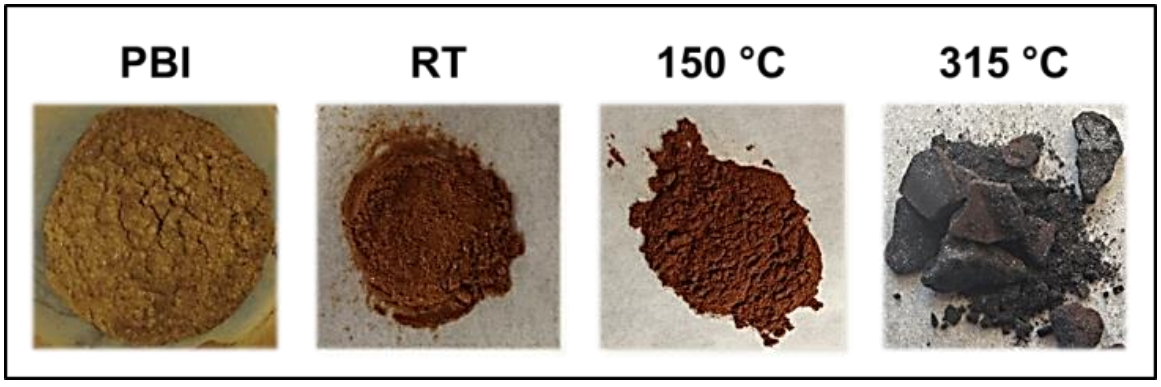

Figure 2.16. Well-dried PBI powder (left) and after treatment with D_2O at the indicated temperatures.

Intrusion of water into the polymer network is the crucial factor when the materials change their morphology or break down due to chemical reactions. Therefore, the interactions of water with the polymers will be studied in more detail in the following. For the ^{1}H and ^{2}H solid-state NMR analysis it is important to reflect on the possible locations of water and protons in hydrated PBI. There are two sorts of backbone protons, aryl protons bound to carbons of the benzene rings, and N-H protons. Aryl C-H protons do not exchange, even under the harsh conditions of steam-treatment at 315 °C.

This is proven by subjecting the molecular model compound benzimidazole, $C_7H_6N_2$, to steam-treatment in the pressure vessels at 150 °C. No C-D deuterated products are found, and therefore one can assume that the hydrogen atoms of the PBI, PEEK, or PEKK backbones will not be exchanged either. Nitrogen-bound protons, on the other hand, can in principle exchange with protons of H_2O, or deuterium, if D_2O is offered (Scheme 2.2). The potentially formed N-D groups are expected to retain the deuterium when PBI is subjected to redrying after D_2O exposure.

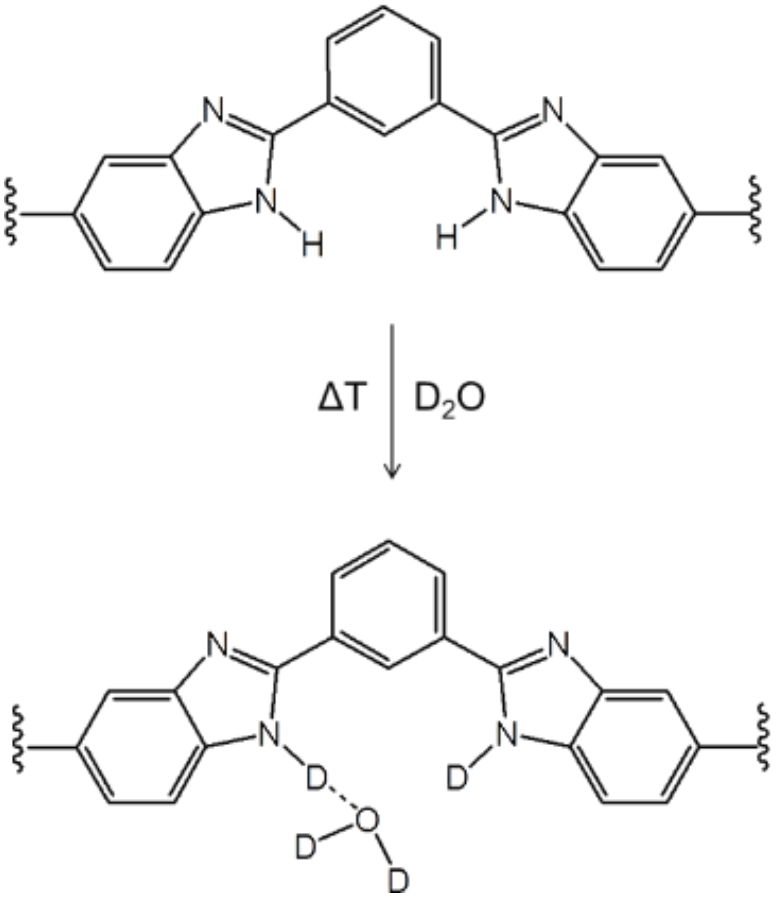

Scheme 2.2. Exchange of protons versus deuterons and hydrogen-bonded D_2O in PBI.

Besides these covalently bound hydrogen or deuterium atoms, D_2O can form hydrogen bonds with the N-H or N-D groups, as shown in Scheme 2.2. In previous work it has been demonstrated with the use of a molecular model compound that one water molecule is hydrogen-bonded per N-H group.[3] Adsorbed water molecules can migrate along the PBI strands and exchange with water molecules in adjacent liquid domains.[3] Hydrogen-bonded water is expected to be removed when redrying the PBI rigorously. Finally, water can also be present in the polymer, residing as a liquid in pockets of the

polymer network, which can also be removed upon drying. While backbone C-H and N-H protons and N-D deuterium atoms are basically immobile, hydrogen-bonded H_2O and D_2O have some mobility even in the solid materials. The water in liquid domains, depending on their size, should be the species with most mobility in the polymer system. The water molecules in large liquid domains can even approach liquid-type mobility with reorientation times in the ns range.[10a]

Since the steam-treatment of PBI leads to obvious changes of the material (Figure 2.16), ^{13}C solid-state NMR has been applied to probe whether decomposition at the molecular level can be detected. Figure 2.17 shows the ^{13}C CP/MAS NMR spectra of all PBI samples before and after exposure to D_2O at the listed conditions. First changes are already visible when PBI is stirred in liquid D_2O at ambient temperatures. The previously merged signals of the carbon nuclei 8 and 9 are split into two signals (Figure 2.17b). Steam-treatment of the PBI at 150 °C leads to an increase of signal intensities of carbons 5-7. Interestingly, after steam-treatment at 315 °C, all signals of the benzimidazole moiety are basically gone, while those of the benzene ring and carbon 1, which is directly bound to it, persist (Figure 2.17d). In order to distinguish whether this result indicates potential decomposition of the imidazole unit, or is due to the exchange of ^{1}H by ^{2}H nuclei, one needs to reflect on the measurement method.

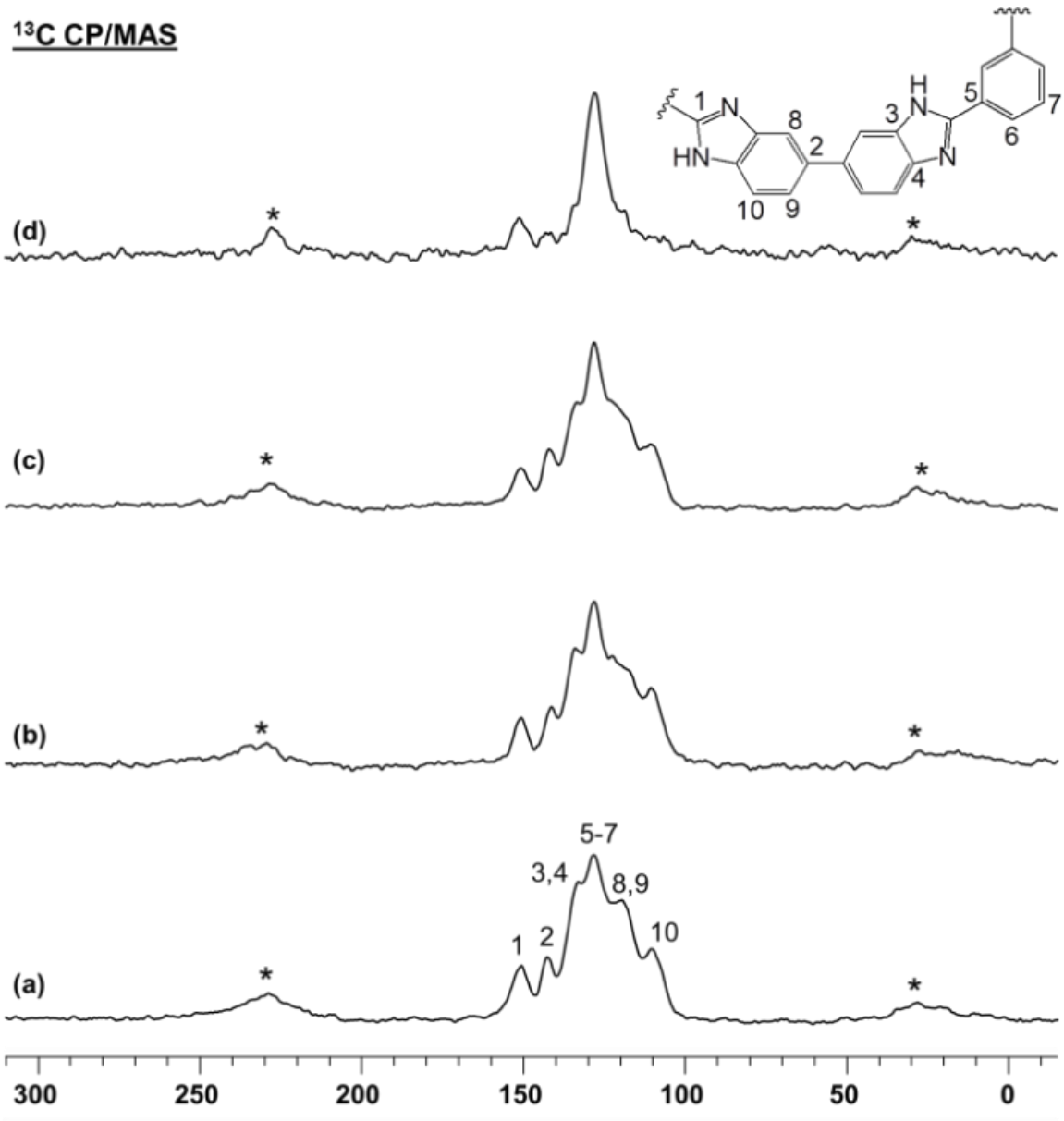

Figure 2.17. ^{13}C CP/MAS NMR spectra of PBI powder after drying at 110 °C for 144 h (a), stirring in liquid D_2O at RT (b), steam-treatment with D_2O at 150 °C (c), and at 315 °C (d).

The spectra in Figure 2.17 are all recorded with cross polarization,[18-6] which means that the ^{13}C signal intensities are boosted by magnetization transfer from protons. Since the original material contains large amounts of protons, a short contact time of 1.5 ms is sufficient to obtain spectra with good signal-to-noise ratio that show all signals. However, in the materials where ^{1}H is largely exchanged with ^{2}H by steam-treatment with D_2O, the magnetization has to be transferred from the remaining aryl protons, which are further away from the corresponding ^{13}C nuclei of the benzimidazole unit. This can be achieved by applying a longer contact time.[6] Indeed, when PBI, steam-treated with D_2O at 315 °C, is measured with a contact time of 10 ms, all ^{13}C signals are visible again (Figure 2.18).

This spectrum allows three conclusions. First, the lines are narrower than in any of the spectra in Figure 2.17, which indicates that the PBI has changed its morphology and is more crystalline after the high-temperature steam-treatment, in accordance with earlier results obtained by ^{13}C T_1 relaxation time measurements.[2] Secondly, the loss of ^{13}C benzimidazole signals after treatment with D_2O and their boost with the longer contact time means that the H_2O and the newly incorporated D_2O mostly reside around the benzimidazole moieties in the polymer. The carbon signal 1 persists throughout, because its signal profits from magnetization transfer of the close-by aryl protons 6 and 7. The third piece of information is that the N-H proton and the protons of the H_2O molecule hydrogen-bonded to the N-H group are a source for magnetization transfer to the ^{13}C nuclei of the benzimidazole unit. Furthermore, this result suggests that the hydrogen-bonded H_2O molecules must stay long enough in the same environment to allow magnetization transfer.

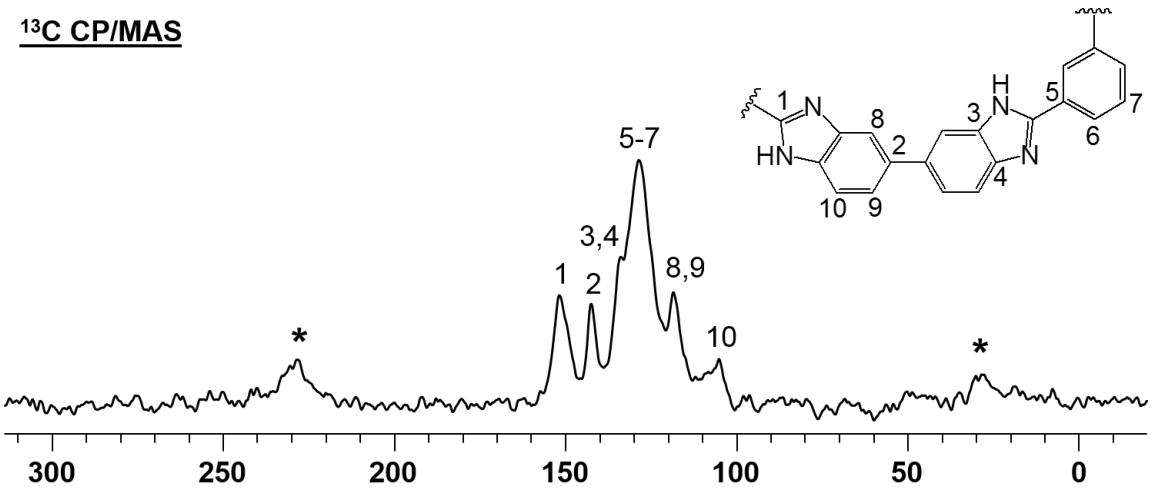

Figure 2.18. ^{13}C CP/MAS NMR spectrum of PBI powder after treatment with D_2O at 315 °C, recorded with a contact time of 10 ms for cross polarization.

In order to further probe the different ^{1}H and ^{2}H locations and characteristics, ^{1}H and ^{2}H solid-state NMR spectroscopy have been applied. ^{1}H MAS NMR, even at very high rotational frequencies of 35 kHz is only of limited use for the polymers investigated here, because only one narrow signal is obtained, surrounded by the corresponding sets of rotational sidebands. However, as demonstrated earlier,[2,10a] ^{1}H wideline NMR spectroscopy without sample spinning is analytically valuable for distinguishing protons of the immobile backbone from mobile H_2O molecules in aqueous domains within the polymer network. Mobile species result in a relatively narrow signal sitting on the broad resonance of the backbone signal.[2]

Figure 2.19 displays the ^{1}H wideline NMR spectra of PBI powder before and after exposure to D_2O under different conditions. Spectrum (a) shows that after drying the sample *in vacuo* for 144 h at 110 °C only immobile C-H and N-H backbone protons are

present, which result in a broad resonance with about 31.0 kHz linewidth. After stirring PBI at RT in D_2O, the proton wideline spectrum (b) shows a narrower line on top of the backbone signal whose half width can be determined to be around 5.1 kHz after deconvolution.[19] The narrow signal might stem from residual, strongly adsorbed H_2O that has been liberated into aqueous domains by exchange with D_2O. Independent of the origin of the protons resulting in the narrow resonance one can conclude that even at RT water can easily move into the polymer and participate in proton exchange.

After steam-treatment of the PBI with D_2O at 150 °C (c) and 315 °C (d), narrow peaks are present with line widths of 2.1 and 4.4 kHz, respectively, but their intensity is diminished as compared to the signal in spectrum (b). Obviously, at the higher temperatures the exchange of protons by deuterium is more complete, leading to reduced ^1H signals of exchangeable protons, because under these conditions more water can penetrate into the polymer network within the given time frame and leave it again.

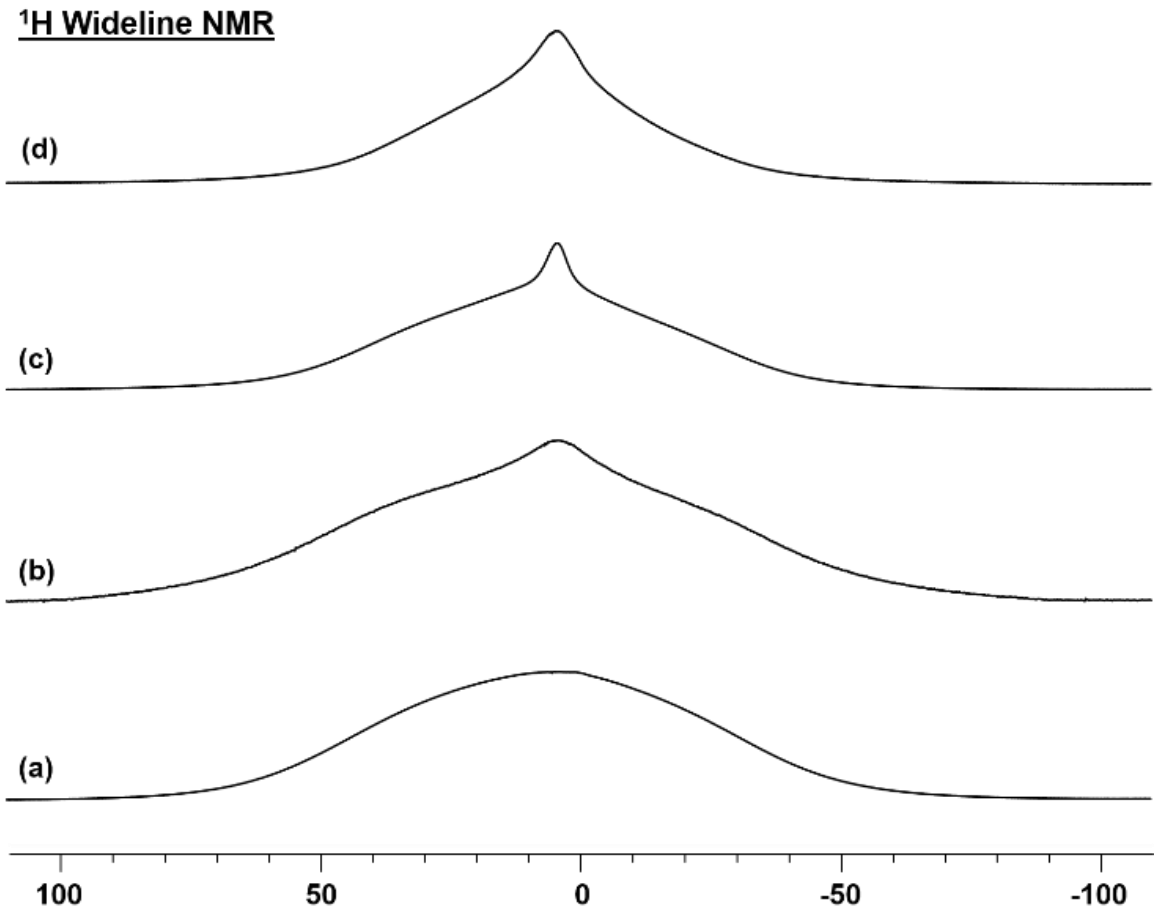

Figure 2.19. ^{1}H Wideline NMR spectra of PBI powder after drying at 110 °C for 144 h (a), stirring in D_2O at RT (b), and steam-treatment with D_2O at 150 °C (c) and 315 °C (d).

In order to gain a more differentiated picture about the various sorts of protons and water present in the PBI, as well as their mobilities, ^{2}H MAS has been applied. Measuring ^{2}H instead of ^{1}H NMR also allows to eliminate any signals from the polymer backbone. Information about the mobilities of the ^{2}H-containing species can be obtained, because ^{2}H has a nuclear spin of 1 and is therefore quadrupolar. The Pake patterns[18,10a,13] of ^{2}H wideline signals in the solid state display a splitting of the two lines with maximal intensity

that allows the calculation of the quadrupolar coupling constant Q_{cc}. When the sample is rotated the Pake pattern is split into sets of rotational sidebands. Q_{cc} can be calculated from spectra of rotated samples as described in the experimental section and in the literature.[20] The quadrupolar coupling constant can be correlated with the mobility, or more precisely, the reorientation time of the species or functional groups containing the measured ^2H nucleus. [13,21]

This correlation between reorientation times and appearances of the corresponding Pake patterns has been described in detail for long alkyl chains.[21] ^2H MAS spectroscopy has previously been applied by us to quantify the mobilities of metallocenes adsorbed on silica surfaces.[10a] But there are also examples for applications in the field of polymers in the literature, and recently ^2H solid-state NMR has been used to obtain more quantitative insight into various dynamic scenarios.[13] For example, the segmental mobilities of polymer chains[13g] and the plasticization of poly(vinyl acetate) adsorbed on silica have been investigated using ^2H solid-state NMR.[13f]

Figure 2.20 shows the ^2H MAS spectra after treating PBI with D_2O under different conditions. Stirring PBI in D_2O at ambient temperature results in spectrum (a). There are two signals with very different characteristics discernible in the spectrum. A signal in the center at ca. 5 ppm with a half width of about 3 kHz is not split into a Pake pattern. This signal is attributed to mobile water present in liquid aqueous domains in the polymer due to a collapsed Pake pattern.[10a,13] The second signal presents as a classic Pake pattern of lower intensity with a Q_{cc} value of 194 kHz (Table 2.1). Due to the sample rotation with

6 kHz the Pake pattern is split into a manifold of rotational sidebands with residual line widths of about 600 Hz.

The origin of this signal must be an immobile species, most probably D_2O strongly hydrogen-bonded to N-H groups of the PBI backbone. This assumption is corroborated by the following experiment: when the PBI sample is redried thoroughly *in vacuo*, there are no longer any ^2H signals emerging in the spectrum (Figure 2.20b), even after prolonged measurement times. Therefore, one can assume that in case PBI is stirred in D_2O at ambient temperature, the merely adsorbed, as well as D_2O residing in liquid domains, can be removed again quantitatively, and there is no chemical exchange of ^1H versus ^2H.

After PBI is steam-treated with D_2O at 150 °C for 48 h, two signals are again visible in the ^2H MAS spectrum, as shown in Figure 2.20c. The only differences as compared with the spectrum in Figure 2.20a are that the Pake pattern shows higher intensity, and that Q_{cc} assumes a slightly larger value of about 195 kHz. When the sample is dried *in vacuo*, a Pake pattern with a larger Q_{cc} of ca. 201 kHz remains, while the broad resonance in the center is gone (Figure 2.20d). The latter finding corroborates our assumption that the broad center peak belongs to domains of liquid D_2O, which are removed during the drying procedure. The persistent Pake pattern can be assigned to N-D groups in the polymer backbone that come into existence by deuterium exchange of the N-H groups with hydrogen-bonded D_2O.

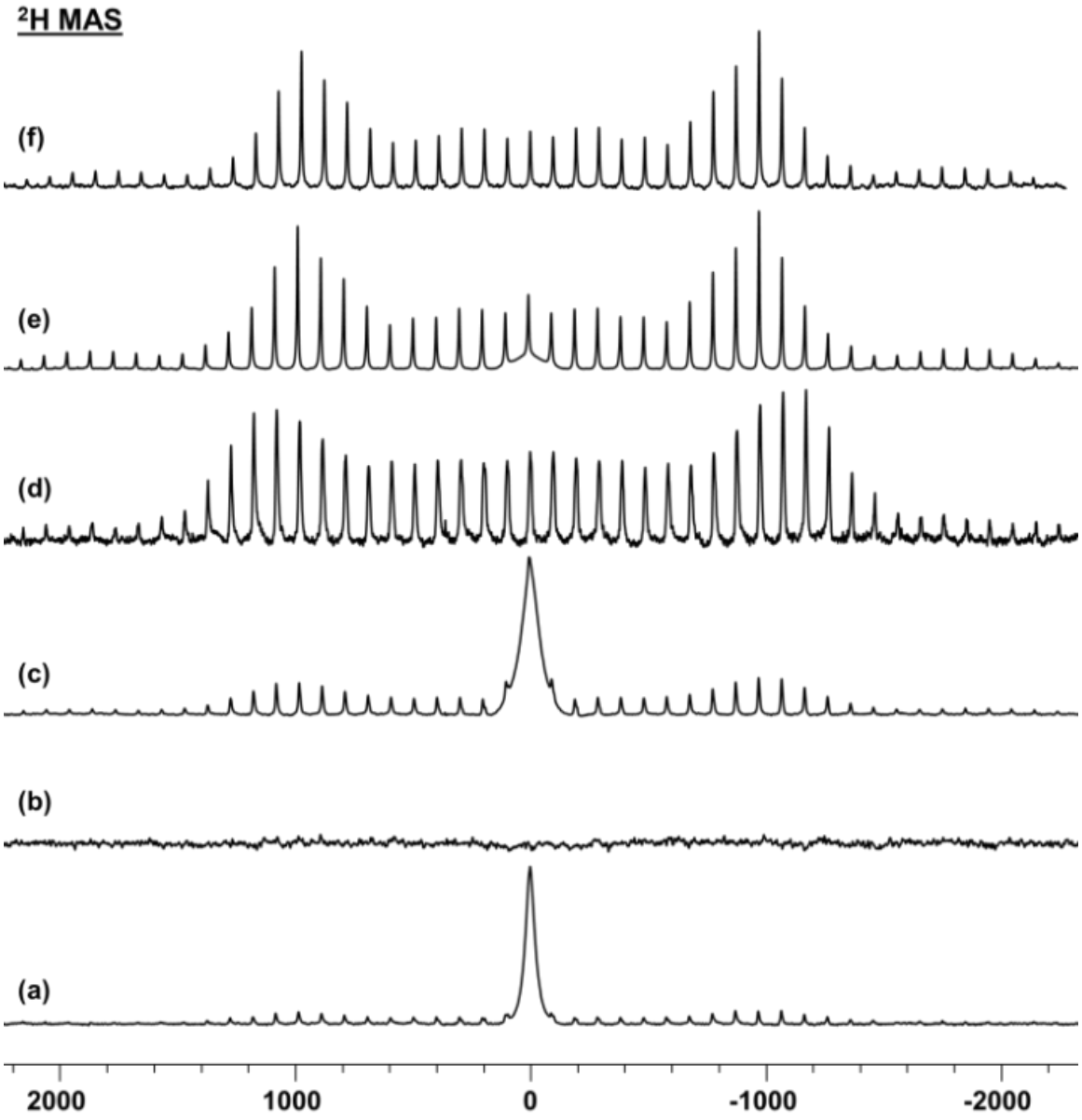

Figure 2.20. ^{2}H MAS spectra of rigorously dried PBI stirred as a powder in D_2O at RT for 48 h (a), and after redrying this sample at 110 °C *in vacuo* for 48 h (b). ^{2}H MAS spectra of dry PBI exposed to D_2O at 150 °C for 48 h (c), and after redrying at 110 °C for 48 h (d). ^{2}H MAS spectra of predried PBI exposed to D_2O at 315 °C for 72 h (e), and after redrying at 110 °C for 48 h (f). The Pake patterns are split into rotational sidebands (spinning frequency 6 kHz for all samples). The Q_{cc} values for (a) and (c-f) are given in Table 2.1.

After PBI is steam-treated with D_2O at 315 °C for 72 h, again two signals are visible in the ^2H MAS spectrum, as shown in Figure 2.20e. When this sample is dried, only the Pake pattern with a Q_{cc} value of 184 kHz remains (Figure 2.20 f). The differences as compared with the spectra (a) and (c) in Figure 2.20 are that the Pake patterns shows higher intensities and Q_{cc} assumes a value of 184 kHz for both spectra (e) and (f).

Regarding the Q_{cc} values obtained from the spectra in Figure 2.20 and compiled in Table 2.1, one should mention that the simulations as described in the experimental section[20] are quite accurate. An example that shows the quality of the fit as the grey simulated spectrum of the measured spectrum (Figure 2.20e) is displayed in Figure 2.21.

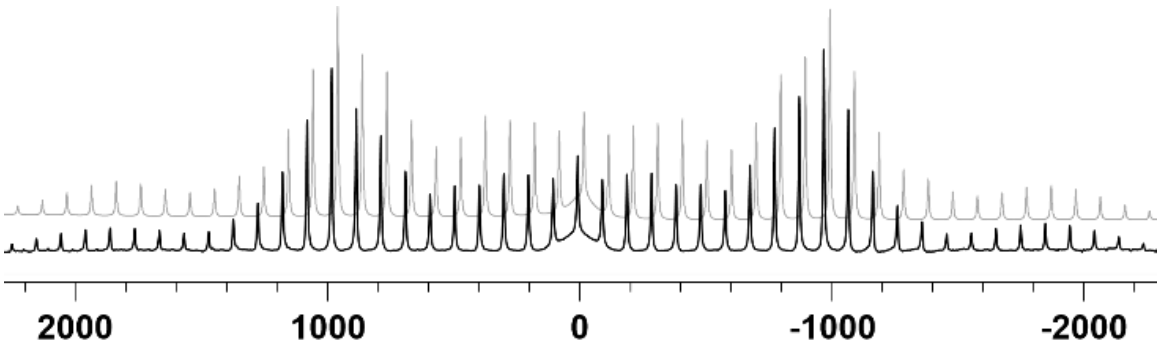

Figure 2.21. ^2H MAS NMR spectrum of PBI powder (spectrum (e) of Figure 2.18) and its simulation (grey) with a slight δ offset for better visibility.

The chemical shift for D_2O is the same whether it resides in liquid domains or is hydrogen-bonded, and $\delta(^2H)$ for N-D should be similar. Therefore, taking the large residual linewidth and the huge chemical shift range of ^2H in the solid state into account,

even the rotational sidebands of the MAS signals of these species overlap. This is why the rotational sidebands of the Pake patterns which stem from the different species are not split into several sets of lines but give only one set. Another consideration is that the hydrogen-bonded D_2O molecules undergo fast exchange with the D_2O molecules in contiguous liquid domains. This means that the Q_{cc} values are variable in the presence of liquid domains. In the absence of liquid D_2O (Figures 2.20 d and f) there is no longer any exchange, and only the signal for N-D groups with maximal Q_{cc} should be present.

The Q_{cc} values of PBI redried after steam-treatment at 150 and 315 °C, however, are 201 and 184 kHz, a difference which is visible to the bare eye when looking at the spectra in Figure 2.20. Therefore, one can assume that the steam-treatment at 315 °C does not only lead to an exchange of N-H protons, but also to a morphological change influencing the overall polymer chain mobility. This assumption is in accordance with the sample becoming more brittle after this treatment (Figure 2.16), and with earlier ^{13}C T_1 relaxation time measurements.

Table 2.1. Q_{cc} (quadrupolar coupling constant) values [kHz] of samples treated with D_2O as liquid and steam at 150 and 315 °C.

	RT	**150 °C**	**315 °C**
PBI*	194	195	184
Redried PBI*	---	201	184
PEEK-PBI#	---	197	184
PEKK-PBI#	---	195	183
PEKK-PBI#,a	---	198	184

*samples exposed as powders, #exposed as melt-blended samples. --- indicates that no Pake pattern has been observed. [a]Sample has been exposed to atmosphere for 1 month after being steam-treated at 315 °C. Error margins of the Q_{cc} values are +/- 0.5 kHz.

Analysis of PEEK-PBI after exposure to D_2O as liquid and steam: In the following it will be analyzed whether the PEEK component in a 50:50 wt% melt-blended PEEK-PBI polymer will change the behavior of the PBI towards water and steam. The ^{13}C CP/MAS NMR spectra of PEEK-PBI samples before and after exposure to D_2O under the indicated conditions are displayed in Figure 2.22. After stirring the blend at RT in D_2O (b) and steam-treatment at 150 °C (c) no major changes of the signals as compared to the dry sample (a) are visible. However, after steam-treatment with D_2O at 315 °C (d), the signals 2 and 10 are no longer present and the peak containing overlapping signals of 8 and 9 is diminished in intensity.

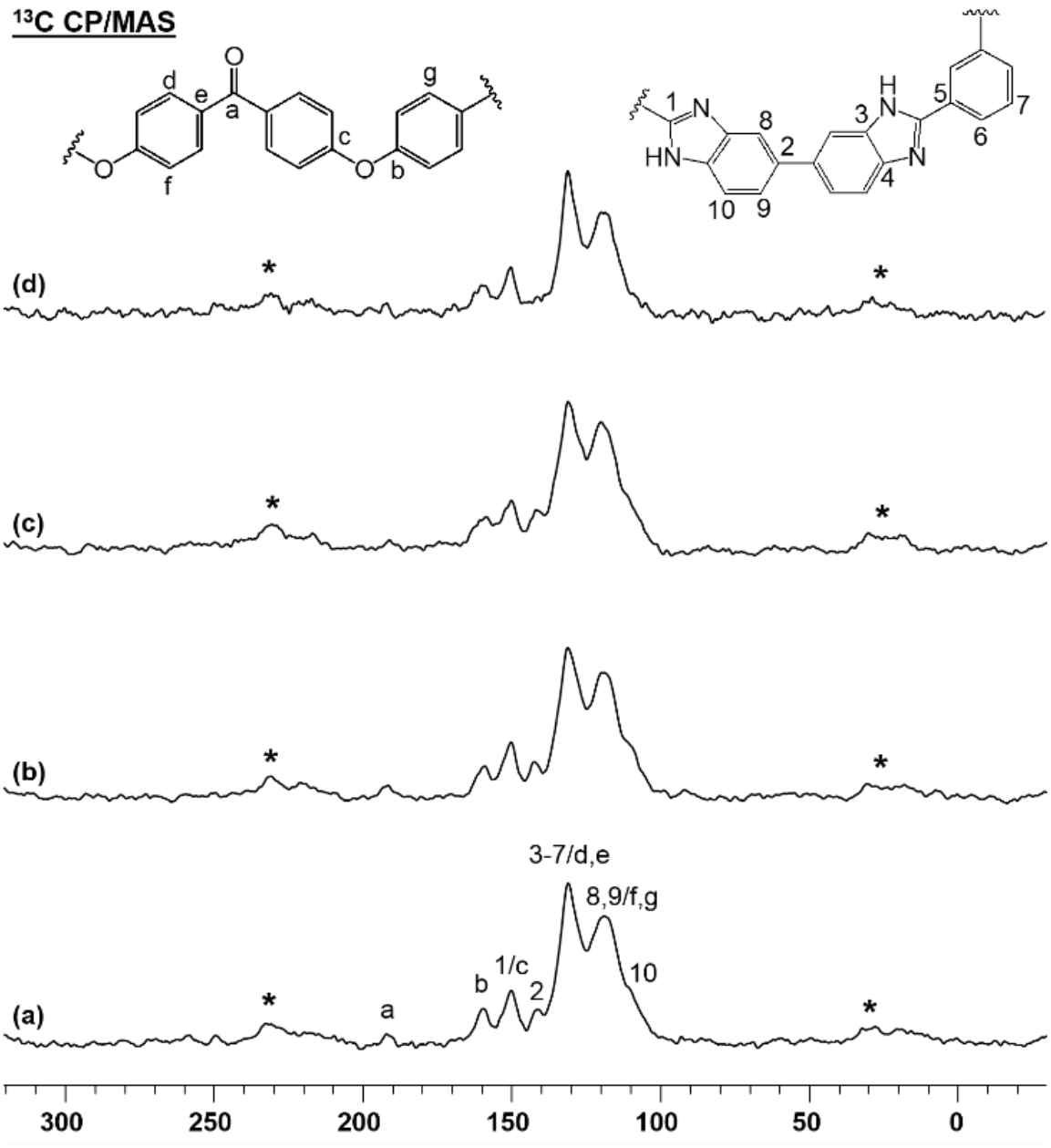

Figure 2.22. ^{13}C CP/MAS NMR spectra of melt-blended PEEK-PBI (50:50 wt%) after drying at 110 °C for 550 h (a), stirring in D_2O at RT (b), steam-treatment with D_2O at 150 °C (c), and immediately after steam-treatment with D_2O at 315 °C (d).

This result can again be attributed to the cross polarization phenomenon discussed above for pure PBI. Therefore, one can conclude that under these harsh conditions, D_2O penetrates the PBI component of the blend, exchanges N-H by N-D and adsorbed H_2O by D_2O, thus depleting the proton pool close to the benzimidazole unit for magnetization transfer at short contact times. As observed for the non-condensed phenyl ring in the PBI component, the aryl protons of PEEK are not exchanged. Furthermore, since the signal intensities of PEEK are not affected by steam-treatment with D_2O, one can conclude that the PEEK component does not contain adsorbed H_2O that contributes to the magnetization transfer.

The ^1H wideline NMR spectra of the melt-blended PEEK-PBI samples before and after treatment with liquid D_2O and D_2O steam are displayed in Figure 2.23. The proton signal with a small line width of about 6 kHz on top of the broad resonance with a half width of ca. 29 kHz in spectrum (a) reveals that even after 550 h of drying in vacuo, the melt-blended tensile specimen still contains adsorbed and mobile H_2O. This result is not surprising taking the drying curve of Figure 2.8 into account that does not reach a constant weight after 600 h. Immersing the specimen in liquid D_2O does not lead to a noticeable change of the spectrum (b). However, after steam-treatment at the higher temperatures of 150 and 315 °C (c, d), immobile N-H protons are exchanged and join mobile species. These lead to the narrower proton signals with halfwidths of 4.9 and 3.5 kHz, respectively.

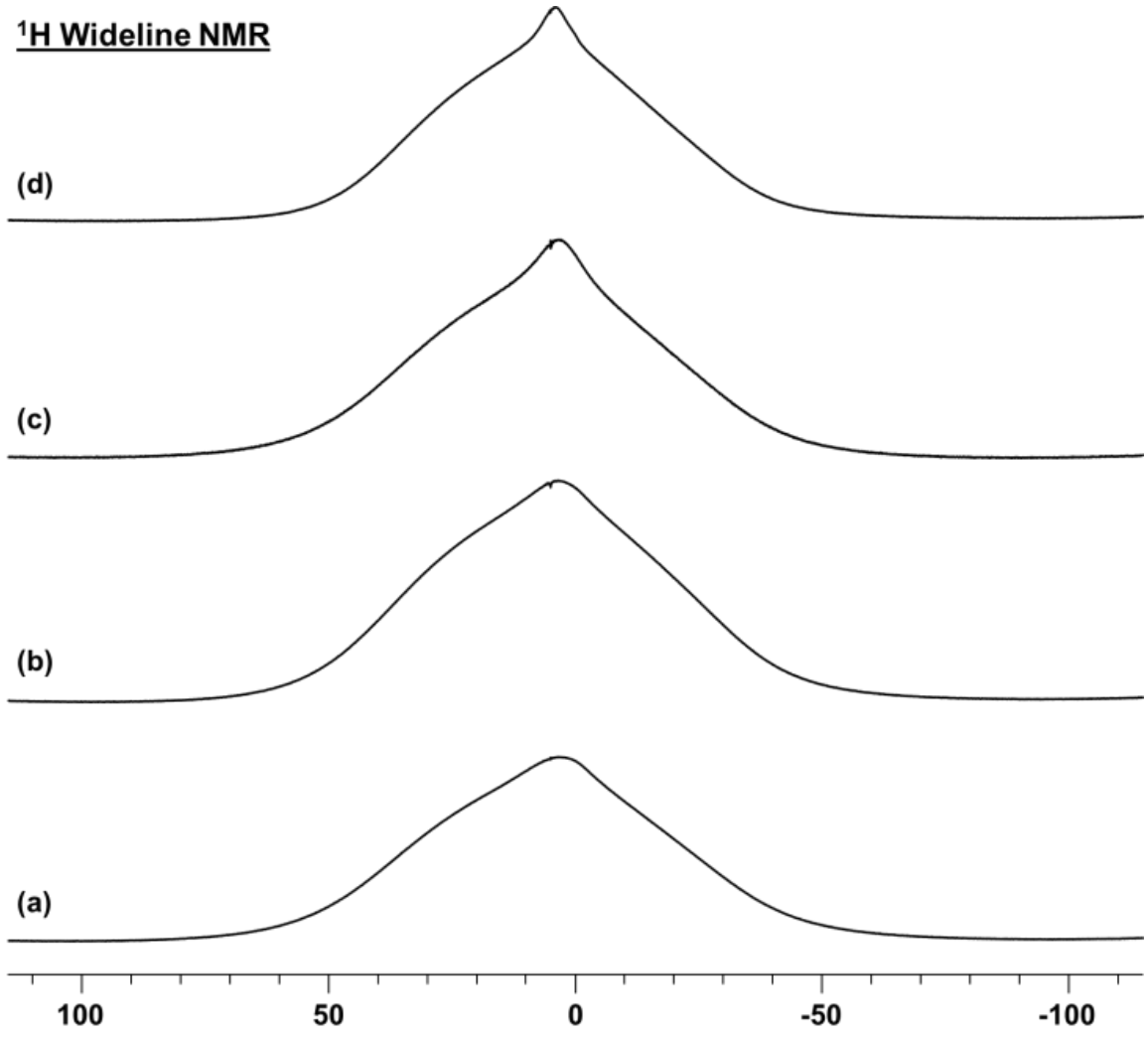

Figure 2.23. ^{1}H Wideline NMR spectra of melt-blended PEEK-PBI after drying at 110 °C for 550 h (a), stirring in liquid D_2O at RT (b), steam-treatment with D_2O at 150 °C (c), and immediately after steam-treatment with D_2O at 315 °C (d).

As the ^{2}H MAS NMR spectra displayed in Figure 2.24 show, it takes steam-treatment at elevated temperatures of 150 and 315 °C to bring substantial amounts of D_2O into the PEEK-PBI melt-blended samples. However, even after stirring the sample in liquid D_2O at RT, a Pake pattern with low intensity emerges. This demonstrates that even

under mild conditions D_2O migrates into the polymer, most probably along the PBI backbone. After 150 °C and 315 °C steam-treatment with D_2O, two signals are visible in each spectrum (b, c). A central signal attributable to mobile D_2O, adsorbed or in liquid domains in the polymer, and Pake patterns.

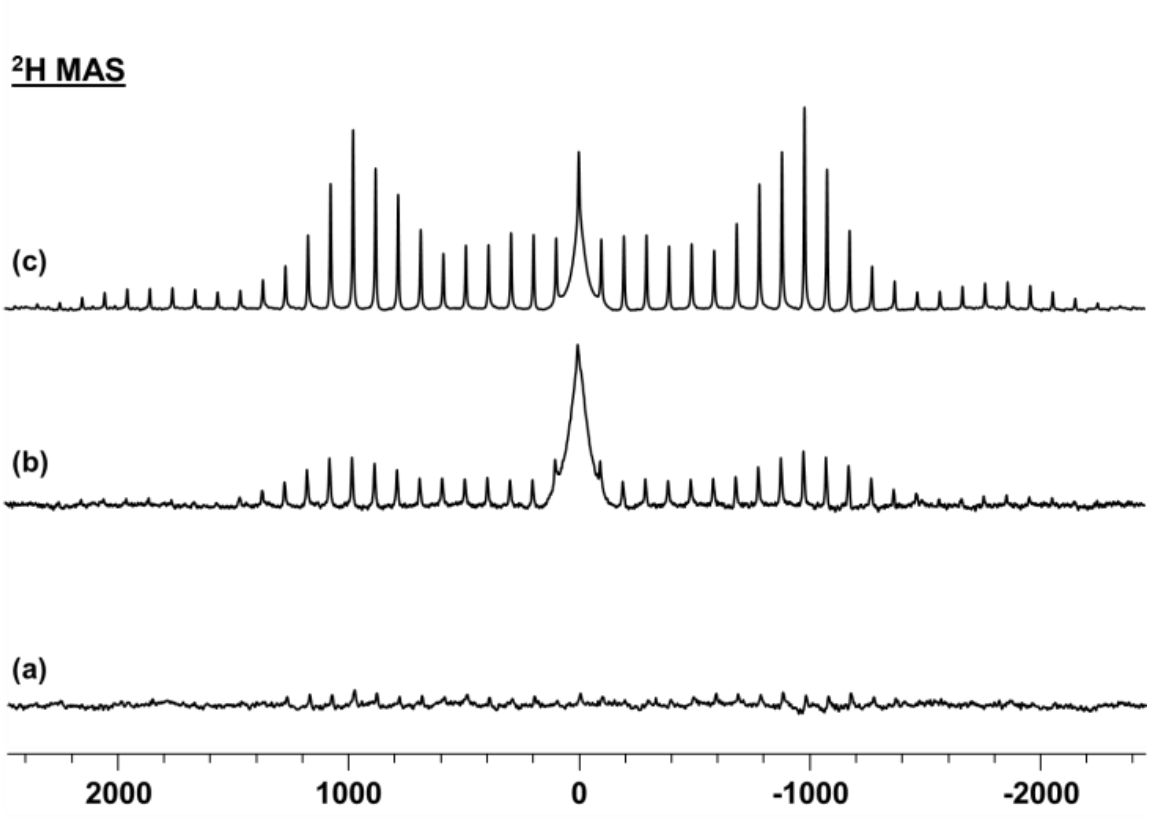

Figure 2.24. ^2H MAS NMR spectra of melt-blended PEEK-PBI after stirring in liquid D_2O at RT (a), steam-treatment with D_2O at 150 °C (b), and immediately after steam-treatment with D_2O at 315 °C (c). The Q_{cc} values of the Pake patterns are given in Table 2.1. The Pake patterns are split into rotational sidebands (spinning frequency 6 kHz for all spectra).

The Q_{cc} values of 197 and 184 kHz are matching those of PBI (195 and 184 kHz) after being subjected to the same D_2O-treatment conditions (Table 2.1). This indicates once more that the PBI component in the blend is dominating the interaction of the blend with water.

Analysis of PEKK-PBI after exposure to D_2O as liquid and steam: The ^{13}C CP/MAS NMR spectra of melt-blended PEKK-PBI samples (Figure 2.25) follow the same trends as observed for pure PBI and PEEK-PBI, when treated with D_2O at ambient and elevated temperatures. After treatment at RT (**b**) and 150 °C (**c**) there are no major changes in the signals as compared to the starting material (**a**). However, steam-treatment with D_2O at 315 °C again leads to a disadvantage for the benzimidazole signals of the PBI component at the short cross polarization time of 1.5 ms. This phenomenon has been observed and discussed for pure PBI and PEEK-PBI. It can be concluded that in the case of PEKK-PBI, too, D_2O is more readily incorporated into the PBI- as compared to the PEKK component.

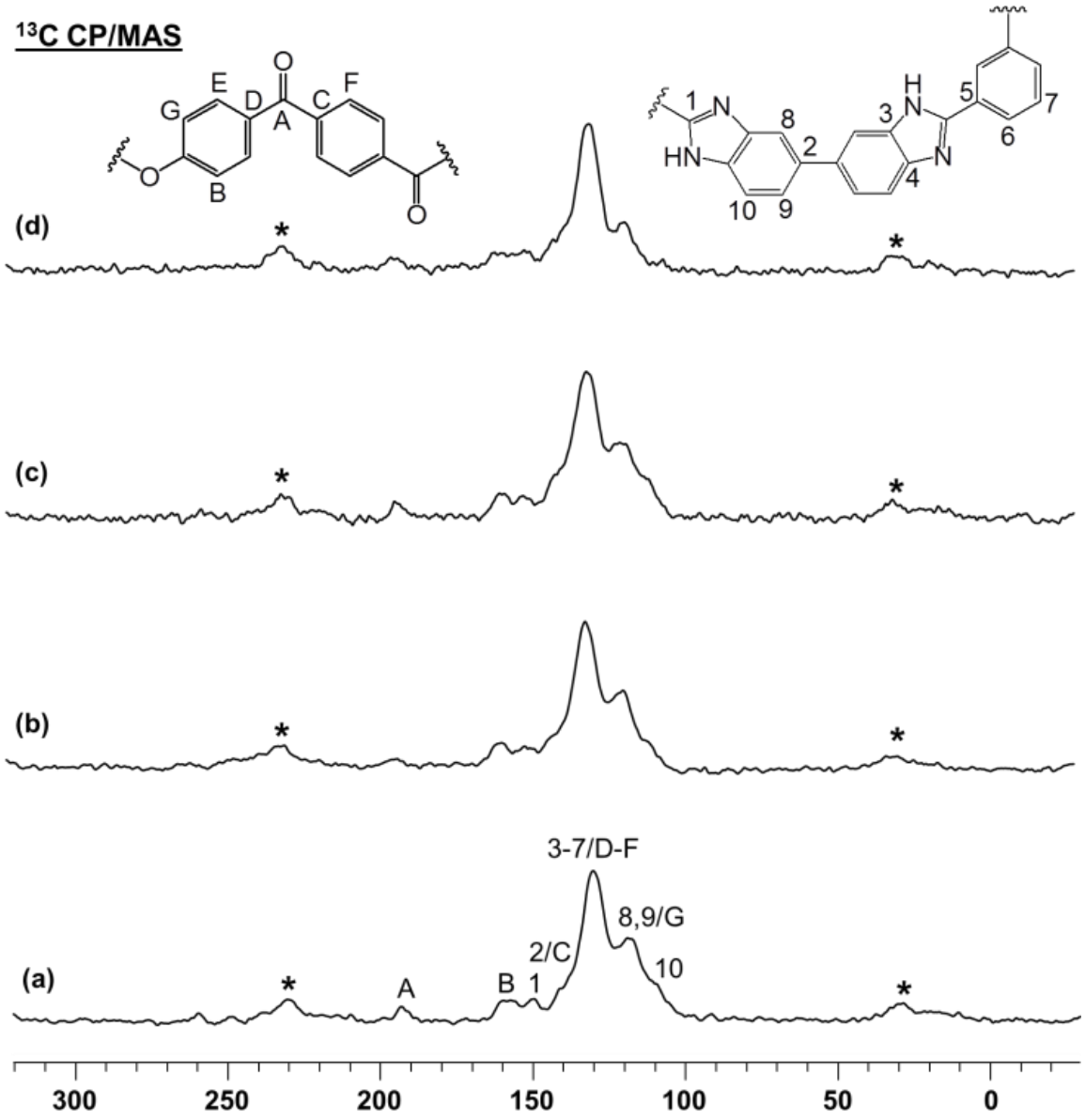

Figure 2.25. ^{13}C CP/MAS NMR spectra of melt-blended PEKK-PBI after drying at 110 °C for 550 h (a), stirring with liquid D_2O at RT (b), steam-treatment with D_2O at 150 °C (c), and immediately after steam-treatment with D_2O at 315 °C (d).

In contrast to the PEEK-PBI, in the case of PEKK-PBI steam-treatment at 150 °C is needed to bring substantial amounts of D_2O into the polymer, as the ^2H MAS spectra in Figure 2.26 show. Even at this elevated temperature most of the D_2O is included in the blend in the form of liquid domains, as the unstructured center signal with a half width of about 430 Hz implies. However, steam-treatment at 150 °C also leads to the formation of less mobile ^2H-containing species (**b**), whose Q_{cc} value of 195 kHz matches the one of PBI after exposure to D_2O under the same conditions (Table 2.1).

After steam-treatment at 315 °C, the polymer contains more of the less mobile ^2H species as indicated by the increase in intensity of the Pake pattern with a Q_{cc} value of 183 kHz. The same phenomena and similar Q_{cc} values of 184 kHz are observed after the treatment of PEEK-PBI and pure PBI with D_2O under identical conditions. Therefore, we conclude that in the case of PEKK-PBI, too, the PBI component is mainly responsible for the interactions with D_2O. As compared to PEEK-PBI, however, the PEKK component fends off D_2O slightly better, as indicated by the nearly complete lack of a Pake pattern in spectrum (**a**).

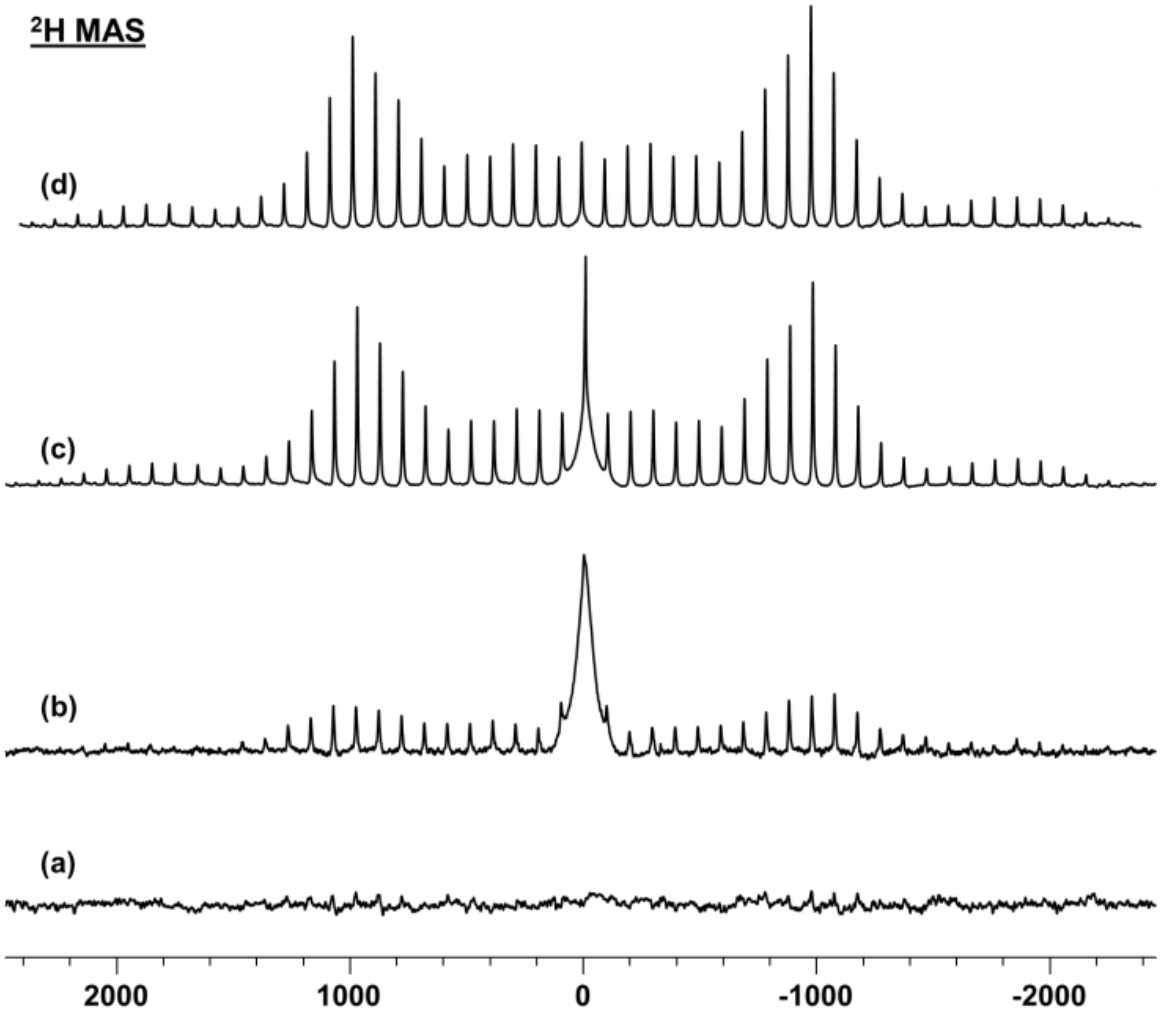

Figure 2.26. ^{2}H MAS NMR spectra of melt-blended PEKK-PBI after stirring in liquid D_2O at RT (a) and steam-treatment with D_2O at 150 °C (b), immediately after steam-treatment with D_2O at 315 °C (c), and one month of exposure to the atmosphere after the latter treatment (d). The Q_{cc} values are listed in Table 2.1. The Pake patterns are split into rotational sidebands (spinning frequency 6 kHz for all spectra).

Interestingly, when the PEKK-PBI that has been steam-treated with D_2O at 315 °C is exposed to the H_2O-containing ambient atmosphere for one month, the D_2O residing in liquid domains is nearly quantitatively exchanged by H_2O, a process that ultimately

removes the broad center ^{2}H signal in the MAS spectrum (Figure 2.26d). In contrast to this, the Pake pattern with a Q_{cc} of 184 kHz is fully retained. This means that the N-D groups do not undergo any D/H exchange with H_2O from the atmosphere.

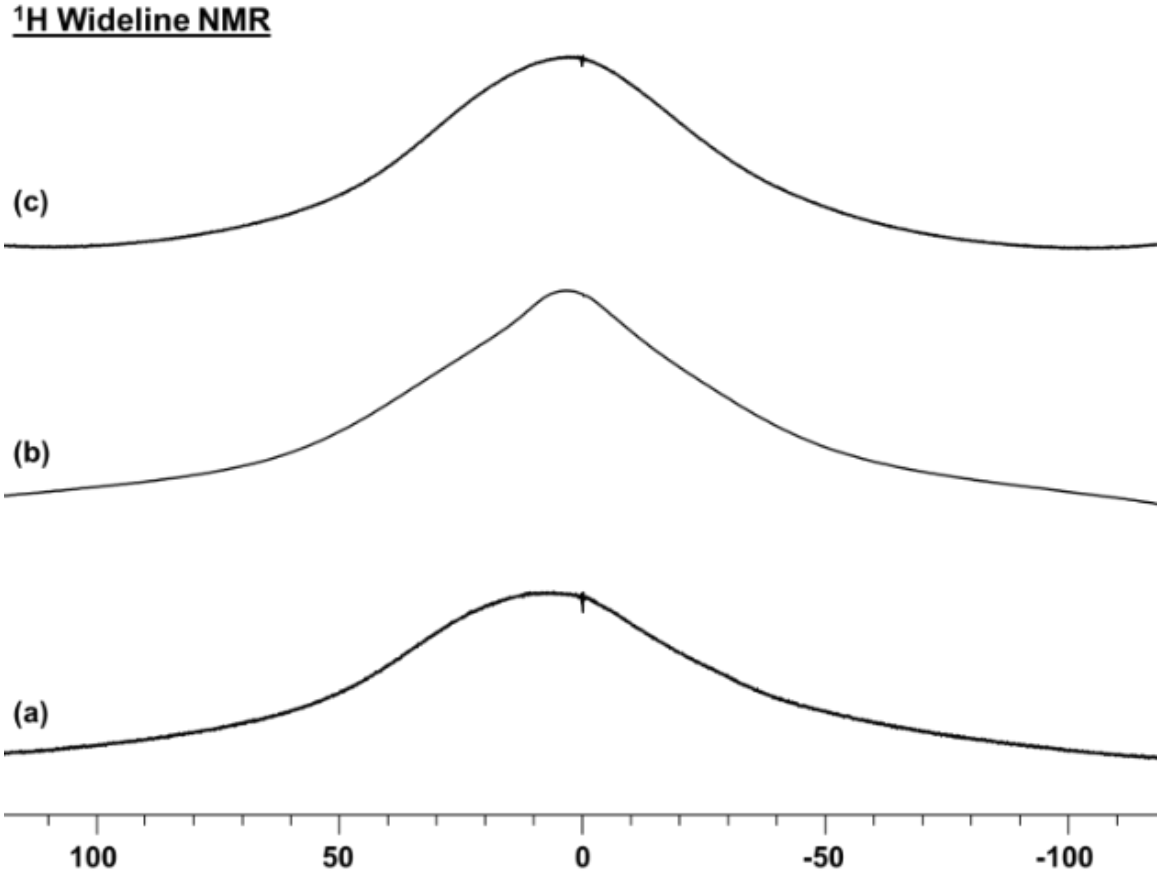

Figure 2.27. ^{1}H Wideline NMR spectra of the PEKK-PBI blend as received (a), after steam-treatment with H_2O at 150 °C in H_2O for 48 h (b), and after steam-treating this sample at 150 °C in D_2O for 48 h (c).

The ^{1}H wideline NMR spectra of the PEKK-PBI (Figures 2.27 and 2.28) provide complementary information and corroborate the conclusions drawn above. The PEKK-

PBI sample as received contains only traces of H_2O (Figure 2.27a), which is in accordance with earlier results.[2] Therefore, only the broad signal for the backbone protons with a line width of about 33 kHz is visible in the spectrum. After steam-treatment with H_2O at 150 °C a narrow peak with a half width of ca. 5 kHz appears on top of the hump, indicating the presence of mobile H_2O (Figure 2.27b). When this sample is steam-treated again with D_2O at 150 °C, the H_2O from the liquid domains and hydrogen-bonded water is quantitatively exchanged by D_2O, and therefore the narrower ^1H NMR signal is gone from the ^1H NMR spectrum in Figure 2.27c.

The ^1H wideline NMR spectrum obtained after steam-treatment of PEKK-PBI with H_2O at 315 °C shows a 30 kHz broad hump and a narrower signal with a half width of 2 kHz on top of it (Figure 2.28a), representing the backbone protons and the mobile H_2O in liquid domains. Steam-treating this sample with D_2O at 315 °C removes nearly all of the narrow ^1H signal, since now it is mainly D_2O residing in the liquid domains (Figure 2.28b). Finally, exposing the sample to the ambient atmosphere reinstates the narrow signal on top of the ^1H backbone hump, because the D_2O in the liquid domains has gradually been exchanged by atmospheric H_2O. A summary of the ^1H Wideline, ^2H MAS, and ^{13}C CP/MAS NMR signal halfwidths ($\Delta\nu_{1/2}$) for all samples is given in Table 2.2.

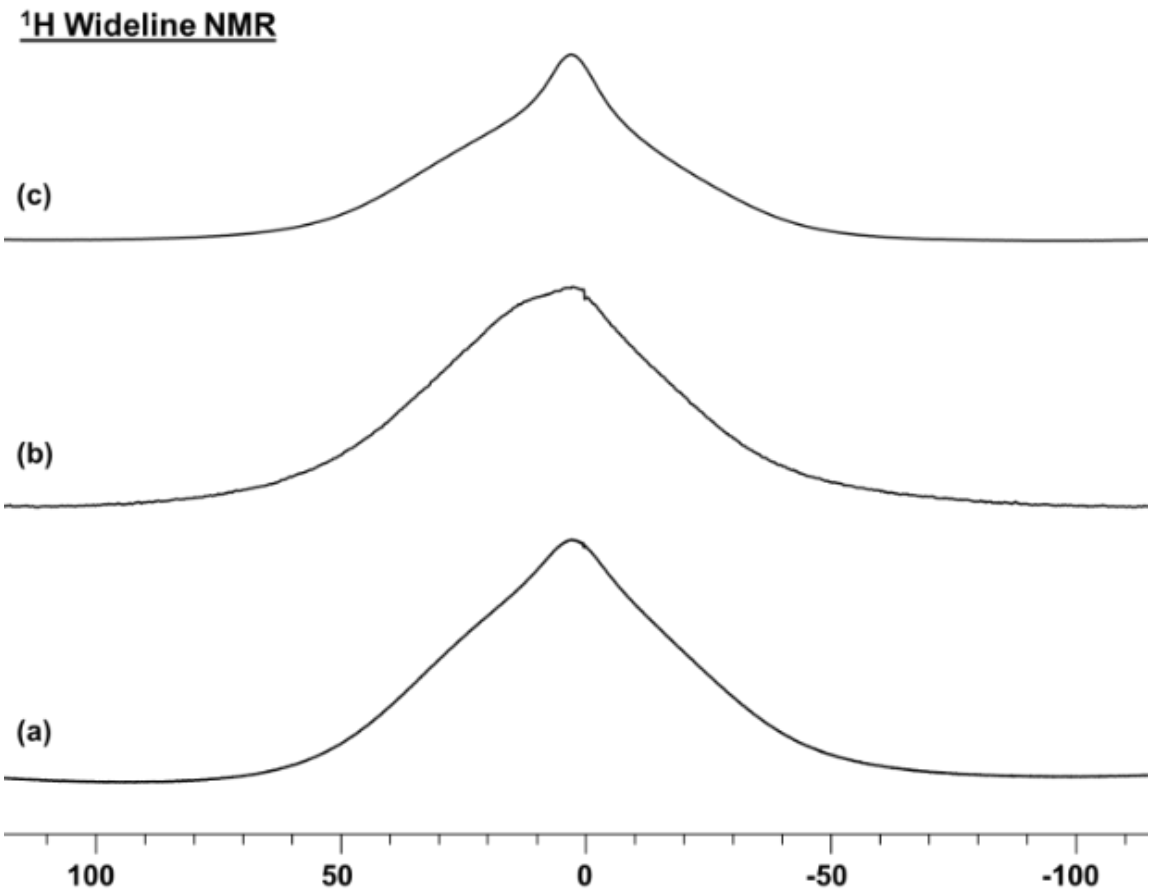

Figure 2.28. ^{1}H Wideline NMR spectra of PEKK-PBI after (a) steam-treatment at 315 °C with H_2O for 72 h (a), steam-treatment of this sample at 315 °C in D_2O for 72 h (b), and after exposure to the atmosphere for one month (c).

Table 2.2. Signal halfwidths $\Delta\nu_{1/2}$ [kHz] of the ^{1}H wideline, ^{2}H MAS, and ^{13}C CP/MAS NMR resonances of the originally rigorously dried samples stirred in liquid D_2O and steam-treated with D_2O at 150 and 315 °C.

	Well-Dried		**RT**		**150 °C**		**315 °C**	
^{1}H	*Broad Signal*	*Narrow Central Signal*	*Broad Signal*	*Narrow Central Signal*	*Broad Signal*	*Narrow Central Signal*	*Broad Signal*	*Narrow Central Signal*
PBI*	28.2	---	35.0	4.9	28.5	2.5	21.7	4.5
PEEK-PBI#	30.2	6.1	28.7	5.8	28.8	4.9	27.3	3.5
PEKK-PBI#	32.5	---	23.2	5.3	31.2	3.7	29.5	2.0
^{2}H	*Central Signal*	*Pake Pattern Signal*	*Central Signal*	*Pake Pattern Signal*	*Central Signal*	*Pake Pattern Signal*	*Central Signal*	*Pake Pattern Signal*
PBI*	---	---	2.8	0.6	5.1	0.6	4.7	0.3
PEEK-PBI#	---	---	---	0.6	4.7	0.5	3.2	0.3
PEKK-PBI#	---	---	---	0.7	4.3	0.5	3.4	0.2
^{13}C	*Signal 1*	*Signals 5-7*	*Signal 1*	*Signals 5-7*	*Signal 1*	*Signals 5-7*	*Signal 1*	*Signals 5-7*
PBI*	0.5	0.3	0.5	0.4	0.5	0.4	0.5	0.7
	Signal a	*Signals 3-7/d,e*	*Signal a*	*Signals 3-7/d,e*	*Signal a*	*Signals 3-7/d,e*	*Signal a*	*Signals 3-7/d,e*
PEEK-PBI#	0.4	0.4	0.3	0.4	0.3	0.6	0.4	0.5
	Signal A	*Signals 3-7/D,F*	*Signal A*	*Signals 3-7/D,F*	*Signal A*	*Signals 3-7/D,F*	*Signal A*	*Signals 3-7/D,F*
PEKK-PBI#	0.4	0.6	0.5	0.6	0.5	0.6	0.6	0.8

*exposed as powders, #exposed as melt-blended samples. --- indicates that no Pake pattern has been observed.

^{7}Li MAS for investigating salt uptake of the PEKK-PBI blend

During the polymerization process of PAEK polymers typically NaCl is formed, which is extracted subsequently with water. This can be counted as another indication that water can diffuse into the polymer and leave it again, carrying NaCl along. It also corroborates the results above which describe how H_2O can be replaced by D_2O in the polymer and *vice versa*. But there are two questions left, (a) whether salts other than NaCl can be extracted by water, and (b) whether salts can also move into the polymers, not only out of them. Therefore, the PEKK-PBI blend has been stirred with an aqueous LiCl solution at 106 °C for two days. In order to qualitatively probe the presence of LiCl, a ^{7}Li MAS spectrum has been recorded (Figure 2.29). Although ^{7}Li is quadrupolar with a nuclear spin of 3/2, it behaves nearly like a spin-1/2 nucleus and can easily be measured in various materials.[14] As the spectrum in Figure 2.29a shows, a substantial amount of ^{7}Li can be found in the polymer blend after its exposure to an aqueous LiCl solution. When this sample is then stirred with H_2O, the LiCl is only partially extracted, as ^{7}Li is found both in the aqueous phase (Figure 2.29c), as well as in the polymer (Figure 2.29b).

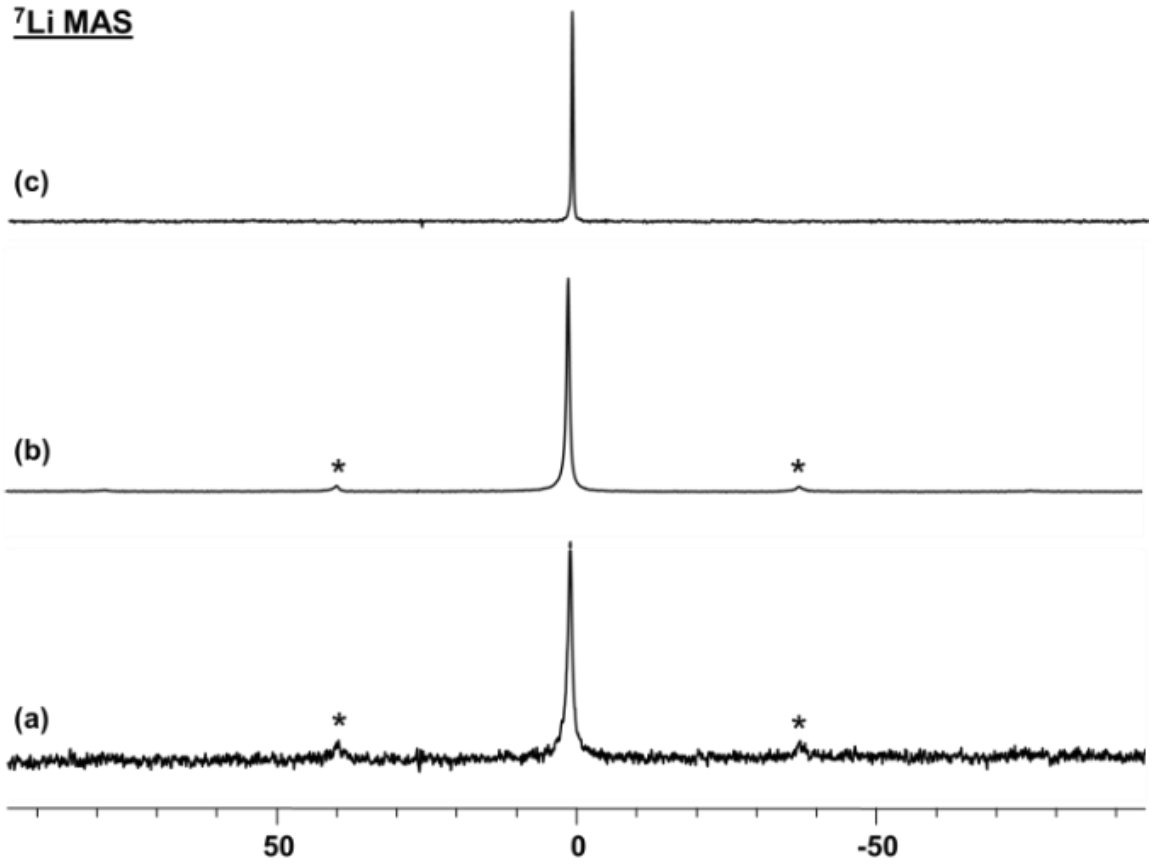

Figure 2.29. ^{7}Li MAS NMR spectra of (a) PEKK-PBI after stirring a melt-blended tensile specimens in a 150 mL solution of 15 g of LiCl (10 wt%) in H_2O at 106 °C for 24 h (6 kHz), (b) PEKK-PBI sample described under (a) after stirring it in H_2O at 100 °C for 48 h (6 kHz), and (c) aqueous phase after stirring the PEKK-PBI sample (b) with H_2O. Asterisks denote rotational sidebands. The halfwidths of the signals are 134.3 Hz (a), 73.2 Hz (b), and 36.6 Hz (c).

In order to test whether the salt uptake is only possible for LiCl or also in the case of other salts, PBI, PEEK-PBI, and PEKK-PBI have been exposed to 5 wt% aqueous $ZnBr_2$ solution. ^{79}Br is quadrupolar with a nuclear spin of 5/2, which means that in the solid state NMR spectrum of a Br nucleus, given that it resides in an electronically

symmetric environment, a center transition and a Pake pattern of lower intensity are visible. As a Br^- anion naturally has a symmetric surroundings, spectra are in principle obtainable. The ^{79}Br MAS NMR spectra in Figure 2.30 show that pure PBI admits the salt readily. Interestingly, no signal can be found after PEEK-PBI is treated with the $ZnBr_2$ solution, and only traces in the case of PEKK-PBI. Therefore, one can conclude that the PEEK and PEKK components make the PBI more resistant towards uptake of $ZnBr_2$.

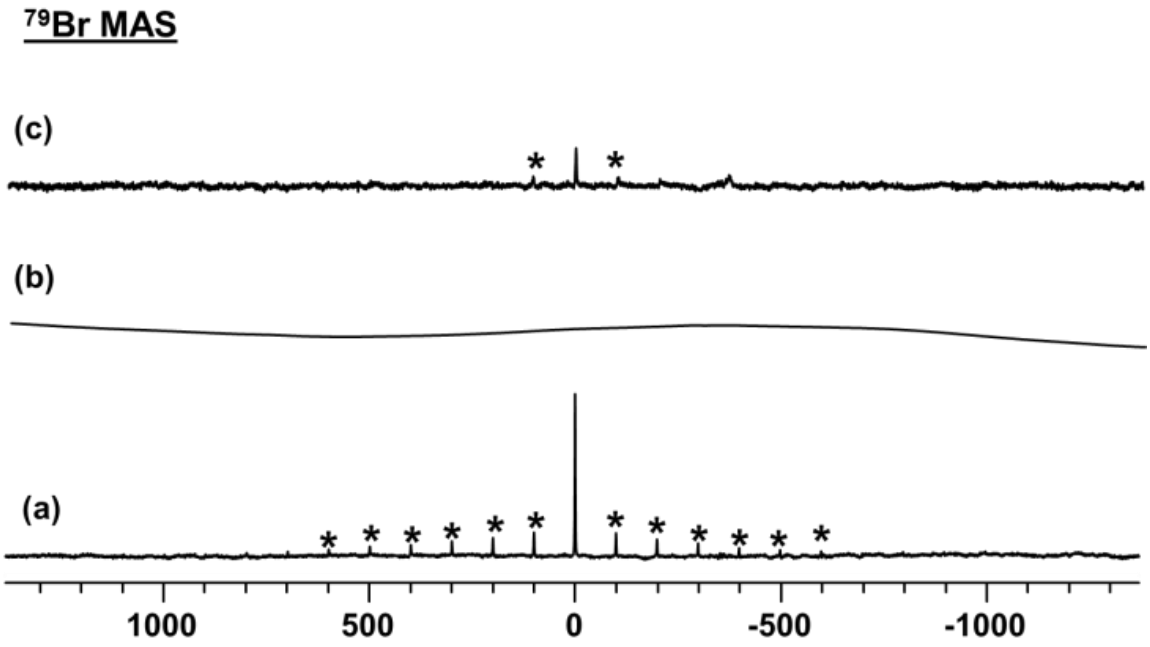

Figure 2.30. ^{79}Br MAS NMR spectra (10 kHz) of melt-molded samples of PBI (a), PEEK-PBI (b), and PEKK-PBI (c) after stirring in 5 wt% aqueous $ZnBr_2$ solution at 102 °C for 48 h.

In future work a quantitative measure of the tenacity of the salts in the polymer networks, as well as their impact on the morphologies and reactivities of the polymers will be pursued.

CONCLUSION

In this chapter we have successfully demonstrated that PEEK and PEKK blends with PBI (50:50 wt%) can be characterized by ^{13}C CP/MAS and all signals can be assigned due to the favorable signal resolution. While physical mixtures of the components cannot be distinguished from their melt-blended versions based on their ^{13}C CP/MAS spectra, more pronounced, albeit not conclusive, differences are visible in the ^{15}N CP/MAS and IR spectra. Furthermore, it is described that the moisture uptake of PEEK-PBI and PEKK-PBI samples is much faster than the reverse process, especially at elevated temperatures. PEEK-PBI incorporates overall more water than PEKK-PBI. With the use of ^{2}H MAS and ^{1}H wideline NMR spectroscopy for samples steam-treated with D_2O and H_2O, three different ^{2}H sites can be distinguished in PBI and in the PEEK- and PEKK-PBI blends.

Mobile D_2O can reside in liquid domains in the polymer network. Less mobile D_2O is attached to N-H (or N-D) groups via hydrogen bonds, and they are exchanging with mobile D_2O molecules in contiguous liquid D_2O domains. Finally, immobile ^{2}H nuclei, covalently bound in N-D groups are found after steam-treatment at higher temperatures. Furthermore, it has been demonstrated with ^{7}Li MAS that LiCl is incorporated into PEKK-PBI by treating the blend with an aqueous LiCl solution at elevated temperatures. This LiCl can partially be extracted again with H_2O at elevated

temperatures. Finally, it has been shown by ^{79}Br MAS NMR that $ZnBr_2$ is readily incorporated into pure PBI out of an aqueous solution, while only traces move into the PEEK-PBI and PEKK-PBI blends.

EXPERIMENTAL

General information and procedures

All polymer samples were provided by the company Hoerbiger Corporation of America, Inc. The PEEK-PBI and PEKK-PBI are based on 50:50 wt% mixtures of the pure components. PBI, PEEK-PBI, and PEKK-PBI powders were dried thoroughly at 110 °C for 144 h under vacuum (0.01 torr). PEEK-PBI and PEKK-PBI melt-blended samples were rigorously dried at 110 °C for 550 h under vacuum (0.01 torr). As described in the corresponding sections, the blends were either used as melt-blended tensile specimens or filed into powders with average particle diameters of about 0.5 mm before being treated or measured by solid-state NMR.

Unless mentioned otherwise in the text, the melt-molded polymer samples were all ASTM D638 Type V tensile specimens, machined from solid compression-molded plaques. The pure components and blends were either stirred in D_2O at RT for 48 h, or steam-treated in Parr pressure reactors (Model 4913) at 150 °C for 48 h and at 315 °C for 72 h. The maximal pressures in the closed vessels amounted to 5 bar (72 psi) and 110 bar (1600 psi), respectively. The redrying procedure consisted of removing the D_2O at 110 °C under vacuum for 48 h.

Instruments and measurements

The solid-state NMR spectra were measured on a *Bruker* AVANCE 400 spectrometer operating at 100.6 MHz for ^{13}C, 40.5 MHz for ^{15}N, 61.4 MHz for ^{2}H, 400.1 MHz for ^{1}H, 155.5 MHz for ^{7}Li NMR, and 100.3 MHz for ^{79}Br. For the processing of the spectra line-broadening factors of 10 Hz (^{1}H, ^{7}Li), 20 Hz (^{79}Br), and 150 Hz (^{2}H, ^{13}C, and ^{15}N) have been applied. All experiments were carried out using densely packed powders of the polymers in 4 mm ZrO_2 rotors. In case no signal was observed in a spectrum, block averaging measurements were performed to prove that the absence of any resonance was not merely due to a spectrometer malfunction.

The ^{13}C CP/MAS (Cross Polarization with Magic Angle Spinning) spectra were recorded at MAS rates of 10 kHz. The ^{1}H $\pi/2$ pulse was 2.5 μs and TPPM (Two Pulse Phase Modulation) decoupling was used during the acquisition. The Hartmann-Hahn matching condition was optimized using the polymer Victrex 450P at a rotational speed of 10 kHz. Adamantane served as the external ^{13}C chemical shift standard (δ = 37.95 and 28.76 ppm). All spectra were measured with a contact time of 1.5 ms and a relaxation delay of 3.0 s, unless stated otherwise, and typically 1024 FIDs were accumulated.

The ^{15}N CP/MAS experiments were carried out at MAS rates of 6 and 10 kHz. The Hartmann-Hahn matching condition was optimized using glycine at a rotational speed of 6 kHz. Glycine also served as the external ^{15}N chemical shift standard (δ = 7.70 ppm). All spectra were measured with a contact time of 2 ms and a relaxation delay of 5 s, and typically 32800 FIDs were accumulated.

The ^{2}H solid-echo measurements were performed at MAS rates of 6 kHz. D_2O served as the ^{2}H chemical shift standard (δ = 4.79 ppm). All spectra were measured with a relaxation delay of 2 s and a quadrupolar echo τ delay of 6 μs. The τ delay was optimized using deuterated PMMA (polymethyl methacrylate) at a rotational speed of 6 kHz. Typically 32800 FIDs were accumulated for the PBI and PAEK polymers and their blends.

The ^{1}H wideline NMR spectra were recorded using the MAS probehead without sample spinning. H_2O was used as the external chemical shift standard (δ = 4.79 ppm). No background ^{1}H NMR signal of the probehead, loaded with an empty rotor, was obtained when a spectrum was recorded with the measurement parameters used for the polymer samples. A $\pi/2$ pulse of 2.7 μs, a deadtime of 5.6 μs, and a pulse delay of 3 s were used and typically 32 FIDs were accumulated.

Deconvolution (^{1}H wideline spectra) and processing of the spectra was accomplished using ACD/NMR Processor Academic Edition.[19] The quadrupolar coupling constants were derived from the ^{2}H MAS NMR spectra using the NMR simulation program Dmfit.[22]

The ^{7}Li MAS experiments were performed at a MAS rate of 10 kHz. Polycrystalline LiCl served as the external ^{7}Li chemical shift standard (δ = 0.00 ppm). All spectra were measured with a deadtime of 5 μs and a relaxation delay of 6 s, and typically 10500 FIDs were accumulated. There was no ^{7}Li background NMR signal from the probehead or rotor, when an empty rotor was measured under these conditions.

The ^{79}Br MAS experiments were carried out at a MAS rate of 10 kHz. Polycrystalline KBr served as the external ^{79}Br chemical shift standard (δ = 0.00 ppm).

All spectra were measured with a deadtime of 5 μs and a relaxation delay of 5 ms, and typically 300000 FIDs were accumulated. There was no ^{79}Br background NMR signal from the probehead or rotor, when an empty rotor was measured under these conditions.

The IR spectra were recorded on a Shimadzu IRAffinity-1 FTIR spectrometer by placing the powdered polymers on top of a Pike Technologies MIRacle ATR diamond plate. Typically 100 scans were accumulated for optimal spectrum quality.

The TGA curves were recorded on the TA Instruments Q500 TGA by placing approximately 10 mg of the melt-molded sample into an Al_2O_3 pan. The thermal decomposition studies were performed over a temperature range of 30-700 °C under air at a heating rate of 20 °C/min. Nitrogen was used as the balance gas at a rate of 40 mL/min and air was used as the sample gas at a rate of 40 mL/min.

CHAPTER III

HIGH-TEMPERATURE STEAM-TREATMENT OF MELT-MOLDED PBI, PEEK, AND PEKK WITH H_2O AND D_2O: A SOLID-STATE NMR STUDY*

INTRODUCTION

Polyaryletherketones (PAEK) represent an important group within the family of thermoplastic polymers.[1] PAEK polymers include PEEK (polyetheretherketone) and PEKK (polyetherketoneketone) polymers (Scheme 3.1), and these are of growing interest in a wide range of applications. In particular, when maximal mechanical strength, corrosion resistance and retention of dimensional and physical properties at high temperatures and pressures are demanded. One important example for such an application would be low-weight downhole materials in oil and gas drilling and fracturing processes. While different commercially available PAEK grades are already indispensable for end users, the demand for even higher temperature applications increases steadily, and therewith the endeavor to also improve their tribological performance.

One approach for meeting these demands is to manufacture blends of PAEK polymers with PBI (polybenzimidazole) resins (Scheme 3.1). The resulting PAEK-PBI blends benefit from the increased service temperatures and some improvement in the wear properties that come with the PBI component. For example, PEKK-PBI blends are manufactured primarily to elevate the service temperature of the PEKK polymer, and to

* Reproduced in part with permission from Pope, J.; Sue, H.-J.; Bremner, T.; Blümel, J. *Polymer* **2014**, doi: 10.1016/j.polymer.2014.07.027. © 2014 Elsevier.

improve its wear performance. However, the PBI blends display comparatively poor chemical stability associated with this component. Furthermore, in contrast to the pure PAEK components, the PBI blends exhibit more complex interactions with aqueous systems, such as water and steam,[2] as well as salt solutions.[23]

Therefore, a deeper understanding and quantification of these interactions of water with the functional groups of the PBI component at the molecular level are indispensable. Furthermore, the hypothesis that the pure PEEK and PEKK polymers display only little affinity to water needs to be tested. In the study presented, the traditional celazole-type PBI (poly[2,2'-(*m*-phenylene)-5,5'-bibenzimidazole]), as well as PEEK and PEKK in the form of dog bones are exposed to H_2O and D_2O at ambient temperature. In order to simulate real-life conditions, as they might be applied in oil and gas drilling and fracturing processes, the polymers have also been steam-treated with H_2O and D_2O at 150 °C (ca. 300 °F) and 315 °C (ca. 600 °F) for 48 and 72 h.

The impact of water or steam on PBI, PEEK, and PEKK polymers has not been extensively reported by other research groups, but has received some attention.[3,24] Using a molecular model compound mimicking PBI, one report discusses two ways in which water could reside in PBI.[3] It can form larger aqueous domains nestled between the PBI polymer strands, or it can be bound to the N-H group of the benzimidazole unit by hydrogen bridges. Furthermore, a single crystal X-ray structure has been obtained, which shows the location of water molecules around a benzimidazole moiety incorporated in a cobalt complex.[25]

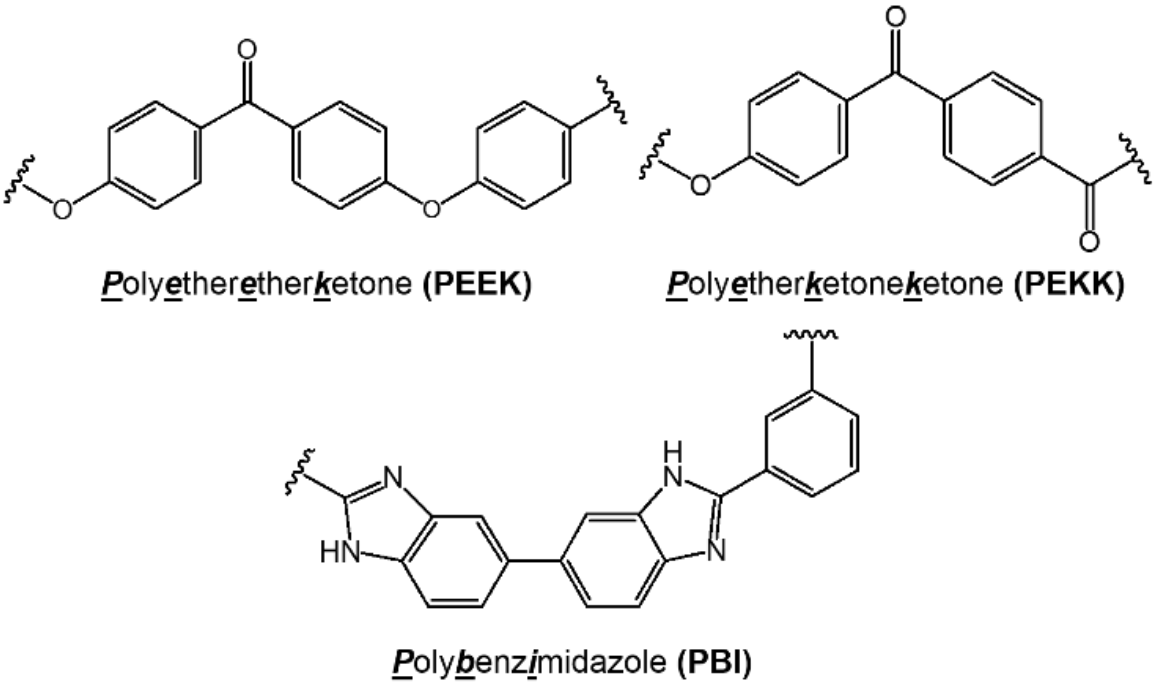

Scheme 3.1. Structures of Polyetheretherketone (PEEK), Polyetherketoneketone (PEKK), and Polybenzimidazole (PBI).

In order to analyze the PBI, PEEK, and PEKK samples before and after exposure to D_2O under various conditions, several methods are applied. In order to assess the overall water content of the samples in a straightforward and quantitative manner, TGA analyses are performed. IR spectroscopy is employed as another powerful tool,[4,5,26,27] especially when investigating potential hydrogen-bonding of water to the C=O group of PEEK or PEKK, which would lead to a decreased value of the stretching frequency for the carbonyl group.[4] Another valuable piece of information can be obtained from the different stretching and vibrational modes of H_2O and D_2O. For example, the stretching band of O-

D appears at about 2500 cm^{-1},[26] a spectral region that is very favorable because it is not populated by any other peaks from the polymers. In this way the O-D stretching band is also easy to distinguish from the O-H stretching peak at around 3400 cm^{-1}.[4,26]

Solid-state NMR spectroscopy is a powerful analytical tool that allows a multitude of diverse measurements of crystalline and amorphous compounds and materials.[2,6-9,12-16,18,20-22] Polymers represent the most prominent and the classic materials for solid-state NMR investigations.[15, 18] The cross polarization (CP) of magnetization from the abundant protons in polymers to the measured nuclei facilitates measurements of materials such as PBI or PAEK polymers, as it improves the signal to noise (S/N) ratio in the spectra.[2,18-6]

The most common nucleus for measuring polymers is ^{13}C,[18,12,15] followed by ^{2}H wideline (no spinning) and MAS (Magic Angle Spinning) NMR.[10,13,21] In this chapter it will be demonstrated that ^{1}H wideline NMR spectroscopy[2,9-10] can give valuable complementary information about the polymer systems on the molecular level as well. ^{1}H wideline NMR spectroscopy allows to distinguish protons of the immobile polymer backbone from mobile H_2O in aqueous domains. Mobile species lead to a relatively narrow signal sitting on the broad hump of the backbone signal in the ^{1}H wideline NMR spectra.[2,10] The method is limited when a distinction between different immobile nuclei, such as C-H and N-H protons in PBI is sought.[2]

For cases where a differentiated picture about the various sorts of protons and water and their mobilities are needed ^{2}H MAS can be applied.[10,13,21] This eliminates any signals from the polymer backbone. ^{2}H is a quadrupolar nucleus with a nuclear spin of 1, and therefore the Pake patterns[18,10,13,21] of ^{2}H wideline signals in the solid state display a

splitting of the two lines with maximal intensity that allows the calculation of the quadrupolar coupling constant Q_{cc}. Sample spinning splits the Pake pattern into sets of rotational sidebands. Q_{cc} can be calculated from spectra of rotated samples as described in the experimental section and in the literature.[19,20] The mobilities of the species or functional groups containing the measured ^2H nucleus can be determined via Q_{cc}.[10,13,21]

The correlation between reorientation times and the shapes of the corresponding Pake patterns has been described in detail for long deuterated alkyl chains.[21] ^2H MAS spectroscopy has previously been applied by us to quantify the mobilities of metallocenes adsorbed on silica surfaces.[10] But there are also examples for applications in the field of polymers in the literature, and recently ^2H solid-state NMR has been applied to gain quantitative insight into different dynamic scenarios.[13] For example, the segmental mobilities of polymer chains[13h] and the plasticization of poly(vinyl acetate) adsorbed on silica have been investigated using ^2H solid-state NMR.[13f]

RESULTS AND DISCUSSION

Steam-treatment of PBI, PEEK, and PEKK with H_2O and D_2O

For testing the moisture uptake of the corresponding tensile specimens under mild conditions at ambient temperatures, they have been stirred in liquid H_2O and D_2O for 48 h. Additionally, in order to mimic more realistic conditions of their exposure to fluids, the PBI, PEEK, and PEKK samples have also been steam-treated with H_2O and D_2O. For this purpose, the samples are placed into stainless steel pressure vessels with the glass sample holders described elsewhere.[23] Then the pressure vessels are filled with 150 mL of liquid

H_2O or D_2O to the height of about 1.5 cm, then sealed and heated. The pressures in the closed vessels reach 5 bar (72 psi) at 150 °C and 110 bar (1600 psi) at 315 °C. The exposure of the samples to water at RT and 150 °C has been maintained for 48 h, and at 315 °C for 72 h.

As described qualitatively in previous work,[2,3,23] PBI is hydrophilic and able to readily incorporate large amounts of water from the atmosphere. The affinity of the benzimidazole moiety to water becomes also obvious, for example, when contemplating the single crystal X-ray structure of a representative molecular species.[25] The water uptake of PBI is reversible when it takes place under mild conditions, and upon drying powdered samples, the material gives the original ^{13}C T_1 relaxation time data[2] again and assumes its previous weight.[23] Hereby, the drying process is faster for powdered samples than for the molded tensile specimens due to the larger specific surface area.[23] By weighing the PBI samples as received before drying them at 110 °*C in vacuo* (0.1 torr) at 110 °C it has been determined that up to 9 wt% of the material consists of water. [23]

For a more refined analysis, melt-molded PBI is subjected to steam-treatment with H_2O under controlled conditions and subsequently analyzed by TGA. Figure 3.1 shows the TGA curves recorded immediately after stirring PBA in water at RT, and after steam-treatment at 150 and 315 °C. Immersing the tensile specimens to liquid water for 48 h leads to a moisture content of 5%. Steam-treatment with water at 150 °C increases the H_2O content significantly and 11% of the weight of the sample is lost (Figure 3.1) during the TGA analysis. The highest temperature leads to a medium moisture content of 9%.

This result is in accordance with earlier analyses performed with different NMR spectroscopic methods.[2,23]

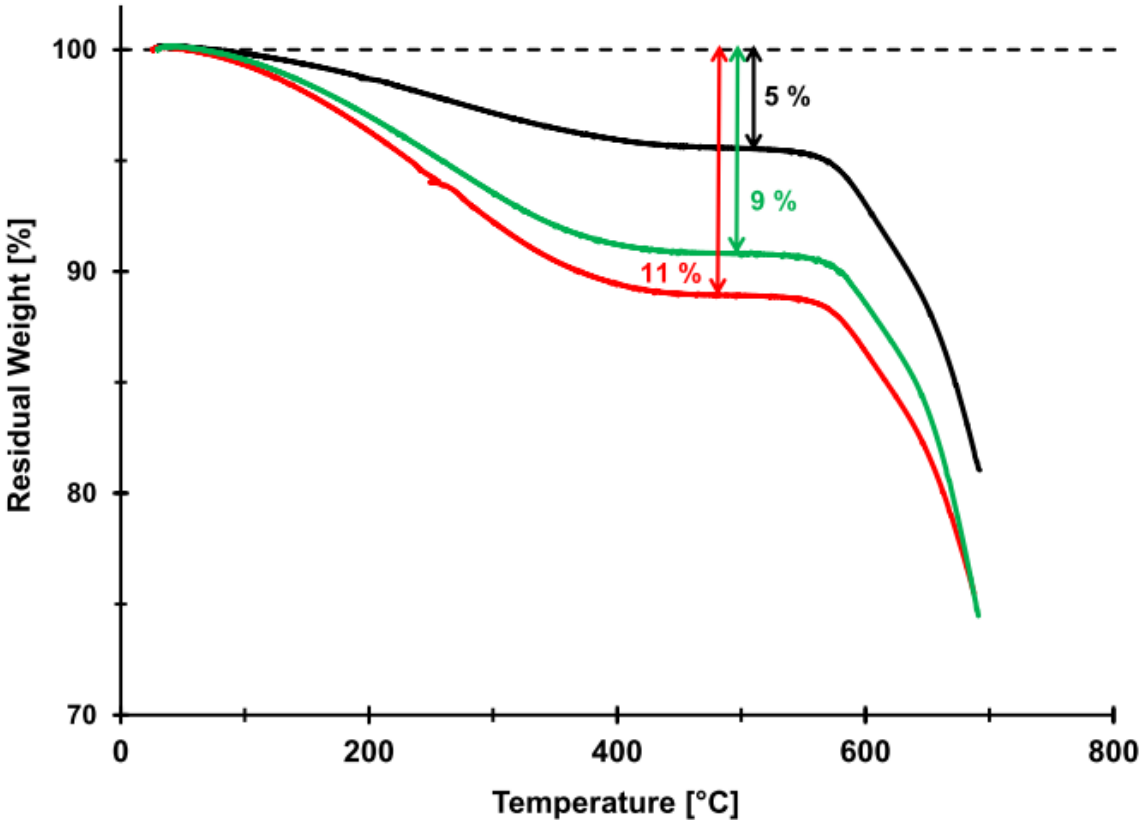

Figure 3.1. TGA of melt-molded PBI after stirring in H_2O at RT and steam-treatment with H_2O at 150 °C and 315 °C.

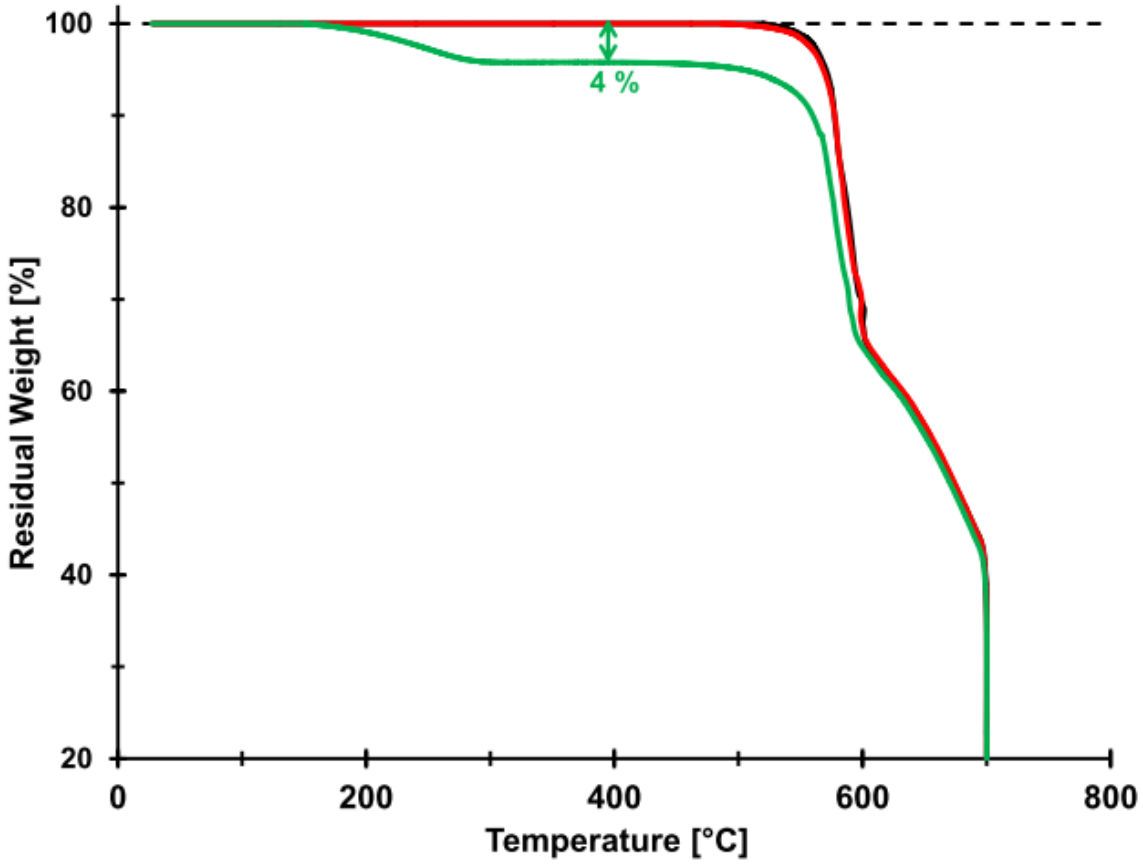

Figure 3.2. TGA of melt-molded PEEK after stirring in D_2O at RT and steam-treatment with D_2O at 150 °C and 315 °C.

As anticipated, regarding the earlier analyses of PEEK-PBI and PEKK-PBI blends,[2,23] the moisture uptake of pure PEEK and PEKK is much less than for PBI. The TGA of PEEK (Figure 3.2) shows that by stirring the sample at RT with D_2O and during steam-treatment at 150 °C with D_2O basically no water is adsorbed. After steam-treatment with D_2O at 315 °C about 4 wt% of D_2O is incorporated into the polymer, which would correspond to a weight loss of 3.6% of non-deuterated water when taking the lower molecular weight of H_2O into account.

For PEKK the corresponding results are displayed in Figure 3.3. The determined moisture contents show the same trends as for PEEK. There is practically no water uptake during the treatment of PEKK with D_2O at ambient temperature and steam-treatment at 150 °C. After steam-treatment with D_2O at 315 °C a weight loss of only about 3% is visible in the TGA curve at the indicated conditions (Figure 3.3), which would correspond to an even lower value for the lighter H_2O. It should also be noted that no moisture is found by TGA after prolonged exposure of PEEK and PEKK to the atmosphere. The NMR and IR measurements (see below) are in accordance with these results.

Overall, the TGA results once more corroborate the assumption that in PEEK and PEKK blends of PBI, the PBI component is the one mainly responsible for any water uptake.

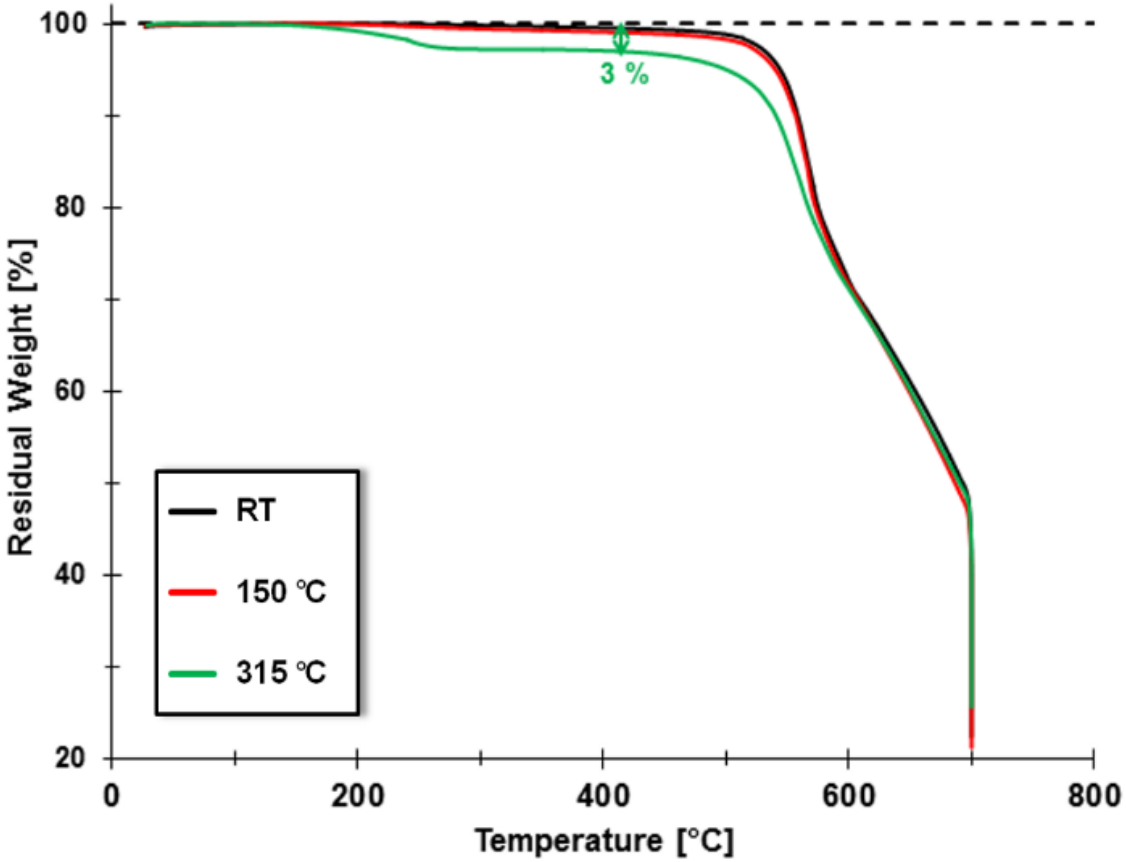

Figure 3.3. TGA of melt-molded PEKK after stirring in D_2O at RT and steam-treatment with D_2O at 150 °C and 315 °C.

^{13}C, ^{1}H, and ^{2}H NMR and IR spectroscopy for probing different H_2O sites in PBI, PEEK, and PEKK

After gaining an overview of water in general incorporated into PBI, PEEK, and PEKK, a more differentiated picture is sought. For this purpose, besides IR and ^{13}C solid-state NMR analysis, ^{1}H wideline NMR and ^{2}H MAS are applied in the following. For ^{2}H solid-state NMR spectroscopy the samples have been treated with D_2O instead of H_2O. Since the largest amount of moisture obviously resides in the PBI, it will be discussed first.

Analysis of PBI after exposure to H_2O and D_2O as liquid and steam

When a molded sample of PBI is stirred in water at ambient temperatures, changes in its appearance are immediately obvious. Its color darkens (Figure 3.4), but no obvious change of its texture takes place. The surface of the material remains smooth and it does not become brittle. The same observation is made after steam-treatment with D_2O at 150 °C, although some first defects on the surface become visible. However, after steam-treatment at 315 °C for 72 h the color is lighter again and the material becomes brittle. Its surface is rough and some pieces have chipped off at the edges of the specimen (Figure 3.4). It is noteworthy that D_2O practically does not differ in its reactivity from H_2O, and the same observations are made using the latter for steam-treatment.

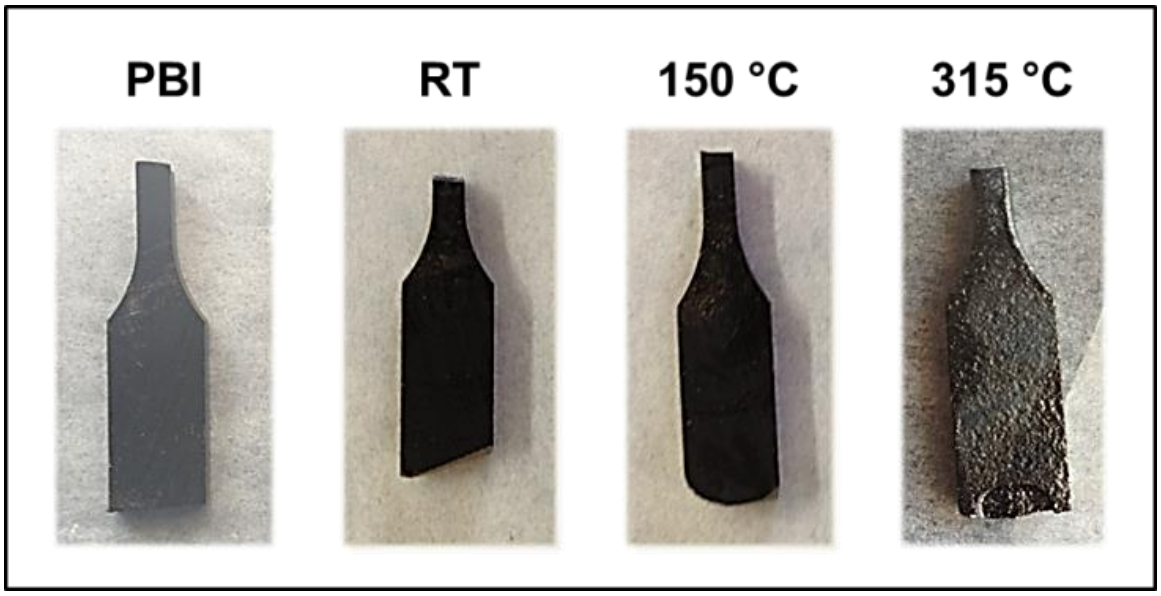

Figure 3.4. Change of physical appearance of melt-molded PBI after stirring in D_2O at RT, and steam-treatment with D_2O at 150 °C and 315 °C.

Since there are massive changes in the appearance of the material occurring after steam-treatment, the IR spectra of PBI have been recorded (Figure 3.5). IR spectroscopy shows that the only major change when steam-treating the PBI with D_2O at 150 °C is that water is incorporated into the polymer network. This can be concluded from the large broad signal in the middle spectrum, with the lowest transmission at 2256 cm^{-1}.[26] The largest difference between the IR spectra is found when proceeding to steam-treatment at 315 °C (Figure 3.5, top). The polymer backbone seems to be affected, as the whole region from 1447 to 600 cm^{-1} is largely changed. In particular, the peaks at 1447, 1377, and 1308 cm^{-1}, representing the D_2O and H_2O bending modes,[26] are shifted. At the same time, the broad water O-H stretching peak around 3100 cm^{-1} increases in intensity. Overall the IR

spectra suggest that D_2O is incorporated into the PBI and that at 315 °C the PBI also undergoes morphological changes.

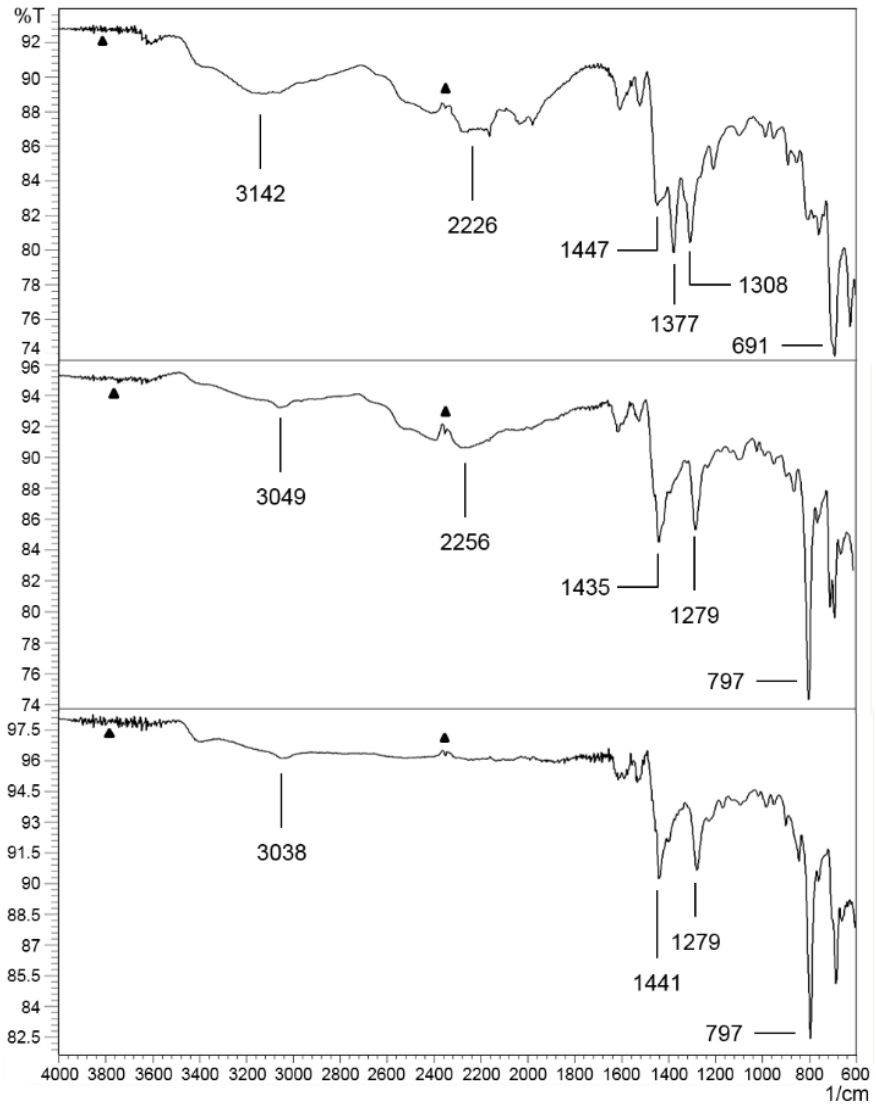

Figure 3.5. IR spectra of rigorously dried PBI powder (bottom), and PBI tensile specimens after steam-treatment with D_2O at 150 °C (middle) and 315 °C (top). The triangles denote artifacts from the instrument and traces of CO_2.

The uptake of water into the polymer network plays a crucial role when the materials change their morphology or break down due to chemical reactions. Therefore, the interactions of water with the polymers will be studied in more detail in the following. For this purpose, the different water and proton sites in fully hydrated PBI need to be contemplated (Scheme 3.2).

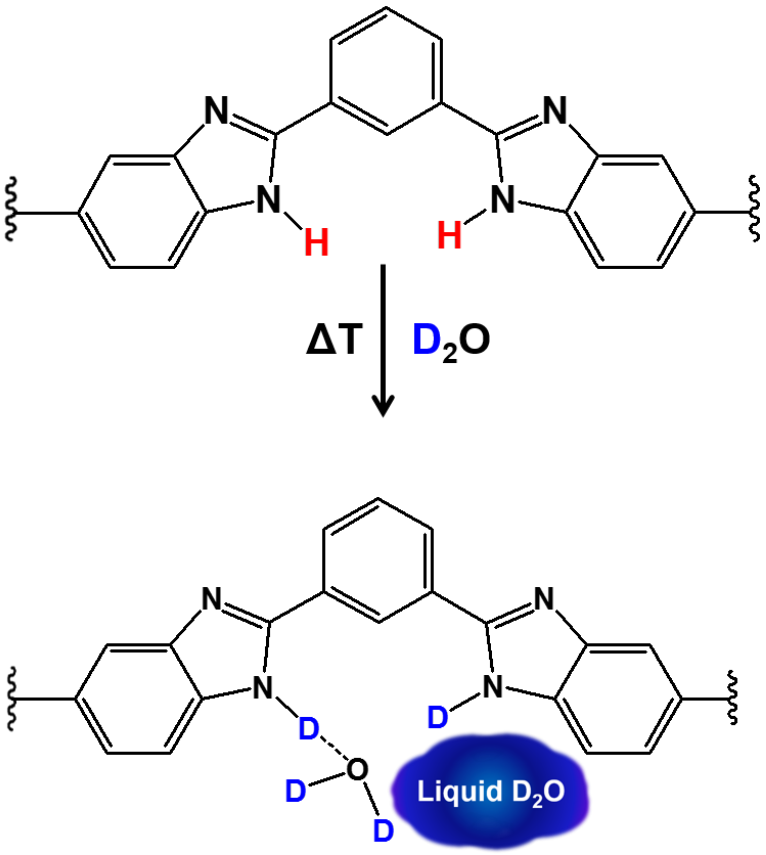

Scheme 3.2. Changes on the molecular level after steam-treatment of PBI with D_2O.

As depicted in the top structure of Scheme 3.2, rigorously dried PBI contains two sorts of backbone protons, aryl protons bound to carbons of the benzene rings and N-H protons. Aryl C-H protons of benzimidazole are not exchangeable, even under the harsh conditions of steam-treatment at 315 °C.[23] Furthermore, C-H protons of non-fused aryl rings do not exchange, even in the presence of a C=O substituent, as demonstrated by steam-treating triptycene and benzophenone with D_2O at 315 °C. Nitrogen-bound protons, on the other hand, can in principle be exchanged with protons of H_2O, or deuterium from D_2O (Scheme 3.2). However, the N-D groups will not lose the deuterium atom when PBI is redried after D_2O exposure.[23]

Besides the covalently bound hydrogen and deuterium atoms, D_2O can form hydrogen bonds with the N-H or N-D groups, as shown in Scheme 3.2. In previous work it has been demonstrated with the use of a molecular model compound that at least one water molecule is hydrogen-bonded per N-H group.[3] The adsorbed water molecules can migrate along the PBI strands.[3] Another publication describes the single crystal X-ray structure of a complex incorporating a benzimidazole moiety,[25] which shows multiple water molecules attached to the molecule. The water can either form hydrogen bridges with the free electron pair at the N via its hydrogen atoms or interact with N-H protons via the oxygen atom.[25] Hydrogen-bonded water can be removed entirely when redrying the PBI rigorously.[23]

Finally, water can also be present in the polymer as a liquid, residing in pockets of the polymer network (Scheme 3.2). Water molecules in the liquid domains can exchange with adjacent hydrogen-bonded water. This water in aqueous domains is lost most easily

during a redrying process. While backbone C-H and N-H protons and N-D deuterium atoms are practically immobile, disregarding movements of the polymer chains, hydrogen-bonded H_2O and D_2O have some mobility even in the solid materials. The water in liquid domains, depending on their size, represents the species with the highest degree of mobility in the polymer. The water molecules in large aqueous domains can even approach liquid-type mobilities with reorientation times in the ns range.[23]

Since the steam-treatment of PBI leads to obvious changes of the material (Figure 4), ^{13}C CP/MAS NMR has been applied to probe whether decomposition at the molecular level can be detected. Figure 3.6 shows the ^{13}C CP/MAS NMR spectra of all PBI tensile specimens before and after exposure to D_2O at the listed conditions. The signal assignments are in agreement with the literature.[2,28,16] Slight changes are already visible when PBI is stirred in liquid D_2O at RT. The overlapping signal of the carbons 5-7 in the center grows, while those for carbons 8, 9, and 10 start to lose some intensity. After steam-treatment of the PBI at 150 °C basically the same overall signal shape is obtained.

However, after steam-treating the sample at 315 °C for 72 h, the resonances for carbons 8-10 and 2 are mostly gone. Only the signals for carbons 1 and the shoulder for 3 and 4, besides the signals 5-7 of the benzene ring remain.

Since the outcome of solid-state NMR measurements is always determined by the measurement programs and parameters in a major way, one needs to contemplate these to decide whether the changed spectra indicate any decomposition of the sample, or the scenario is just a consequence of the exchange of ^{1}H by ^{2}H.

The spectra in Figure 3.6 are all recorded with cross polarization,[7-6] which means that the ^{13}C NMR signal intensities are boosted by magnetization transfer from the proton reservoir to the corresponding carbon nuclei. Since hydrated PBI contains large amounts of protons in adsorbed water, as visible, for example, in the X-ray structure of a benzimidazole-containing complex,[25] a short contact time of 1.5 ms is sufficient to obtain spectra with good signal-to-noise ratio that show all signals. This also indicates that adsorbed H_2O stays long enough in one place to allow for the magnetization transfer.

For those PBI samples, however, where ^{1}H is largely exchanged with ^{2}H by steam-treatment with D_2O, the magnetization has to be transferred from the remaining aryl protons. But cross polarization from aryl protons to heteronuclei requires longer contact times.[18,6]

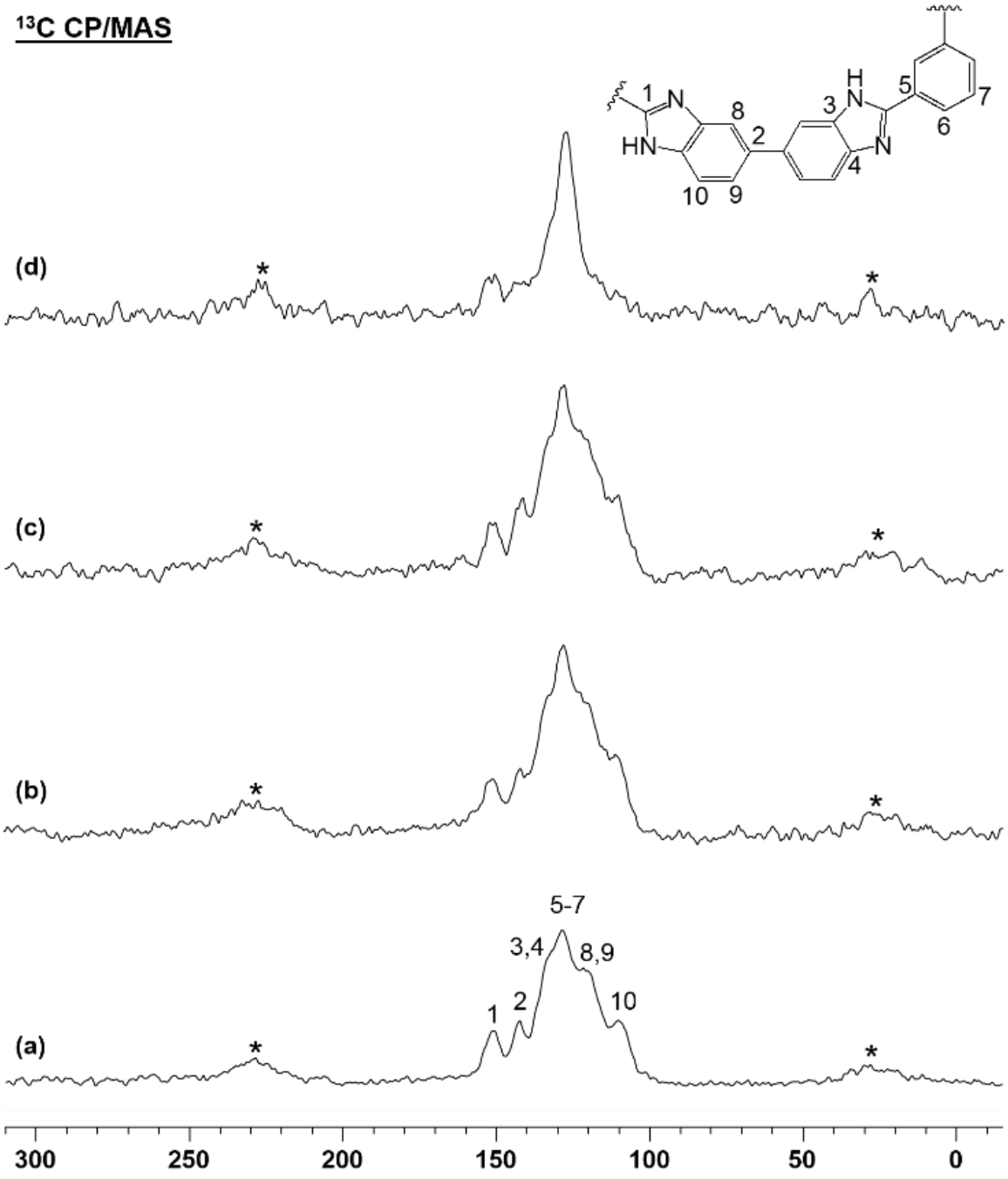

Figure 3.6. ^{13}C CP/MAS NMR spectra of melt-molded PBI after drying at 110 °C for 550 h (a), stirring in D_2O at RT (b), steam-treatment with D_2O at 150 °C (c), and steam-treatment with D_2O at 315 °C (d). The spinning speed is 10 kHz for all spectra, and the asterisks denote rotational sidebands.

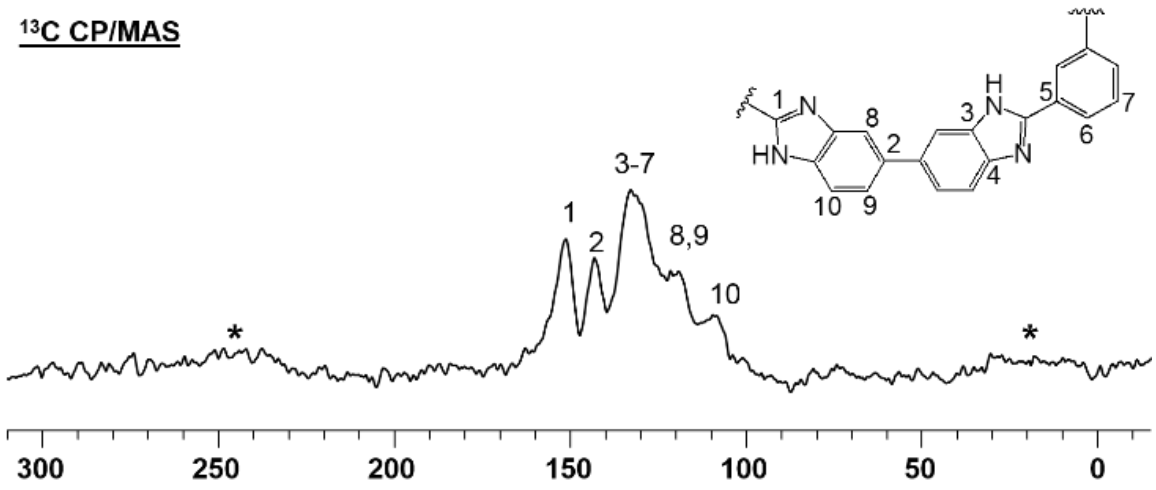

Figure 3.7. ^{13}C CP/MAS NMR spectrum of melt-molded PBI after steam-treatment with D_2O at 315 °C, recorded with a cross-polarization contact time of 10 ms. The spinning speed is 10 kHz, and the asterisks denote rotational sidebands.

To test this hypothesis, PBI, steam-treated with D_2O at 315 °C, has been measured with a contact time of 10 ms. As the ^{13}C CP/MAS spectrum in Figure 3.7 shows, all ^{13}C signals that do not overlap with the peak in the center are visible again with about the same intensities as seen in the spectrum for the original PBI (Figure 3.6a). The loss of ^{13}C benzimidazole signals after treatment with D_2O and their boost with the longer contact time means that the H_2O and the newly incorporated D_2O mostly reside around the benzimidazole moieties in the polymer. This is in accord with the X-ray analysis described in the literature.[25] The carbon signal 1 persists throughout, because its signal profits from magnetization transfer of the close-by aryl protons 6 and 7. Furthermore, the result indicates that the N-H proton and the protons of the H_2O molecule hydrogen-bonded to

the N-H group are a source for magnetization transfer to the ^{13}C nuclei of the benzimidazole moiety.

In order to further probe the different ^{1}H locations and characteristics, ^{1}H solid-state NMR spectroscopy has been applied. ^{1}H MAS NMR, recorded with high spinning speeds of up to 35 kHz is analytically not very favorable for the polymers investigated in this chapter, because only one narrow signal is obtained, which is surrounded by the corresponding sets of rotational sidebands. However, as demonstrated earlier,[2,23] ^{1}H wideline NMR spectroscopy without sample spinning provides valuable information for distinguishing protons of the immobile backbone from those in mobile H_2O molecules in aqueous domains within the polymer network. Mobile species result in a relatively narrow signal sitting on the broad resonance of the polymer backbone ^{1}H NMR signal.[2,23]

Figure 3.8 displays the ^{1}H wideline NMR spectra of melt-molded PBI prior to and after exposure to D_2O under different conditions. Spectrum (a) shows that after drying the sample *in vacuo* for 550 h at 110 °C only immobile C-H and N-H backbone protons are present, which result in a broad resonance with a line width of about 26.8 kHz. After stirring PBI at RT in D_2O, the proton wideline spectrum (b) shows a narrow line on top of the 27.7 kHz broad backbone signal, whose half width can be determined to be about 8.3 kHz after deconvolution.[19] The narrow signal might originate from residual, strongly adsorbed H_2O that has been liberated into aqueous domains by exchange with D_2O. Independent of the origin of the protons resulting in the narrow resonance one can conclude that even at RT D_2O can migrate into the polymer and participate in proton exchange. After steam-treatment of the PBI sample with D_2O at 150 °C (c) and 315 °C

(d), narrow peaks are present with line widths of 5.8 and 7.3 kHz, respectively. The scenario shows that for (c) the water content is highest, in accordance with the TGA (Figure 3.1) and earlier results obtained with different methods.[2,23] Obviously at the higher temperature of 315 °C the equilibrium water content is lower.

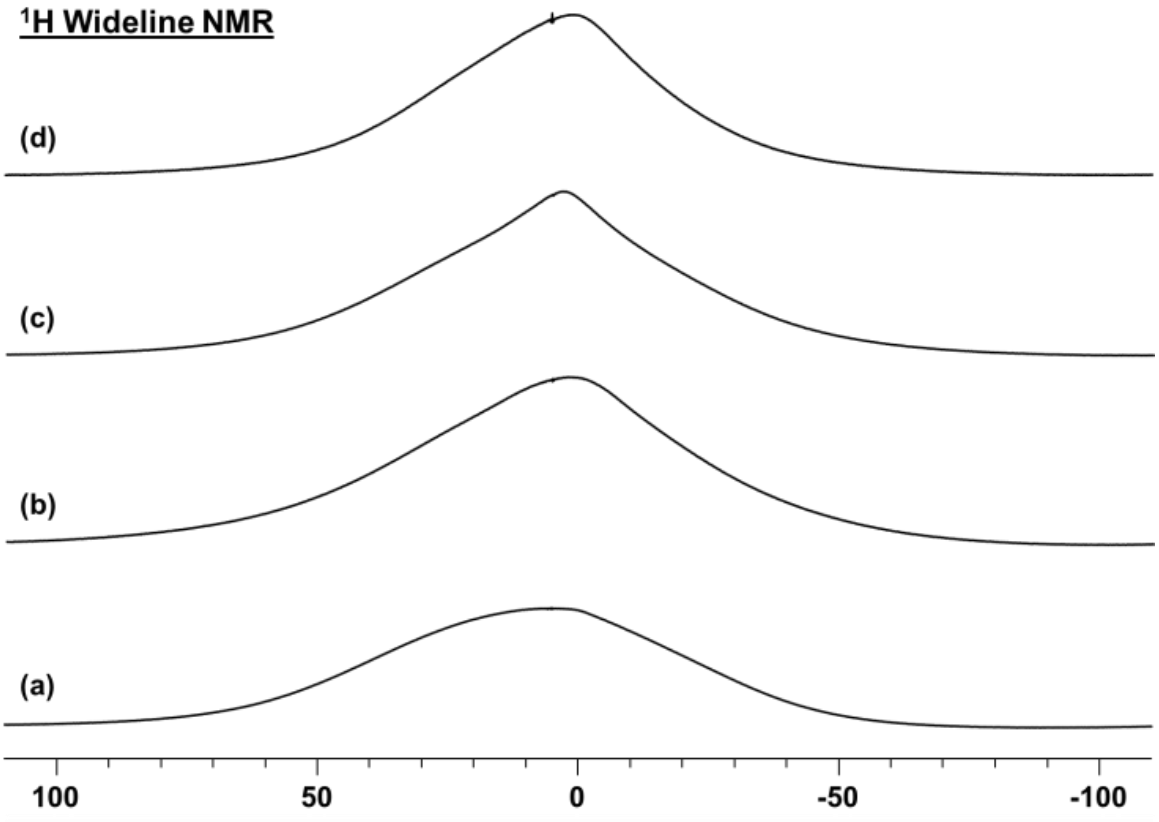

Figure 3.8. ^{1}H Wideline NMR spectra of melt-molded PBI after drying at 110 °C for 550 h (a), stirring in D_2O at RT (b), steam-treatment with D_2O at 150 °C (c), and steam-treatment with D_2O at 315 °C (d).

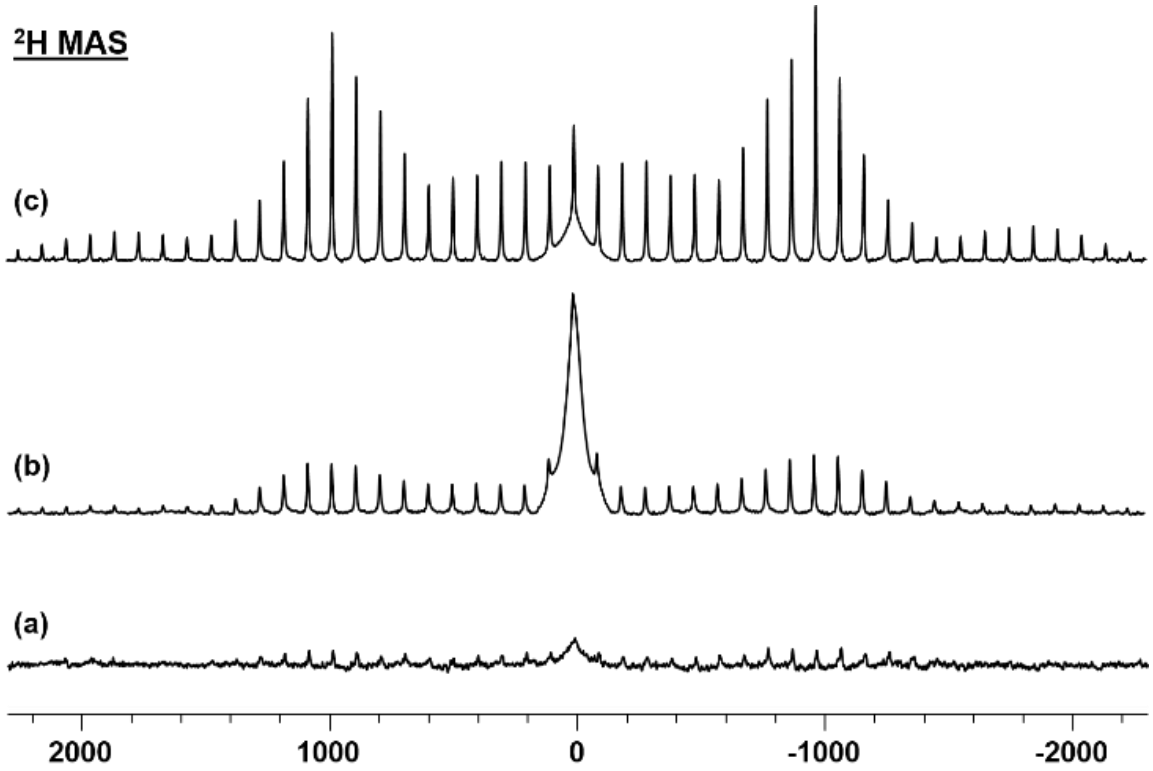

Figure 3.9. ^{2}H MAS NMR spectra of melt-molded PBI after stirring in D_2O at RT (a), steam-treatment with D_2O at 150 °C (b), and immediately after steam-treatment with D_2O at 315 °C (c). The Pake patterns are split into rotational sidebands (spinning frequency 6 kHz for all samples). Their Q_{cc} values are given in Table 3.1.

Figure 3.9 displays the ^{2}H MAS spectra obtained before and after exposure of PBI to D_2O under various conditions. After immersing a tensile specimen of PBI in D_2O at RT, two signals with very different characteristics are visible in the ^{2}H MAS spectrum (a). The central signal must be due to mobile D_2O present in aqueous domains within the polymer based on its small half width of 3.7 kHz and the fact that it is not a Pake pattern. The second signal represents a classical Pake pattern that is split into rotational sidebands because of the spinning frequency of 6 kHz. The residual linewidths of the rotational

sidebands is small with only about 500 Hz. The quadrupolar coupling constant Q_{cc} with a value of 194 kHz indicates that the ^2H nuclei responsible for the signal are basically immobile.[21] Therefore, we conclude that this Pake pattern stems from strongly adsorbed D_2O or N-D groups.

The quadrupolar coupling constants Q_{cc} of all ^2H MAS spectra are summarized in Table 3.1, together with key data obtained earlier.[23] The Q_{cc} values have been obtained after deconvolution[19] and simulating the Pake patterns in the spectra.[20] The simulated spectra obtained as described in the experimental section and in the literature[20] are quite accurate. Figure 3.10 shows as an example the simulated spectrum in grey fitting the measured spectrum of PBI after steam-treatment with D_2O at 315 °C (Figure 3.9c).

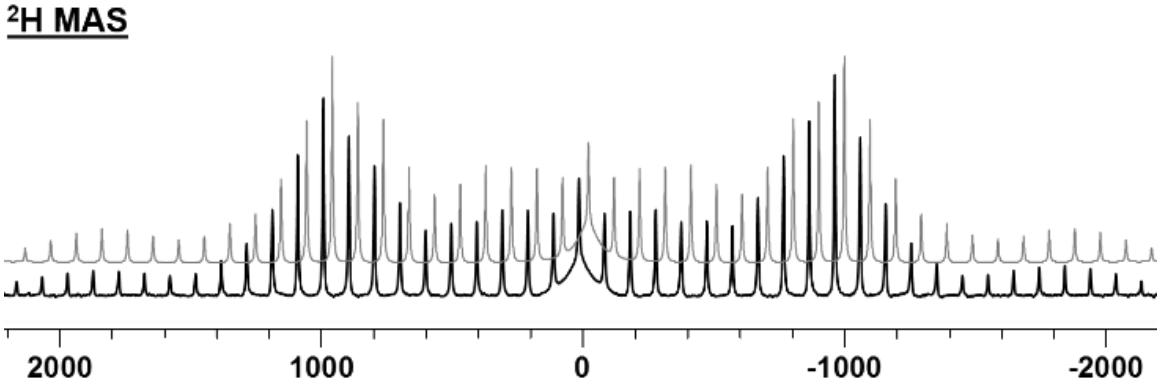

Figure 3.10. ^2H MAS NMR spectrum of melt-molded PBI after steam-treatment with D_2O at 315 °C (Figure 3.7c) and the simulated spectrum in grey with a slight δ offset for improved visibility.[20]

As Figure 3.9 shows, after steam-treatment of the PBI sample with D_2O at 150 °C (b) and 315 °C (c), the same two unstructured center signals with halfwidths of only about 3.8 khZ and 500 Hz, are again visible. The main difference is that the signal assigned to mobile D_2O in liquid domains is more intense after steam-treatment at 150 °C (b), while it shrinks again after 315 °C (c). This is in accordance with the above TGA and ^1H MAS results. The Pake pattern, however, is most intense after steam-treating the PBI at 315 °C. Its Q_{cc} value matches the ones obtained after steam-treatment of its PEEK and PEKK blends very well (Table 3.1). It can tentatively be assigned to strongly adsorbed D_2O or deuterium nuclei in N-D groups, also taking into account that it has previously been found that the Pake patterns do not disappear after redrying the PEEK-PBI and PEKK-PBI blends.[23]

The chemical shift for D_2O is the same whether it resides in liquid domains or is hydrogen-bonded, and $\delta(^2H)$ for N-D should be similar. Therefore, taking the large residual linewidth and the huge signal span of ^2H in the solid state into account, even the rotational sidebands of the MAS signals of these species overlap. This is why the rotational sidebands of the Pake patterns which stem from the different species are not split into several sets of lines but give only one set. Another consideration is that the D_2O molecules bound via hydrogen bridges undergo fast exchange with the D_2O molecules in contiguous liquid domains. This means that the Q_{cc} values connected to specific types of ^2H environments are averaged out and variable to some degree in the presence of liquid domains. In the absence of liquid D_2O, there is no longer any exchange and only the signal for N-D groups with maximal Q_{cc} is present.[23]

Table 3.1. Q_{cc} (quadrupolar coupling constant) values [kHz] of melt-molded samples treated with D_2O as liquid at RT and steam at 150 and 315 °C.

Melt-Molded	***RT***	***150 °C***	***315 °C***
PBI	194	196	184
PEEK	-	-	186*
PEKK	-	-	182*
PEEK Redried	-	-	182*
PEKK Redried	-	-	183*
PEEK-PBI[23]	-	197	184
PEKK-PBI[23]	-	195	183

- indicates that no Pake pattern has been observed. *indicates signals with low intensity. The data for the melt-blends (50:50 wt%) have been taken from the literature.[23] Error margins of the Q_{cc} values are +/- 0.5 kHz.

Table 3.1 shows that the Q_{cc} values for melt-molded PEEK-PBI, PEKK-PBI, and PBI after steam-treatment with D_2O at 315 °C are practically the same. Taking into account that at this temperature the amount of water in liquid domains is minimal (Figure 3.9c), one can conclude that the Pake pattern stems from N-D groups and that any water uptake of the blends is basically due to the PBI component. The Q_{cc} values of PBI and its blends (Table 3.1) are larger after treatment with liquid D_2O and steam at 150 °C, although the exchange of deuterium nuclei with the increased amount of water in aqueous domains can take place and therewith a diminished splitting of the Pake patterns should be

expected. Therefore, a morphological change influencing the overall polymer chain mobility has to take place at the higher temperature of 315 °C. This assumption is in accordance with the sample becoming more brittle after this treatment (Figure 3.4), with the IR results presented above, and with earlier ^{13}C T_1 relaxation time measurements.[2]

Analysis of PEEK after exposure to D_2O as liquid and steam

In the following melt-molded PEEK samples are exposed to liquid D_2O and its steam as described for PBI above. Figure 3.11 shows that at ambient temperature and 150 °C only the color changes slightly, while the texture of the sample remains the same. After steam-treatment with D_2O at 315 °C, however, the color of the sample changes to black, and it becomes deformed and brittle with a charcoal-type texture.

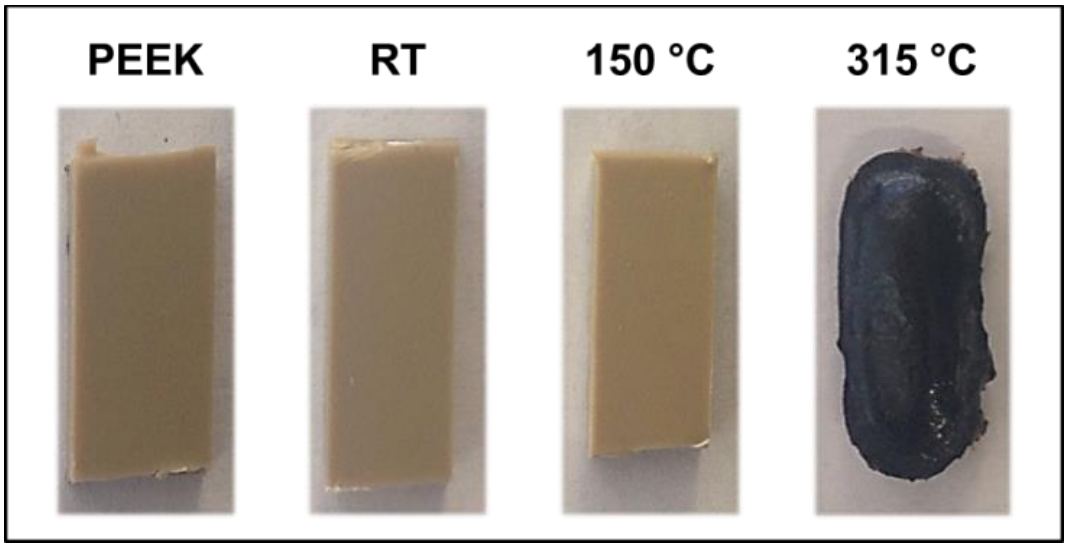

Figure 3.11. Change of physical appearance of melt-molded PEEK after stirring in D_2O at RT, and steam-treatment at 150 °C and 315 °C.

PAEK and PBI polymers and their incorporation of water are in general amenable to investigation by IR spectroscopy.[2,4,5,23,25,26] Changes of the carbonyl stretching band and modifications in the fingerprint area, for example, are indicators for both chemical and morphological transformations.[23] After steam-treatment of PBI with D_2O it has been of interest whether the N-D stretching band would be visible, or any hydrogen bridges with D_2O molecules. Figure 3.12 displays the IR spectra of the original sample, which is practically identical to the spectrum after steam-treatment at 150 °C, and after steam-treatment at 315 °C. The constant value of the C=O stretching band of the PEEK sample at 1647 cm^{-1} does not support the presence of a large number of D_2O molecules bound via hydrogen bridges, as this should decrease its wavenumber.

The same observation is made regarding the C-O stretching band of the ether group of the PEEK at 1219 cm^{-1}. However, the two low intensity bands at the shoulder of this peak around 1300 cm^{-1} experience a change. While they have equal intensities in the IR spectrum of the original sample, the band with the higher wavenumber loses intensity. This effect has been reported in the literature, and attributed to an increase in crystallinity of the sample.[27] This is again in accord with the ^2H MAS results described above and earlier investigations.[2]

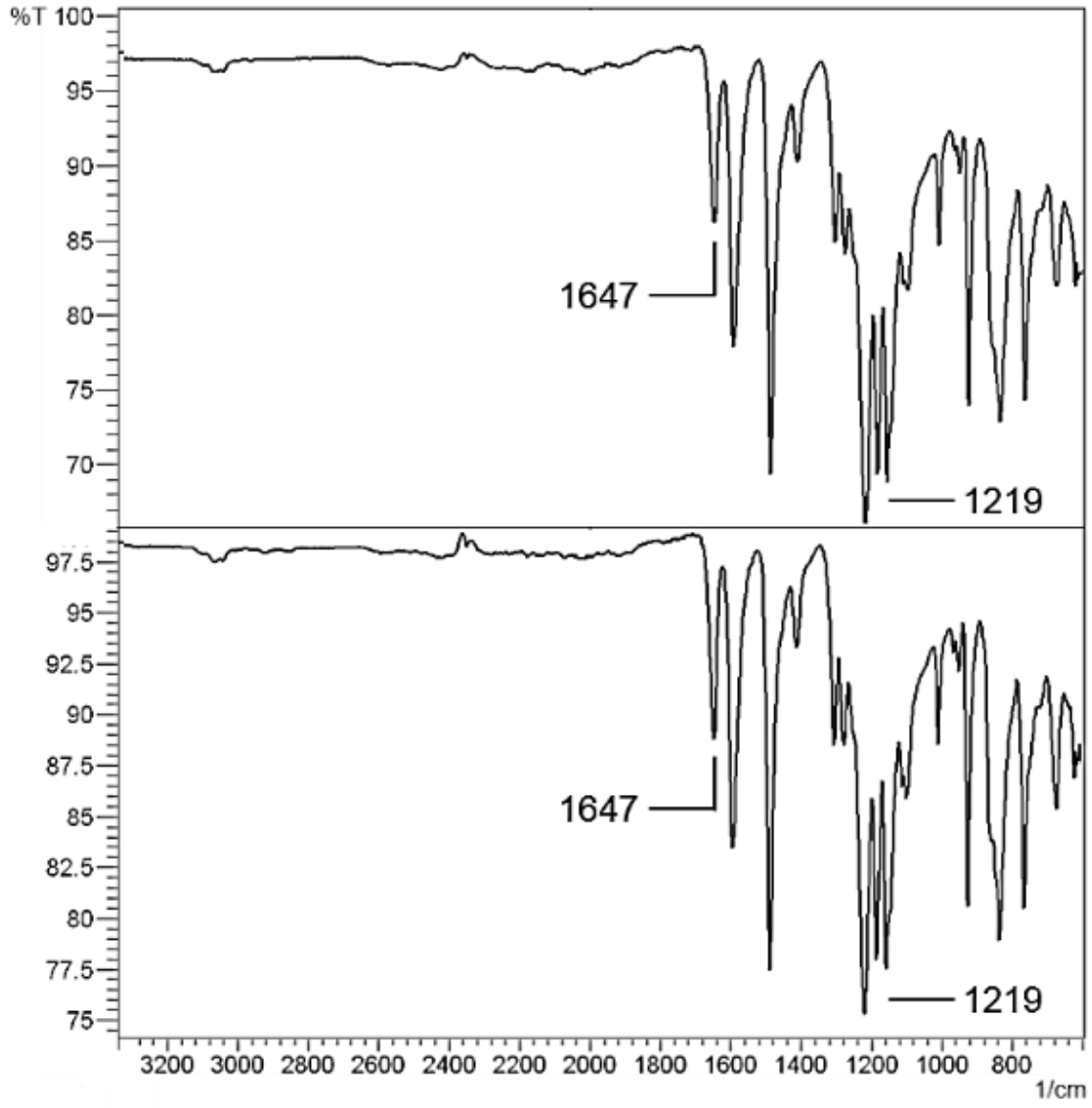

Figure 3.12. IR spectra of melt-molded PEEK as received (bottom) and after steam-treatment with D_2O at 315 °C (top).

The ^{13}C CP/MAS NMR spectra of PEEK samples before and after exposure to D_2O under the indicated conditions are displayed in Figure 3.13. All signals can be assigned in accordance with the literature.[2,27] After stirring the dried PEEK (a) at RT in

D_2O (b), steam-treatment at 150 °C (c) and at 315 °C with D_2O (d), no obvious changes are visible in the ^{13}C CP/MAS spectra. In particular, the resonance a for the carbonyl carbon at 193.4 ppm does not change its chemical shift. Therefore, one can conclude that the carbonyl group does not undergo hydrogen-bonding with potentially incorporated H_2O or D_2O. The same accounts for the signals b and c of the carbon nuclei at 160.5 and 161.2 ppm, bound to the ether oxygen atom. None of the ^{13}C CP/MAS signals changes its intensity.

Regarding the cross polarization mechanism discussed above,[18-6] one can conclude that either no magnetization transfer from exchangeable protons to the carbon nuclei takes place in the original sample, or that the D_2O does not replace any protons in PEEK even under harsh reaction conditions. The following ^{1}H wideline and ^{2}H MAS NMR results show that the first interpretation is the most likely. As observed for the non-condensed phenyl ring in PBI, the aryl protons of PEEK are not exchanged and it can be concluded that PEEK does not contain adsorbed H_2O that contributes to the magnetization transfer.

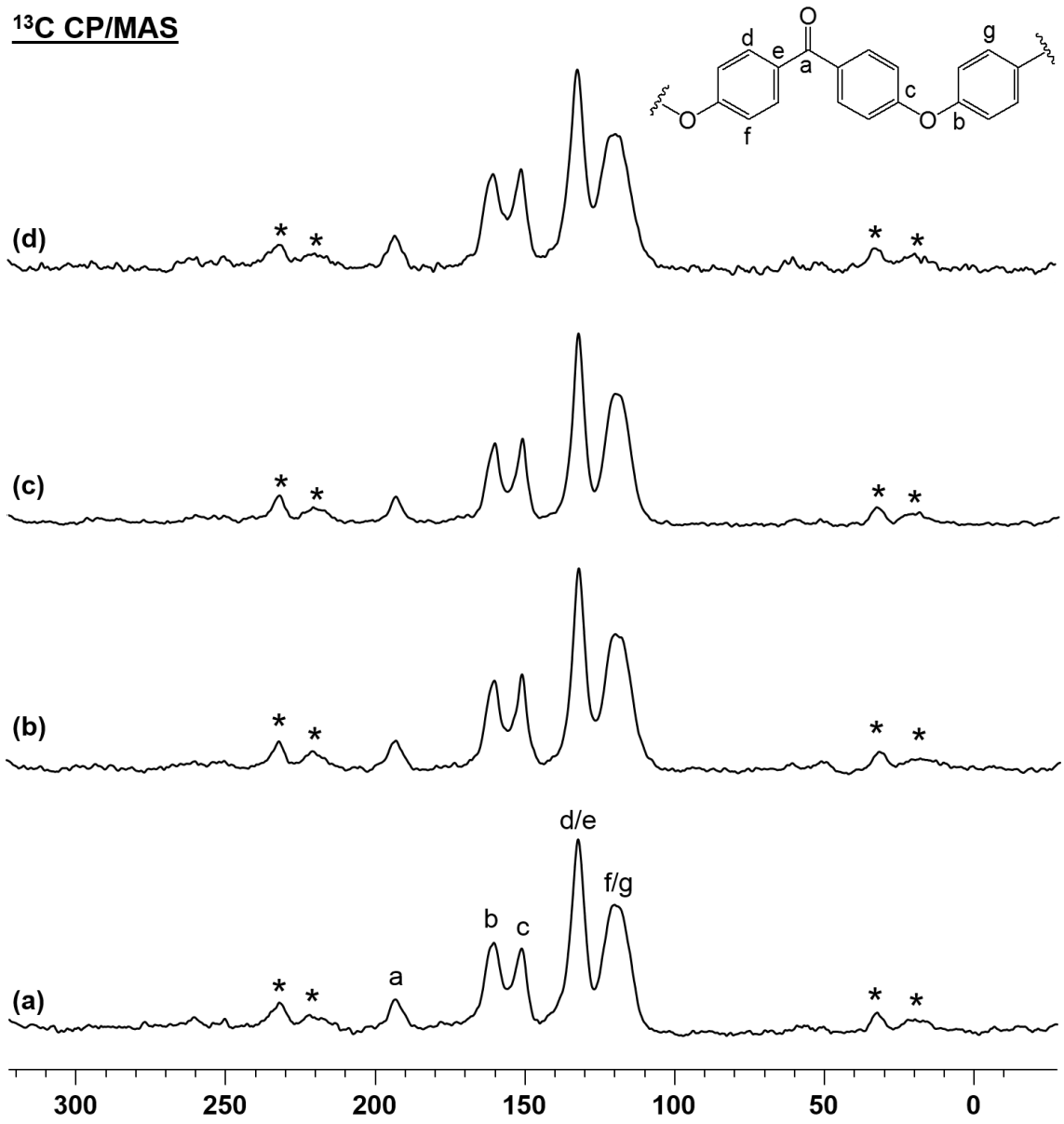

Figure 3.13. ^{13}C CP/MAS NMR spectra of melt-molded PEEK after drying at 110 °C for 550 h (a), stirring in D_2O at RT (b), steam-treatment with D_2O at 150 °C (c), and immediately after steam-treatment with D_2O at 315 °C (d).

The ^{1}H wideline NMR spectra of the melt-molded PEEK samples before and after treatment with liquid D_2O and D_2O steam are displayed in Figure 3.14. The absence of any substantial proton signals with smaller line widths on top of the broad resonances with halfwidths of ca. 29 kHz in the spectra (a) and (b) reveals that under ambient conditions the melt-molded sample does not contain adsorbed and mobile H_2O. This is in accordance with its TGA curves and the IR and ^{13}C CP/MAS results. However, after steam-treatment at the higher temperatures of 150 and 315 °C (c, d), low intensity signals with halfwidths of about 1.7 and 2.6 kHz appear. These are tentatively attributed to tiny amounts of exchangeable protons in the original sample, potentially stemming from traces of plasticizers. Their decomposition might also explain the color change of PEEK when exposed to the most demanding conditions (Figure 3.11). It is noteworthy that molecular benzophenone does not exchange protons of the phenyl rings for deuterium atoms when steam-treated at 315 °C for 72 h.

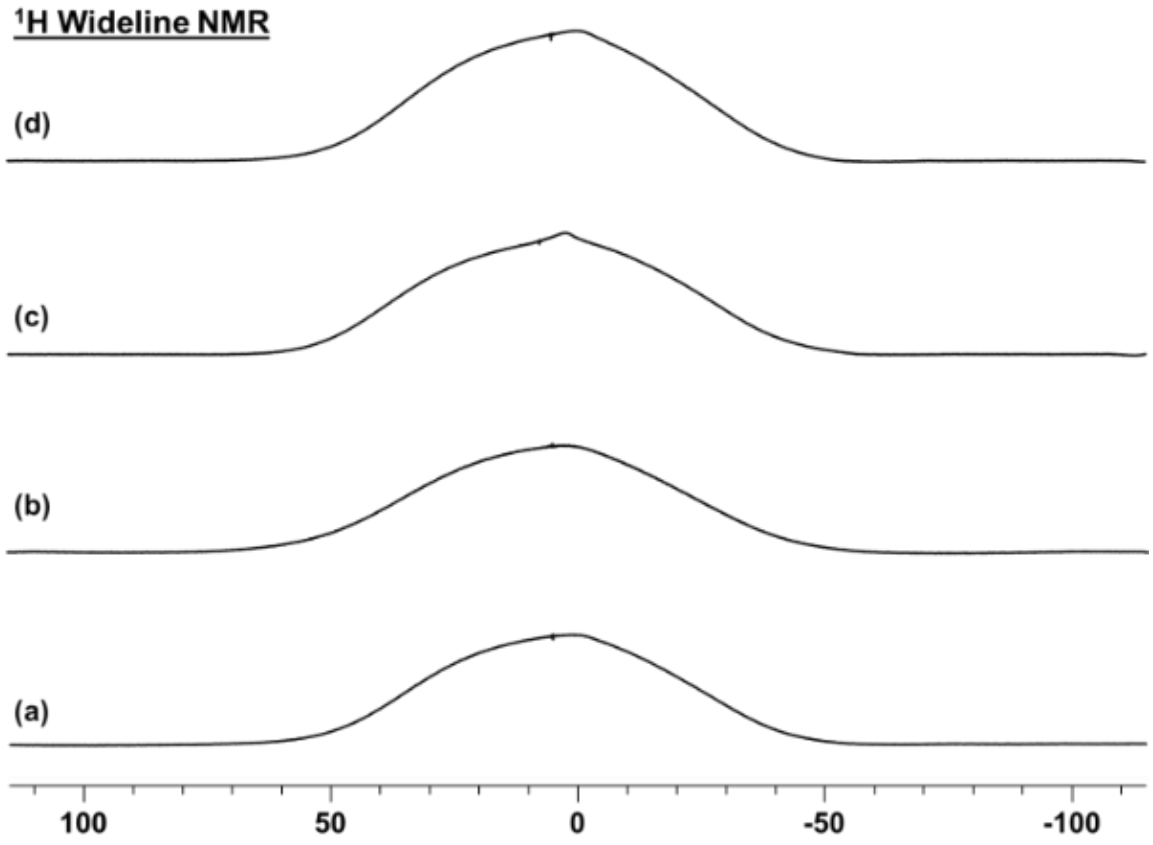

Figure 3.14. ^{1}H Wideline NMR spectra of melt-molded PEEK as received (a), after stirring in D_2O at RT (b), steam-treatment with D_2O at 150 °C (c), and immediately after steam-treatment with D_2O at 315 °C (d).

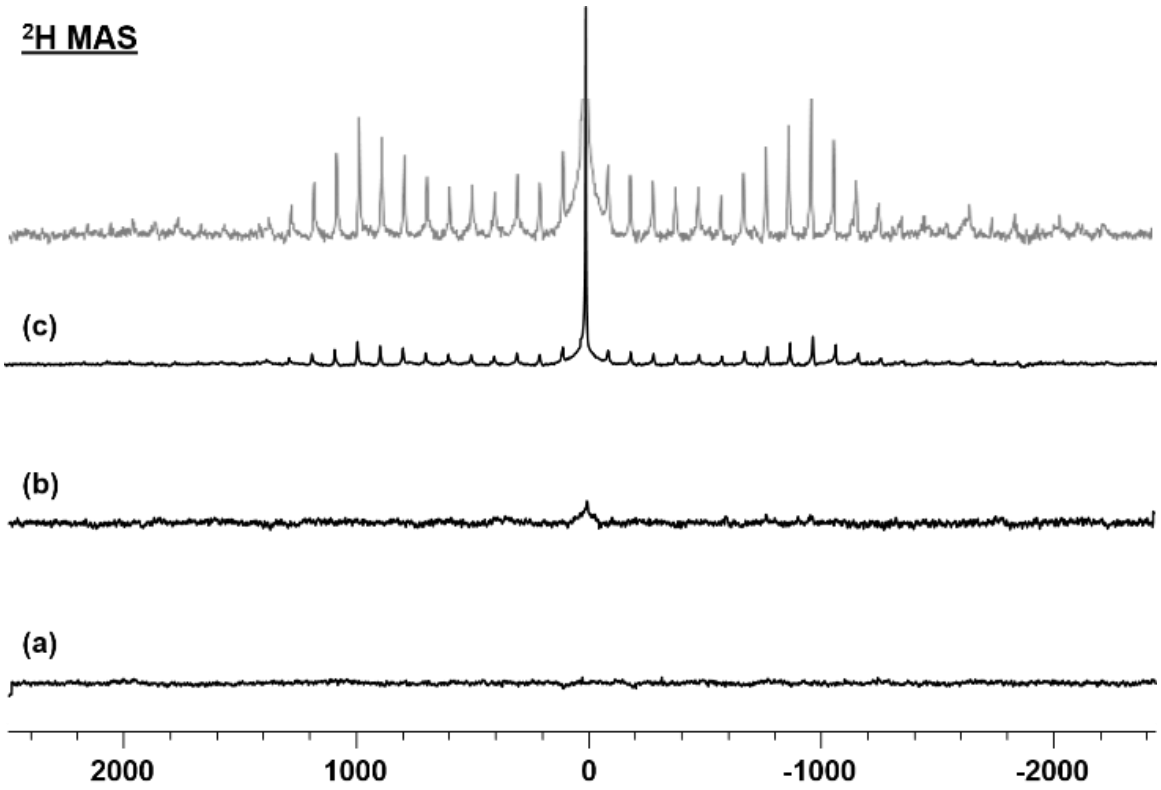

Figure 3.15. ^{2}H MAS NMR spectra of melt-molded PEEK after stirring in D_2O at RT (a), steam-treatment with D_2O at 150 °C (b), and immediately after steam-treatment with D_2O at 315 °C (c). The grey top trace shows the vertical expansion of (c) to improve the visibility of the Pake pattern, which is split into rotational sidebands (spinning frequency 6 kHz for all samples). The Q_{cc} value is given in Table 3.1.

As the ^{2}H MAS NMR spectra displayed in **Figure 3.15** show, it takes steam-treatment at 315 °C to bring substantial amounts of D_2O into the melt-molded PEEK samples. No ^{2}H MAS signal is found after exposure of PEEK to D_2O at RT even after prolonged measurement times. After steam-treatment at 150 °C a low intensity central signal with a halfwidths of about 2 kHz appears, indicating traces of mobile D_2O. A low intensity Pake pattern is obtained after steam-treatment with D_2O at 315 °C. In contrast to

the PBI samples, where the Pake pattern becomes obvious after only 512 scans, the PEEK measurements required 32000 scans to render the Pake pattern visible (Figure 3.15c). Besides the Pake pattern with a Q_{cc} value of 186 kHz (Table 3.1), a central signal attributable to mobile D_2O, adsorbed or in liquid domains in the polymer, emerges with a halfwidth of about 700 Hz. After redrying this sample at 110 °C for 48 h, the ^2H NMR spectrum was recorded (Figure 3.16). A Pake pattern with a Q_{cc} of 183 kHz remains. This can be attributed to deuterium exchange in the fillers and stabilizers in the polymer.

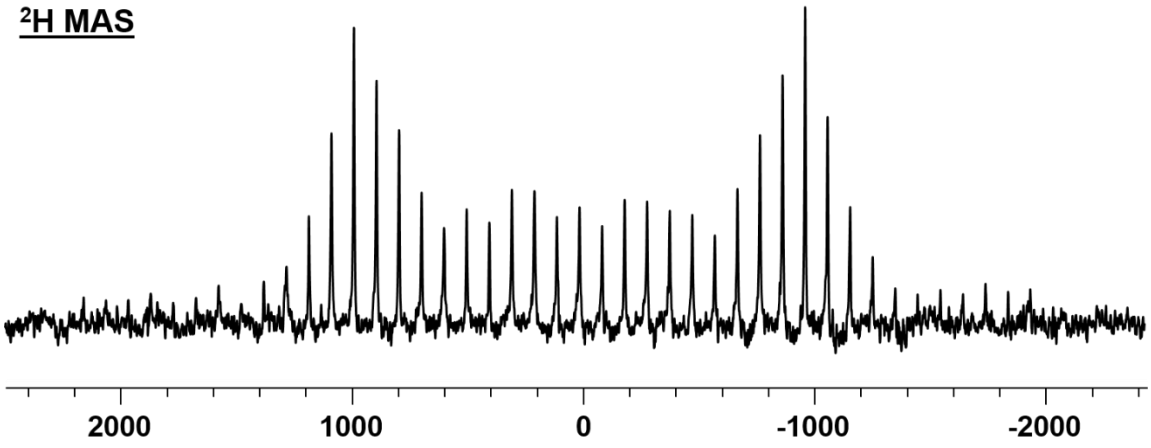

Figure 3.16. ^2H MAS NMR spectra of melt-molded PEEK that has been redried after steam-treatment with D_2O at 315 °C. The Pake pattern is split into rotational sidebands (spinning frequency 6 kHz). The Q_{cc} value is given in Table 3.1.

Analysis of PEKK after exposure to D_2O as liquid and steam

When melt-molded PEKK is exposed to D_2O under various conditions, the physical appearance of the specimen changes as displayed in Figure 3.17. Stirring the

sample in liquid D_2O and steam-treatment at 150 °C leaves the color of the sample practically unchanged. The surface also remains smooth under these conditions. However, steam-treatment of PEKK with D_2O at 315 °C leads to a notable color change to black, while astonishingly, the surface of the polymer remains smooth (Figure 3.17).

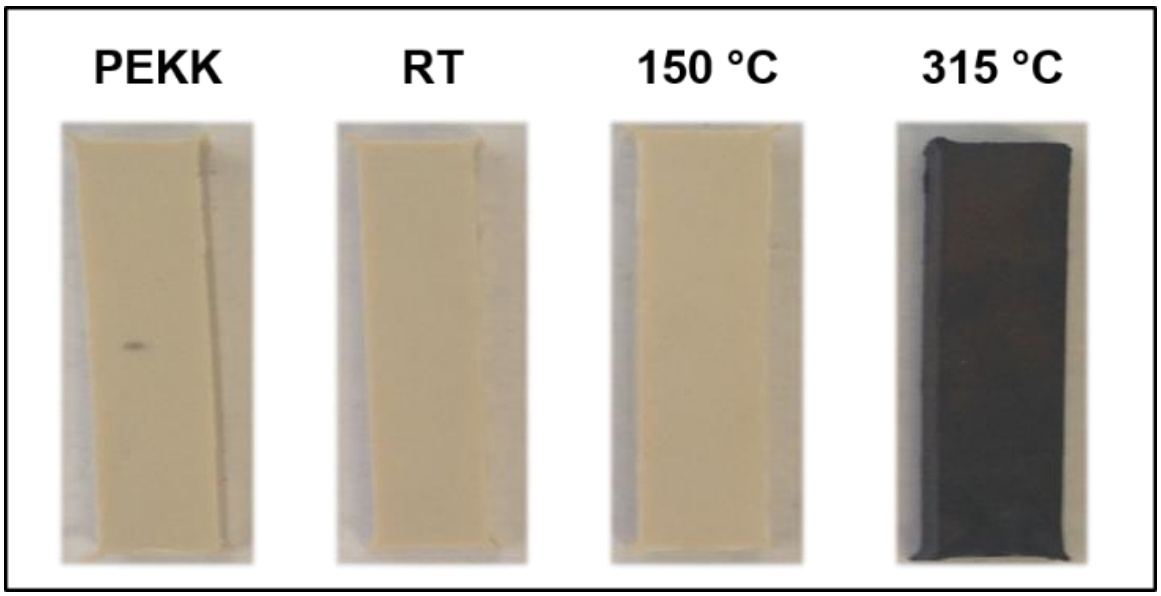

Figure 3.17. Change of the physical appearance of melt-molded PEKK after stirring in D_2O at RT, and steam-treatment at 150 °C and 315 °C.

Figure 3.18 displays the IR spectra of the original melt-molded PEKK sample (bottom), and the PEKK samples after steam-treatment at 315 °C. There are no obvious differences in the spectra and in particular the wavenumbers of the C=O and C-O stretching bands retain their values of 1647 cm^{-1} and 1231 cm^{-1}, respectively. Therefore,

one can conclude that there is practically no D_2O hydrogen-bonded to the carbonyl or ether groups in the treated sample, as this would lead to weaker C=O and C-O bonds and therewith lower wavenumbers of their stretching bands.

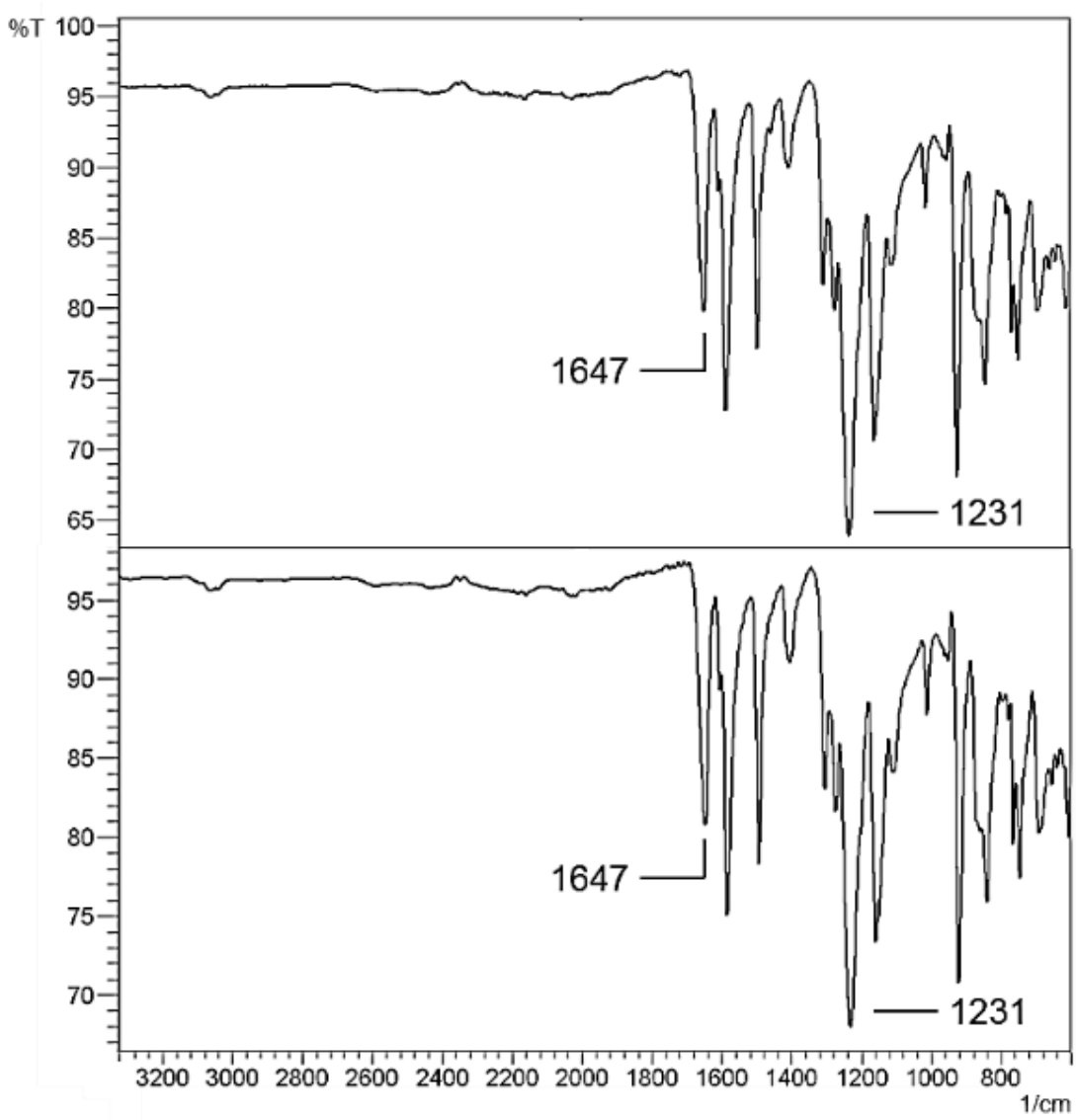

Figure 3.18. IR spectra of melt-molded PEKK as received (bottom) and after steam-treatment with D_2O at 315 °C (top).

The ^{13}C CP/MAS NMR spectra of melt-molded PEKK samples follow the trend observed for PEEK, when treated with D_2O at ambient and elevated temperatures (Figure 3.19). After treatment of the original sample (a) with D_2O at RT (b) and 150 °C (c) there are no major changes in the ^{13}C CP/MAS signals. However, steam-treatment with D_2O at 315 °C leads to a different result (d) as compared to the PBI and PEEK polymers. Disregarding negligible changes of the intensities of all signals, the spectrum (d) is indistinguishable from the spectra (a) to (c).

Therefore, taking the CP characteristics discussed for PBI and PEEK into account, one can conclude that untreated PEKK does not contain any significant amount of H_2O in its network, which could be replaced by D_2O during the steam-treatment and subsequently change the CP dynamics of the sample. This is in accordance with the TGA and IR results presented above, which indicate that PEKK contains only traces of water when in equilibrium with the atmosphere or exposed to it under the harsh conditions of steam-treatment.

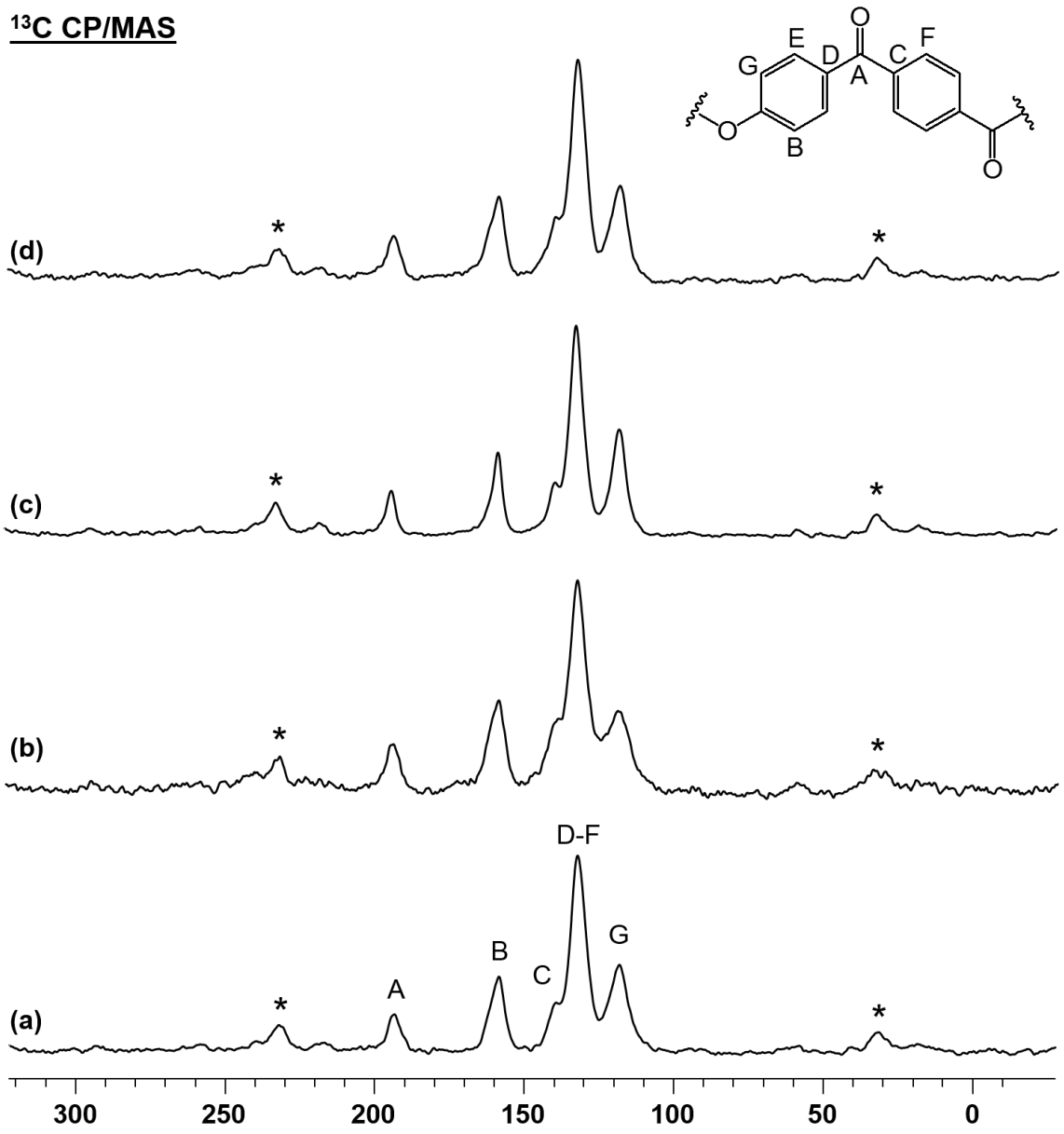

Figure 3.19. ^{13}C CP/MAS NMR spectra of melt-molded PEKK as received (a), after stirring in D_2O at RT (b), steam-treatment with D_2O at 150 °C (c), and immediately after steam-treatment with D_2O at 315 °C (d).

The ^{1}H NMR spectra of melt-molded PEKK before and after exposure to D_2O are displayed in Figure 3.20. The original sample shows traces of water in the form of a narrow signal with a half width of about 5 kHz on top of the broad resonance from the polymer backbone protons with a half width of ca. 30 kHz (a). Stirring the molded specimen in D_2O at ambient temperature and steam-treatment at 150 °C basically do not change the appearance of the signals, as seen in the traces (b) and (c).

This suggests that D_2O does not penetrate into the polymer network, as in this case changes of the narrow resonance on top of the backbone signal would be expected. Steam-treatment of the PEKK sample with D_2O at 315 °C, however, liberates more H_2O, and the narrow signal with a half width of about 2 kHz on top of the 26 kHz broad hump increases in intensity (d). This result is in accordance with the TGA analysis, and it can be concluded that very harsh conditions are needed to bring at least moderate amounts of D_2O into the polymer.

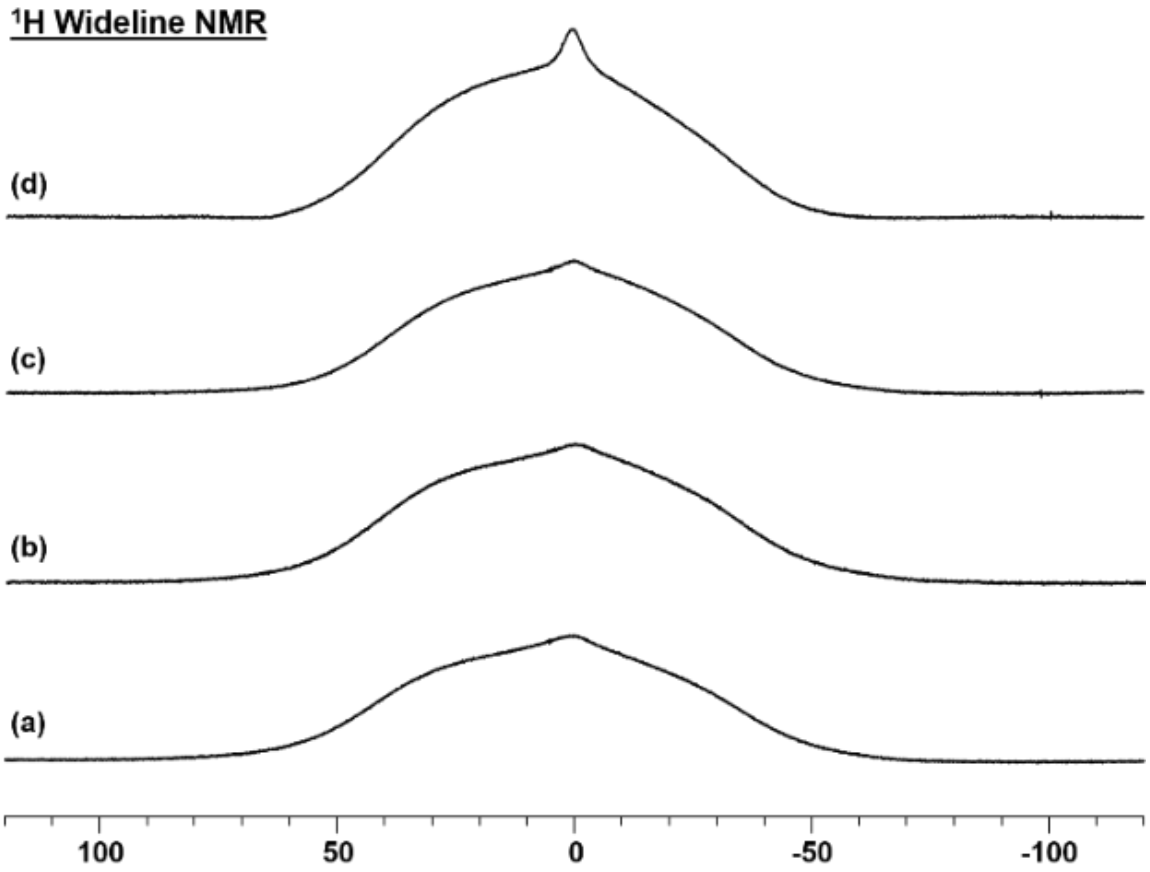

Figure 3.20. ^{1}H Wideline NMR spectra of melt-molded PEKK as received (a), after stirring in D_2O at RT (b), steam-treatment with D_2O at 150 °C (c), and immediately after steam-treatment with D_2O at 315 °C (d).

The ^{2}H MAS spectra (a) and (b) displayed in Figure 3.21 corroborate the ^{1}H wideline NMR results. After treatment with D_2O at RT and 150 °C, no ^{2}H NMR signals emerge even after prolonged measurement times. Block averaging techniques prove that the absence of a signal is not due to any instrument malfunction. This means that under these conditions no D_2O penetrates into the polymer network, which is in agreement with

the hypothesis that PEKK should fend off water when teaming up with PBI in PBI-PEKK blends.[2,23]

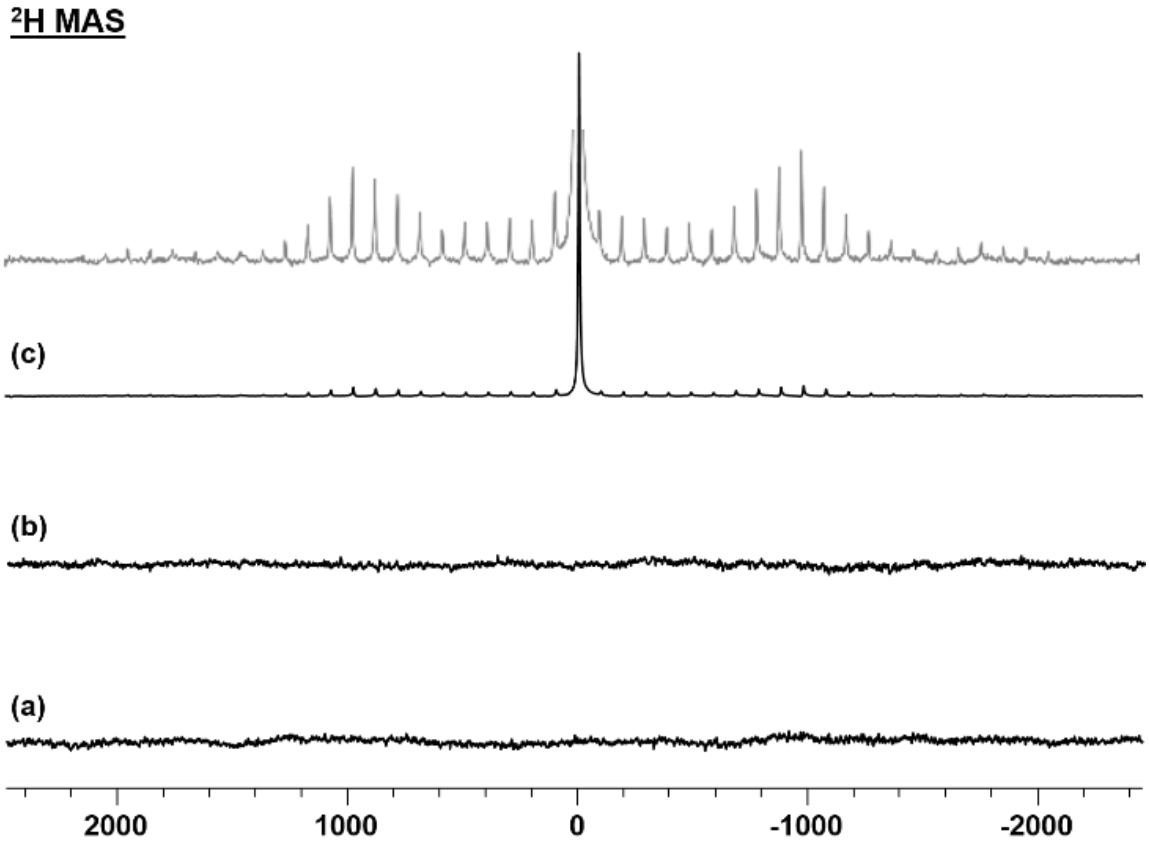

Figure 3.21. ^{2}H MAS NMR spectra of melt-molded PEKK after stirring in D_2O at RT (a), steam-treatment with D_2O at 150 °C (b), and immediately after steam-treatment with D_2O at 315 °C (c). The grey top spectrum shows the vertical expansion of (c). The Pake pattern is split into rotational sidebands (spinning frequency 6 kHz). The Q_{cc} value is given in Table 3.1.

Steam-treatment of a melt-molded PEKK sample with D_2O at 315 °C leads to a ^2H MAS spectrum with two signals (Figure 3.21c). An unstructured central signal with a half width of merely 200 Hz, attributable to mobile water in the polymer, is the dominant feature. The second signal emerges as a low intensity Pake pattern with a Q_{cc} of 182 kHz. Only a large vertical expansion of the spectrum renders this signal visible (Figure 3.21c, gray trace). After redrying this sample at 110 °C for 48 h, the ^2H NMR spectrum was recorded (Figure 3.22). A Pake pattern with a Q_{cc} of 183 kHz remains. As with the pure PEEK sample that was redried (Figure 3.16), this can be attributed to deuterium exchange in the fillers and stabilizers in the polymer. A summary of the ^1H Wideline, ^2H MAS, and ^{13}C CP/MAS NMR signal halfwidths ($\Delta\nu_{1/2}$) for all samples is given in Table 3.2.

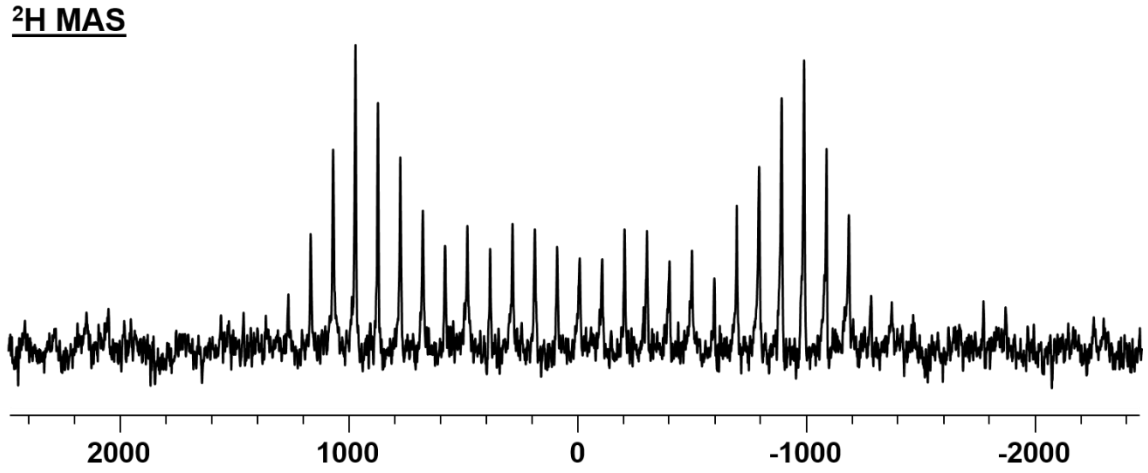

Figure 3.22. ^2H MAS NMR spectra of melt-molded PEKK that has been redried after steam-treatment with D_2O at 315 °C. The Pake pattern is split into rotational sidebands (spinning frequency 6 kHz). The Q_{cc} value is given in Table 3.1.

Table 3.2. Signal halfwidths $\Delta\nu_{1/2}$ [kHz] of the ^{1}H wideline, ^{2}H MAS, and ^{13}C CP/MAS NMR spectra of thoroughly dried samples that were treated with D_2O as liquid and steam at 150 and 315 °C.

	Well-Dried		**RT**		**150 °C**		**315 °C**	
^{1}H	*Broad Signal*	*Narrow Central Signal*	*Broad Signal*	*Narrow Central Signal*	*Broad Signal*	*Narrow Central Signal*	*Broad Signal*	*Narrow Central Signal*
PBI[#]	26.4	---	27.7	8.3	24.3	5.8	21.7	7.3
PEEK[#]	28.3	---	28.8	---	29.8	1.7	29.3	2.6
PEKK[#]	28.9	5.4	29.0	4.2	27.5	3.4	26.2	1.7
^{2}H	*Central Signal*	*Pake Pattern Signal*	*Central Signal*	*Pake Pattern Signal*	*Central Signal*	*Pake Pattern Signal*	*Central Signal*	*Pake Pattern Signal*
PBI[#]	---	---	3.7	0.5	3.8	0.4	3.6	0.3
PEEK[#]	---	---	---	---	1.7	---	0.5	0.3
PEKK[#]	---	---	---	---	---	---	0.2	0.3
^{13}C	*Signal 1*	*Signals 5-7*	*Signal 1*	*Signals 5-7*	*Signal 1*	*Signals 5-7*	*Signal 1*	*Signals 5-7*
PBI[#]	0.6	0.4	0.6	0.4	0.6	0.3	0.6	0.7
	Signal a	*Signal d/e*	*Signal a*	*Signal d/e*	*Signal a*	*Signal d/e*	*Signal a*	*Signal d/e*
PEEK[#]	0.6	0.4	0.5	0.3	0.4	0.4	0.5	0.4
	Signal A	*Signals D-F*	*Signal A*	*Signals D-F*	*Signal A*	*Signals D-F*	*Signal A*	*Signals D-F*
PEKK[#]	0.5	0.6	0.5	0.6	0.5	0.6	0.4	0.6

[#]exposed as melt-molded samples. --- indicates that no Pake pattern has been observed

Clearly, most of the water incorporated in the PEKK resides in aqueous domains and only a trace might be present hydrogen-bound to C=O or C-O groups. Regarding the Q_{cc} values in Table 3.1 it should also be noted that the Pake patterns found for PEEK and PEKK have the largest deviation from the values of 183 and 184 kHz obtained for PBI, PEEK-PBI, and PEKK-PBI. Therefore, the Pake patterns in the pure PEEK and PEKK might also be the consequence of proton exchange in traces of plasticizer in the polymers. However, in the PBI component and its blends clearly the Pake patterns are associated with D_2O either strongly adsorbed to the PBI strands, or to N-D groups of the benzimidazole moiety after proton exchange.

CONCLUSION

In this contribution it has successfully been demonstrated that the single components of important PAEK-PBI blends, namely PBI, PEEK, and PEKK, can be characterized by ^{13}C CP/MAS and all signals can be assigned due to the favorable signal resolution. Furthermore, the melt-molded samples can be analyzed by TGA, IR, ^{1}H wideline solid-state NMR, and ^{2}H MAS NMR after steam-treatment. When the samples are stirred at ambient temperature in D_2O or steam-treated with it at 150 °C, only the PBI sample takes up large amounts of water. Under harsh conditions of steam-treatment at 315 °C, D_2O is incorporated in trace amounts and mainly in the form of liquid domains into the PEEK and PEKK samples. The PBI, however, incorporates a smaller amount of D_2O into its polymer network when subjected to steam-treatment at 315 °C, as compared to the outcome at lower temperatures. The physical appearance of the samples implies that

PEEK is least resistant to steam-treatment at the highest temperature of 315 °C, showing signs of major decomposition. The PEKK sample keeps up best, and only undergoes a color change to black, while PBI becomes more brittle and rough on its surface. Overall it can be concluded that both PEEK and PEKK are valuable components in blends with PBI, being able to fend off water even under harsh reaction conditions. PEEK-PBI and PEKK-PBI blends, and their salt uptake are being investigated in a parallel project.

EXPERIMENTAL

General information and procedures

All polymer samples were provided by the company Hoerbiger Corporation of America, Inc. PBI, PEEK, and PEKK were dried thoroughly at 110 °C for 550 h under vacuum (0.01 torr) prior to treatment with D_2O. Unless mentioned otherwise in the text, the melt-molded polymer samples were all ASTM D638 Type V tensile specimens, machined from solid compression molded plaques. To prepare fine powders for solid-state NMR spectroscopy, solid samples were filed into powders with average particle diameters of about 0.5 mm. The polymers were either stirred in D_2O at RT for 48 h, or steam-treated in Parr pressure reactors (Model 4913) at 150 °C for 48 h and at 315 °C for 72 h. The maximal pressures in the closed vessels amounted to 5 bar (72 psi) and 110 bar (1600 psi), respectively. Unless mentioned otherwise, the drying procedure consisted of removing the H_2O or D_2O at 110 °C under vacuum for 48 h.

Instruments and measurements

The solid-state NMR spectra were measured on a *Bruker* AVANCE 400 spectrometer operating at 100.6 MHz for ^{13}C, 61.4 MHz for ^{2}H, and 400.1 MHz for ^{1}H. For the processing of the spectra line-broadening factors of 10 Hz (^{1}H) and 150 Hz (^{2}H, ^{13}C) have been applied. All experiments were carried out using densely packed powders of the polymers in 4 mm ZrO_2 rotors. In case no signal was observed in a spectrum, block averaging measurements were performed to prove that the absence of any resonance was not merely due to a spectrometer malfunction.

The ^{13}C CP/MAS (Cross Polarization with Magic Angle Spinning) spectra were recorded at MAS rates of 10 kHz. The ^{1}H $\pi/2$ pulse was 2.5 μs and TPPM (two pulse phase modulation) decoupling was used during the acquisition. The Hartmann-Hahn matching condition was optimized using the polymer Victrex 450P at a rotational speed of 10 kHz. Adamantane served as the external ^{13}C chemical shift standard (δ = 37.95 and 28.76 ppm). All spectra were measured with a contact time of 1.5 ms and a relaxation delay of 3.0 s, and typically 1024 FIDs were accumulated.

The ^{2}H solid-echo measurements were performed at MAS spinning speeds of 6 kHz. D_2O served as the ^{2}H chemical shift standard (δ = 4.79 ppm). All spectra were measured with a relaxation delay of 2 s and a quadrupolar echo τ delay of 6 μs. The τ delay was optimized using deuterated PMMA (polymethyl methacrylate) at a rotational speed of 6 kHz. Typically 32800 FIDs were accumulated for the PBI, PEEK, and PEKK samples.

The ^{1}H wideline NMR spectra were recorded using the MAS probehead without sample spinning. H_2O was used as the external chemical shift standard (δ = 4.79 ppm). No

background ^{1}H NMR signal of the probehead, loaded with an empty rotor, was obtained when a spectrum was recorded with the measurement parameters used for the polymer samples. A $\pi/2$ pulse of 2.7 μs, a deadtime of 5.6 μs, and a pulse delay of 3 s were used and typically 32 FIDs were accumulated.

Deconvolution (^{1}H wideline spectra) and processing of the spectra was accomplished using ACD/NMR Processor Academic Edition.[19] The quadrupolar coupling constants were derived from the ^{2}H MAS NMR spectra using the NMR simulation program Dmfit.[22]

The IR spectra were recorded on a Shimadzu IRAffinity-1 FTIR spectrometer by placing the powdered polymers on top of a Pike Technologies MIRacle ATR diamond plate. Typically 100 scans were accumulated for optimal spectrum quality.

The TGA curves were recorded on the TA Instruments Q500 TGA by placing approximately 10 mg of the melt-molded sample into an Al_2O_3 pan. The thermal decomposition studies were performed over a temperature range of 30-700 °C under air at a heating rate of 20 °C/min. Nitrogen was used as the balance gas at a rate of 40 mL/min and air was used as the sample gas at a rate of 40 mL/min.

CHAPTER IV

IMMOBILIZED SONOGASHIRA CATALYST SYSTEMS FOR C-C COUPLING REACTIONS: NEW INSIGHTS AND IMPROVED RECYCLABILITY

INTRODUCTION

Pd-catalyzed carbon-carbon bond forming reactions have dominated homogeneous catalysis over the last decade.[29,30] In particular, the Pd-catalyzed cross-coupling reactions, which can be used to build a variety of compounds, have become of immense interest. Some of the most important representatives of these Pd-catalyzed cross-coupling reactions that form sp^2-hybridized products are shown in Scheme 4.1.[31]

One of the most widely used Pd-mediated cross-coupling reactions is the Sonogashira coupling of aryl halides with terminal acetylenes.[32,33] This reaction is catalyzed by a Pd(0)/Cu(I) system and is believed to follow the mechanism outlined in Scheme 4.2.[32] However, despite the importance and intensive use of the Sonogashira catalyst system, detailed mechanistic studies remain scarce.[32]

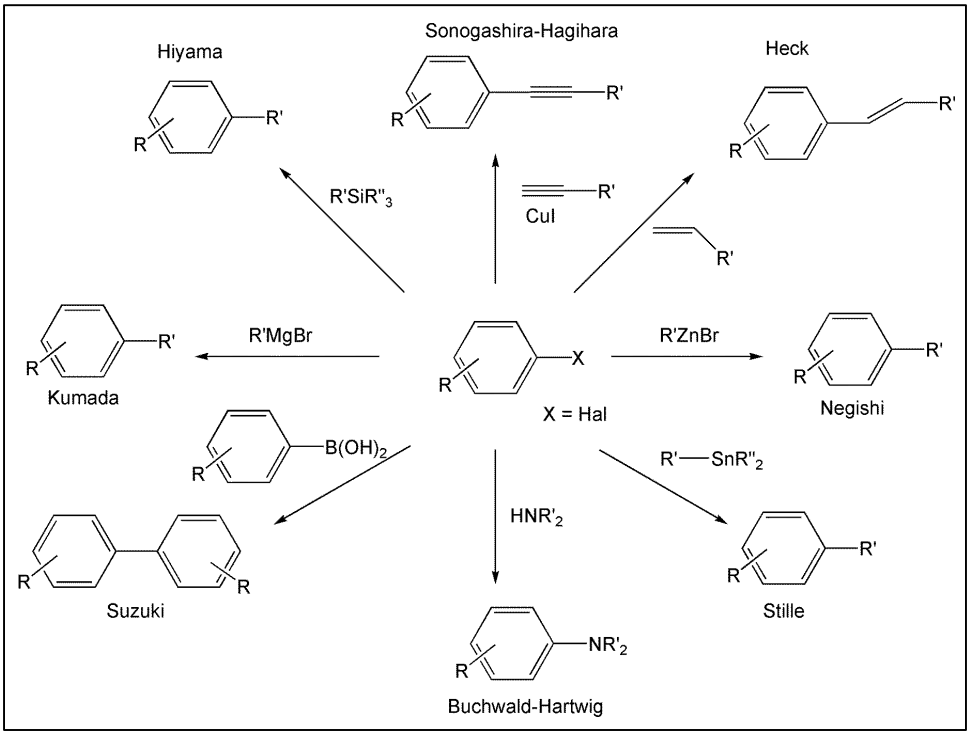

Scheme 4.1. Representative Pd-catalyzed cross-coupling reactions.

In homogeneous solution, mechanistic studies are complicated by the presence of many different species,[32] and it is often unclear whether Pd-catalyzed reactions are achieved by molecular entities or metallic Cu[34,35] or Pd[36] nanoparticles that form during the course of the reaction. Catalyst immobilization helps to disentangle the different components and effects.[37] Furthermore, tethering the catalyst system to a solid support offers the advantage that the catalysts can easily be removed from the reaction mixtures and recycled.[37]

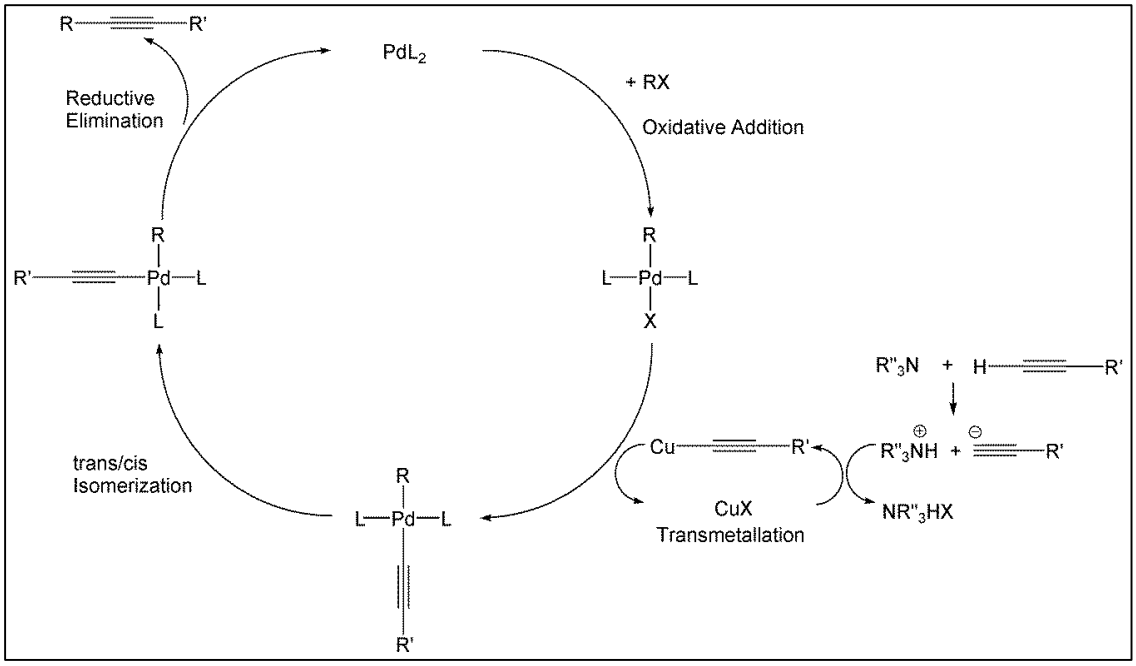

Scheme 4.2. Proposed catalytic cycle of the Sonogashira reaction.[32]

In order to categorize different catalysts it is necessary to make the distinction between homogeneous and heterogeneous catalysts. Homogeneous catalysts are often highly active and selective; they are in general well understood and amenable to finetuning.[38] On the other hand, homogeneous catalysts often decompose under the reaction conditions or during work-up and only rarely can they be recovered and reused. Heterogeneous catalysts on the other hand are often cheaper to produce and are conveniently separated and recycled.[38] However, they are usually less active and selective due to the presence of many different species which display different activities and selectivities.[38]

An immobilized catalyst combines the advantages of both homogeneous and heterogeneous catalysts.[39,40] The idea is to tether a homogeneous catalyst to support materials such as zeolites, carbon black, metal oxides like silica,[35,41] or polymers[42] that are not soluble in the reaction mixture. For most applications, silica turns out to be the most favorable support. Once tethered, it is possible to retain the activity and selectivity of the homogeneous catalyst and to overcome the problem of separation and recycling.[43]

Immobilized species have had a major impact in such diverse areas as combinatorial chemistry,[44,45] solid-phase synthesis,[46] and catalysis.[47-48] Therefore, they are of immense academic and industrial interest. Being recyclable, immobilized catalysts reduce energy and resource consumption, and help to make chemistry "greener". Many analytical methods are available that enable the researcher to characterize surface-bound catalysts, elucidate their mechanistic features, and thus direct the researcher to improved catalysts.[50-53] The most useful methods are solid-state NMR,[49,50] *in situ* IR spectroscopy,[51] X-ray powder diffraction,[51] electron microscopy,[51] and methods for probing surface and particle characteristics.[52]

The major goals of this project are to **(1)** synthesize and immobilize phosphine linkers, which readily bind to Pd and Cu centers,[37a,51-53] **(2)** determine optimal conditions for this catalytic reaction, and **(3)** test the activities and lifetimes of the corresponding immobilized Pd and Cu catalysts with the Sonogashira cross-coupling reaction. Using the Sonogashira Pd(0)/Cu(I) catalyst system, this project will address basic questions in homogeneous and heterogeneous catalysis. Dynamic effects as well as ligand coordination strength will be investigated, so that highly active and recyclable catalyst systems can be synthesized.

RESULTS AND DISCUSSION

Synthesis

The ligands synthesized for this project are listed in Figure 4.1. The class of chelate ligands includes phosphine ligands with phenyl (**1**) and cyclohexyl (**2**) substituents. The phosphine **3** was synthesized to allow comparisons with a monodentate ligand. It will be demonstrated in this chapter that the chelate functionalities of phosphine ligands **1** and **2** coordinate more strongly to both Pd and Cu complexes than the monodentate ligand **3**.

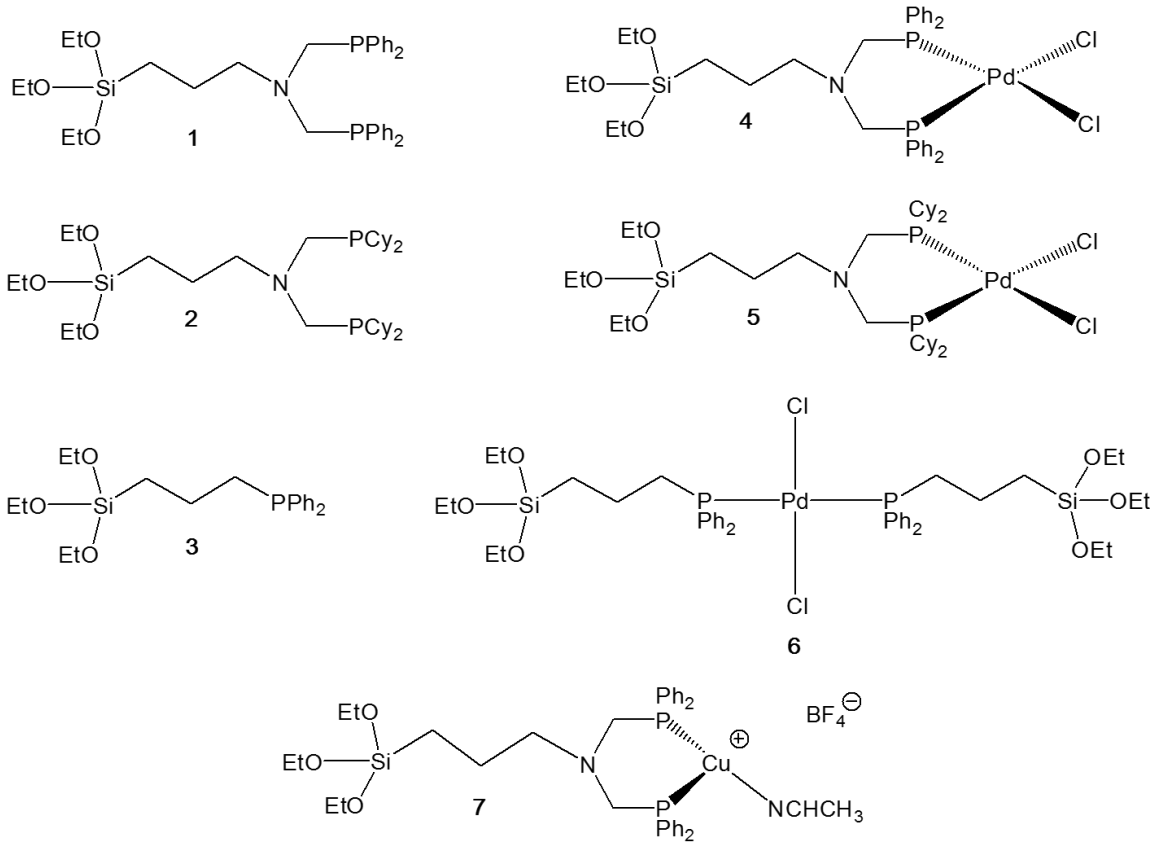

Figure 4.1. Relevant molecular species for studies of the Songoashira Pd/Cu catalyst system.

Ligand **1** has been synthesized in high yields via three routes. Therefore, the synthetic approach can be modified if needed for ligands with substituents at P other than phenyl. Route 1 is the traditional route utilizing (3-aminopropyl)triethoxysilane, diphenylphosphine, and paraformaldehyde.[37a] The solvent and unreacted educts can be removed *in vacuo* leaving a clear viscous oil as the product in yields of up to 96%.

Route 2 is a Mannich-type reaction.[53] Ligand **1** is synthesized by refluxing the phosphonium salt $[Ph_2P(CH_2OH)_2]Cl$, (3-aminopropyl)triethoxysilane and triethylamine in H_2O/EtOH. After aqueous workup, a clear viscous oil is obtained in yields of up to

97%. The phosphonium salt in this route is easier to handle than diphenylphosphine due to its stability in air.

Route 3 is similar to route 1, however, the phosphinoalcohol $HOCH_2PPh_2$[54] is used instead of diphenylphosphine and paraformaldehyde. The phosphinoalcohol allows for a more accurate stoichiometric ratio to be achieved, in contrast to route 1, because only one reactant has to be weighed in. The phosphinoalcohol and (3-aminopropyl)triethoxysilane are reacted under the same conditions as described in route 1. The product is obtained in yields of up to 95%. The products from all three routes give clean ^1H, ^{13}C, and ^{31}P NMR spectra in $CDCl_3$ (Figure 4.2) and the signal assignments can be made in agreement with the literature.[37b]

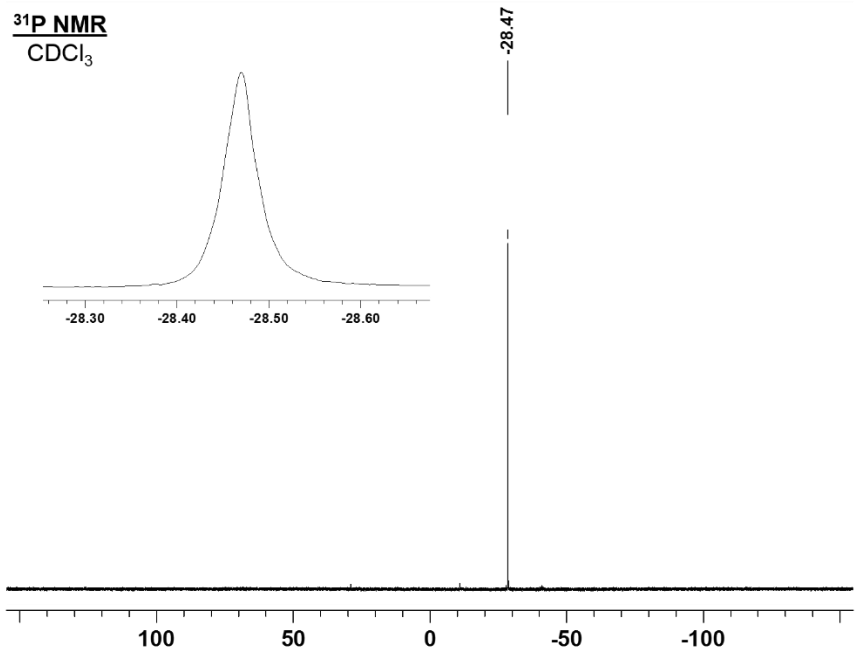

Figure 4.2. ^{31}P NMR spectrum of ligand **1** in $CDCl_3$.

Ligand **1** can easily coordinate to Pd, forming complex **4**. Ligand **1** is stirred with $PdCl_2(NCPh)_2$ in toluene at RT for 2 h. After 2 h, the a yellow solid precipitates upon addition of pentane and a yellow-orange powder is obtained after filtration and drying in yields of up to 70%,[37b] resulting in a single ^{31}P NMR peak in solution at 7.79 ppm. While ligand **1** easily coordinates to Cu, complex **7** is insoluble when synthesized in solution. This could be attributed to the formation of Cu agglomerates, rendering the red-orange solid insoluble in all solvents, both polar and non-polar.

Ligand **2**, with cyclohexyl substituents, has been successfully synthesized in high yields, according to the same procedure as applied for ligand **1** (Route 1), except with dicyclohexylphosphine instead of diphenylphosphine. The ^{1}H-^{1}H COSY and ^{13}C-^{1}H HSQC spectra of the ligand in solution have been obtained (Figures 4.3, 4.4, and 4.5), which allow all NMR signal assignments of the ligand. The ^{1}H-^{1}H COSY NMR spectrum shows overlapping proton signals for the cyclohexyl ring between 1.15-1.79 ppm. However, when utilizing the ^{13}C-^{1}H HSQC, the overlapping signals can be distinguished. The ^{13}C NMR signals for the cyclohexyl rings were assigned according to the literature.[55]

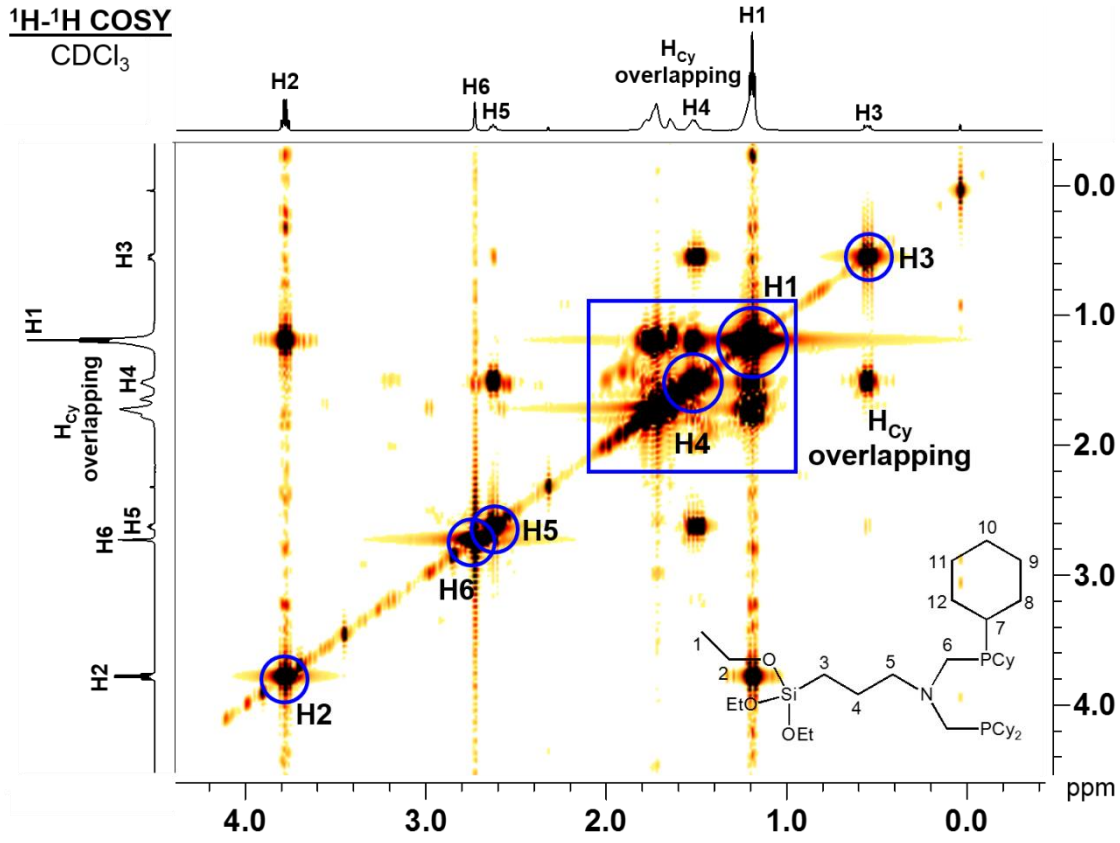

Figure 4.3. ^{1}H-^{1}H COSY NMR spectrum of ligand **2** in $CDCl_3$.

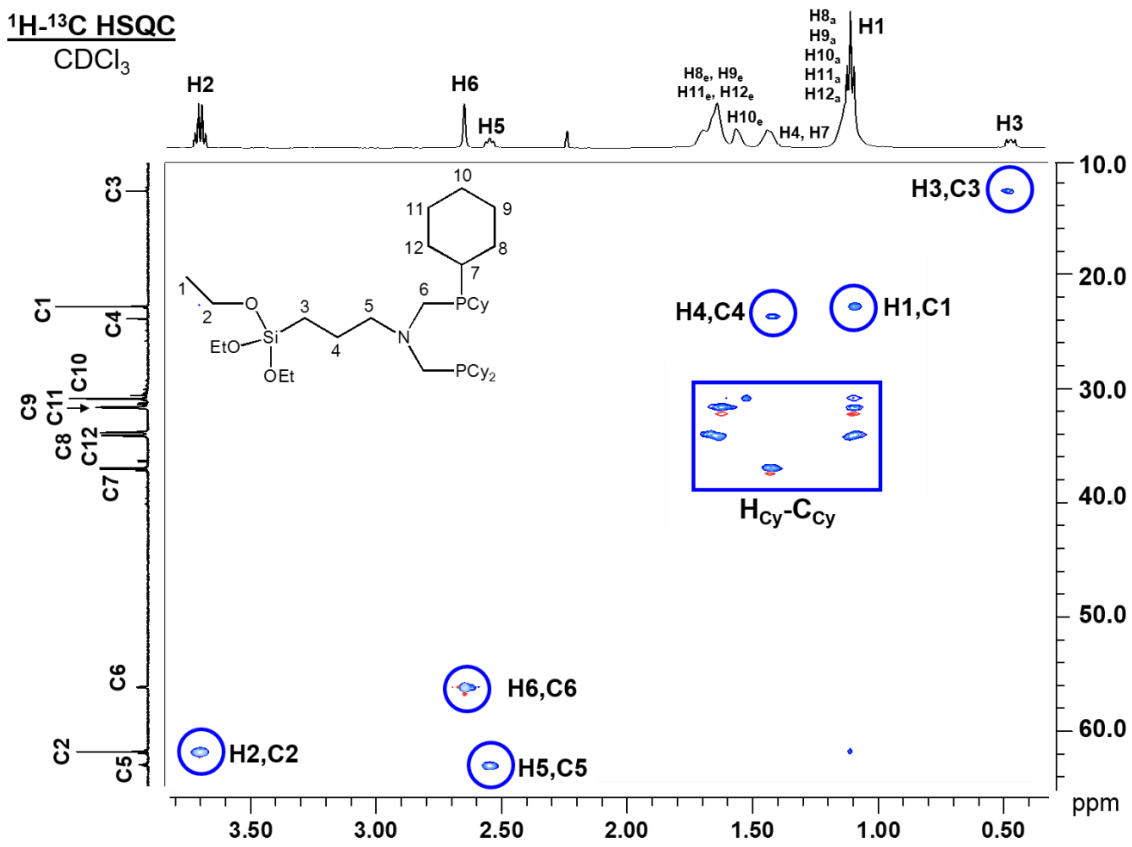

Figure 4.4. ^{13}C-^{1}H HSQC of ligand **2** in $CDCl_3$.

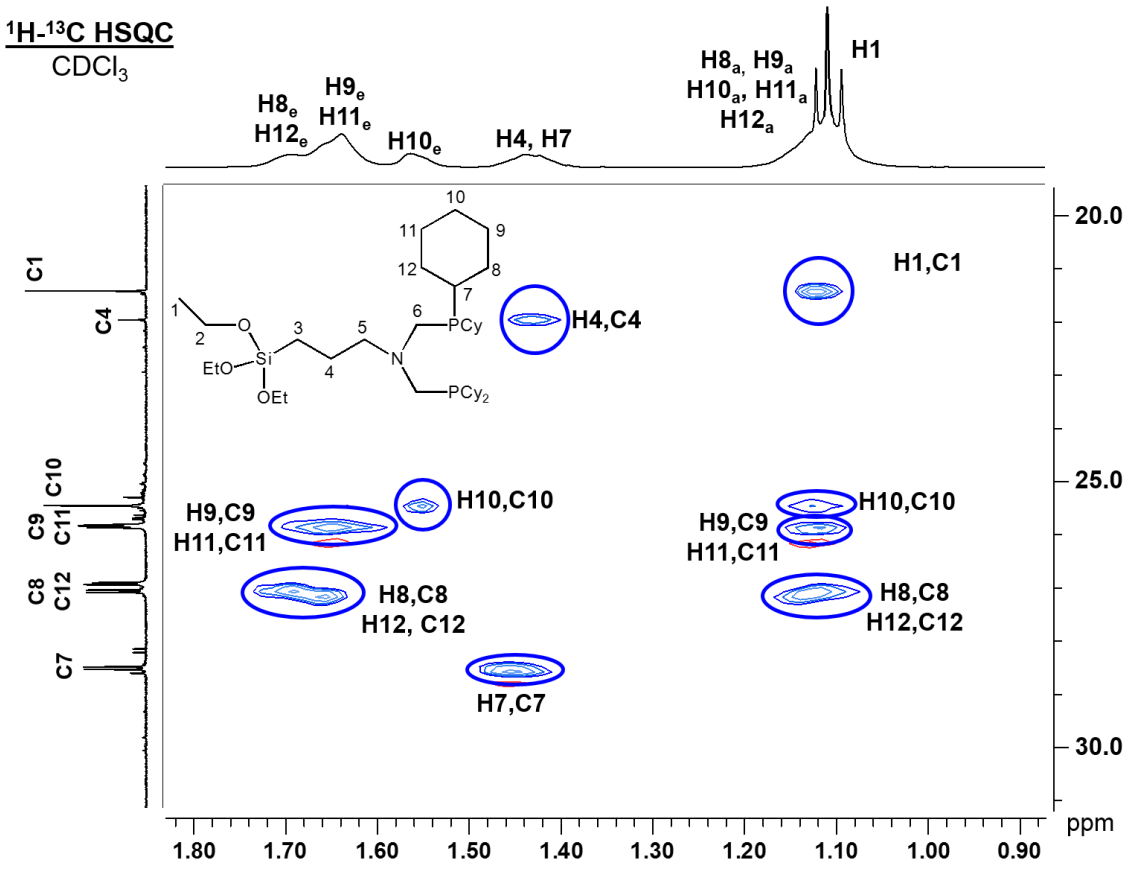

Figure 4.5. Cyclohexyl region of the ^{13}C-^{1}H HSQC NMR spectrum of ligand **2** in $CDCl_3$.

Similarly to ligand **1**, ligand **2** readily coordinates to Pd, forming complex **5** when using the same procedure as described previously. The product is a yellow powder obtained in yields of up to 87%, with a single ^{31}P NMR peak in solution at 29.60 ppm. The ligand was fully characterized using ^{31}P, ^{13}C, and ^{1}H NMR in $CDCl_3$. The data can be seen in both the experimental section and in Appendix B.

Ligand **3** and complex **6** are synthesized according to literature procedures.[55,56] They are characterized by solution NMR, and all signals are in agreement with the

literature.[55,56] Pd complex **6** resulted in single crystals after crystallization at -19.6 °C in a mixture of pentane and toluene (Figure 4.6). The P and Pd atoms are positioned *trans* to each other. This will play an important role when this complex is immobilized on SiO_2. The complex is perfectly planar.

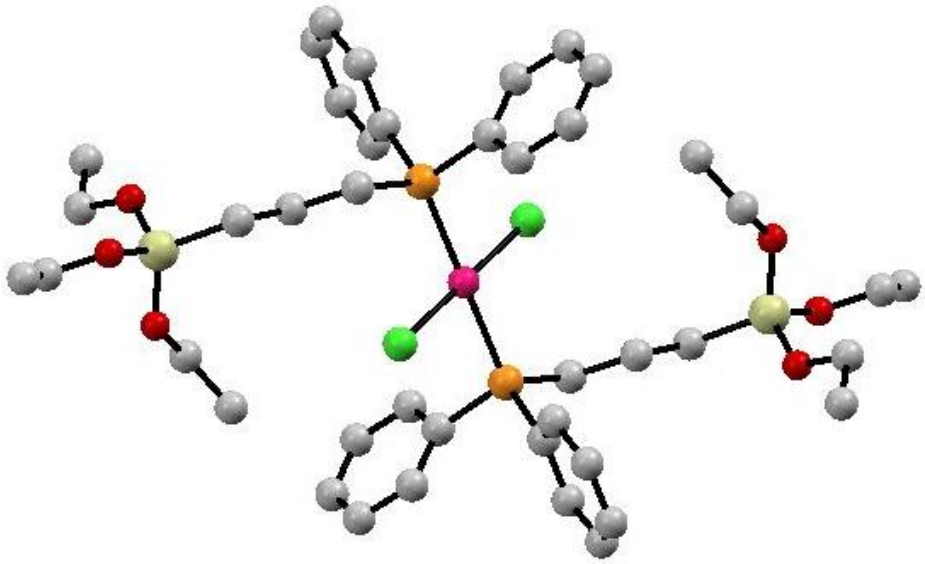

Figure 4.6. Single crystal X-ray structure of Pd complex **6**.

Immobilization

As established in earlier publications of our group, phosphines can be cleanly immobilized on oxide supports via $(EtO)_3Si$ groups under suitable reaction conditions.[6, 37,43,57-58] Based on this experience, ligands **1-3**, and the Pd (**4-6**) and Cu (**7**) components of the Sonogashira catalyst system have been immobilized on silica (Figure 4.7).

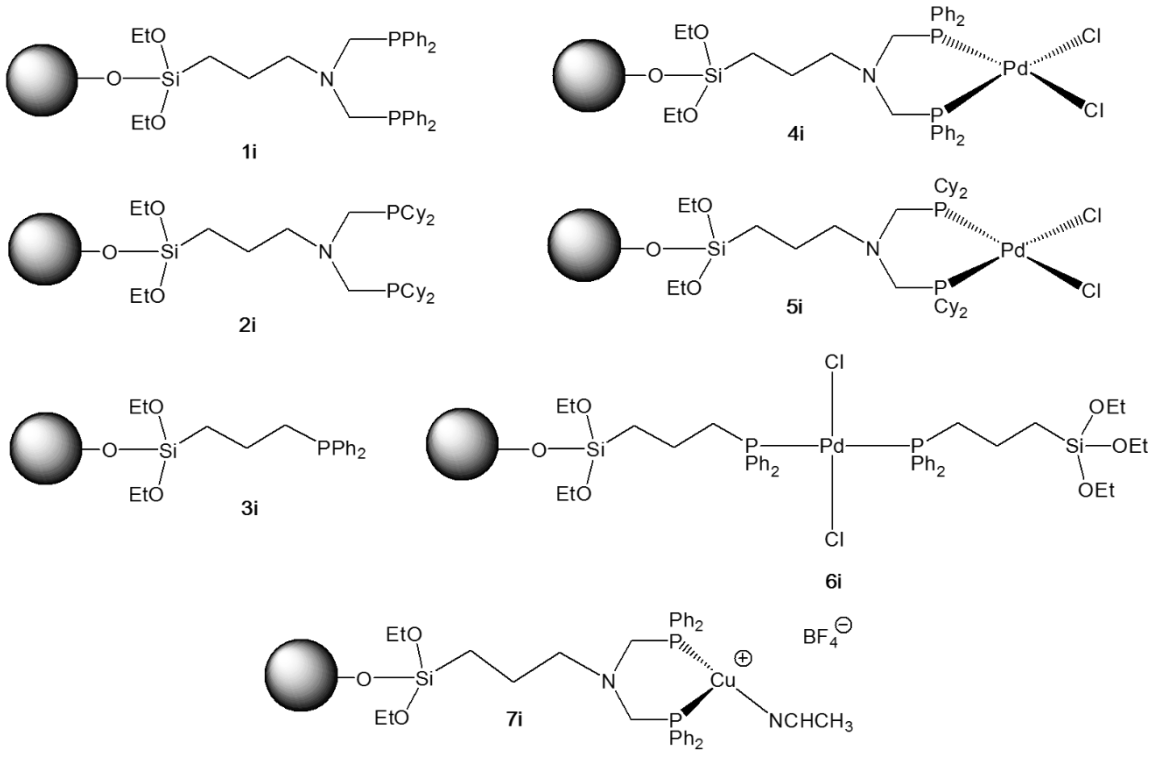

Figure 4.7. Immobilized species used for studies of the Sonogashira Pd/Cu catalyst system.

The Bluemel group has always used and optimized solid-state NMR as a powerful technique for characterizing surface-bound species[6,39,43,57-58] and has, for example, improved classical CP/MAS measurements of the dry materials.[59] Recently, the group has pioneered the solid-state NMR measurement of immobilized linkers and catalysts in the presence of solvents (HRMAS, High Resolution MAS).[39,43] The advantages of our technique lay in the reduction of the chemical shift anisotropy (CSA) and the residual linewidth. Therefore, the lines obtained are much narrower than the corresponding CP/MAS signals of dry materials, as demonstrated for the immobilized ligand **1i** (Figure 4.6).

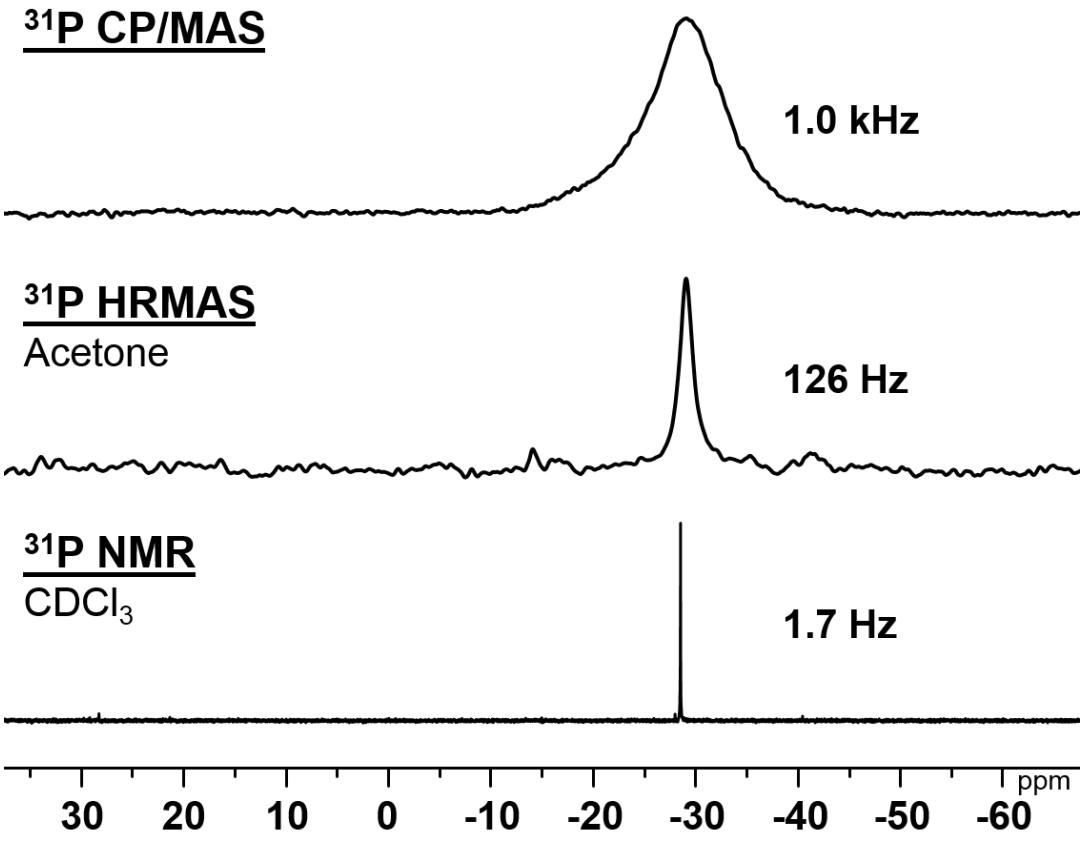

Figure 4.8. ^{31}P CP/MAS NMR of immobilized chelate ligand **1i** on silica (top, rotational speed 4 kHz), ^{31}P HRMAS of **1i** as a slurry in acetone (middle, 2 kHz) and ^{31}P NMR of **1** dissolved in $CDCl_3$ (bottom).

Further improvement of the HRMAS spectra can be obtained when the solvents are optimally chosen. As shown in Figure 4.7, nine different solvents have been screened for the immobilized ligand **1**. Typically, the less viscous a solvent is, the more mobile a ligand on the SiO_2 support will be. Furthermore, solvent polarity plays a crucial role on the mobility of ligands on the SiO_2 support. Usually, the more polar a solvent is, the more mobile the ligands are. This is due to the inability of the ligand to interact with the surface

the silica surface, and thus get slowed down, when a polar solvent is bound more strongly to the support. Minimal viscosity and maximal polarity are combined in the solvents diethyl ether and THF, and therefore the narrowest signals are obtained from slurries of **1** in these solvents (Table 4.1). The chemical shifts and halfwidths are shown in Table 4.1.

Table 4.1. Chemical shifts $\delta(^{31}P)$ and halfwidths $\nu_{1/2}$ of the ^{31}P HRMAS NMR signals of **1i** in the indicated solvents. Surface coverage 0.103 g (0.167 mmol, 13.4 molecules of **1** on 100 nm^2 of surface) of **1** on 1 g SiO_2.

Solvent	**$\delta(^{31}P)$ [ppm]**	**$\nu_{1/2}$ [Hz]**
Diethyl ether	-29.52	111
THF	-29.41	115
Methanol	-29.63	119
Acetone	-29.65	126
Acetonitrile	-29.75	128
DMF	-29.63	138
Dichloromethane	-29.55	142
Toluene	-29.33	265
Hexanes	-29.19	944

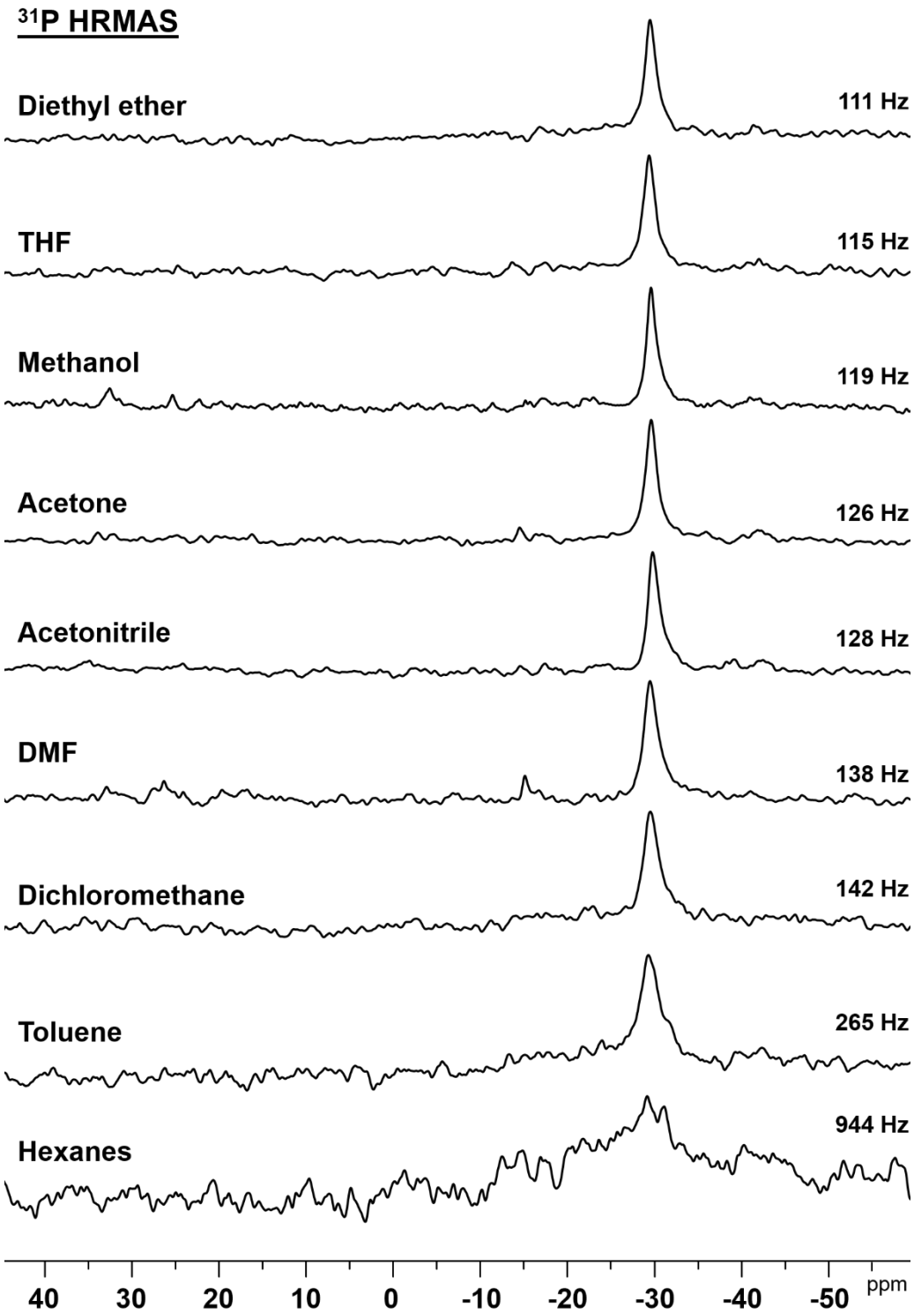

Figure 4.9. ^{31}P HRMAS NMR spectra of the immobilized chelate ligand **1i** as a slurry in the indicated solvents. Solvents are arranged in decreasing halfwidths.

Complex **4** can be immobilized via two different routes (Scheme 4.3). The first route involves the immobilization of ligand **1** in toluene at 60 °C, followed by the addition of $PdCl_2(NCPh)_2$ in solution at RT to give immobilized **4i**. The second route starts with the formation of complex **4** in solution. Then, complex **4** is added in toluene to a silica slurry and allowed to react at 60 °C for 16 h to form the immobilized **4i**. Both result in a single peak at 6.83 ppm in the ^{31}P HRMAS NMR spectrum of a slurry of **4i** in acetone.

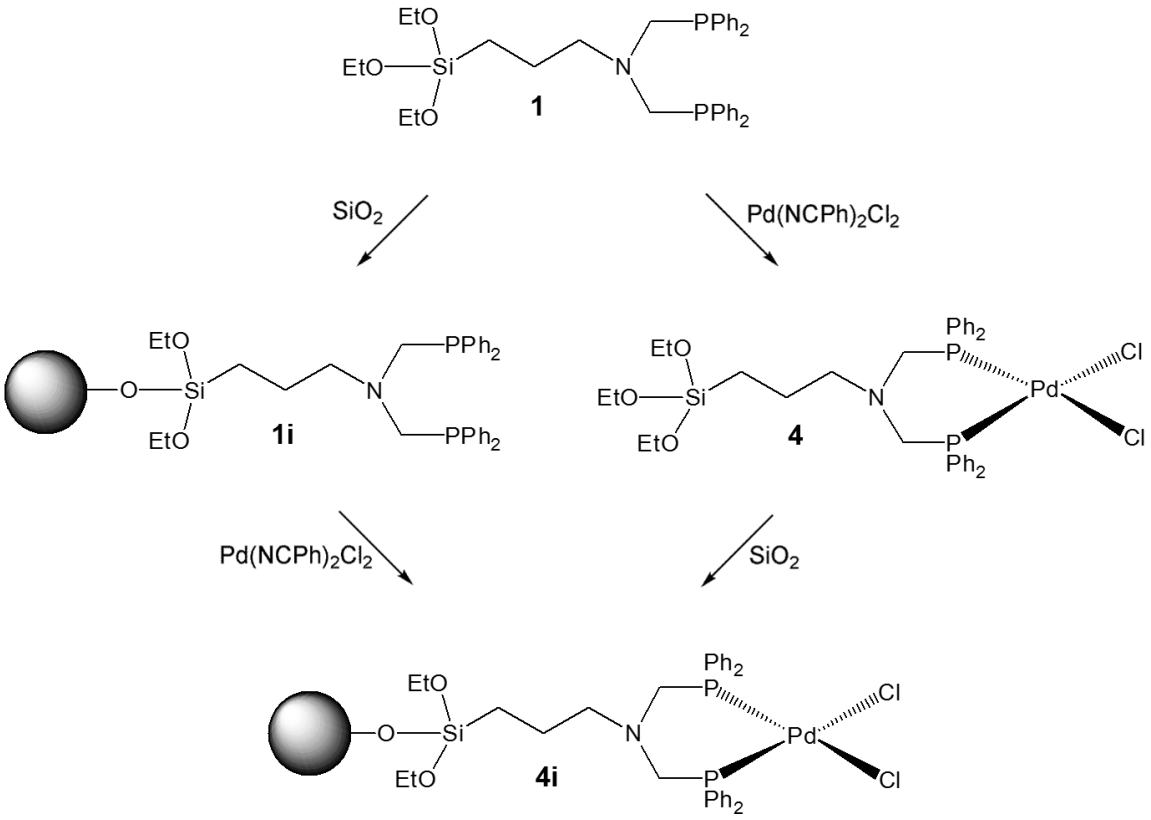

Scheme 4.3. Immobilization of Pd complex **4.**

Due to the insolubility of complex **7**, the immobilized Cu complex **7i** can only be formed via one route (Scheme 4.4.). This route starts with the immobilization of ligand **1** using the same procedure described above, followed by the addition of $[Cu(NCCH_3)_4]BF_4$ in acetone at RT. This leads to the immobilized Cu complex **7i** which results in a single signal at -17.11 ppm in the ^{31}P HRMAS NMR spectrum of its slurry in acetone.

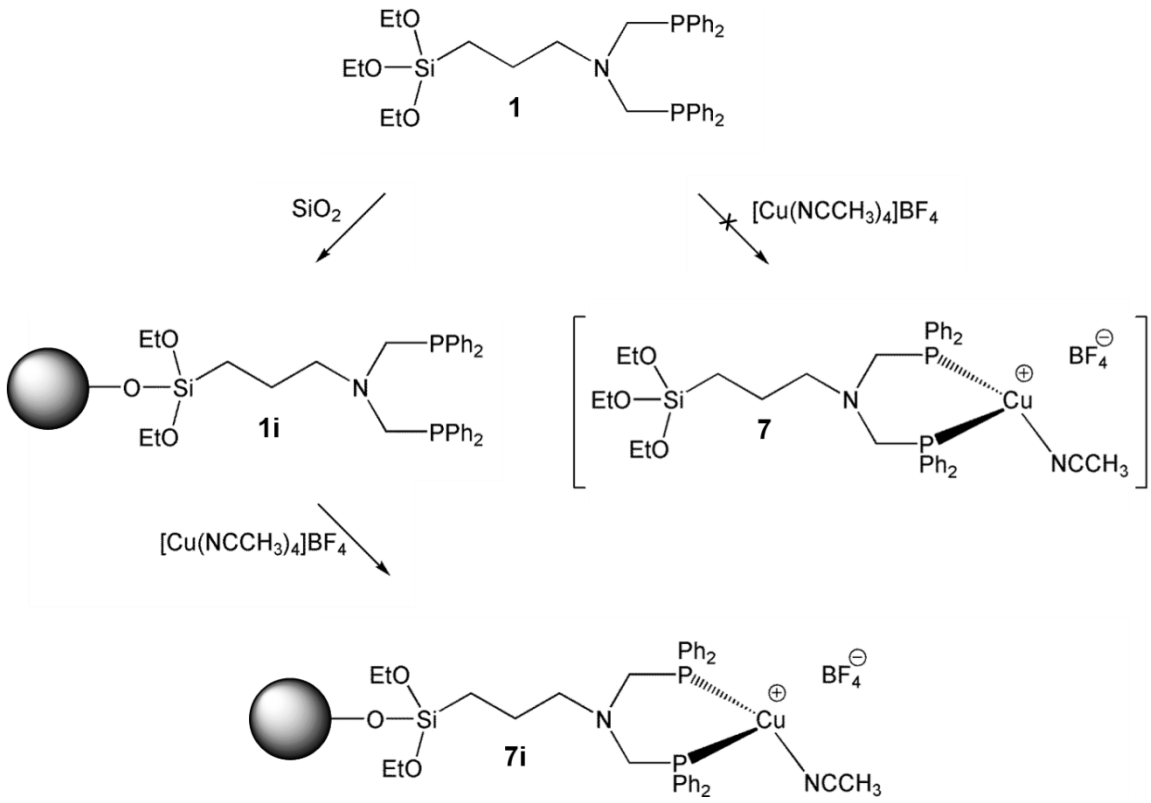

Scheme 4.4. Immobilization of Cu complex **7**.

Ligands **2** and **3** are cleanly immobilized on silica via the same procedure as described above for ligand **1**. However, the immobilization of **5** and **6** has to be different. Complex **5** can only be immobilized via one route due to complications when trying to form the Pd complex **6** on the SiO_2 support. When attempting to coordinate the Pd complex to the immobilized **2i**, no signal is visible in the ^{31}P HRMAS NMR spectrum. This might be due to a dynamic effect that is not fully understood at this point. However, when the Pd complex **5** is first synthesized in solution, and then immobilized on silica at 60 °C in toluene, a signal at 27.57 ppm is visible in the ^{31}P HRMAS NMR spectrum of a slurry of **5i** in acetone (Scheme 4.5).

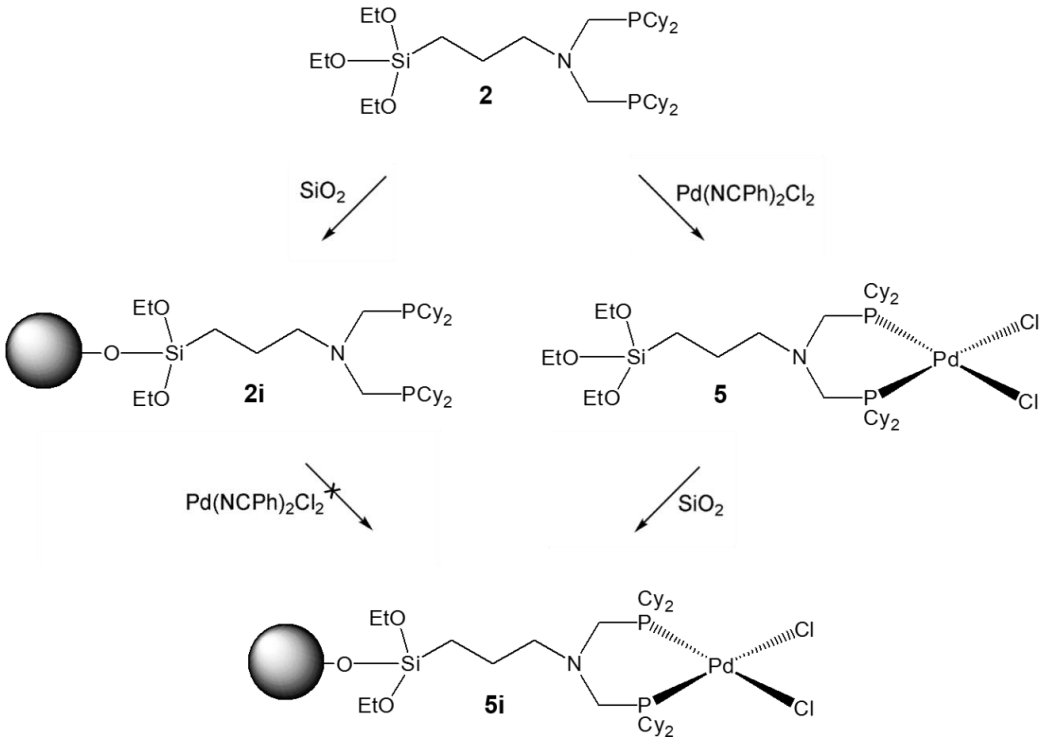

Scheme 4.5. Immobilization of Pd complex **5**.

The same holds true for the immobilization of complex **6** (Scheme 4.6). When first immobilizing ligand **3** in toluene at 60 °C, then adding $Pd(NCPh)_2Cl_2$ to the functionalized silica support, no signal is visible in the ^{31}P HRMAS NMR spectrum of an acetone slurry. However, when first synthesizing complex **6** in solution, then immobilizing the complex directly onto silica by stirring at 60 °C in toluene for 16 h, a single ^{31}P peak at 14.80 is visible in the ^{31}P HRMAS NMR spectrum of a slurry of **6i** in acetone.

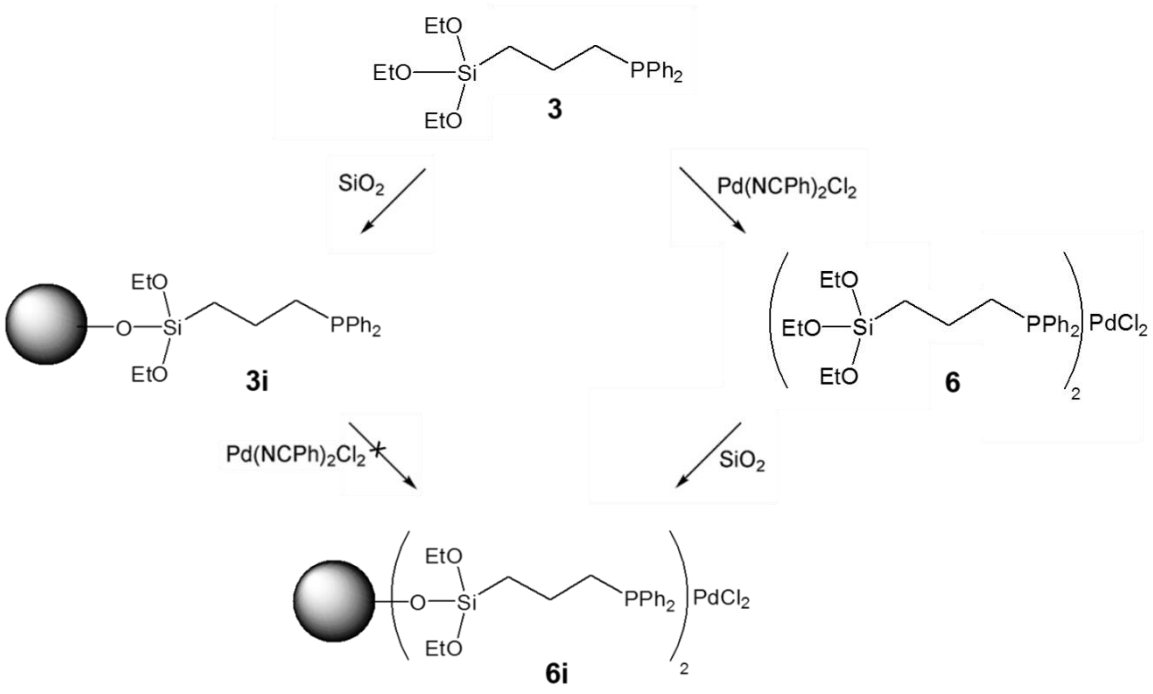

Scheme 4.6. Immobilization of Pd complex **6.**

Table 4.2 lists the chemical shifts and halfwidth of the immobilized ligands and complexes. Figure 4.10 shows the ^{31}P HRMAS NMR spectra of these immobilized ligands and complexes in acetone. The spectra prove that all ligands are cleanly immobilized by the presence of one dominant peak in each case.

Table 4.2. Chemical shifts δ(^{31}P) [ppm] and halfwidths [Hz] of the ^{31}P HRMAS NMR signals of immobilized ligands and metal complexes in acetone.

Ligand or Complex	**δ(^{31}P) [ppm]**	**$\nu_{1/2}$ [Hz]**
1i	-29.29	35.6
2i	-18.76	77.1
3i	-18.21	201.5
4i	6.83	53.4
5i	27.57	17.8
6i	14.80	23.7
7i	-17.11	62.9

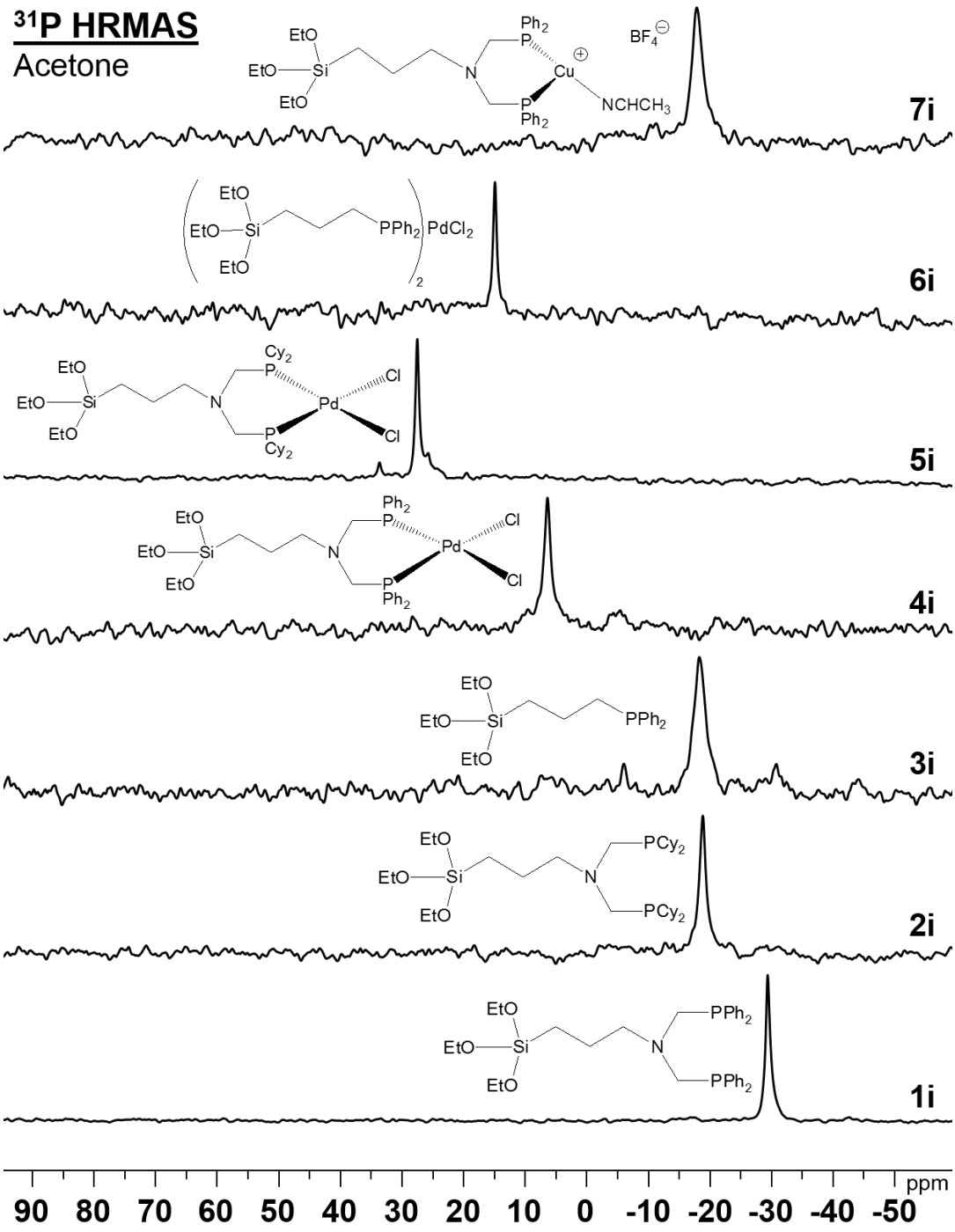

Figure 4.10. ^{31}P HRMAS NMR spectra of slurries of the immobilized ligands **1i** -**3i** and metal complexes **4i**-**7i** in acetone at a spinning speed of 2 kHz.

In order to have a better understanding of the amount of the ligands on the silica support, Table 4.3 contains the values of the surface coverage, which corresponds to 100 % of the maximal coverage of the silica with a monolayer of the molecular linker or complex. The 100% maximal surface coverage was determined by dissolving an excess amount of linker and adding it to a silica slurry. After immobilization, the silica was washed with solvent, and the supernatant was collected. Then the excess ligand in the supernatant was weighed to determine the maximal surface coverage.

Table 4.3. Surface coverages of the modified silica **1i**-**3i** and catalysts **4i**-**7i** with linkers and complexes.

Linker/complex	molecules per 100 nm^2 of SiO_2	mg of linker/complex per g of SiO_2	mmol of linker/complex per g of SiO_2
1i	13.4	103	0.167
2i	11.8	94	0.147
3i	10.5	51	0.131
4i	9.4	94	0.118
5i	11.2	115	0.140
6i	5.6	67	0.070
7i	11.0	111	0.137

[a)] All surface coverages correspond to 100% of the maximal coverage of the surface with a monolayer of the molecular linker or complex.

Ligand coordination strength

In 1977, Chad Tolman published a review[60] covering the methods which he had developed for ordering a wide variety of phosphine ligands in terms of their coordinating strength. This was based on their electron donating ability. In order to test the phosphine ligands' electron donating abilities, he reacted one equivalent of the phosphine with $Ni(CO)_4$ to make the tricarbonyl complex $Ni(CO)_3PR_3$. He then measured the carbonyl IR stretching frequency ν_{CO} of the complexes and determined that the more electron density the phosphine donates to the metal center, the more π back-bonding to the CO ligands takes place. This weakens the CO triple bond, thus lowering the ν_{CO} value. The lower the ν_{CO} IR stretching frequency, the more donating a phosphine ligand is, thus resulting in stronger coordination to the metal center. The order of the coordinating strengths for representative phosphine ligands is as follows: $PCy_3 > {}^nPBu_3 > PPh_3$. This will be illustrated in the palladium migration experiments discussed below.

Having thoroughly characterized all immobilized species, next we sought to study (a) whether the $PdCl_2$ fragment can be detached from a phosphine linker, and (b) whether it is scavenged again by a more strongly coordinating linker *in situ*, in which case a ranking of the ligands with respect to their coordinating strength was desired. For this purpose, migration and competition experiments have been performed where two different linkers or Pd complexes were immobilized on separate silica batches. Then the batches were mixed and combined with acetone.

The potential migration of the $PdCl_2$ fragment has been monitored over time *in situ* with ^{31}P HRMAS. Representative spectra are displayed in Figure 4.11.[61]

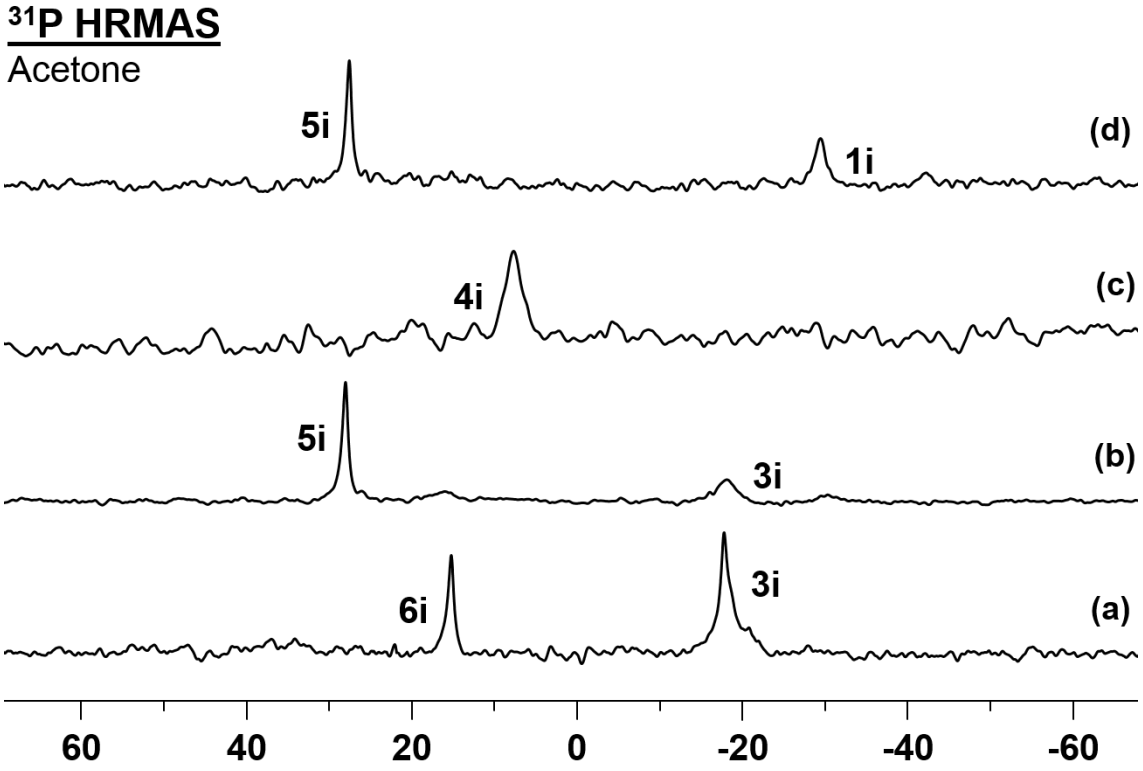

Figure 4.11. ^{31}P HRMAS spectra of the following batches after being mixed together in acetone: **6i** and **3i** (a), **5i** and **3i** (b), **4i** and **8i** (c), and **5i** and **1i** (d).

Regarding the batches **6i** and **3i** (Figure 4.11a), initially both their ^{31}P HRMAS signals are present at 14.8 and -18.2 ppm, with small halfwidths of 24 and 202 Hz, respectively. In the course of couple hours their intensity diminishes and a broad resonance emerges, indicating that the Pd center has migrated from one to

the other batch and is diluted on the surfaces of both batches, displaying the dynamic "Pd hopping" process described earlier.[39a] This process could again be stopped by adding borane as the protecting group, resulting in an intense signal at 14.4 ppm for **3i-BH$_3$**. In contrast to this, no dynamic process is observed when **5i** is mixed with **2i**, which means that Pd does not leave the chelate ligand. When batches of **4i** or **5i** (Figure 4.11b) are mixed with **3i**, Pd remains coordinated to the chelate linkers even after days. Only the narrow signals of **4i** (6.8 ppm, 53 Hz) and **5i** (28 Hz, 18 Hz) are visible besides the resonance of **3i**. When the experiment is reversed and **2i** is mixed with **6i**, the signal of **5i** becomes visible immediately. This means that the migration of Pd from the monodentate to the chelate linker takes place readily.[61]

When the chelate complex **4i** is competing with the immobilized amine linker **8i** it retains the coordinated Pd and only the signal for **4i**, but no trace of **1i** is visible in the ^{31}P HRMAS spectrum (Figure 4.11c). A mixture of batches of **1i** with **9i** results in the signal of **4i** emerging within one hour, which means that the leaching of the Pd from the monodentate amine linker and the scavenging by the chelate linker **2i** are fast processes. Finally, the chelate linkers **1i** and **2i** were set up to compete with each other. When **5i** is mixed with **1i**, the spectrum shown in Figure 4.11d persists with an undiminished intensity of the narrow signal for **1i** at -29.3 ppm.[61]

Therefore, it is concluded that the ligand retaining and scavenging the $PdCl_2$ fragment best is **2i**, followed by **1i**, while **3i** and **8i** are prone to leaching.[61]

Catalysis

The Sonogashira cross-coupling reaction is catalyzed under a wide range of conditions. It can be catalyzed by both homogeneous and heterogeneous metal catalysts, and a Pd(0)/Cu(I) is often applied. However, other metal catalysts have been used, such as Au,[62] In,[63] Fe,[64] Ni,[65] Ag,[66] Co,[67] Rh,[68] and Ru.[69] Furthermore, the reaction has been catalyzed by Pd-[70] and Cu-free[71] systems. In addition, the catalysis has been shown to work under ligand-,[72] phosphine-,[73] base-,[74] amine-,[75] and solvent-free[76] conditions.

The catalyst system **4i**/**7i** has shown high activity for the Sonogashira coupling of phenylacetylene with iodobenzene in the presence of piperidine, which functions as both the solvent and the base.[37a] It is especially noteworthy that only at ambient temperature (25 °C) is the reaction catalyzed by both Pd (**4i**) and CuI (Figure 4.12), resulting in nearly 100% yield after the first cycle, and approximately 20% yield after the second cycle. The reaction is only minimally catalyzed by Pd (**4i**) at RT, but at elevated temperatures the reaction is catalyzed by Pd to almost 100% conversion (Figure 4.13).

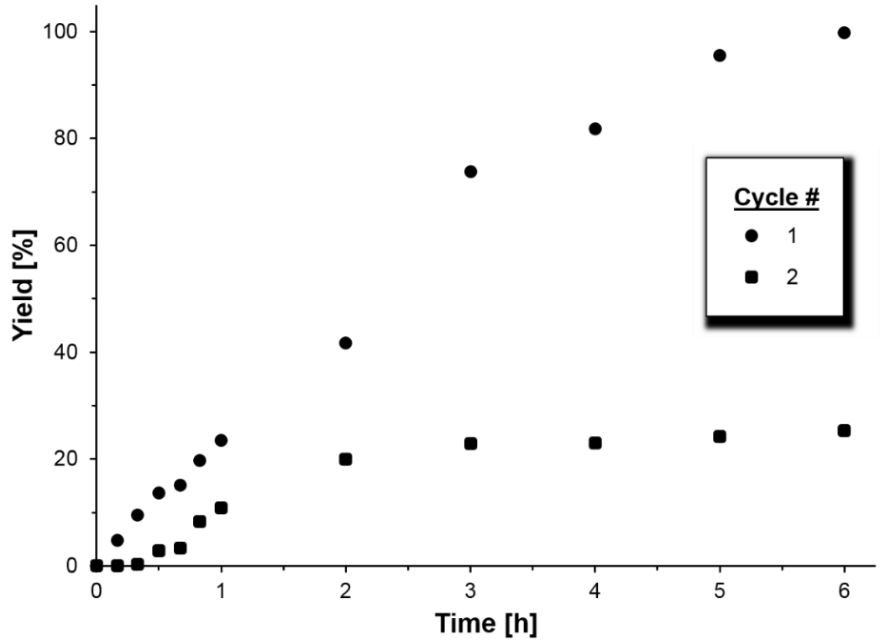

Figure 4.12. Catalysis with Pd complex **4i**, CuI, and piperidine in toluene at RT.

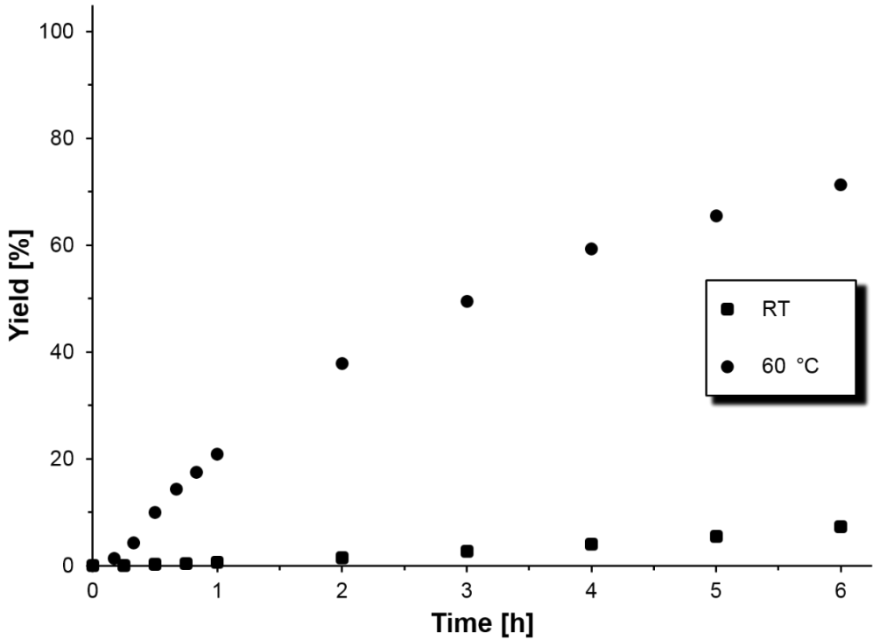

Figure 4.13. Catalysis with Pd complex **4i** and piperidine in toluene at RT and at 60 °C.

However, when the reaction is carried out only with Cu(I) (**7i**) at ambient or higher temperatures (Figure 4.14), no catalytic activity is noted during 6 h of the reaction. This demonstrates that it is necessary to have Pd in the reaction mixture in order for the reaction to be catalyzed.

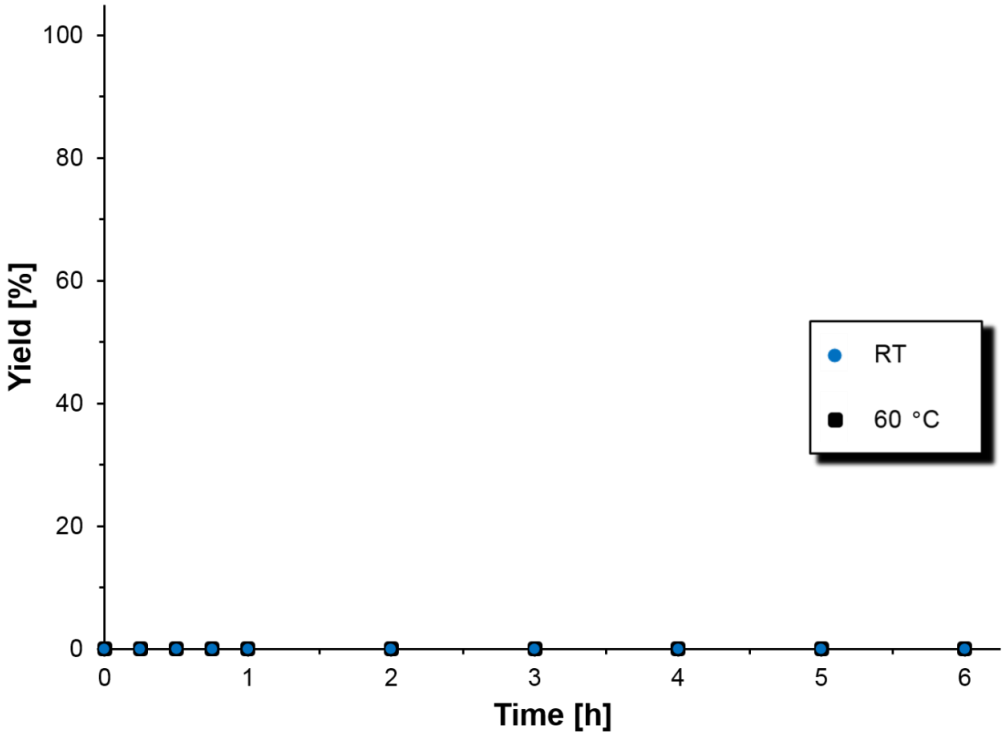

Figure 4.14. Catalysis with Cu complex **7i** and piperidine in toluene at RT and at 60 °C.

After probing various conditions for the Sonogashira cross-coupling reaction, such as different Pd and Cu amounts, as well as the solvent to base ratios, the optimal conditions for the Sonogashira reaction have been determined and they are given in Table 4.4. After

screening various aryl halides at different temperatures, the reaction has also been shown to proceed fastest when iodobenzene is coupled with phenylacetylene at RT (25 °C).

Table 4.4. Optimal conditions for Sonogashira cross-coupling of phenylacetylene and iodobenzene.

Cu Complex	Pd Complex	Phenyl-acetylene	Iodobenzene	Toluene	Piperidine
12 mg	100 mg	0.17 mL	0.14 mL	2.5 mL	2.5 mL
0.0063 mmol	0.0126 mmol	1.55 mmol	1.26 mmol	24 mmol	25 mmol
0.5 mol%	1.0 mol%	120 mol%	100 mol%	1900 mol%	2000 mol%

When the Sonogashira reaction is carried out under the optimal conditions, the immobilized Pd catalyst **2i** displays no significant decline in activity, even though four times less Pd is used, 1 mol% compared to 4 mol% (Figure 4.15). This shows that even when four times more immobilized Pd is used, the catalyst loses activity quickly. It might become deactivated by agglomeration or leaching into solution, and subsequently being removed when the silica is washed in between the catalytic cycles. This confirms once again the basic principle of all immobilized catalysts that a larger immobilized amount does not necessarily lead to prolonged lifetime and better recyclability.[43]

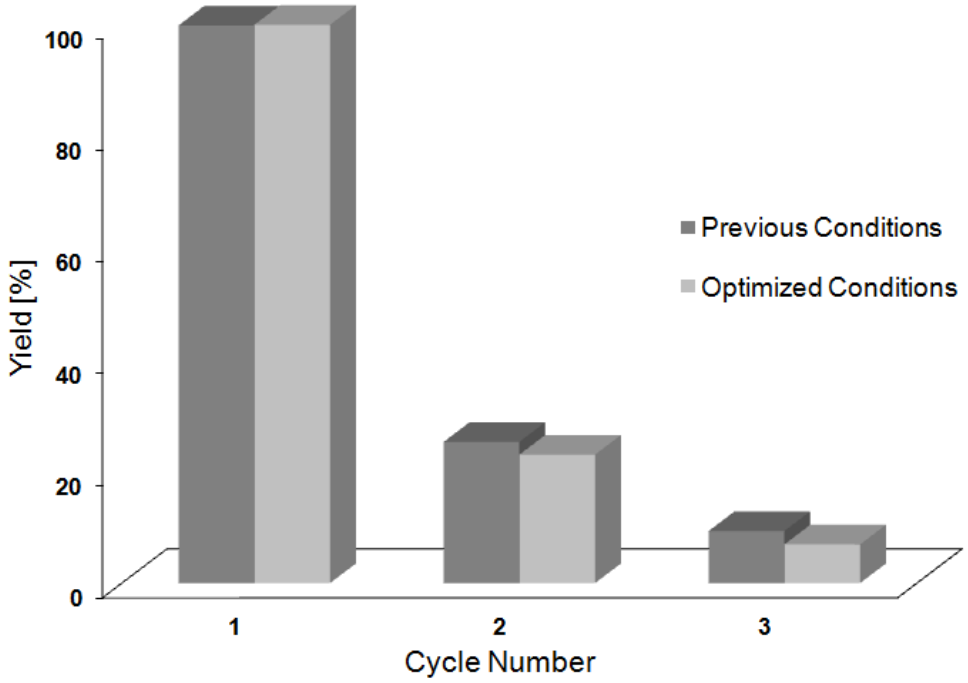

Figure 4.15. Catalysis with immobilized Pd complex **4i** and CuI. Note that with optimized conditions only a fraction of the amount of Pd is used as compared to the reaction under previous conditions (see text).

The immobilized Cu complex **7i** shows an increase in activity and prolonged lifetime when the reaction is conducted under the optimized conditions (Figure 4.16). This could be attributed to agglomeration or to the amount of base present. It has been determined in the base optimization experiments that the greater the amount of base present, the more the catalytic activity is hindered.

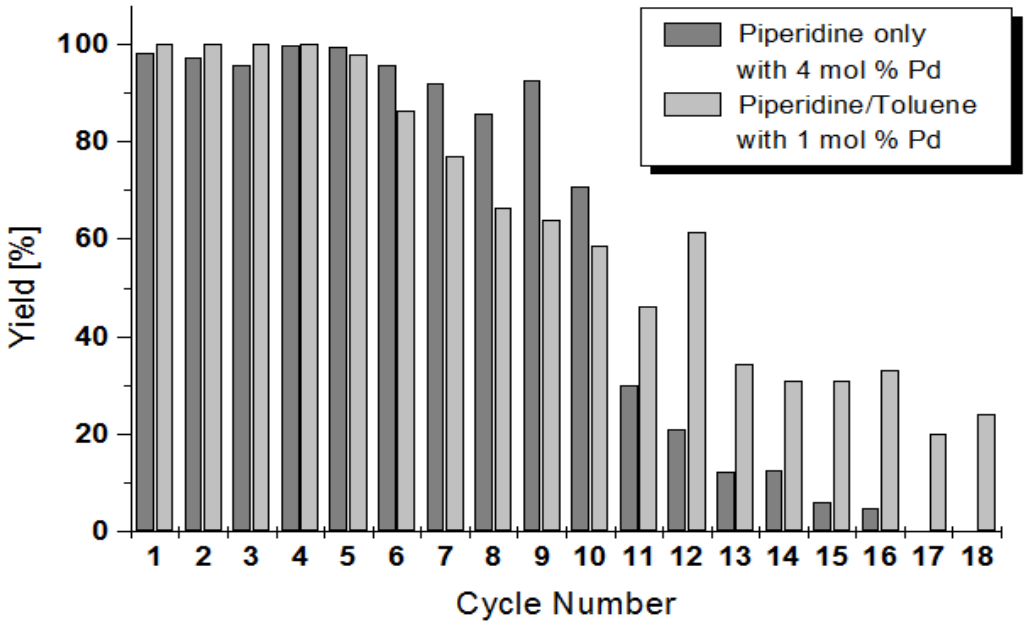

Figure 4.16. Catalysis with immobilized Cu complex **7i** and $Pd(PPh_3)_2Cl_2$ added prior to each cycle under optimal conditions as compared to reaction conditions used earlier.[37a]

Using the cross-coupling of phenylacetylene with iodobenzene to yield diphenylacetylene, a correlation can be established between the coordinating strength of the immobilized linker for $PdCl_2$ and the catalytic activity of the Sonogashira catalyst system. The more strongly the phosphine linker coordinates the Pd complex, the lower the catalytic activity is.

This was shown when attempting catalysis with immobilized **5i** and CuI under the optimized conditions, minimal activity (13% conversion in 6 h) is observed during the first cycle (Figure 4.17). This can be attributed to the increased coordinating strength of **2**[60, 77] as compared to **1**, which proves that in order to generate the catalytically active system, the Pd component has to become detached from the support and get into contact

with the Cu complex. If the Pd is held back too firmly by a strongly coordinating linker, catalysis is impeded, since its mechanism is not of a consecutive nature.

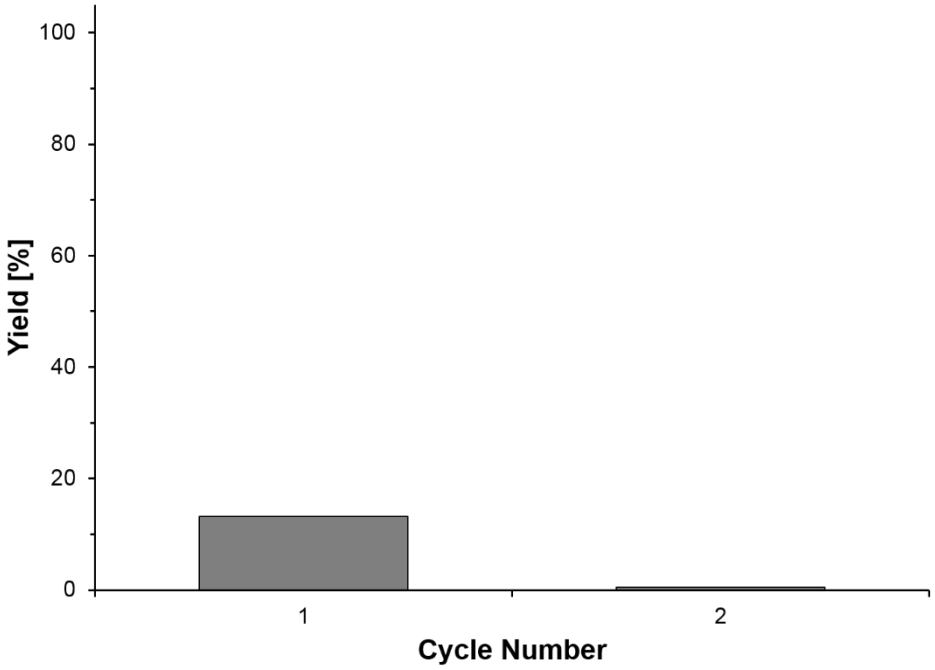

Figure 4.17. Catalysis with immobilized Pd complex **5i** and added CuI under optimal conditions.

This was also shown when using PCy_3 and $^nPBu_3$ as ligands in combination with $PdCl_2(PPh_3)_2$ and CuI. Minimal catalytic activity was observed in both cases even in solution and under the optimized reaction conditions (Appendix C).

CONCLUSION

It has been illustrated that molecular catalysts immobilized on oxide supports are both easy to design and they are as selective and active as their homogeneous analogues. They assume the properties of heterogeneous catalysts with respect to the ease of separation from reaction mixtures and efficient recycling. Chelating phosphine linkers, which are bound to silica via ethoxysilane groups have been synthesized and characterized. The ligands readily coordinate to the Pd and Cu complexes needed for the Sonogashira reaction. Using these linkers immobilized Pd(0)/Cu(I) Sonogashira catalyst systems for the coupling of aryl halides with terminal acetylenes have been generated successfully and characterized thoroughly.

The characterization and *in situ* measurements of all immobilized species was performed by classical solid-state CP/MAS and by HRMAS NMR spectroscopy of slurries. New insights concerning the synthesis, immobilization and characterization of Pd(0)/Cu(I) Sonogashira catalyst systems have been described. After optimization of the reaction conditions, a recyclable catalyst with unprecedented activities and lifetimes has been obtained.

In addition, it has been demonstrated that the coordinating strength of the phosphine moieties to the metal catalysts plays an important role in catalysis. By *in situ* ^{31}P HRMAS NMR studies, it has been shown that ligand **2** coordinates to Pd centers more strongly than to ligands **1** and **3**. This affected catalysis by significantly reducing the catalytic activity when utilizing the immobilized Pd complex **5i** in combination with CuI

under optimized conditions. Finally, the chelate phopsphine linker **1** was shown to coordinate Pd more strongly as compared to the amine ligand **8**.

EXPERIMENTAL SECTION

General remarks

The ^{1}H, ^{13}C, and ^{31}P NMR spectra of liquids were recorded at 499.70, 125.66, and 470.17 MHz on a 500 MHz Varian spectrometer and referenced as follows: ^{1}H: residual internal $CHCl_3$ (δ, 7.26 ppm) or benzene-d_6 (δ, 7.16 ppm); ^{13}C: internal $CDCl_3$ (δ, 77.23 ppm) or benzene-d_6 (δ, 128.06 ppm). ^{31}P NMR spectra are referenced to neat Ph_2PCl (δ, 81.92 ppm) which is placed in a capillary centered in the NMR sample tube. The ^{13}C and ^{31}P spectra are recorded with ^{1}H decoupling if not stated otherwise. The solid-state NMR spectra are measured with a Bruker Avance 400 widebore NMR spectrometer with a multinuclear 4 mm MAS probehead. For the ^{31}P HRMAS and MAS measurements ^{1}H high-power decoupling was applied. The recycle delays are 5 s for HRMAS and 10 s for MAS spectra.

GC analyses are carried out on a Shimadzu GC 2010 gas chromatograph equipped with a SHRXI-5MS column (15 m × 0.25 mm × 0.25 μm) and a flame ionization detector (GC:FID). All reactions are carried out using standard Schlenk techniques and a purified N_2 atmosphere, if not stated otherwise. Reagents purchased from Sigma Aldrich or VWR are used without further purification. Solvents are dried by boiling them over Na, distilled, and stored under N_2. CH_2Cl_2 is obtained from a solvent purification system. The silica (Merck, 40 Å average pore diameter, 0.063 to 0.2 mm average particle size, specific

surface area 750 m^2/g) is rigorously dried in vacuo at 250 °C for 4 days to remove adsorbed water and condense surface silanol groups.

General procedure for the immobilization of phosphine linkers 1-3 and Pd complexes 5 and 6

Phosphine linker **1** (135 mg, 0.065 mmol) is dissolved in toluene (15 ml) and added to a suspension of 0.8272 g of SiO_2 in toluene (40 ml). The mixture is stirred overnight at 60 °C. The silica is allowed to settle and the supernatant is removed. The functionalized silica **1i** is then washed with toluene (3×10 ml). Subsequently the silica is dried *in vacuo* for several hours. The supernatant and the solvents from the washing process are combined, and all volatile matter is removed *in vacuo*. The remaining material is then weighed, and the weight difference is calculated to determine the amount of linker **1** that is immobilized on the support, resulting in **1i** with about 13.4 molecules per 100 nm^2 of silica surface (data for all immobilized species are given in Table 2.1).

Procedure for crystallization of Pd complex 6

Pd complex **6** (50-100 mg) is dissolved in 2 mL of toluene at RT, then 25 mL of pentane is added to precipitate the product (yellow powder). This flask is then placed in the freezer (-19.6 °C) for approximately 4 weeks. After leaving it undisturbed during this time, the flask is checked, and yellow crystals of X-ray quality were formed.

General procedure for the catalyst preparation (4i and 7i)

$PdCl_2(NCPh)_2$ (27 mg, 0.070 mmol), dissolved in 10 ml of toluene, is added to a slurry of the functionalized silica **1i** (0.5032 g, 0.069 mmol ligand) in 20 ml of toluene. The mixture is stirred overnight at RT, then the silica is allowed to settle and the supernatant is removed. The catalyst-containing silica 4**i** is washed with toluene (3×10 ml) and dried *in vacuo* for 4 h.

General procedure for ligand hopping experiments

The immobilized chelate ligand **1i** (0.022 g, 0.0288 mmol. 0.131 mmol/g, 10.5 molecules per 100 nm^2) is added in a 1:1 ratio to the immobilized complex **5i** (0.020 g, 0.0288 mmol; 0.147 mmol/g). The two are mixed thoroughly together, then placed in a 4 mm HRMAS rotor. After adding acetone to the rotor and sealing it, the rotor is placed in the magnet and the first measurement is started. The measurements are recorded every 1024 scans (approximately every 1.5 hours) using a block averaging program.

General information for Sonogashira C-C bond forming cross-coupling reactions

The catalytic coupling of iodobenzene and phenylacetylene results in diphenylacetylene as the product. Both reactants and the product are analyzed by gas chromatography using a CP-Sil5 column (10 m x 0.25 mm, film thickness 0.35 μm). The retention times of the substrates and products for the column are reported in Table 4.5. The GC temperature program is given in Table 4.6.

Table 4.5. GC Retention Times [minutes]

	Substrate *Phenylacetylene*	**Substrate** *Iodobenzene*	**Product** *Diphenylacetylene*
Line 1	5.10	13.77	25.30
Line 2	4.72	12.94	25.04

Table 4.6. GC Temperature Program

Column Starting Temperature	50 °C
Column Ending Temperature	270 °C
Heating Rate	5 °C/min
Holding Time	2 min
Total Time for Heating Program	46 min

The reactions with both immobilized and homogeneous catalysts are carried out under a nitrogen atmosphere at RT unless stated otherwise. In a 50 mL Schlenk flask various mol% (which are given in the tables) of Pd(II) and Cu(I) catalysts are added (all mol% are determined based on the iodobenzene amount). The immobilized catalyst is first added to the flask, followed by dissolved $Pd(PPh_3)_2Cl_2$ or CuI (based on catalytic reaction) in toluene. For all catalytic reactions, piperidine is used as the base and toluene is used as the solvent, unless it is stated otherwise. Then freshly distilled phenylacetylene is added

via syringe, followed by iodobenzene. 0.1 mL samples are taken at time increments indicated in the graphical displays during the catalytic reaction with a glass pipette. These samples are then filtered through a glass Pasteur pipette with approximately 100 mg of silica gel and toluene as the solvent.

Between each catalytic cycle with an immobilized catalyst, the supernatant is decanted, and the salt formed during the catalytic reaction is dissolved with 75 mL of THF. The THF is then decanted, and the silica gel is washed three times with 10 mL of toluene. The silica is dried under high vacuum for 30 minutes and is ready for use in the next catalytic cycle.

N,N-Bis((diphenylphosphino)methyl)-3-(triethoxysilyl)propan-1-amine (1)

Route 1: Diphenylphosphine (754 mg, 4.05 mmol) is dissolved in 20 mL of toluene and paraformaldehyde (0.1215 g, 4.05 mmol). 3-aminopropyltriethoxysilane (0.4450 g, 2.01 mmol) is then added. The reaction mixture is stirred at 60°C for 16 h. Then the solvent is removed under vacuum resulting in **1** as an opaque viscous oil[37a] with a yield of 1.2534 g (2.02 mmol, 95%).

Route 2: The phosphinoalcohol $HOCH_2PPh_2$[15] (501 mg, 2.32 mmol) is dissolved in 20 mL of toluene, and 3-aminopropyltriethoxysilane (256 mg, 1.16 mmol) is added. The reaction is stirred at 60 °C for 16 h. Then, the solvent is removed under vacuum resulting in **1** as an opaque viscous oil in a yield of 0.7365 g (1.19 mmol, 97%).

Route 3: The phosphonium salt $[Ph_2P(CH_2OH)_2]Cl$ (176 mg, 0.62 mmol) and 3-aminopropyltriethoxysilane (69 mg, 0.311 mmol) are dissolved in 7 mL of water and 3.5

mL ethanol. Triethylamine (0.16 mL, 1.15 mmol) is added. The reaction mixture is stirred at 80 °C for 2 h. After aqueous workup with dichloromethane as organic phase, **1** is obtained as an opaque viscous oil in a yield of 0.198 g (0.320 mmol, 97%). The product is characterized by NMR and the signals are in accordance with the literature.[40b]

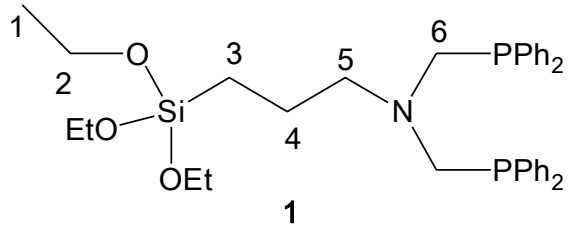

1

$C_{35}H_{45}NO_3P_2Si$
617.7692 g/mol

^{1}H NMR ($CDCl_3$, 499.70 MHz): δ [ppm] = 7.85 – 7.31 (m, 20H, Aryl-H), 3.74 (q, 6H, H2, $^{3}J(^{1}H\text{-}^{1}H)$ = 6.5 Hz), 3.55 (d, 4H, H6, $^{3}J(^{31}P\text{-}^{1}H)$ = 2.8 Hz), 2.82 (t, 2H, H5, $^{3}J(^{1}H\text{-}^{1}H)$ = 6.7 Hz), 1.50 (qui, 2H, H4, $^{3}J(^{1}H\text{-}^{1}H)$ = 7.0 Hz), 1.17 (t, 9H, H1, $^{3}J(^{1}H\text{-}^{1}H)$ = 7.1 Hz), 0.46 (t, 2H, H3, $^{3}J(^{1}H\text{-}^{1}H)$ = 9.0 Hz); **^{13}C NMR** ($CDCl_3$, 125.66 MHz): δ [ppm] = 138.24 (d, C_i, $^{1}J(^{31}P\text{-}^{13}C)$ = 15.1 Hz), 133.01 (d, C_o, $^{2}J(^{31}P\text{-}^{13}C)$ = 9.5 Hz), 128.3 (s, C_p), 128.22 (d, C_m, $^{3}J(^{31}P\text{-}^{13}C)$ = 6.51 Hz,), 59.18 (t, C5, ^{3}J(P-C) = 9.1 Hz), 58.59 (dd, C6, $^{1}J(^{31}P\text{-}^{13}C)$ = 9.3 Hz, $^{3}J(^{31}P\text{-}^{13}C)$ = 4.2 Hz), 58.24 (s, C2), 19.68 (s, C4), 18.28 (s, C1), 7.64 (s, C3); **^{31}P NMR** ($CDCl_3$, 202.28 MHz): δ [ppm] = -28.47 (s).

2-(3-Triethoxysilylpropyl)-aza-1,3-bis(dicyclohexylphosphino)propane (2)

Dicyclohexylphosphine (842 mg, 4.24 mmol) is dissolved in 20 mL of toluene and paraformaldehyde (127 mg, 4.24 mmol). 3-aminopropyltriethoxysilane (470 g, 2.12 mmol) is then added. The reaction mixture is stirred at 60°C for 16 h. Then the solvent is

removed under vacuum resulting in the product as a clear viscous oil in a yield of 1.27 g (1.98 mmol, 94%).

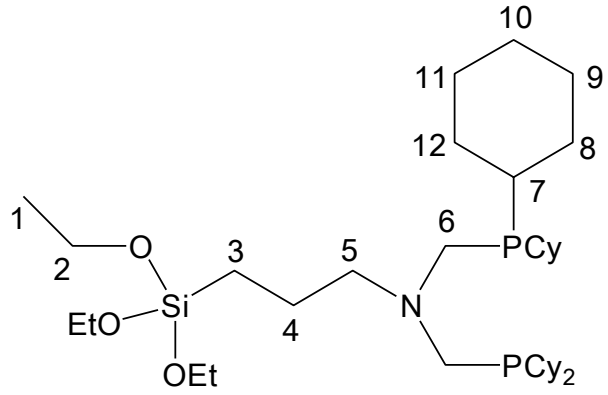

2

$C_{35}H_{69}NO_3P_2Si$

641.9603 g/mol

^{1}H NMR ($CDCl_3$, 499.70 MHz): δ [ppm] = 3.74 (q, 6H, H2, $^{3}J(^{1}H\text{-}^{1}H)$ = 7.0 Hz), 2.69 (s, 4H, H6), 2.59 (t, 2H, H5, $^{3}J(^{1}H\text{-}^{1}H)$ = 7.2 Hz), 1.81-1.63 (m, 19H, H8, H9, H11, and H12), 1.61 (s, 4H, H10), 1.48 (m, 6H, H4 and H7), 1.15 (t, 29H, H1 and H8, H9, H10, H11, H12*, $^{3}J(^{1}H\text{-}^{1}H)$ = 7.0 Hz,), 0.51 (t, 2H, H3, $^{3}J(^{1}H\text{-}^{1}H)$ = 8.4 Hz), ($^{*}H_{Cy}$ is overlapping with H1); **^{13}C NMR** ($CDCl_3$, 125.66 MHz): δ [ppm] = 59.32 (t, C5, $^{3}J(^{31}P\text{-}^{13}C)$ = 9.3 Hz), 58.14 (s, C2), 52.36 (dd, C6, $^{1}J(^{31}P\text{-}^{13}C)$= 8.4 Hz, $^{3}J(^{31}P\text{-}^{13}C)$ = 5.9 Hz), 32.72 (d, C7, $^{1}J(^{31}P\text{-}^{13}C)$ = 12.6 Hz), 29.75 (d, C8, $^{2}J(^{31}P\text{-}^{13}C)$ = 11.8 Hz), 29.46 (d, C12, $^{2}J(^{31}P\text{-}^{13}C)$ = 10.1 Hz), 27.27 (d, C9, $^{3}J(^{31}P\text{-}^{13}C)$ = 10.1 Hz), 27.22 (d, C11, $^{3}J(^{31}P\text{-}^{13}C)$ = 9.3 Hz), 26.49 (s, C10), 19.33 (s, C4), 18.21 (s, C1), 7.82 (s, C3); **^{31}P NMR** ($CDCl_3$, 202.28 MHz): δ [ppm] = -18.10 (s).

[(3-Triethoxysilyl)propyl]diphenylphosphine (3)

Route 1: Diphenylphosphine (1.09 g, 5.8 mmol) is added to allyltriethoxysilane (939 mg, 4.59 mmol) with AIBN (75 mg, 0.459 mmol). The reaction mixture is stirred at 70 °C for 96 h. Then, additional AIBN (75 mg, 0.459 mmol) is added, and the reaction mixture is stirred for 48 h. After purification by column chromatography (6:1 hexanes to ethyl acetate as the mobile phase; SiO_2 60 Å as the stationary phase), **3** results as a clear oil in a yield 1.13 g (2.89 mmol, 63%).

Route 2: Potassium diphenylphosphide solution (13.7 mL of a 0.5 molar solution in THF, 6.85 mmol) is placed in a 500 mL flask. Chloropropyltriethoxysilane (1.65 g, 6.86 mmol) is dissolved in 150 mL of THF, precooled in an ice bath, and added dropwise over the course of 1 h under cooling to the Schlenk flask. After stirring for 3 h under cooling the solution is brought to RT and stirred for an additional 16 h. Then 200 mL of pentane is added to precipitate the potassium chloride and extract the product. The solution is filtered, and the filtrate collected. The solvent is removed under vacuum and after purification by column chromatography (6:1 hexanes to ethyl acetate as the mobile phase; SiO_2 60 Å as the stationary phase), **3** results as a clear oil in a yield of 1.26 g (3.24 mmol, 47%).

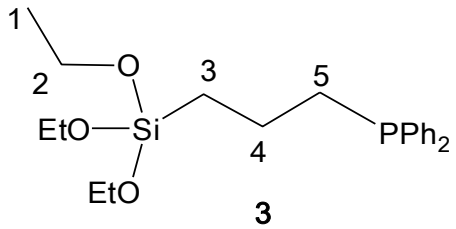

3

$C_{21}H_{31}O_3PSi$
390.5283 g/mol

^{1}H NMR ($CDCl_3$, 499.70 MHz): δ [ppm] = 7.47-7.29 (m, 10H, Aryl-H), 3.81 (q, 6H, H2, $^{3}J(^{1}H\text{-}^{1}H)$ = 7.1 Hz), 2.17 (t, 2H, H5, $^{3}J(^{1}H\text{-}^{1}H)$ = 7.8 Hz), 1.67-1.60 (m, 2H, H4), 1.22 (t, 9H, H1, $^{3}J(^{1}H\text{-}^{1}H)$ = 6.8 Hz, 0.86 (t, 2H, H3, $^{3}J(^{1}H\text{-}^{1}H)$ = 8.1 Hz); **^{13}C NMR** ($CDCl_3$, 125.66 MHz): δ [ppm] = 138.8 (d, C_i, $^{1}J(^{31}P\text{-}^{13}C)$ = 13.3 Hz), 132.54 (d, C_o, $^{2}J(^{31}P\text{-}^{13}C)$ = 18.4 Hz), 128.2 (s, C_p), 128.1 (d, C_m, $^{3}J(^{31}P\text{-}^{13}C)$ = 6.7 Hz), 58.1 (s, C2), 31.4 (d, C5, $^{1}J(^{31}P\text{-}^{13}C)$ = 11.4 Hz), 19.4 (d, C4, $^{2}J(^{31}P\text{-}^{13}C)$ = 17.9 Hz), 18.1 (s, C1), 12.1 (d, C3, $^{3}J(^{31}P\text{-}^{13}C)$ = 12.6 Hz; **^{31}P NMR** ($CDCl_3$, 202.28 MHz): δ [ppm] = -17.08 (s).

Bis(cyanophenyl)palladium(II)chloride

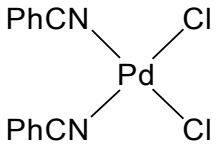

$C_{14}H_{10}Cl_2N_2Pd$
390.5283 g/mol

Palladium (II) chloride (0.237 g, 1.336 mmol) is weighed out and dissolved in 30 mL of benzonitrile. The solution is stirred at 100°C for 1 h. The red solution is filtered and hot hexanes (50 mL) are added to produce a yellow solid. An additional 100 mL of hexanes are added to wash the filtrate and to ensure all of the product is precipitated. The solution is then filtered, and the precipitate is further washed twice with 10 mL of hexanes. The product is dried in vacuo to result in the product a yellow powder in a yield of 0.2866 g (0.747 mmol, 56%).

[N,N-Bis((diphenylphosphino)methyl)-3-(triethoxysilyl)propan-1-amine]-palladium (II)chloride (4)

Bis(cyanophenyl)palladium (II) chloride (760 mg, 0.198 mmol) is dissolved in 30 mL of toluene. Ligand **1** (121 mg, 0.196 mmol) is dissolved in 5 mL toluene and added dropwise to the dissolved Pd complex. The solution changes from a dark red to a light orange color. The solution is stirred at RT for 2 h. The light orange solution is then concentrated to approximately 2 mL, and 30 mL of pentane is added to precipitate a solid. The solvent is then decanted, and the solid is washed 3 times with 10 mL of pentane. The solid is then dried *in vacuo* resulting in **4** as a yellow-orange powder in a yield of 0.110 g (0.147 mmol, 71%).

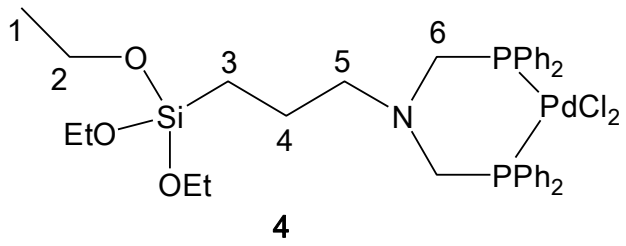

4

$C_{35}H_{45}Cl_2NO_3P_2PdSi$
795.0957 g/mol

^{1}H NMR ($CDCl_3$, 499.70 MHz): δ [ppm] = 7.96 – 7.35 (m, 20H, Aryl-H), 3.77 (q, 6H, H2, $^3J(^1H\text{-}^1H)$ = 7.0), 3.34 (s, 4H, H6), 2.68 (t, 2H, H5, $^3J(^1H\text{-}^1H)$ = 8.1 Hz), 1.55 (s, 2H, H4), 1.18 (t, 9H, H1, $^3J(^1H\text{-}^1H)$ = 7.0 Hz), 0.43 (t, 2H, H3, $^3J(^1H\text{-}^1H)$ = 7.8 Hz); **^{13}C NMR** ($CDCl_3$, 125.66 MHz): δ [ppm] = 133.81 (virt. t, C_m, $^2J(^{31}P\text{-}^{13}C)$ = 5.4 Hz), 131.39 (s, C_p), 129.26 (d, C_i, $^1J(^{31}P\text{-}^{13}C)$ = 51.6 Hz), 128.53 (virt. t, C_o, $^2J(^{31}P\text{-}^{13}C)$ = 5.8 Hz), 65.08 (t, C5, $^3J(^{31}P\text{-}^{13}C)$ = 10.0 Hz), 58.41 (s, C2), 56.38 (d, C6, $^1J(^{31}P\text{-}^{13}C)$ = 47.7 Hz),

18.60 (s, C4), 18.25 (s, C1), 7.64 (s, C3); **P NMR** ($CDCl_3$, 202.28 MHz): δ [ppm] = 7.79 ppm (s).

2-(3-triethoxysilylpropyl)-aza-1,3-bis(dicyclohexylphosphino)propane (5)

Bis(cyanophenyl)palladium (II) chloride (145 mg, 0.379 mmol) is dissolved in 40 mL of toluene. Ligand **2** (243 mg, 0.379 mmol) is dissolved in 10 mL of toluene and added dropwise. The solution changes from a dark red to a light orange color. The solution is stirred at RT for 2 h. The light orange solution is then concentrated to approximately 2 mL, and 30 mL of pentane is added to precipitate a solid. The solvent is then decanted, and the solid is washed 3 times with 10 mL of pentane. The solid is then dried *in vacuo* resulting in **5** as a yellow powder in a yield of 0.269 g (0.328 mmol, 87%).

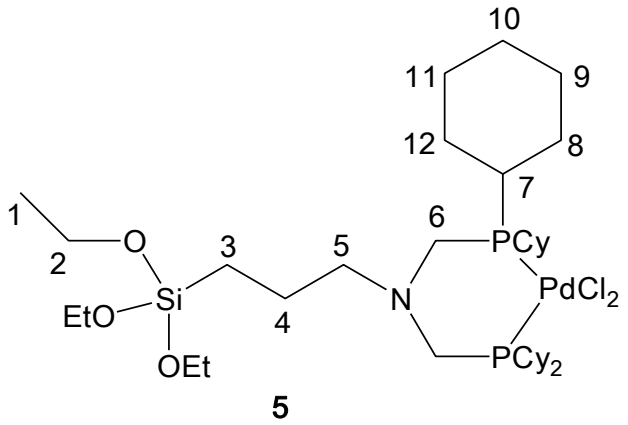

5

$C_{35}H_{69}Cl_2NO_3P_2PdSi$
819.2863 g/mol

^{1}H NMR ($CDCl_3$, 499.70 MHz): δ [ppm] = 3.78 (q, 6H, H2, $^3J(^1H\text{-}^1H)$ = 7.0 Hz), 2.65 (s, 4H, H6), 2.56 (t, 2H, H5, $^3J(^1H\text{-}^1H)$ = 7.6 Hz), 2.41 (m, 4H, H7), 2.31 (m, 4H, H8), 1.88 (m, 4H, H12), 1.73 (m, 8H, H9 and H11), 1.62 (m, 5H, H10), 1.59 (m, 5H, H4 and H8*), 1.40 (m, 4H, H12), 1.25 (m, 8H, H9, H10, and H11), 1.18 (t, 13H, H1, H9, H10,

and H11*, $^{3}J(^{1}H\text{-}^{1}H)$ = 7.0 Hz), 0.54 (t, 2H, H3, $^{3}J(^{1}H\text{-}^{1}H)$ = 7.8 Hz), ($^{*}H_{Cy}$ is overlapping with H4 and H1); **^{13}C NMR** ($CDCl_3$, 125.66 MHz): δ [ppm] = 65.45 (t, C5, $^{3}J(^{31}P\text{-}^{13}C)$ = 10.0 Hz), 58.31 (s, C2), 48.64 (d, C6, $^{1}J(^{31}P\text{-}^{13}C)$ = 42.6 Hz), 36.77 (d, C7, $^{1}J(^{31}P\text{-}^{13}C)$ = 28.1), 30.10 (s, C8), 29.31 (s, C12), 27.00 (t, C9, $^{3}J(^{31}P\text{-}^{13}C$) = 7.0 Hz), 26.77 (t, C11, $^{3}J(^{31}P\text{-}^{13}C)$ = 6.0 Hz), 25.72 (s, C10), 19.84 (s, C1), 18.16 (s, C1), 7.78 (s, C3); **^{31}P NMR** ($CDCl_3$, 202.28 MHz): δ [ppm] = 29.60 (s).

Bis-[(3-Triethoxysilyl)propyl]diphenylphosphine]-Palladium(II)-chloride (6)

Bis(cyanophenyl)palladium (II) chloride (122 mg, 0.318 mmol) is dissolved in 50 mL of toluene. Ligand **3** (243 mg, 0.379 mmol) is dissolved in 10 mL of toluene and added dropwise to the dissolved Pd complex. The solution changes from a dark red to yellow. The solution is stirred at RT for 2 h. The light orange solution is then concentrated to approximately 2 mL, and 30 mL of pentane is added to precipitate a solid. Then the solvent is decanted, and the solid is washed 3 times with 10 mL of pentane. The solid is then dried *in vacuo* resulting in **6** as a yellow powder in a yield of 0.188 g (0.196 mmol, 62%).

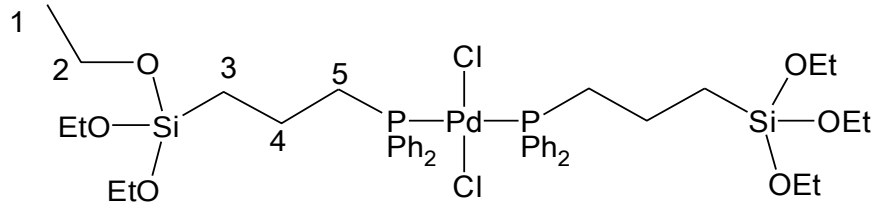

6

$C_{42}H_{62}Cl_2O_6P_2PdSi$
958.3826 g/mol

^{1}H NMR ($CDCl_3$, 499.70 MHz): δ [ppm] = 7.82 - 6.98 (m, 44H, Aryl-H), 3.69 (q, 12H, H2, $^{3}J(^{1}H\text{-}^{1}H)$ = 7.1 Hz), 2.68 – 2.62 (m, 4H, H5), 1.86 - 1.78 (m, 4H, H4), 1.07 (t,

18H, H1, $^{3}J(^{1}H\text{-}^{1}H)$ = 7.0 Hz), 0.76 (t, 4H, H3, $^{3}J(^{1}H\text{-}^{1}H)$ = 7.8 Hz); **^{13}C NMR** ($CDCl_3$, 125.66 MHz): δ [ppm] = 133.70 (t, C_o, $^{2}J(^{31}P\text{-}^{13}C)$ = 6.1 Hz), 130.84 (t, C_i, $^{1}J(^{31}P\text{-}^{13}C)$ = 10.0 Hz), 130.24 (s, C_p), 128.12 (t, C_m, $^{3}J(^{31}P\text{-}^{13}C)$ = 5.1 Hz), 58.30 (s, C2), 28.13 (t, C5, $^{1}J(^{31}P\text{-}^{13}C)$ = 14.0 Hz), 18.22 (s, C4), 17.95 (s, C1), 12.05 (s, C3); **^{31}P NMR** ($CDCl_3$, 202.28 MHz): δ [ppm] = 15.73 (s).

CHAPTER V

CONCLUSIONS

After a brief overview of solid-state NMR and its relevance to the various areas of chemistry in chapter I, chapter II demonstrated that PEEK and PEKK blends with PBI (50:50 wt%) can be characterized by ^{13}C CP/MAS and all signals can be assigned due to the favorable signal resolution. While physical mixtures of the components cannot be distinguished from their melt-blended versions based on their ^{13}C CP/MAS spectra, more pronounced, albeit not conclusive, differences are visible in the ^{15}N CP/MAS and IR spectra. Furthermore, it is described that the moisture uptake of PEEK-PBI and PEKK-PBI samples is much faster than the reverse process, especially at elevated temperatures. PEEK-PBI incorporates overall more water than PEKK-PBI.

With the use of ^{2}H MAS and ^{1}H wideline NMR spectroscopy for samples steam-treated with D_2O and H_2O, three different ^{2}H sites can be distinguished in PBI and in the PEEK- and PEKK-PBI blends. Mobile D_2O can reside in liquid domains in the polymer network. Less mobile D_2O is attached to N-H (or N-D) groups via hydrogen bonds, and they are exchanging with mobile D_2O molecules in contiguous liquid D_2O domains. Finally, immobile ^{2}H nuclei, covalently bound in N-D groups are found after steam-treatment at higher temperatures.

Furthermore, it has been illustrated with ^{7}Li MAS that LiCl is incorporated into PEKK-PBI by treating the blend with an aqueous LiCl solution at elevated temperatures. This LiCl can partially be extracted again at higher temperatures with H_2O. It has also

been shown by ^{79}Br MAS NMR that $ZnBr_2$ is readily incorporated into pure PBI out of an aqueous solution, while only traces move into the PEEK-PBI and PEKK-PBI blends.

In chapter III, it has been demonstrated that the single components of important PAEK-PBI blends, namely PBI, PEEK, and PEKK, can be characterized by ^{13}C CP/MAS and all signals can be assigned. Furthermore, the melt-molded samples can be analyzed by TGA, IR, ^{1}H wideline solid-state NMR, and ^{2}H MAS NMR after steam-treatment. When the samples are stirred at ambient temperature in D_2O or steam-treated with it at 150 °C, only the PBI sample takes up large amounts of water. Under harsh conditions of steam-treatment at 315 °C, D_2O is incorporated in trace amounts and mainly in the form of liquid domains into the PEEK and PEKK samples.

The PBI, however, incorporates a smaller amount of D_2O into its polymer network when subjected to steam-treatment at 315 °C, as compared to the outcome at lower temperatures. The physical appearance of the samples implies that PEEK is least resistant to steam-treatment at the highest temperature of 315 °C, showing signs of major decomposition. The PEKK sample keeps up best, and only undergoes a color change to black, while PBI becomes more brittle and rough on its surface. Overall it can be concluded that both PEEK and PEKK are valuable components in blends with PBI, being able to fend off water even under harsh reaction conditions. PEEK-PBI and PEKK-PBI blends, and their salt uptake are being investigated in a parallel project.

In the previous chapters it has been demonstrated that using PEKK instead of PEEK in combination with PBI water is fended off better and this could lead to polymers with longer lifetimes in industrial applications. Further work will be conducted to study a

PBI with a different monomers in order to determine whether it will lead to different water uptake and longer polymer lifetimes.

In chapter IV, it has been demonstrated that molecular catalysts immobilized on oxide supports are both easy to design and they are as selective and active as their homogeneous analogues. They assume the properties of heterogeneous catalysts with respect to the ease of separation from reaction mixtures and efficient recycling. Chelating phosphine linkers, which are bound to silica via ethoxysilane groups have been synthesized and characterized. The ligands readily coordinate to the Pd and Cu complexes needed for the Sonogashira reaction. Using these linkers immobilized Pd(0)/Cu(I) Sonogashira catalyst systems for the coupling of aryl halides with terminal acetylenes have been generated successfully and characterized thoroughly.

The characterization and *in situ* measurements of all immobilized species was performed by classical solid-state CP/MAS and by HRMAS NMR spectroscopy of slurries. New insights concerning the synthesis, immobilization and characterization of Pd(0)/Cu(I) Sonogashira catalyst systems have been described. After optimization of the reaction conditions, a recyclable catalyst with unprecedented activities and lifetimes has been obtained.

In addition, it has been demonstrated that the coordinating strength of the phosphine moieties to the metal catalysts plays an important role in catalysis. By *in situ* ^{31}P HRMAS NMR studies, it has been shown that ligand **2** coordinates to Pd centers more strongly than to ligands **1** and **3**. This affected catalysis by significantly reducing the catalytic activity when utilizing the immobilized Pd complex **5i** in combination with CuI

under optimized conditions. Finally, the chelate phopsphine linker **1** was shown to coordinate Pd more strongly as compared to the amine ligand **8**.

REFERENCES

1. Kemmish, D., *Updates on the Technology and Applications of Polyaryletherketones*; iSmithers: Shropshire, United Kingdom, 2010.
2. Guenther, J.; Wong, M.; Sue, H.-J.; Bremner, T.; Blümel, J. *J. Appl. Polym. Sci.* **2013**, *128*, 4395-4404.
3. Brooks, N. W.; Duckett, R. A.; Rose, J.; Ward, I. M.; Clements, J. *Polymer* **1993**, *34*, 4038-4042.
4. Larkin, P., *Infrared and Raman Spectroscopy, Principles and Spectral Interpretation*; Academic Press, Elsevier: 2011.
5. Hilliard, C. R.; Bhuvanesh, N.; Gladysz, J. A.; Blümel, J. *Dalton Trans.* **2012**, *41*, 1742-1754.
6. Reinhard, S.; Behringer, K. D.; Blümel, J. *New J. Chem.* **2003**, *27*, 776-778.
7. Menczel, J. D. *J. Therm. Anal. Calorim.* **2000**, *59*, 1023-1027.
8. Vogel, H.; Marvel, C. S. *J. Polym. Sci.* **1961**, *50*, 511-539.
9. Herrmann, W. A.; Scherer, W.; Fischer, R. W.; Blümel, J.; Kleine, M.; Mertin, W.; Gruehn, R.; Mink, J.; Boysen, H. *J. Am. Chem. Soc.* **1995**, *117*, 3231-3243.
10. (a) Cluff, K. J.; Bhuvanesh, N.; Blumel, J. *Organometallics* **2014**, *33*, 2671-2680; (b) Cluff, K. J.; Schnellbach, M.; Hilliard, C. R.; Blumel, J. *J. Organomet. Chem.* **2013**, *744*, 119-124.

11. Herrmann, W. A.; Kratzer, R. M.; Blümel, J.; Friedrich, H. B.; Fischer, R. W.; Apperley, D. C.; Mink, J.; Berkesi, O. *J. Mol. Catal. A: Chem.* **1997**, *120*, 197-205.

12. Stejskal, E. O.; Memory, J. D., *High Resolution NMR in the Solid State: Fundamentals of CP/MAS*; Oxford University Press: Oxford, New York, 1994.

13. (a) Schmidt-Rohr, K.; Saalwaechter, K.; Liu, S.-F.; Hong, M. *J. Am. Chem. Soc.* **2001**, *123*, 7168-7169; (b) Brown, S. P.; Spiess, H. W. *Chem. Rev.* **2001**, *101*, 4125-4155; (c) Lee, Y. J.; Murakhtina, T.; Sebastiani, D.; Spiess, H. W. *J. Am. Chem. Soc.* **2007**, *129*, 12406-12407; (d) Blümich, B.; Hagemeyer, A.; Schafer, D.; Schmidt-Rohr, K.; Spiess, H. W. *Adv. Mater.* **1990**, *2*, 72-81; (e) Albunia, A. R.; Graf, R.; Grassi, A.; Guerra, G.; Spiess, H. W. *Macromolecules* **2009**, *42*, 4929-4931; (f) Nambiar, R. R.; Blum, F. D. *Macromolecules* **2009**, *42*, 8998-9007; (g) Hetayothin, B.; Cabaniss, R. A.; Blum, F. D. *Macromolecules* **2012**, *45*, 9128-9138; (h) Metin, B.; Blum, F. D. *Langmuir* **2010**, *26*, 5226-5231; (i) Fyfe, C. A.; Diaz, A. C.; Grondey, H.; Lewis, A. R.; Foerster, H. *J. Am. Chem. Soc.* **2005**, *127*, 7543-7558; (j) Hepp, M. A.; Ramamurthy, V.; Corbin, D. R.; Dybowski, C. *J. Phys. Chem.* **1992**, *96*, 2629-2632.

14. Blümel, J.; Born, E.; Megzger, T. *J. Phys. Chem. Solids* **1994**, *55*, 589-593.

15. Schmidt-Rohr, K.; Spiess, H. W., *Multidimensional Solid-State NMR and Polymers*; Academic Press Inc.: San Diego, CA, 1999.

16. Poliks, M. D.; Schaefer, J. *Macromolecules* **1990**, *23*, 3426-3431.

17. Pope, J. C.; Sue, H.-J.; Bremner, T.; Blümel, J. *Polymer* **2014**, doi: 10.1016/j.polymer.2014.07.027.

18. Fyfe, C., *Solid-State NMR for Chemists*; C.F.C. Press: Guelph, Canada, 1983.

19. *ACD/NMR Processor Academic Edition*, 12.01; Advanced Chemistry Development, Inc: Toronto, Canada, 2010.

20. Massiot, D.; Fayon, F.; Capron, M.; King, I.; Le Calve, S.; Alonso, B.; Durand, J.-O.; Bujoli, B.; Gan, Z.; Hoatson, G. *Magn. Reson. Chem.* **2002**, *40*, 70-76.

21. Xiong, J.; Lock, H.; Chuang, I. S.; Keeler, C.; Maciel, G. E. *Environ. Sci. Technol.* **1999**, *33*, 2224-2233.

22. Akbey, U.; Graf, R.; Chu, P. P.; Spiess, H. W. *Aust. J. Chem.* **2009**, *62*, 848-856.

23. Pope, J. C.; Sue, H.-J.; Bremner, T.; Blümel, J. *J. Appl. Polym. Sci.* **2014**, *submitted*.

24. Keinath, S. E.; Morgan, R. J. *Thermochim. Acta* **1990**, *166*, 17-26.

25. Xie, X.-N.; Lu, M.; Yuan, J.; Yang, H.-X. *Acta Crystallogr. Sect. E: Struct. Rep. Online* **2012**, *E68*, m754.

26. Lappi, S. E.; Smith, B.; Franzen, S. *Spectrochim. Acta, Part A* **2004**, *60A*, 2611-2619.

27. Voice, A. M.; Bower, D. I.; Ward, I. M. *Polymer* **1993**, *34*, 1164-1173.

28. Torchia, D. A. *J. Magn. Reson.* **1978**, *30*, 613-616.

29. (a) Brandsma, L., *Synthesis of Acetylenes, Allenes, and Cumulenes: Methods and Techniques*; Elsevier: Oxford, 2004; (b) *Handbook of Organopalladium Chemistry for Organic Synthesis*; Negishi, E.; Meijere, A. D., Eds.; Wiley-Interscience: New

York, 2002; (c) *Metal-Catalyzed Cross-Coupling Reactions*; Diederich, F.; Meijere, A. D., Eds.; Wiley-VCH: Weinheim, 2004; (d) Beller, M.; Bolm, C., *Transition Metals for Organic Synthesis: Building Block and Fine Chemicals*; 2nd ed.; Wiley-VCH: Weinheim, 2004.

30. (a) Torborg, C.; Beller, M. *Adv. Synth. Catal.* **2009**, *351*, 3027-3043; (b) Vlaar, T.; Ruijter, E.; Orru, R. V. A. *Adv. Synth. Catal.* **2011**, *353*, 809-841; (c) Pal, M. *Synlett* **2009**, 2896-2912; (d) Karimi, B.; Behzadnia, H.; Farhangi, E.; Jafari, E.; Zamani, A. *Curr. Org. Synth.* **2010**, *7*, 543-567.

31. (a) Kochi, J. K.; Tamura, M. *J. Amer. Chem. Soc.* **1971**, *93*, 1483-1485; (b) Heck, R. F.; Nolley, J. P., Jr. *J. Org. Chem.* **1972**, *37*, 2320-2322; (c) Sonogashira, K.; Tohda, Y.; Hagihara, N. *Tetrahedron Lett.* **1975**, 4467-4470; (d) Negishi, E.; King, A. O.; Okukado, N. *J. Org. Chem.* **1977**, *42*, 1821-1823; (e) Milstein, D.; Stille, J. K. *J. Am. Chem. Soc.* **1979**, *101*, 4992-4998; (f) Miyaura, N.; Yamada, K.; Suzuki, A. *Tetrahedron Lett.* **1979**, 3437-2440; (g) Hatanaka, Y.; Hiyama, T. *J. Org. Chem.* **1988**, *53*, 918-920; (h) Paul, F.; Patt, J.; Hartwig, J. F. *J. Am. Chem. Soc.* **1994**, *116*, 5969-5970.

32. Chinchilla, R.; Najera, C. *Chem. Soc. Rev.* **2011**, *40*, 5084-5121.

33. (a) Chinchilla, R.; Najera, C. *Chem. Rev.* **2007**, *107*, 874-922; (b) Doucet, H.; Hierso, J.-C. *Angew. Chem., Int. Ed.* **2007**, *46*, 834-871.

34. (a) Thathagar, M. B.; Beckers, J.; Rothenberg, G. *Green Chem.* **2004**, *6*, 215-218; (b) Yuan, Y.; Zhu, H.; Zhao, D.; Zhang, L. *Synthesis* **2011**, 1792-1798.

35. Zhang, L.-Y.; Wang, L. *Chin. J. Chem.* **2008**, *26*, 1601-1606.

36. (a) Gaikwad, A. V.; Holuigue, A.; Thathagar, M. B.; Elshof, J. E.; Rothenberg, G. *Chem. Eur. J.* **2007**, *13*, 6908-6913, S6908/1-S6908/7; (b) Chen, Z.; Cui, Z.-M.; Niu, F.; Jiang, L.; Song, W.-G. *Chem. Commun.* **2010**, *46*, 6524-6526; (c) Gao, S.; Zhao, N.; Shu, M.; Che, S. *Appl. Catal., A* **2010**, *388*, 196-201; (d) Teratani, T.; Ohtaka, A.; Kawashima, T.; Shimomura, O.; Nomura, R. *Synlett* **2010**, 2271-2274; (e) Rumi, L.; Scheuermann, G. M.; Muelhaupt, R.; Bannwarth, W. *Helv. Chim. Acta* **2011**, *94*, 966-976.

37. (a) Posset, T.; Blümel, J. *J. Am. Chem. Soc.* **2006**, *128*, 8394-8395; (b) Posset, T.; Guenther, J.; Pope, J. C.; Oeser, T.; Blümel, J. *Chem. Commun.* **2011**, *47*, 2059-2061; (c) Posset, T.; Pope, J. C.; Oeser, T.; Blümel, J. *Adv. Synth. Catal.* **2014**, *in preparation*.

38. Fadhel, A. Z.; Pollet, P.; Liotta, C. L.; Eckert, C. A. *Molecules* **2010**, *15*, 8400-8424.

39. Blümel, J. *Inorg. Chem.* **1994**, *33*, 5050-5056.

40. Behringer, K. D.; Blümel, J. *J. Liq. Chromatogr. Relat. Technol.* **1996**, *19*, 2753-2765.

41. (a) Tyrrell, E.; Whiteman, L.; Williams, N. *Synthesis* **2009**, 829-835; (b) Lee, D.-H.; Jung, J.-Y.; Jin, M.-J. *Green Chem.* **2010**, *12*, 2024-2029; (c) Lee, G.; Youn, H.-K.; Jin, M.-J.; Cheong, W.-J.; Ahn, W.-S. *Microporous Mesoporous Mater.* **2010**, *132*, 232-238.

42. (a) Ye, Z.-W.; Yi, W.-B. *J. Fluorine Chem.* **2008**, *129*, 1124-1128; (b) Bakherad, M.; Keivanloo, A.; Bahramian, B.; Jajarmi, S. *Appl. Catal., A* **2010**, *390*, 135-140;

(c) Islam, S. M.; Mondal, P.; Roy, A. S.; Mondal, S.; Hossain, D. *Tetrahedron Lett.* **2010**, *51*, 2067-2070; (d) He, Y.; Cai, C. *J. Organomet. Chem.* **2011**, *696*, 2689-2692.

43. Blümel, J. *Coord. Chem. Rev.* **2008**, *252*, 2410-2423.

44. *Combinatorial Chemistry*; Bannworth, W.; Felder, E., Eds.; Wiley-VCH: Weinheim, 2000.

45. Seneci, P., *Solid-Phase Synthesis and Combinatorial Technologies*; John Wiley & Sons: New York, 2000.

46. Zaragoza, F. D., *Organic Synthesis on Solid Phase*; Wiley-VCH: Weinheim, 2000.

47. Linares, N.; Sepulveda, A. E.; Pacheco, M. C.; Berenguer, J. R.; Lalinde, E.; Najera, C.; Garcia-Martinez, J. *New J. Chem.* **2011**, *35*, 225-234.

48. Rothenberg, G., *Catalysis: Concepts and Green Applications*; Wiley-VCH: Weinheim, 2008.

49. Duer, M. J., *Introduction to Solid-State NMR Spectroscopy*; Blackwell Publishing: Oxford, 2000.

50. *NMR Techniques in Catalysis*; Bell, A. T.; Pines, A., Eds.; Marcel Dekker, Inc.: New York, 1994.

51. Niemantsverdriet, J. W., *Spectroscopy in Catalysis*; 2nd ed.; Wiley-VCH: Weinheim, 2000.

52. Webb, P. A.; Orr, C., *Analytical Methods in Fine Particle Technology*; Micrometrics Instrument Corporation: Norcross, GA, 1997.

53. Keles, M.; Keles, T.; Serindag, O.; Yasar, S.; Ozdemir, I. *Phosphorus, Sulfur Silicon Relat. Elem.* **2010**, *185*, 165-170.

54. Kuhl, O.; Blaurock, S.; Sieler, J.; Hey-Hawkins, E. *Polyhedron* **2001**, *20*, 2171-2177.

55. Capka, M. *Synth. React. Inorg. Met.-Org. Chem.* **1977**, *7*, 347-354.

56. Posset, T. Immobilisierte Nickel-, Palladium- und Kupfer-Katalysatoren: Neue Einblicke durch klassische CP/MAS- und Suspensions- HRMAS-NMR-Spektroskopie. Ph.D., University of Heidelberg, 2006.

57. Piestert, F.; Fetouaki, R.; Bogza, M.; Oeser, T.; Blümel, J. *Chem. Commun.* **2005**, 1481-1483.

58. Posset, T.; Rominger, F.; Blümel, J. *Chem. Mater.* **2005**, *17*, 586-595.

59. Brenna, S.; Posset, T.; Furrer, J.; Blümel, J. *Chem.--Eur. J.* **2006**, *12*, 2880-2888.

60. Tolman, C. A. *Chem. Rev.* **1977**, *77*, 313-348.

61. Pope, J. C.; Posset, T.; Bhuvanesh, N.; Blümel, J. *Chem. Commun.* **2014**, *in preparation*.

62. Gonzalez-Arellano, C.; Abad, A.; Corma, A.; Garcia, H.; Iglesias, M.; Sanchez, F. *Angew. Chem., Int. Ed.* **2007**, *46*, 1536-1538.

63. Borah, H. N.; Prajapati, D.; Boruah, R. C. *Synlett* **2005**, 2823-2825.

64. Carril, M.; Correa, A.; Bolm, C. *Angew. Chem., Int. Ed.* **2008**, *47*, 4862-4865.

65. Wang, L.; Li, P.; Zhang, Y. *Chem. Commun.* **2004**, 514-515.

66. Li, P.; Wang, L. *Synlett* **2006**, 2261-2265.

67. Feng, L.; Liu, F.; Sun, P.; Bao, J. *Synlett* **2008**, 1415-1417.

68. Kanuru, V. K.; Humphrey, S. M.; Kyffin, J. M. W.; Jefferson, D. A.; Burton, J. W.; Armbruester, M.; Lambert, R. M. *Dalton Trans.* **2009**, 7602-7605.

69. Park, S.; Kim, M.; Koo, D. H.; Chang, S. *Adv. Synth. Catal.* **2004**, *346*, 1638-1640.

70. (a) Biffis, A.; Scattolin, E.; Ravasio, N.; Zaccheria, F. *Tetrahedron Lett.* **2007**, *48*, 8761-8764; (b) Chen, G.; Zhu, X.; Cai, J.; Wan, Y. *Synth. Commun.* **2007**, *37*, 1355-1361; (c) Monnier, F.; Turtaut, F.; Duroure, L.; Taillefer, M. *Org. Lett.* **2008**, *10*, 3203-3206.

71. (a) Guan, J. T.; Weng, T. Q.; Yu, G.-A.; Liu, S. H. *Tetrahedron Lett.* **2007**, *48*, 7129-7133; (b) Lu, N.; Chen, Y.-C.; Chen, W.-S.; Chen, T.-L.; Wu, S.-J. *J. Organomet. Chem.* **2009**, *694*, 278-284; (c) de Carne-Carnavalet, B.; Archambeau, A.; Meyer, C.; Cossy, J.; Folleas, B.; Brayer, J.-L.; Demoute, J.-P. *Org. Lett.* **2011**, *13*, 956-959.

72. (a) Basu, B.; Das, S.; Das, P.; Mandal, B.; Banerjee, D.; Almqvist, F. *Synthesis* **2009**, 1137-1146; (b) Pan, C.; Luo, F.; Wang, W.; Ye, Z.; Cheng, J. *Tetrahedron Lett.* **2009**, *50*, 5044-5046; (c) Zhou, M.-B.; Wei, W.-T.; Xie, Y.-X.; Lei, Y.; Li, J.-H. *J. Org. Chem.* **2010**, *75*, 5635-5642.

73. Lee, D.-H.; Lee, Y. H.; Harrowfield, J. M.; Lee, I.-M.; Lee, H. I.; Lim, W. T.; Kim, Y.; Jin, M.-J. *Tetrahedron* **2009**, *65*, 1630-1634.

74. Wang, X.; Qin, W.; Kakusawa, N.; Yasuike, S.; Kurita, J. *Tetrahedron Lett.* **2009**, *50*, 6293-6297.

75. Li, P.-H.; Wang, L. *Adv. Synth. Catal.* **2006**, *348*, 681-685.

76. Thorwirth, R.; Stolle, A.; Ondruschka, B. *Green Chem.* **2010**, *12*, 985-991.

77. (a) Crabtree, R. H., *The Organometallic Chemistry of Transition Metals*; 5th ed.; John Wiley & Sons, Inc.: Hoboken, New Jersey, 2009; (b) Hartwig, J., *Organotransition Metal Chemistry From Bonding to Catalysis*; University Science Books: Herndon, VA, 2010; (c) Leyssens, T.; Peeters, D.; Orpen, A. G.; Harvey, J. N. *Organometallics* **2007**, *26*, 2637-2645; (d) Neuwald, B.; Oelscher, F.; Goettker-Schnetmann, I.; Mecking, S. *Organometallics* **2012**, *31*, 3128-3137; (e) Tolman, C. A. *J. Amer. Chem. Soc.* **1970**, *92*, 2956-2965.

APPENDIX A

CRYSTALLOGRAPHIC DATA FOR THE STRUCTURE OF 6

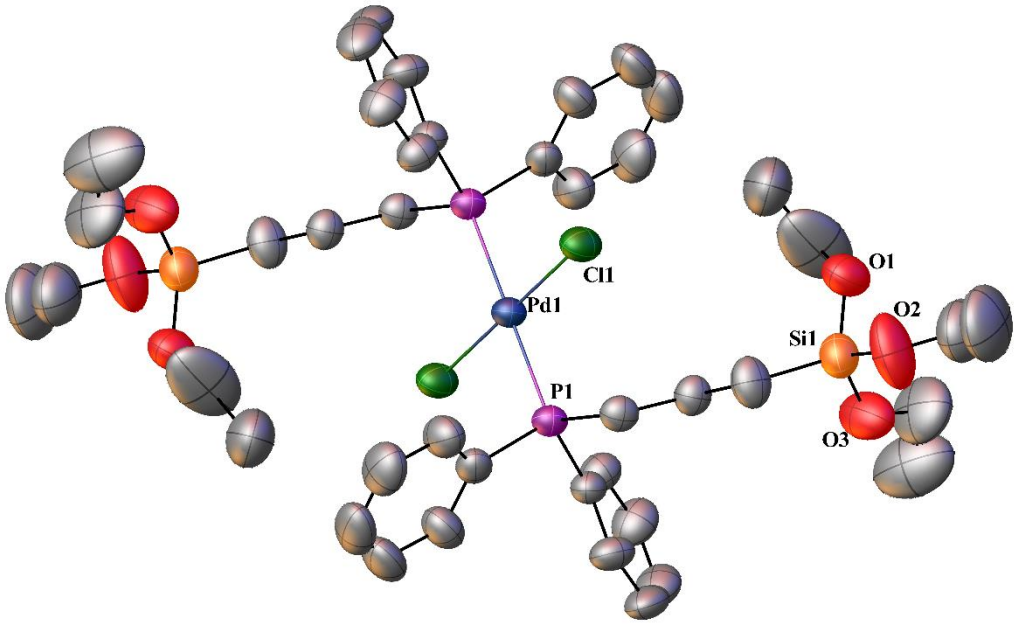

Table A-1. Crystal data and structure refinement for JBB_JP_275.

Identification code	jbb	
Empirical formula	C42 H62 Cl2 O6 P2 Pd Si2	
Formula weight	958.34	
Temperature	273(2) K	
Wavelength	0.71073 Å	
Crystal system	Monoclinic	
Space group	P2(1)/c	
Unit cell dimensions	a = 13.564(2) Å	α = 90°.
	b = 8.8285(14) Å	β = 96.056(2)°.
	c = 20.404(3) Å	γ = 90°.
Volume	2429.8(7) $Å^3$	
Z	2	
Density (calculated)	1.310 Mg/m^3	
Absorption coefficient	0.648 mm^{-1}	
F(000)	1000	
Crystal size	0.57 x 0.20 x 0.05 mm^3	
Theta range for data collection	2.01 to 27.48°.	
Index ranges	-17<=h<=14, -11<=k<=11, -26<=l<=26	

Reflections collected	18486
Independent reflections	5523 [R(int) = 0.0438]
Completeness to theta = 27.48°	99.2 %
Absorption correction	Semi-empirical from equivalents
Max. and min. transmission	0.9683 and 0.7090
Refinement method	Full-matrix least-squares on F^2
Data / restraints / parameters	5523 / 16 / 278
Goodness-of-fit on F^2	1.049
Final R indices [I>2sigma(I)]	R1 = 0.0410, wR2 = 0.1034
R indices (all data)	R1 = 0.0582, wR2 = 0.1147
Largest diff. peak and hole	0.661 and -0.568 e.$Å^{-3}$

Table A-2. Atomic coordinates (x 10^4) and equivalent isotropic displacement parameters ($Å^2$ x 10^3) for JBB_JP_275. U(eq) is defined as one third of the trace of the orthogonalized U^{ij} tensor.

	x	y	z	U(eq)
Pd(1)	0	5000	5000	40(1)
Cl(1)	-454(1)	2853(1)	5530(1)	60(1)
P(1)	-98(1)	6265(1)	5992(1)	43(1)
Si(1)	2987(1)	10479(1)	5966(1)	70(1)
O(1)	3421(6)	10123(7)	5297(3)	91(2)
O(2)	3123(3)	12319(4)	5963(2)	134(1)
O(3)	3574(3)	9763(4)	6614(2)	107(1)
C(1)	236(2)	8272(3)	6001(1)	49(1)
C(2)	1358(2)	8488(3)	6030(2)	54(1)
C(3)	1662(3)	10136(4)	5977(2)	72(1)
C(4)	638(2)	5568(4)	6728(1)	48(1)
C(5)	1314(3)	4414(4)	6693(2)	60(1)
C(6)	1914(3)	3986(5)	7253(2)	78(1)
C(7)	1849(4)	4713(5)	7835(2)	84(1)
C(8)	1189(3)	5852(5)	7882(2)	77(1)
C(9)	575(3)	6294(4)	7330(1)	64(1)
C(10)	-1372(2)	6185(4)	6184(1)	52(1)

C(11)	-1654(3)	5291(4)	6694(2)	72(1)
C(12)	-2636(4)	5233(5)	6812(3)	91(1)
C(13)	-3338(3)	6042(6)	6418(3)	98(2)
C(14)	-3078(3)	6910(6)	5921(2)	94(1)
C(15)	-2088(3)	6976(5)	5797(2)	74(1)
C(16)	3916(5)	13217(7)	5920(3)	135(2)
C(17)	3718(6)	14752(8)	5832(4)	171(3)
C(18)	4574(8)	9480(30)	6737(16)	142(8)
C(19)	4759(19)	8340(30)	7263(11)	178(9)
C(20)	3552(11)	8702(12)	5020(6)	176(7)
C(21)	3228(9)	7964(14)	4430(6)	139(4)
O(1A)	3446(8)	9346(10)	5442(4)	91(2)
C(18A)	4347(14)	8770(20)	6745(19)	163(11)
C(19A)	5169(18)	9440(30)	7178(14)	178(9)
C(20A)	2993(13)	9320(20)	4787(7)	176(7)
C(21A)	3675(12)	8570(20)	4429(10)	139(4)

Table A-3. Bond lengths [Å] and angles [°] JBB_JP_275

Pd(1)-Cl(1)	2.2978(8)
Pd(1)-Cl(1)#1	2.2978(8)
Pd(1)-P(1)	2.3273(7)
Pd(1)-P(1)#1	2.3273(7)
P(1)-C(10)	1.813(3)
P(1)-C(4)	1.820(3)
P(1)-C(1)	1.829(3)
Si(1)-O(1)	1.575(5)
Si(1)-O(3)	1.600(3)
Si(1)-O(2)	1.635(4)
Si(1)-O(1A)	1.635(7)
Si(1)-C(3)	1.826(4)
O(1)-C(20)	1.395(8)
O(2)-C(16)	1.346(6)

O(3)-C(18A)	1.371(10)
O(3)-C(18)	1.376(9)
C(1)-C(2)	1.529(4)
C(1)-H(1A)	0.9700
C(1)-H(1B)	0.9700
C(2)-C(3)	1.519(4)
C(2)-H(2A)	0.9700
C(2)-H(2B)	0.9700
C(3)-H(3A)	0.9700
C(3)-H(3B)	0.9700
C(4)-C(5)	1.378(5)
C(4)-C(9)	1.397(4)
C(5)-C(6)	1.383(4)
C(5)-H(5)	0.9300
C(6)-C(7)	1.361(6)
C(6)-H(6)	0.9300
C(7)-C(8)	1.357(6)
C(7)-H(7)	0.9300
C(8)-C(9)	1.383(5)
C(8)-H(8)	0.9300
C(9)-H(9)	0.9300
C(10)-C(15)	1.376(5)
C(10)-C(11)	1.391(5)
C(11)-C(12)	1.379(6)
C(11)-H(11)	0.9300
C(12)-C(13)	1.379(7)
C(12)-H(12)	0.9300
C(13)-C(14)	1.348(7)
C(13)-H(13)	0.9300
C(14)-C(15)	1.394(5)
C(14)-H(14)	0.9300
C(15)-H(15)	0.9300
C(16)-C(17)	1.390(8)

C(16)-H(16A)	0.9700
C(16)-H(16B)	0.9700
C(17)-H(17A)	0.9600
C(17)-H(17B)	0.9600
C(17)-H(17C)	0.9600
C(18)-C(19)	1.473(12)
C(18)-H(18A)	0.9700
C(18)-H(18B)	0.9700
C(19)-H(19A)	0.9600
C(19)-H(19B)	0.9600
C(19)-H(19C)	0.9600
C(20)-C(21)	1.398(10)
C(20)-H(20A)	0.9700
C(20)-H(20B)	0.9700
C(21)-H(21A)	0.9600
C(21)-H(21B)	0.9600
C(21)-H(21C)	0.9600
O(1A)-C(20A)	1.411(11)
C(18A)-C(19A)	1.472(12)
C(18A)-H(18C)	0.9700
C(18A)-H(18D)	0.9700
C(19A)-H(19D)	0.9600
C(19A)-H(19E)	0.9600
C(19A)-H(19F)	0.9600
C(20A)-C(21A)	1.406(11)
C(20A)-H(20C)	0.9700
C(20A)-H(20D)	0.9700
C(21A)-H(21D)	0.9600
C(21A)-H(21E)	0.9600
C(21A)-H(21F)	0.9600
Cl(1)-Pd(1)-Cl(1)#1	180.00(3)
Cl(1)-Pd(1)-P(1)	86.79(3)
Cl(1)#1-Pd(1)-P(1)	93.22(3)

Cl(1)-Pd(1)-P(1)#1	93.21(3)
Cl(1)#1-Pd(1)-P(1)#1	86.79(3)
P(1)-Pd(1)-P(1)#1	180.0
C(10)-P(1)-C(4)	105.08(14)
C(10)-P(1)-C(1)	106.04(14)
C(4)-P(1)-C(1)	101.85(14)
C(10)-P(1)-Pd(1)	108.25(9)
C(4)-P(1)-Pd(1)	118.59(10)
C(1)-P(1)-Pd(1)	115.90(9)
O(1)-Si(1)-O(3)	116.0(3)
O(1)-Si(1)-O(2)	98.2(3)
O(3)-Si(1)-O(2)	110.5(2)
O(1)-Si(1)-O(1A)	26.8(3)
O(3)-Si(1)-O(1A)	96.2(4)
O(2)-Si(1)-O(1A)	123.7(4)
O(1)-Si(1)-C(3)	115.9(3)
O(3)-Si(1)-C(3)	109.23(19)
O(2)-Si(1)-C(3)	106.06(18)
O(1A)-Si(1)-C(3)	110.5(4)
C(20)-O(1)-Si(1)	127.3(7)
C(16)-O(2)-Si(1)	132.6(4)
C(18A)-O(3)-C(18)	29.5(15)
C(18A)-O(3)-Si(1)	135.9(17)
C(18)-O(3)-Si(1)	128.1(12)
C(2)-C(1)-P(1)	111.5(2)
C(2)-C(1)-H(1A)	109.3
P(1)-C(1)-H(1A)	109.3
C(2)-C(1)-H(1B)	109.3
P(1)-C(1)-H(1B)	109.3
H(1A)-C(1)-H(1B)	108.0
C(3)-C(2)-C(1)	113.1(3)
C(3)-C(2)-H(2A)	109.0
C(1)-C(2)-H(2A)	109.0

C(3)-C(2)-H(2B)	109.0
C(1)-C(2)-H(2B)	109.0
H(2A)-C(2)-H(2B)	107.8
C(2)-C(3)-Si(1)	115.7(2)
C(2)-C(3)-H(3A)	108.4
Si(1)-C(3)-H(3A)	108.4
C(2)-C(3)-H(3B)	108.4
Si(1)-C(3)-H(3B)	108.4
H(3A)-C(3)-H(3B)	107.4
C(5)-C(4)-C(9)	119.2(3)
C(5)-C(4)-P(1)	121.2(2)
C(9)-C(4)-P(1)	119.5(3)
C(4)-C(5)-C(6)	119.8(3)
C(4)-C(5)-H(5)	120.1
C(6)-C(5)-H(5)	120.1
C(7)-C(6)-C(5)	120.3(4)
C(7)-C(6)-H(6)	119.8
C(5)-C(6)-H(6)	119.8
C(8)-C(7)-C(6)	121.0(4)
C(8)-C(7)-H(7)	119.5
C(6)-C(7)-H(7)	119.5
C(7)-C(8)-C(9)	119.8(3)
C(7)-C(8)-H(8)	120.1
C(9)-C(8)-H(8)	120.1
C(8)-C(9)-C(4)	119.9(3)
C(8)-C(9)-H(9)	120.0
C(4)-C(9)-H(9)	120.0
C(15)-C(10)-C(11)	119.0(3)
C(15)-C(10)-P(1)	119.1(2)
C(11)-C(10)-P(1)	121.8(3)
C(12)-C(11)-C(10)	119.9(4)
C(12)-C(11)-H(11)	120.0
C(10)-C(11)-H(11)	120.0

C(11)-C(12)-C(13)	119.9(4)
C(11)-C(12)-H(12)	120.1
C(13)-C(12)-H(12)	120.1
C(14)-C(13)-C(12)	121.0(4)
C(14)-C(13)-H(13)	119.5
C(12)-C(13)-H(13)	119.5
C(13)-C(14)-C(15)	119.6(4)
C(13)-C(14)-H(14)	120.2
C(15)-C(14)-H(14)	120.2
C(10)-C(15)-C(14)	120.7(4)
C(10)-C(15)-H(15)	119.7
C(14)-C(15)-H(15)	119.7
O(2)-C(16)-C(17)	116.1(6)
O(2)-C(16)-H(16A)	108.3
C(17)-C(16)-H(16A)	108.3
O(2)-C(16)-H(16B)	108.3
C(17)-C(16)-H(16B)	108.3
H(16A)-C(16)-H(16B)	107.4
C(16)-C(17)-H(17A)	109.5
C(16)-C(17)-H(17B)	109.5
H(17A)-C(17)-H(17B)	109.5
C(16)-C(17)-H(17C)	109.5
H(17A)-C(17)-H(17C)	109.5
H(17B)-C(17)-H(17C)	109.5
O(3)-C(18)-C(19)	110.2(16)
O(3)-C(18)-H(18A)	109.6
C(19)-C(18)-H(18A)	109.6
O(3)-C(18)-H(18B)	109.6
C(19)-C(18)-H(18B)	109.6
H(18A)-C(18)-H(18B)	108.1
O(1)-C(20)-C(21)	136.5(13)
O(1)-C(20)-H(20A)	103.0
C(21)-C(20)-H(20A)	103.0

O(1)-C(20)-H(20B)	103.0
C(21)-C(20)-H(20B)	103.0
H(20A)-C(20)-H(20B)	105.1
C(20A)-O(1A)-Si(1)	118.1(8)
O(3)-C(18A)-C(19A)	112.1(18)
O(3)-C(18A)-H(18C)	109.2
C(19A)-C(18A)-H(18C)	109.2
O(3)-C(18A)-H(18D)	109.2
C(19A)-C(18A)-H(18D)	109.2
H(18C)-C(18A)-H(18D)	107.9
C(18A)-C(19A)-H(19D)	109.5
C(18A)-C(19A)-H(19E)	109.5
H(19D)-C(19A)-H(19E)	109.5
C(18A)-C(19A)-H(19F)	109.5
H(19D)-C(19A)-H(19F)	109.5
H(19E)-C(19A)-H(19F)	109.5
C(21A)-C(20A)-O(1A)	104.7(13)
C(21A)-C(20A)-H(20C)	110.8
O(1A)-C(20A)-H(20C)	110.8
C(21A)-C(20A)-H(20D)	110.8
O(1A)-C(20A)-H(20D)	110.8
H(20C)-C(20A)-H(20D)	108.9
C(20A)-C(21A)-H(21D)	109.5
C(20A)-C(21A)-H(21E)	109.5
H(21D)-C(21A)-H(21E)	109.5
C(20A)-C(21A)-H(21F)	109.5
H(21D)-C(21A)-H(21F)	109.5
H(21E)-C(21A)-H(21F)	109.5

Table A-4. Anisotropic displacement parameters ($Å^2 x\ 10^3$) for JBB_JP_275. The anisotropic displacement factor exponent takes the form: $-2\pi^2[h^2 a^{*2} U^{11} + ... + 2 h k a^* b^* U^{12}]$

	U^{11}	U^{22}	U^{33}	U^{23}	U^{13}	U^{12}
Pd(1)	44(1)	41(1)	35(1)	1(1)	8(1)	2(1)
Cl(1)	81(1)	51(1)	48(1)	5(1)	13(1)	-9(1)
P(1)	47(1)	45(1)	38(1)	-2(1)	8(1)	2(1)
Si(1)	65(1)	71(1)	74(1)	5(1)	4(1)	-11(1)
O(1)	106(3)	95(5)	74(3)	1(3)	28(3)	-22(4)
O(2)	98(2)	83(2)	225(5)	15(3)	29(3)	-29(2)
O(3)	77(2)	159(4)	85(2)	22(2)	4(2)	17(2)
C(1)	55(2)	42(2)	50(2)	-3(1)	9(1)	5(1)
C(2)	54(2)	47(2)	60(2)	-3(1)	4(1)	1(1)
C(3)	65(2)	49(2)	100(3)	8(2)	6(2)	-2(2)
C(4)	52(2)	53(2)	40(1)	1(1)	6(1)	-4(1)
C(5)	67(2)	58(2)	54(2)	2(1)	0(2)	2(2)
C(6)	82(3)	72(2)	75(2)	11(2)	-15(2)	8(2)
C(7)	92(3)	94(3)	59(2)	21(2)	-17(2)	-11(2)
C(8)	98(3)	92(3)	38(2)	1(2)	0(2)	-20(3)
C(9)	84(2)	66(2)	42(2)	-3(1)	8(2)	0(2)
C(10)	50(2)	58(2)	49(2)	-13(1)	12(1)	-3(1)
C(11)	66(2)	78(3)	77(2)	0(2)	26(2)	-6(2)
C(12)	78(3)	109(4)	94(3)	-13(2)	44(3)	-21(3)
C(13)	55(2)	129(4)	115(4)	-40(3)	30(3)	-15(3)
C(14)	55(2)	120(4)	106(3)	-16(3)	2(2)	7(2)
C(15)	53(2)	100(3)	68(2)	-1(2)	8(2)	2(2)
C(16)	147(5)	112(5)	142(5)	0(4)	6(4)	-46(4)
C(17)	189(8)	106(5)	216(9)	-1(5)	14(6)	-74(5)
C(18)	88(9)	180(20)	145(14)	13(19)	-36(8)	29(10)
C(19)	148(18)	230(20)	146(9)	-10(17)	-15(11)	95(16)
C(20)	230(17)	89(9)	233(13)	-64(9)	131(12)	-3(8)
C(21)	117(9)	176(12)	123(6)	-20(8)	2(7)	-46(6)
O(1A)	106(3)	95(5)	74(3)	1(3)	28(3)	-22(4)
C(18A)	220(30)	133(18)	126(14)	3(15)	-39(19)	72(17)

C(19A)	148(18)	230(20)	146(9)	-10(17)	-15(11)	95(16)
C(20A)	230(17)	89(9)	233(13)	-64(9)	131(12)	-3(8)
C(21A)	117(9)	176(12)	123(6)	-20(8)	2(7)	-46(6)

Table A-5. Hydrogen coordinates (x 10^4) and isotropic displacement parameters ($Å^2$ x 10^3) for JBB_JP_275.

	x	y	z	U(eq)
H(1A)	-82	8757	5607	59
H(1B)	-4	8756	6380	59
H(2A)	1668	8076	6442	65
H(2B)	1603	7920	5673	65
H(3A)	1438	10686	6345	86
H(3B)	1317	10555	5577	86
H(5)	1367	3925	6295	72
H(6)	2365	3198	7231	93
H(7)	2264	4424	8206	100
H(8)	1148	6333	8283	92
H(9)	121	7073	7361	77
H(11)	-1181	4734	6955	87
H(12)	-2824	4648	7157	110
H(13)	-4000	5988	6497	118
H(14)	-3557	7461	5662	113
H(15)	-1909	7560	5449	88
H(16A)	4260	12866	5556	161
H(16B)	4363	13094	6320	161
H(17A)	3096	14880	5567	257
H(17B)	4236	15213	5614	257
H(17C)	3687	15225	6253	257
H(18A)	4920	10412	6869	171
H(18B)	4827	9117	6338	171
H(19A)	4338	7481	7162	267
H(19B)	4619	8773	7675	267

H(19C)	5440	8029	7294	267
H(20A)	3356	8012	5352	212
H(20B)	4268	8610	5043	212
H(21A)	2725	7240	4507	209
H(21B)	3777	7453	4266	209
H(21C)	2959	8694	4111	209
H(18C)	4588	8467	6334	195
H(18D)	4113	7872	6953	195
H(19D)	5620	9936	6915	267
H(19E)	5512	8659	7437	267
H(19F)	4910	10168	7466	267
H(20C)	2367	8783	4758	212
H(20D)	2874	10344	4622	212
H(21D)	4097	9296	4248	209
H(21E)	3323	7999	4078	209
H(21F)	4071	7893	4717	209

APPENDIX B

NMR SPECTRA

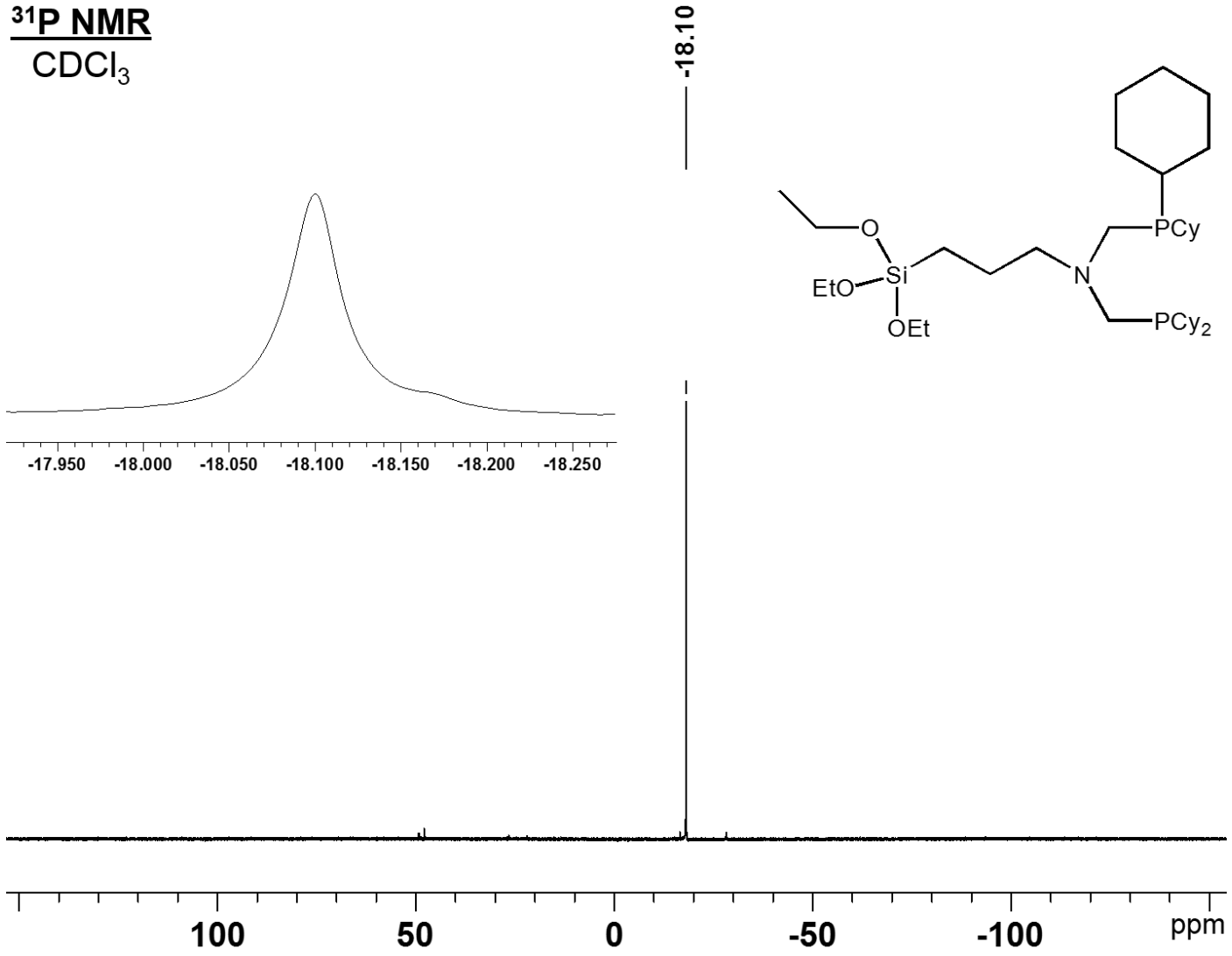
31P NMR
CDCl3
-18.10
O
EtO
Si
OEt
N
PCy
PCy2
-17.950
-18.000
-18.050
-18.100
-18.150
-18.200
-18.250
100
50
0
-50
-100
ppm

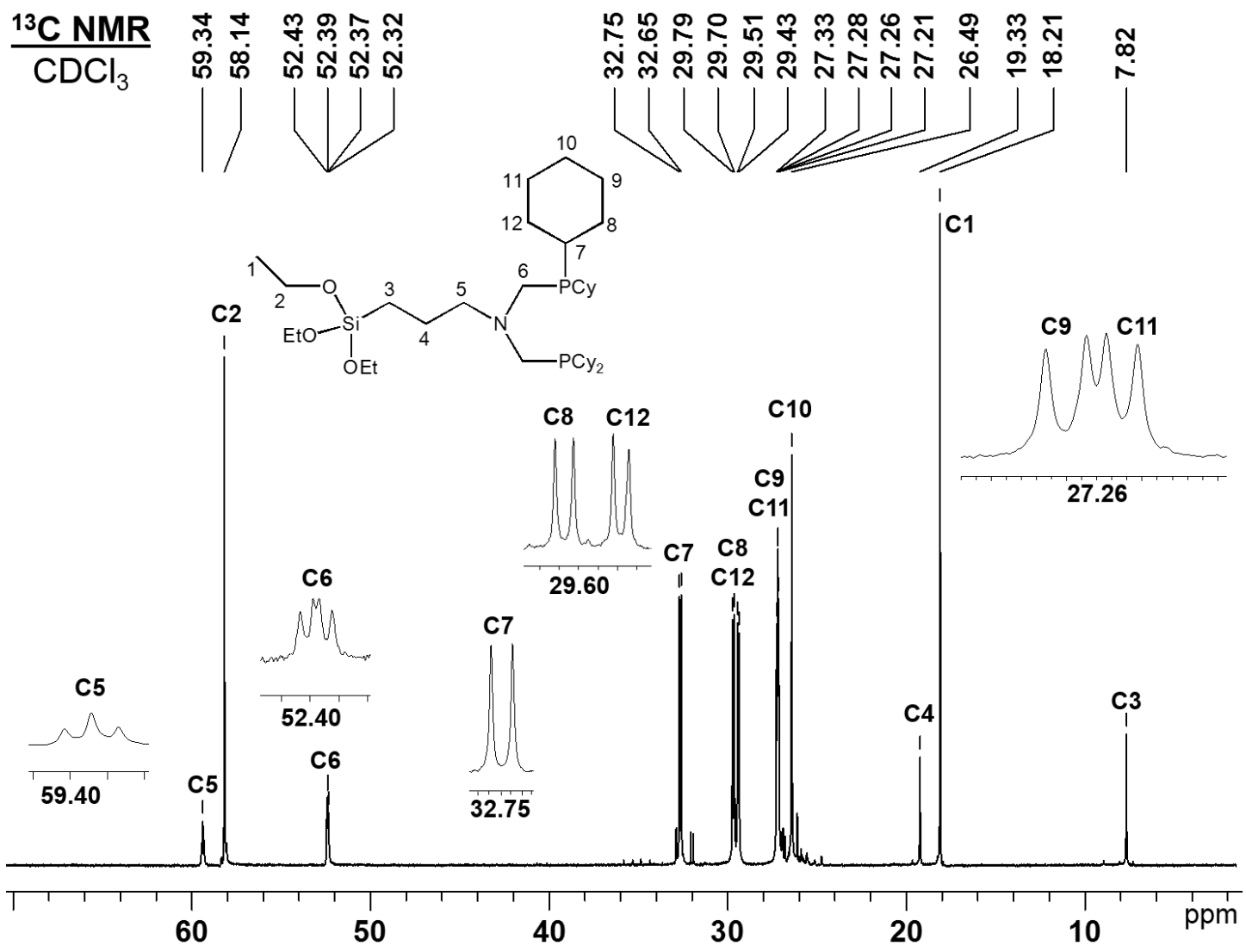
13C NMR
CDCl3
59.34
58.14
52.43
52.39
52.37
52.32
32.75
32.65
29.79
29.70
29.51
29.43
27.33
27.28
27.26
27.21
26.49
19.33
18.21
7.82
C1
C2
C3
C4
C5
C6
C7
C8
C12
C9
C11
C10
59.40
52.40
32.75
29.60
27.26
PCy
PCy2
EtO
OEt
Si
N
O
ppm
60
50
40
30
20
10

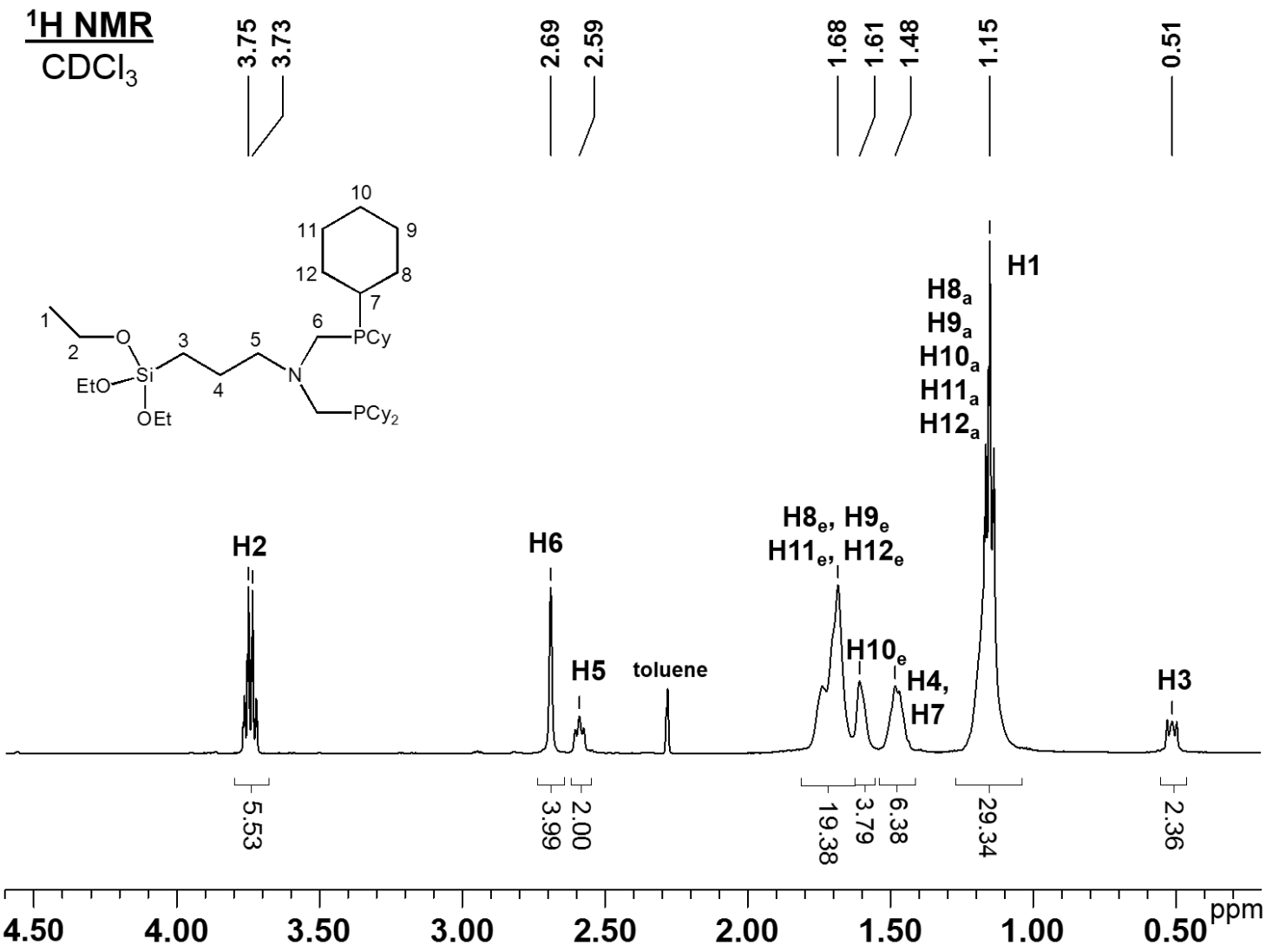
1H NMR
CDCl3
3.75
3.73
2.69
2.59
1.68
1.61
1.48
1.15
0.51
H1
H8a
H9a
H10a
H11a
H12a
H2
H6
H8e, H9e
H11e, H12e
H10e
H5
toluene
H4,
H7
H3
5.53
3.99
2.00
19.38
3.79
6.38
29.34
2.36
4.50
4.00
3.50
3.00
2.50
2.00
1.50
1.00
0.50
ppm

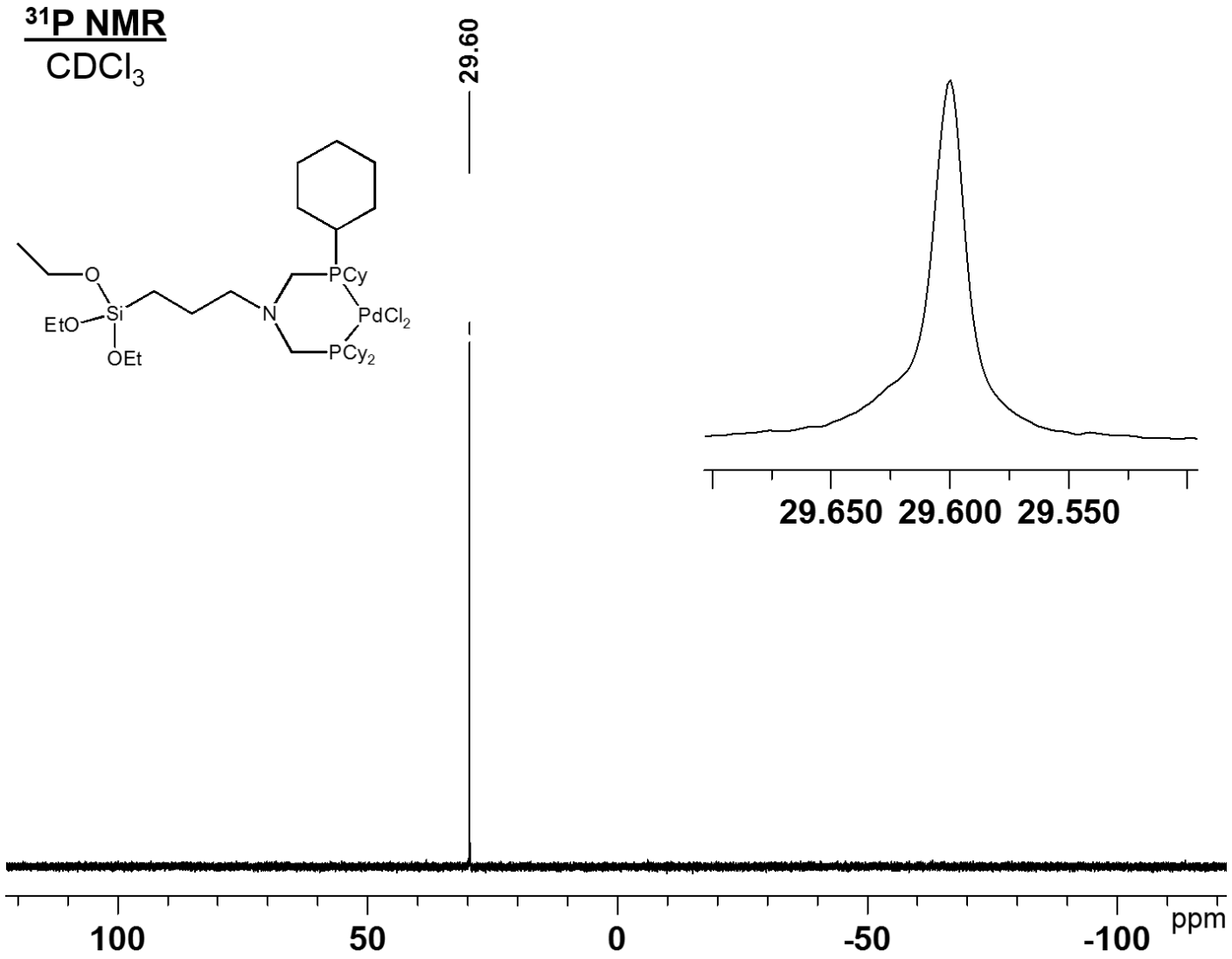
31P NMR
CDCl3
29.60
O
EtO
Si
OEt
N
PCy
PdCl2
PCy2
29.650 29.600 29.550
100
50
0
-50
-100
ppm

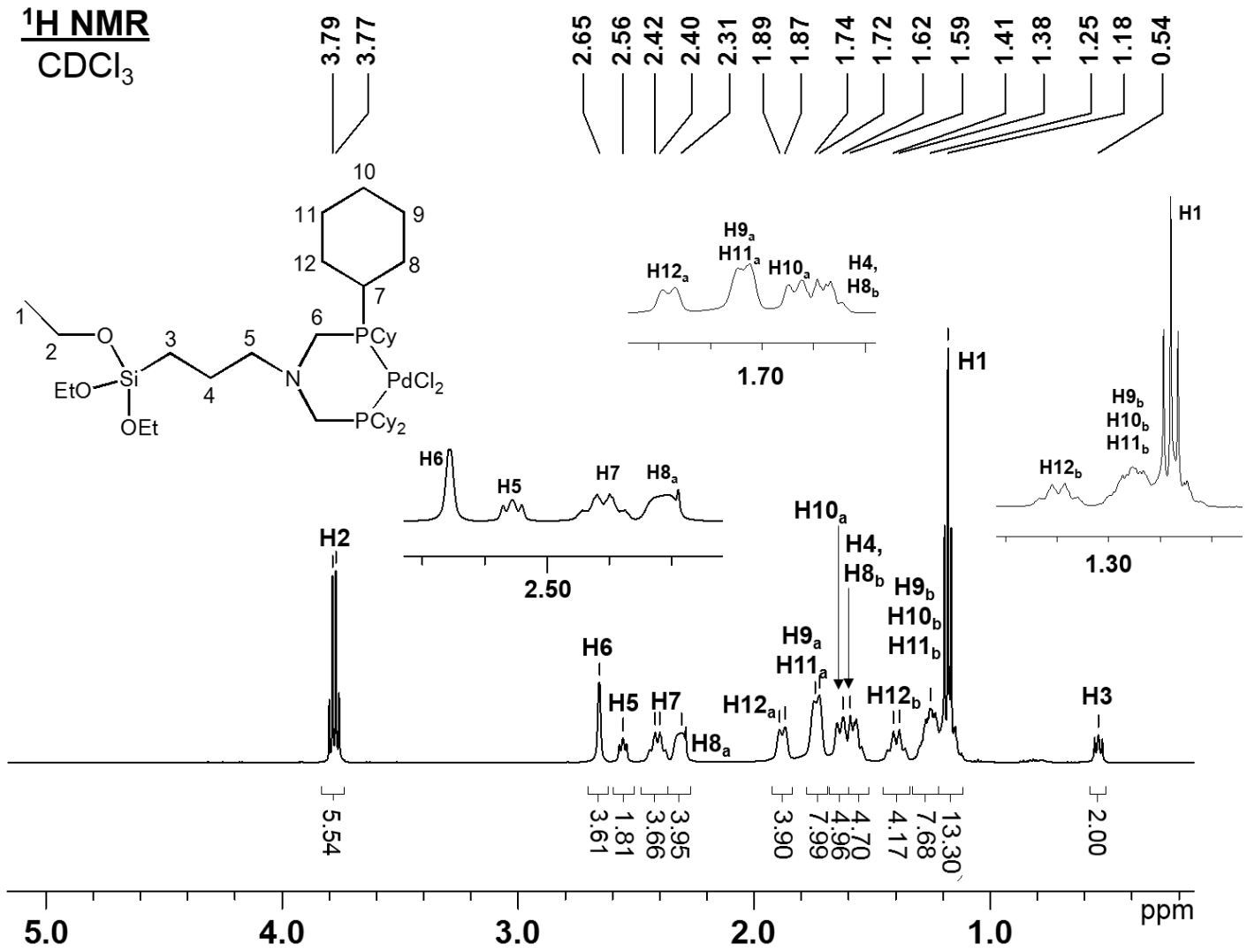
1H NMR
CDCl3
3.79
3.77
2.65
2.56
2.42
2.40
2.31
1.89
1.87
1.74
1.72
1.62
1.59
1.41
1.38
1.25
1.18
0.54
PCy
PdCl2
PCy2
EtO
OEt
Si
O
N
H1
H2
H3
H4, H8b
H5
H6
H7
H8a
H9a H11a
H9b H10b H11b
H10a
H12a
H12b
1.70
2.50
1.30
5.54
3.61
1.81
3.66
3.95
3.90
7.99
4.96
4.70
4.17
7.68
13.30
2.00
5.0
4.0
3.0
2.0
1.0
ppm

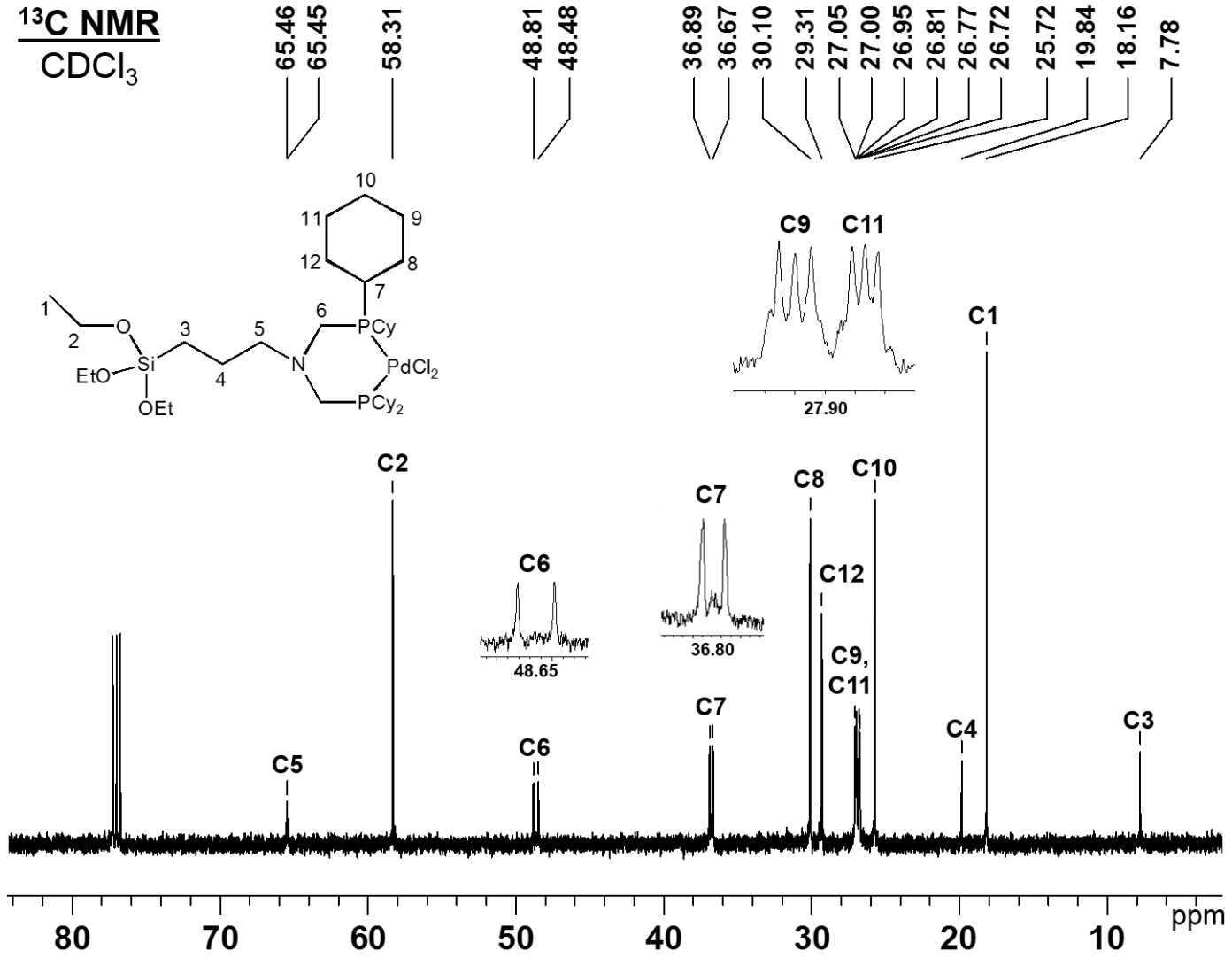
13C NMR
CDCl3
65.46
65.45
58.31
48.81
48.48
36.89
36.67
30.10
29.31
27.05
27.00
26.95
26.81
26.77
26.72
25.72
19.84
18.16
7.78
C9
C11
27.90
C1
C2
C7
C8
C10
C6
C12
48.65
36.80
C9,
C11
C7
C4
C3
C5
C6
80
70
60
50
40
30
20
10
ppm

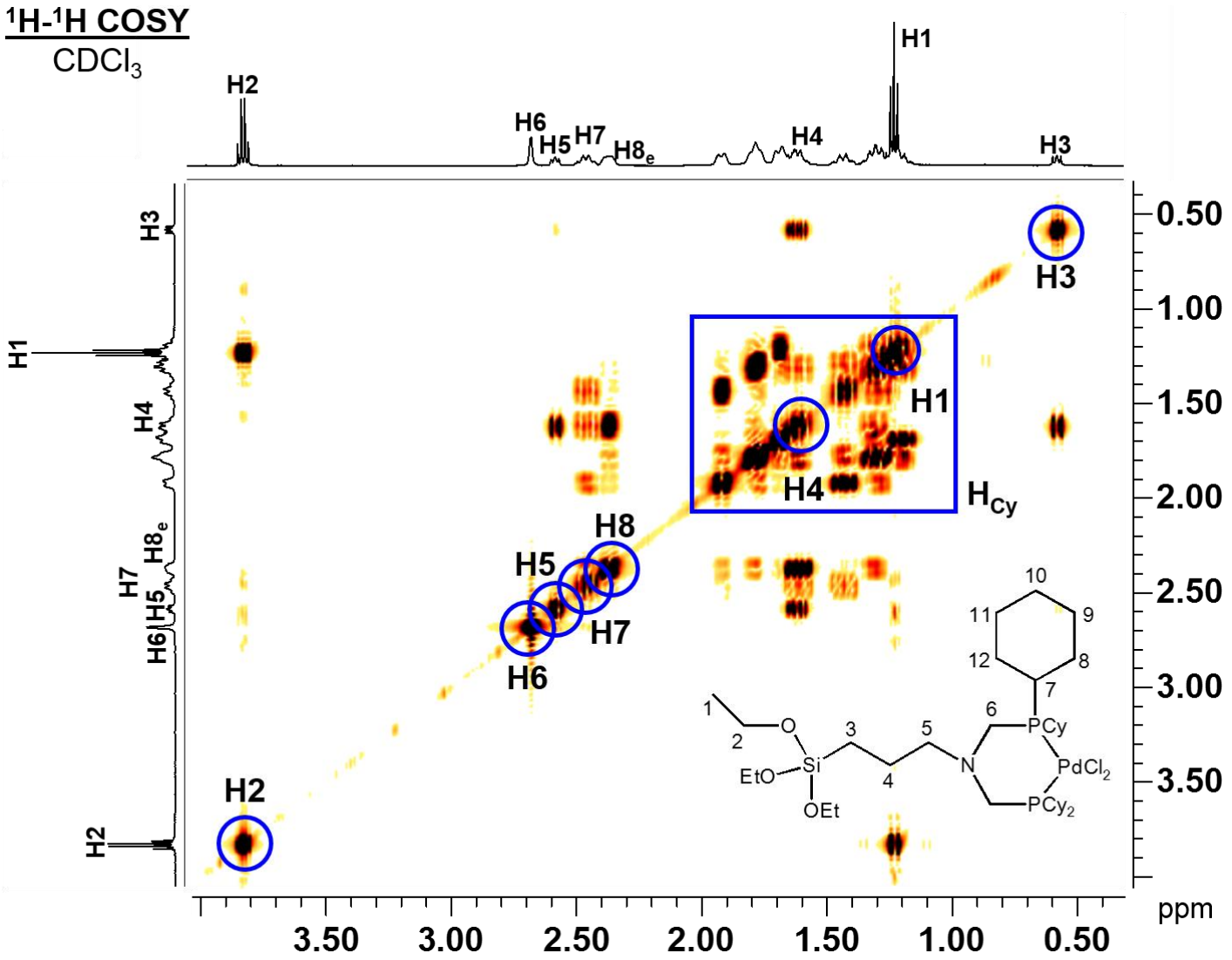
¹H-¹H COSY
CDCl3
H2
H6
H5
H7
H8e
H4
H1
H3
H1
H4
HCy
H8
H5
H7
H6
H2
H3
H1
H4
H8e
H7
H5
H6
H2
10
11
9
12
8
7
6
PCy
PdCl2
PCy2
1
2
O
3
5
Si
EtO
4
N
OEt
0.50
1.00
1.50
2.00
2.50
3.00
3.50
ppm
3.50
3.00
2.50
2.00
1.50
1.00
0.50

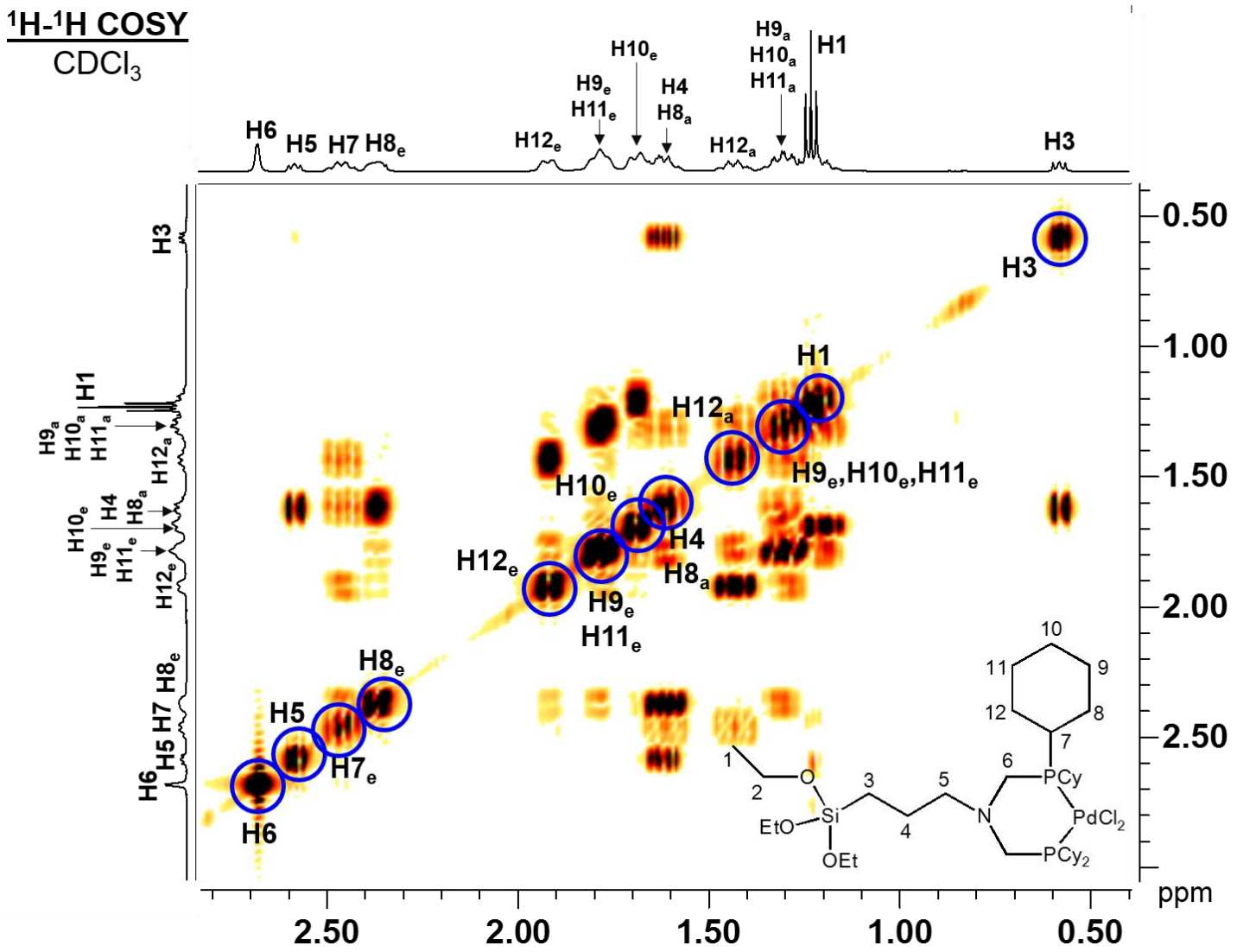
¹H-¹H COSY
CDCl3
H6
H5
H7
H8e
H12e
H9e
H11e
H10e
H4
H8a
H12a
H9a
H10a
H11a
H1
H3
H3
H1
H12a
H9e,H10e,H11e
H10e
H4
H8a
H12e
H9e
H11e
H8e
H5
H7e
H6
H9a H10a H11a H1
H12a
H10e H4 H8a
H9e H11e
H12e
H8e H7 H5 H6
0.50
1.00
1.50
2.00
2.50
ppm
2.50
2.00
1.50
1.00
0.50
10
11
9
12
8
7
6
PCy
PdCl2
PCy2
N
5
3
4
Si
O
1
2
EtO
OEt

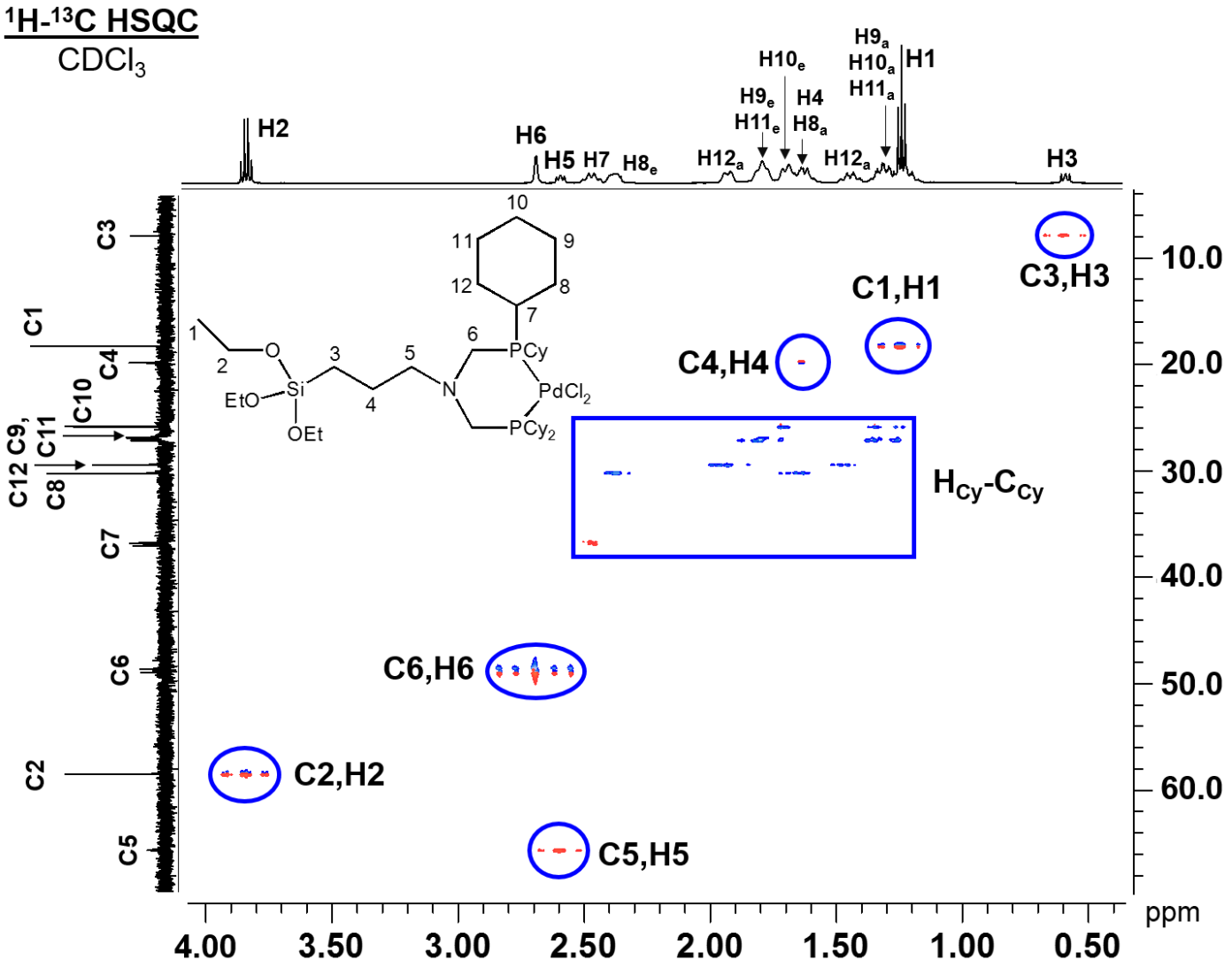
^{1}H-^{13}C HSQC
$CDCl_3$
H2
H6
H5
H7
H8$_e$
H12$_a$
H9$_e$
H11$_e$
H10$_e$
H4
H8$_a$
H12$_a$
H9$_a$
H10$_a$
H11$_a$
H1
H3
C3
C1
C4
C10
C9, C11
C12
C8
C7
C6
C2
C5
C3,H3
C1,H1
C4,H4
H_{Cy}-C_{Cy}
C6,H6
C2,H2
C5,H5
PCy
PdCl$_2$
PCy$_2$
EtO
Si
OEt
O
N
ppm
4.00
3.50
3.00
2.50
2.00
1.50
1.00
0.50
10.0
20.0
30.0
40.0
50.0
60.0

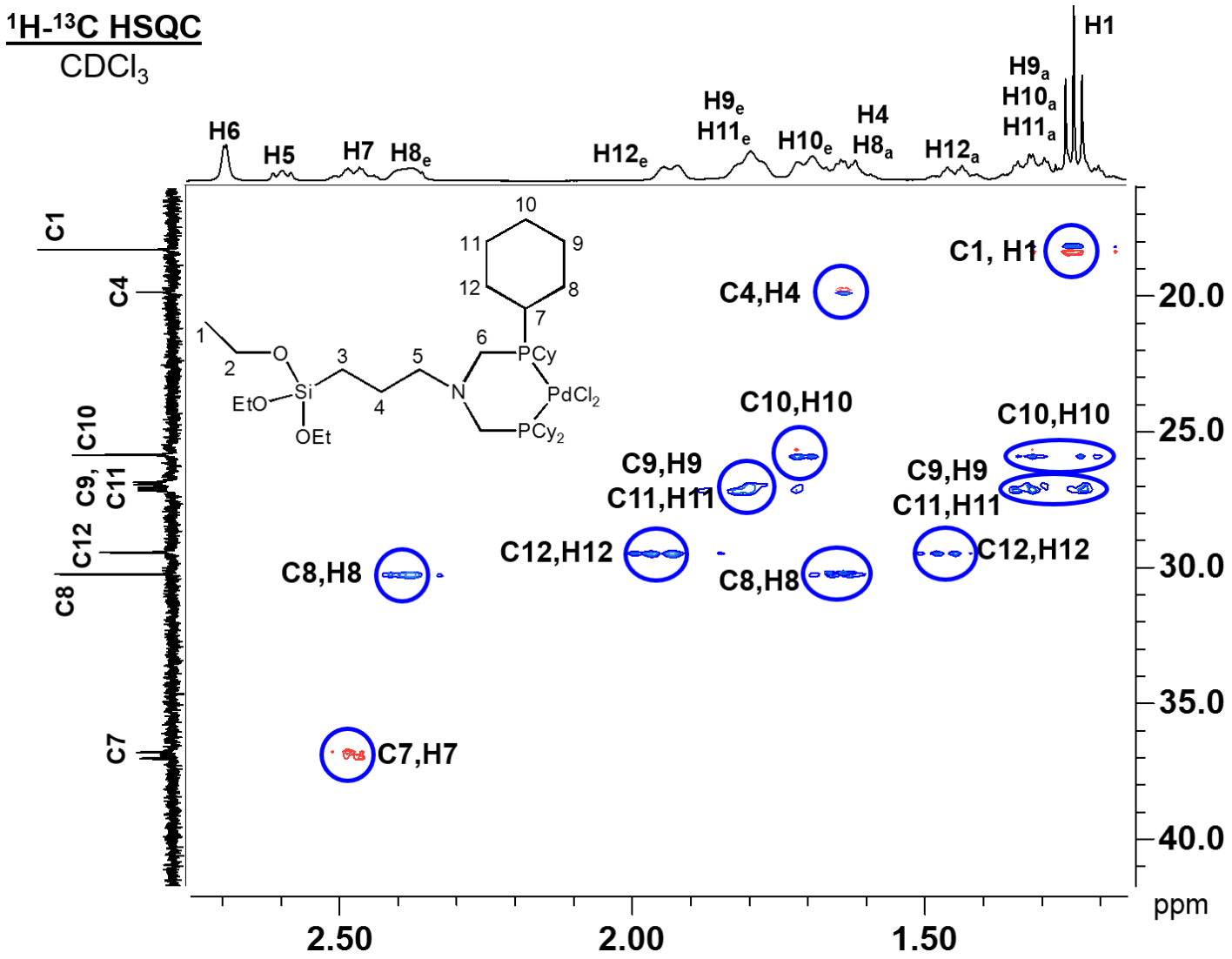
1H-13C HSQC
CDCl3
H6
H5
H7
H8e
H12e
H9e
H11e
H10e
H4
H8a
H12a
H9a
H10a
H11a
H1
C1
C4
C10
C9,
C11
C12
C8
C7
C1, H1
C4,H4
C10,H10
C9,H9
C11,H11
C12,H12
C8,H8
C7,H7
PCy
PdCl2
PCy2
EtO
OEt
Si
N
O
20.0
25.0
30.0
35.0
40.0
ppm
2.50
2.00
1.50

APPENDIX C

CATALYSIS DATA

Homogeneous catalysis with 4 and CuI

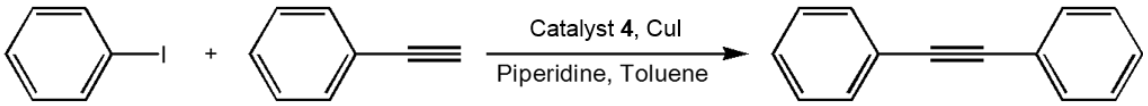

Catalyst 4	CuI	Phenylacetylene	Iodobenzene	Toluene	Piperidine
4 mol%	5 mol%	100 mol%	120 mol%		
0.018 mmol	0.022 mmol	0.634 mmol	0.462 mmol		
14.10 mg	4.0 mg	0.07 ml	0.05 ml	7.4 ml	3.7 ml

Time [h]	Substrate [%] Iodobenzene	Product [%] Diphenylacetylene
0	100.00	0.00
1	18.63	81.37
2	8.11	91.89
3	4.15	95.85
4	3.41	96.59
5	1.10	98.90
6	0.61	99.39

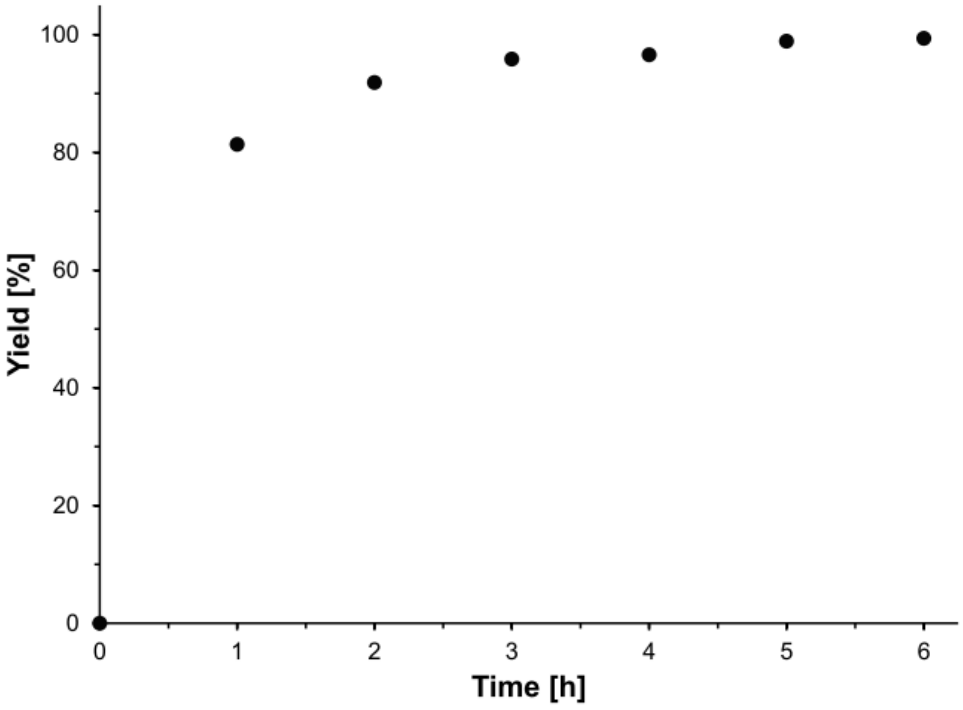
Yield [%]
100
80
60
40
20
0
0
1
2
3
4
5
6
Time [h]

Catalysis with 4i and CuI

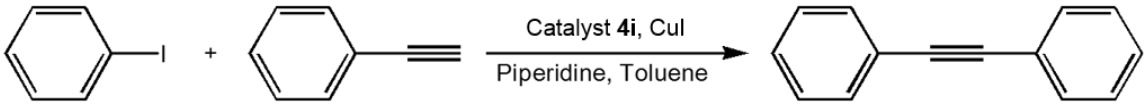

Catalyst 4i	CuI	Phenylacetylene	Iodobenzene	Toluene	Piperidine
4 mol%	5 mol%	120 mol%	100 mol%		
0.021 mmol	0.026 mmol	0.720 mmol	0.525 mmol		
166.7 mg	4.9 mg	0.08 ml	0.06 ml	8.6 ml	4.3 ml

Cycle #1		
Time [h]	**Substrate [%] Iodobenzene**	**Product [%] Diphenylacetylene**
0.00	100.00	0.00
0.17	95.21	4.79
0.33	90.53	9.47
0.50	86.34	13.66
0.67	84.95	15.05
0.83	80.25	19.75
1.00	76.49	23.51
2.00	58.29	41.71
3.00	26.17	73.83
4.00	18.17	81.83
5.00	4.53	95.48
6.00	0.17	99.83

Cycle #2		
Time [h]	**Substrate [%] Iodobenzene**	**Product [%] Diphenylacetylene**
0.00	100.00	0.00
0.17	100.00	0.00
0.33	99.66	0.34
0.50	97.16	2.85
0.67	96.68	3.32
0.83	91.69	8.31
1.00	89.10	10.90
2.00	80.01	19.99
3.00	77.10	22.90
4.00	76.95	23.05
5.00	75.79	24.20
6.00	74.73	25.27

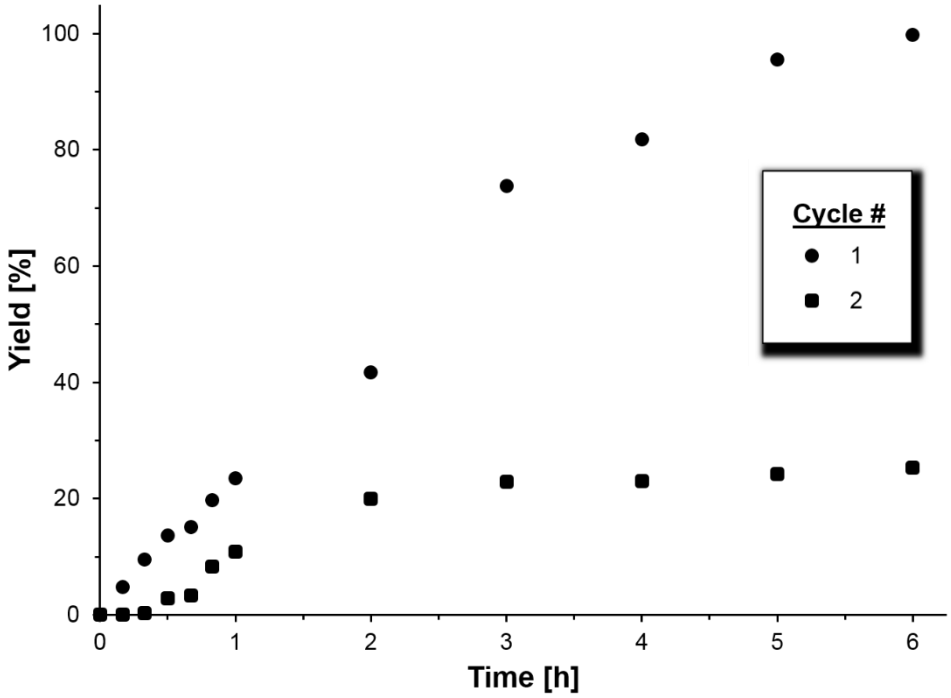
Yield [%]
Time [h]
Cycle #
1
2
0
20
40
60
80
100
0
1
2
3
4
5
6

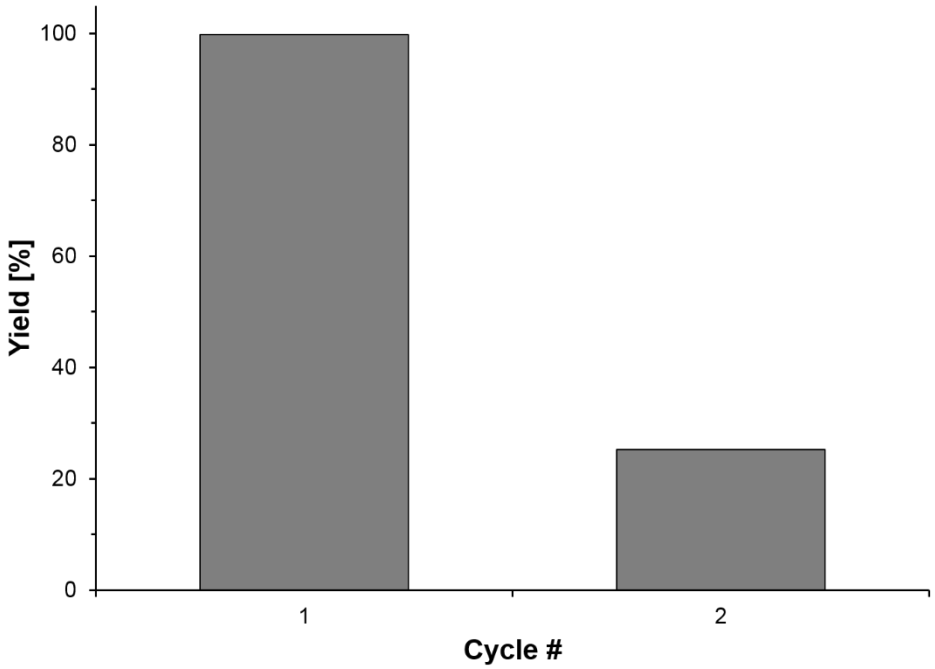
Yield [%]
Cycle #
0
20
40
60
80
100
1
2

Catalysis with 4i at RT and 60 °C

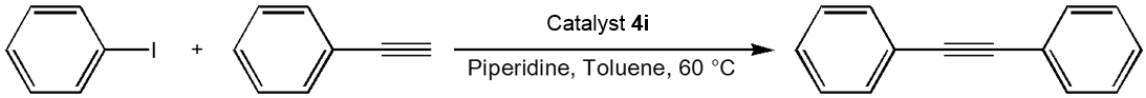

Catalyst 4i	Phenylacetylene	Iodobenzene	Toluene	Piperidine
4 mol%	120 mol%	100 mol%		
0.020 mmol	0.686 mmol	0.500 mmol		
0.1643 g	0.08 ml	0.06 ml	8.2 ml	4.1 ml

Time [h]	Substrate [%] Iodobenzene	Product [%] Diphenylacetylene
0.00	100.00	0.00
0.17	95.21	4.79
0.33	90.53	9.47
0.50	86.34	13.66
0.67	84.95	15.05
0.83	80.25	19.75
1.00	76.49	23.51
2.00	58.29	41.71
3.00	26.17	73.83
4.00	18.17	81.83
5.00	4.53	95.48
6.00	0.17	99.83

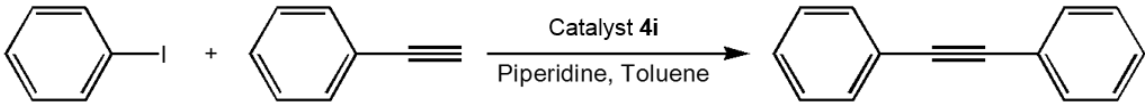

Catalyst 4i	Phenylacetylene	Iodobenzene	Toluene	Piperidine
1.0 mol%	120 mol%	100 mol%		
0.0063 mmol	0.73 mmol	0.63 mmol		
4.59 mg	0.08 ml	0.07 ml	10 ml	5 ml

Time [h]	Substrate [%] Iodobenzene	Product [%] Diphenylacetylene
0.0	100.00	0.00
0.25	100.00	0.00
0.50	99.68	0.32
0.75	99.55	0.45
1.0	99.41	0.59
2	98.47	1.53
3	97.31	2.69
4	85.97	4.03
5	94.50	5.50
6	92.69	7.31

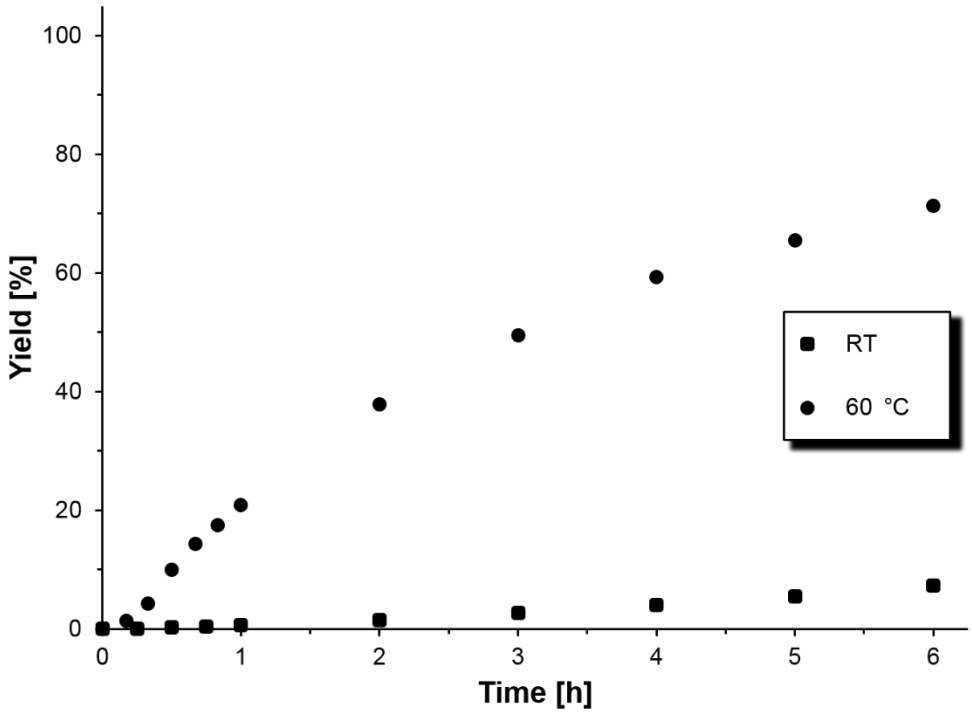
100
80
60
40
20
0
Yield [%]
0
1
2
3
4
5
6
Time [h]
RT
60 °C

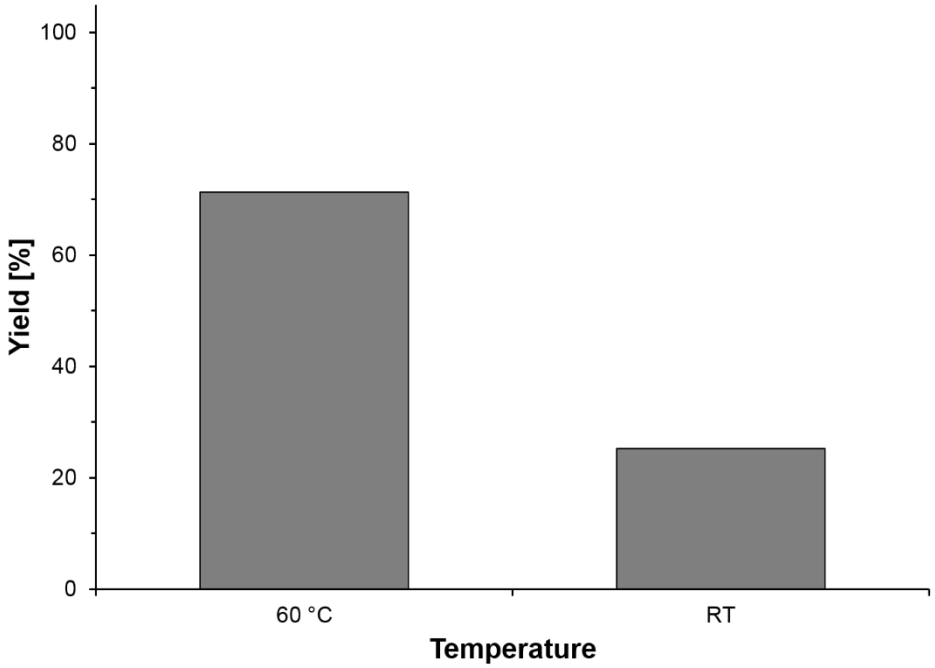
100
80
60
40
20
0
Yield [%]
60 °C
RT
Temperature

Catalysis with 7i at RT and at 60 °C

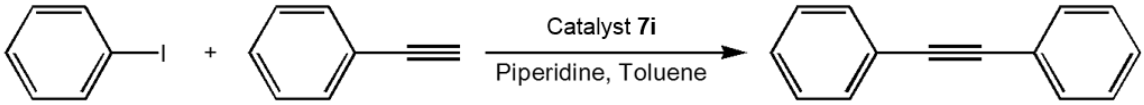

Catalyst 7i	Phenylacetylene	Iodobenzene	Toluene	Piperidine
5 mol%	120 mol%	100 mol%		
0.022 mmol	0.637 mmol	0.449 mmol		
0.1567 g	0.07 ml	0.05 ml	10.8 ml	5.4 ml

Time [h]	Substrate [%] Iodobenzene	Product [%] Diphenylacetylene
0.0	100.00	0.00
0.25	100.00	0.00
0.50	100.00	0.00
0.75	100.00	0.00
1.0	100.00	0.00
2	100.00	0.00
3	100.00	0.00
4	100.00	0.00
5	100.00	0.00
6	100.00	0.00

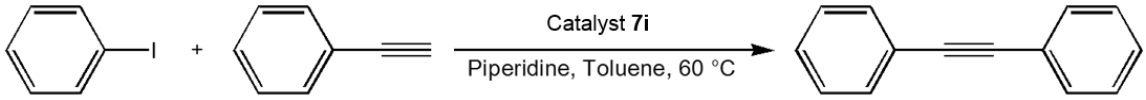

Catalyst 7i	Phenylacetylene	Iodobenzene	Toluene	Piperidine
5 mol%	120 mol%	100 mol%		
0.022 mmol	0.637 mmol	0.449 mmol		
0.1567 g	0.07 ml	0.05 ml	10.8 ml	5.4 ml

Time [h]	Substrate [%] Iodobenzene	Product [%] Diphenylacetylene
0.0	100.00	0.00
0.25	100.00	0.00
0.50	100.00	0.00
0.75	100.00	0.00
1.0	100.00	0.00
2	100.00	0.00
3	100.00	0.00
4	100.00	0.00
5	100.00	0.00
6	100.00	0.00

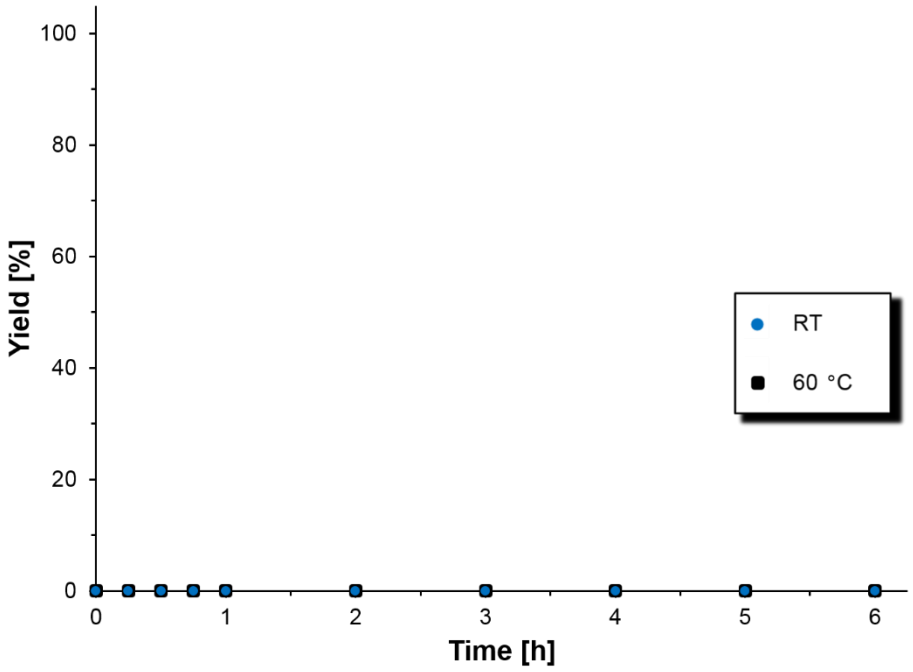
100
80
60
40
20
0
Yield [%]
0
1
2
3
4
5
6
Time [h]
RT
60 °C

Optimization of amount of Pd complex 4 with 1 mol% CuI

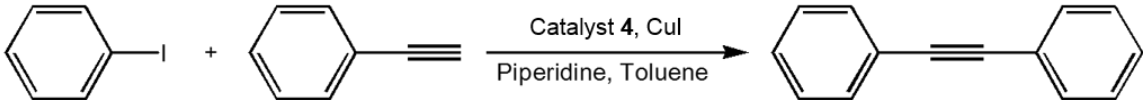

Catalyst 4	CuI	Phenylacetylene	Iodobenzene	Piperidine
0.1 mol%	1.0 mol%	120 mol%	100 mol%	
0.0024 mmol	0.024 mmol	2.82 mmol	2.33 mmol	
1.9 mg	4.6 mg	0.31 ml	0.26 ml	5 ml

Time [h]	Substrate [%] Iodobenzene	Product [%] Diphenylacetylene
0.0	100.00	0.00
0.25	92.21	7.79
0.50	85.56	14.44
0.75	81.85	18.15
1.0	79.31	20.69
2	76.65	23.35
3	73.65	26.35
4	70.61	29.39
5	68.09	31.91
6	66.64	33.37

Catalyst 4	CuI	Phenylacetylene	Iodobenzene	Piperidine
1.0 mol%	1.0 mol%	120 mol%	100 mol%	
0.0064 mmol	0.0063 mmol	0.73 mmol	0.63 mmol	
5.1 mg	1.2 mg	0.08 ml	0.07 ml	5 ml

Time [h]	Substrate [%] Iodobenzene	Product [%] Diphenylacetylene
0.0	100.00	0.00
0.25	68.72	31.28
0.50	51.07	48.93
0.75	35.96	64.04
1.0	30.11	69.89
2.0	14.35	85.65
3.0	8.44	91.56
4.0	4.79	95.21
5.0	2.83	97.17
6.0	1.56	98.44

Catalyst 4	CuI	Phenylacetylene	Iodobenzene	Piperidine
2.0 mol%	1.0 mol%	120 mol%	100 mol%	
0.0088 mmol	0.0047 mmol	0.55 mmol	0.45 mmol	
7.0 mg	0.9 mg	0.06 ml	0.05 ml	5 ml

Time [h]	Substrate [%] Iodobenzene	Product [%] Diphenylacetylene
0.0	100	0
0.25	83.90	16.10
0.50	67.52	32.48
0.75	50.71	49.29
1.0	34.63	65.37
2.0	6.67	93.33
3.0	0.28	99.72
4.0	0.00	100.00
5.0	0.00	100.00
6.0	0.00	100.00

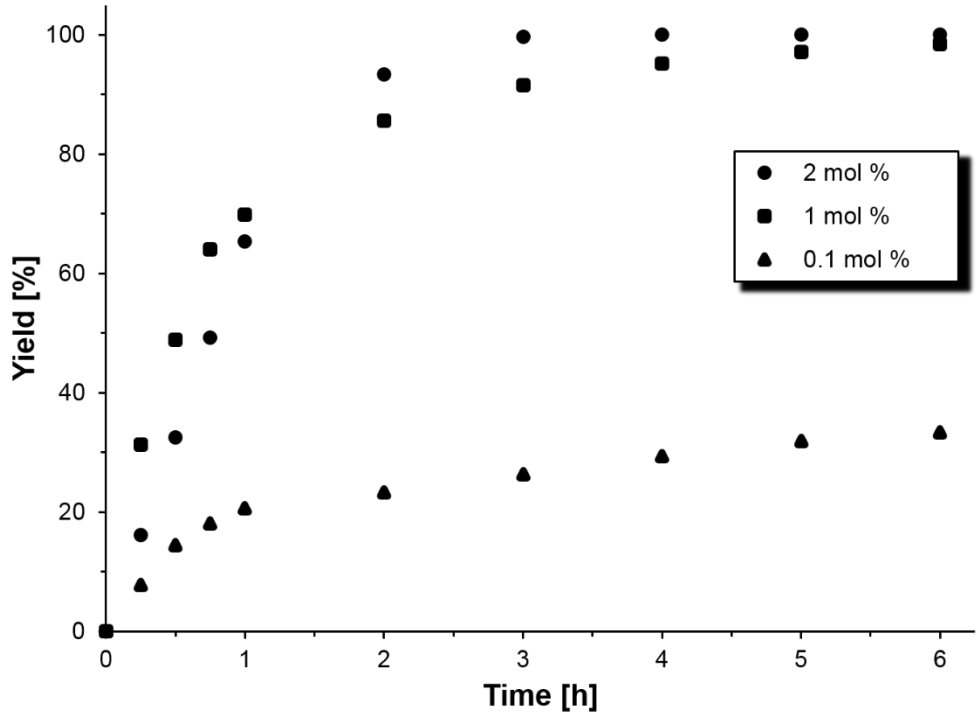
100
80
60
40
20
0
Yield [%]
0
1
2
3
4
5
6
Time [h]
2 mol %
1 mol %
0.1 mol %

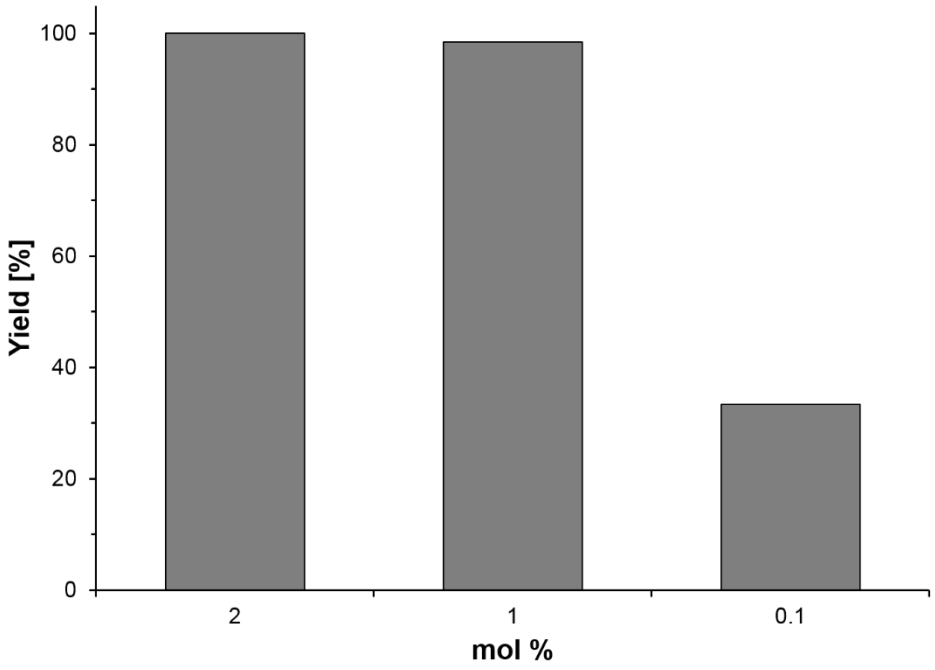
100
80
60
40
20
0
Yield [%]
2
1
0.1
mol %

Optimization of amount of CuI with 1 mol% catalyst 4

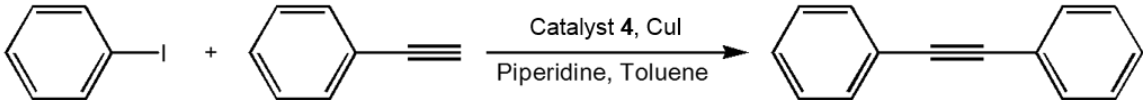

Catalyst 4	CuI	Phenylacetylene	Iodobenzene	Piperidine
1.0 mol%	2.0 mol%	120 mol%	100 mol%	
0.0078 mmol	0.0158 mmol	1.00 mmol	0.81 mmol	
6.2 mg	3.0 mg	0.11 ml	0.09 ml	5 ml

Time [h]	Substrate [%] Iodobenzene	Product [%] Diphenylacetylene
0.0	100.00	0.00
0.25	86.35	13.65
0.50	76.98	23.02
0.75	72.51	27.49
1.0	70.07	29.93
2.0	63.11	36.89
3.0	58.62	41.38
4.0	55.69	44.31
5.0	52.89	47.11
6.0	50.72	49.28

Catalyst 4	CuI	Phenylacetylene	Iodobenzene	Piperidine
1.0 mol%	1.0 mol%	120 mol%	100 mol%	
0.0064 mmol	0.0063 mmol	0.73 mmol	0.63 mmol	
5.1 mg	1.2 mg	0.08 ml	0.07 ml	5 ml

Time [h]	Substrate [%] Iodobenzene	Product [%] Diphenylacetylene
0.0	100.00	0.00
0.25	68.72	31.28
0.50	51.07	48.93
0.75	35.96	64.04
1.0	30.11	69.89
2.0	14.35	85.65
3.0	8.44	91.56
4.0	4.79	95.21
5.0	2.83	97.17
6.0	1.56	98.44

Catalyst 4	CuI	Phenylacetylene	Iodobenzene	Piperidine
1.0 mol%	0.5 mol%	120 mol%	100 mol%	
0.0126 mmol	0.0063 mmol	1.55 mmol	1.26 mmol	
10.0 mg	1.2 mg	0.17 ml	0.14 ml	5 ml

Time [h]	Substrate [%] Iodobenzene	Product [%] Diphenylacetylene
0.0	100	0
0.25	77.72	22.28
0.50	55.03	44.97
0.75	40.75	59.25
1.0	30.30	69.70
2.0	12.57	87.43
3.0	6.18	93.82
4.0	3.02	96.98
5.0	1.18	98.82
6.0	0.42	99.58

Catalyst 4	CuI	Phenylacetylene	Iodobenzene	Piperidine
1.0 mol%	0 mol%	120 mol%	100 mol%	
0.0050 mmol	0 mmol	0.55 mmol	0.45 mmol	
4.0 mg	0 mg	0.06 ml	0.05 ml	5 ml

Time [h]	Substrate [%] Iodobenzene	Product [%] Diphenylacetylene
0.0	0.00	100.00
0.25	0.25	99.35
0.50	0.50	98.92
0.75	0.75	97.82
1.0	1.00	96.78
2.0	2.00	91.98
3.0	3.00	85.40
4.0	4.00	79.41
5.0	5.00	72.15
6.0	6.00	64.90

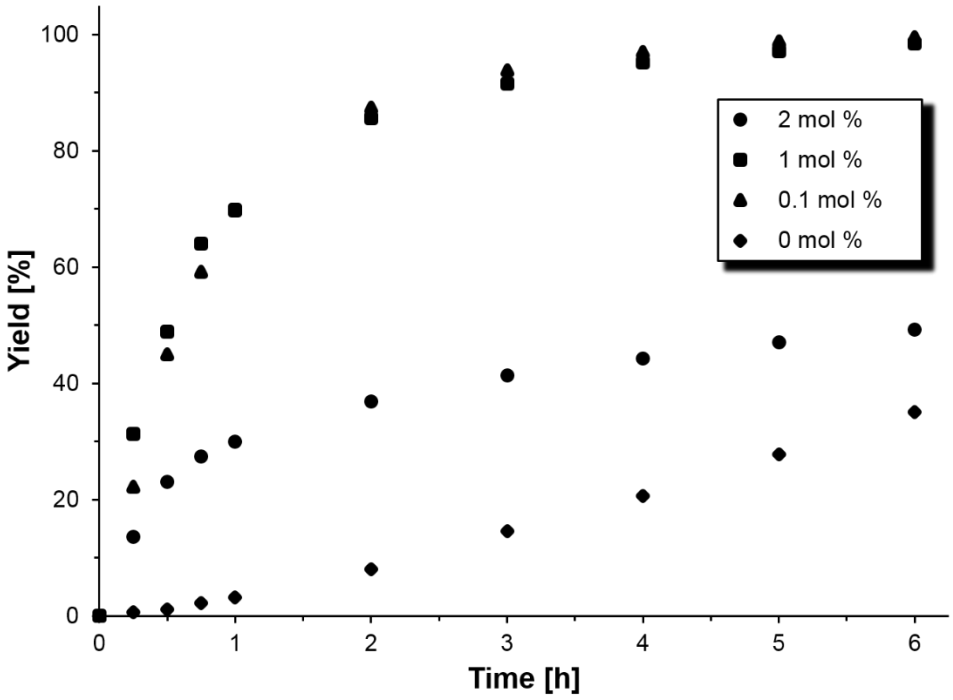
Yield [%]
Time [h]
2 mol %
1 mol %
0.1 mol %
0 mol %
0
20
40
60
80
100
0
1
2
3
4
5
6

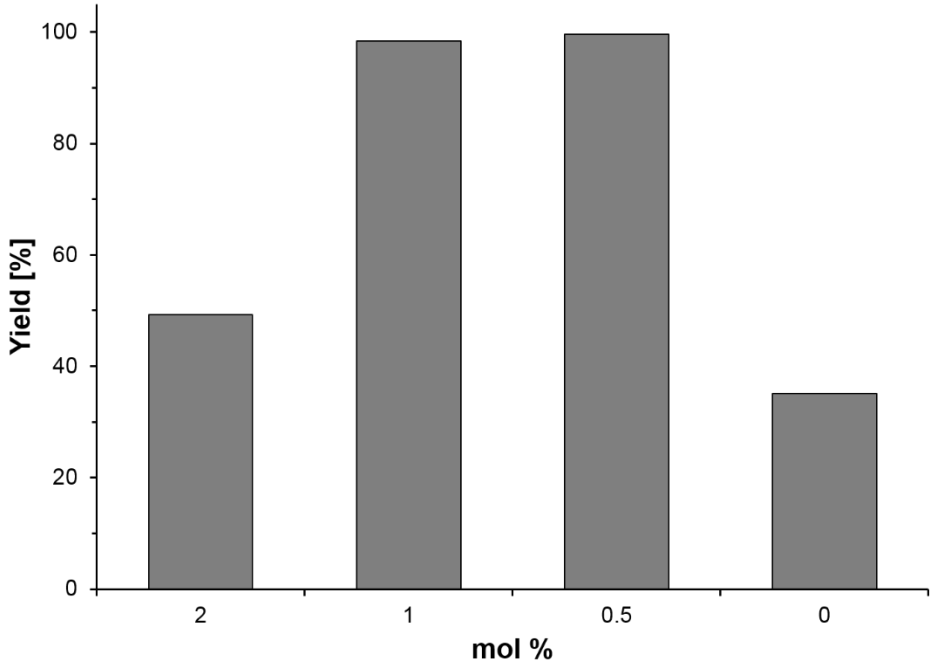
Yield [%]
mol %
0
20
40
60
80
100
2
1
0.5
0

Optimization of the amount of piperidine with 1 mol% Pd complex 4 and 0.5 mol% CuI

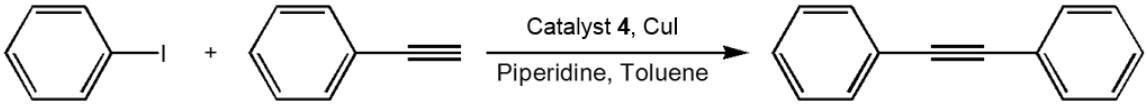

Catalyst 4	CuI	Phenylacetylene	Iodobenzene	Toluene	Piperidine
1.0 mol%	0.5 mol%	120 mol%	100 mol%		
0.0126 mmol	0.0063 mmol	1.55 mmol	1.26 mmol		
10.0 mg	1.2 mg	0.17 ml	0.14 ml	0 ml	5 ml

Time [h]	Substrate [%] Iodobenzene	Product [%] Diphenylacetylene
0.0	100	0
0.25	77.72	22.28
0.50	55.03	44.97
0.75	40.75	59.25
1.0	30.30	69.70
2	12.57	87.43
3	6.18	93.82
4	3.02	96.98
5	1.18	98.82
6	0.42	99.58

Catalyst 4	CuI	Phenylacetylene	Iodobenzene	Toluene	Piperidine
1.0 mol%	0.5 mol%	120 mol%	100 mol%		
0.0126 mmol	0.0068 mmol	1.53 mmol	1.27 mmol		
10.0 mg	1.3 mg	0.17 ml	0.14 ml	1 ml	4 ml

Time [h]	Substrate [%] Iodobenzene	Product [%] Diphenylacetylene
0.0	100.00	0.00
0.25	80.33	19.67
0.50	61.14	38.86
0.75	43.69	56.31
1.0	30.03	69.97
2.0	5.68	94.32
3.0	0.19	99.81
4.0	0.00	100.00
5.0	0.00	100.00
6.0	0.00	100.00

Catalyst 4	CuI	Phenylacetylene	Iodobenzene	Toluene	Piperidine
1.0 mol%	0.5 mol%	120 mol%	100 mol%		
0.0155 mmol	0.0079 mmol	1.82 mmol	1.53 mmol		
12.3 mg	1.5 mg	0.20 ml	0.17 ml	2 ml	3 ml

Time [h]	Substrate [%] Iodobenzene	Product [%] Diphenylacetylene
0.0	100.00	0.00
0.25	76.58	23.42
0.50	48.71	51.29
0.75	32.64	67.36
1.0	19.67	80.33
2.0	1.80	98.20
3.0	0.04	99.96
4.0	0.02	99.98
5.0	0.01	99.99
6.0	0.01	99.99

Catalyst 4	CuI	Iodobenzene	Phenylacetylene	Toluene	Piperidine
1.0 mol%	0.5 mol%	120 mol%	100 mol%		
0.0126 mmol	0.0068 mmol	1.53 mmol	1.27 mmol		
10.0 mg	1.3 mg	0.17 ml	0.14 ml	2.5 ml	2.5 ml

Time [h]	Substrate [%] Iodobenzene	Product [%] Diphenylacetylene
0.0	100.00	0.00
0.25	64.30	35.70
0.50	36.51	63.49
0.75	18.28	81.72
1.0	8.78	91.22
2.0	0.17	99.83
3.0	0.00	100.00
4.0	0.00	100.00
5.0	0.00	100.00
6.0	0.00	100.00

Catalyst 4	CuI	Phenyacetylene	Iodobenzene	Toluene	Piperidine
1.0 mol%	0.5 mol%	120 mol%	100 mol%		
0.0171 mmol	0.0084 mmol	2.06 mmol	1.73 mmol		
13.6 mg	1.6 mg	0.23 ml	0.19 ml	3 ml	2 ml

Time [h]	Substrate [%] Iodobenzene	Product [%] Diphenylacetylene
0.0	100	0
0.25	68.74	31.26
0.50	42.17	57.83
0.75	24.61	75.39
1.0	13.77	86.23
2.0	1.04	98.86
3.0	0.00	100.00
4.0	0.00	100.00
5.0	0.00	100.00
6.0	0.00	100.00

Catalyst 4	CuI	Phenylacetylene	Iodobenzene	Toluene	Piperidine
1.0 mol%	0.5 mol%	120 mol%	100 mol%		
0.0146 mmol	0.0074 mmol	1.71 mmol	1.46 mmol		
11.7 mg	1.4 mg	0.19 ml	0.16 ml	4 ml	1 ml

Time [h]	Substrate [%] Iodobenzene	Product [%] Diphenylacetylene
0.0	100.00	0.00
0.25	78.6673	21.33
0.50	54.9365	45.06
0.75	39.3914	60.61
1.0	26.3302	73.67
2.0	8.6572	91.34
3.0	3.0562	96.94
4.0	1.2975	98.70
5.0	0.3785	99.62
6.0	0.00	100.00

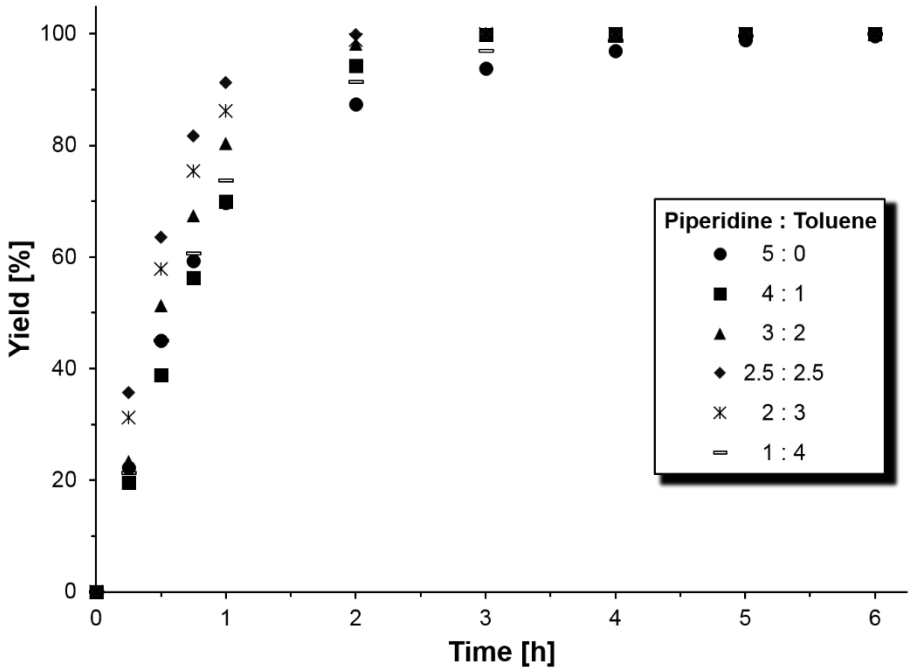
Yield [%]
Time [h]
Piperidine : Toluene
5 : 0
4 : 1
3 : 2
2.5 : 2.5
2 : 3
1 : 4

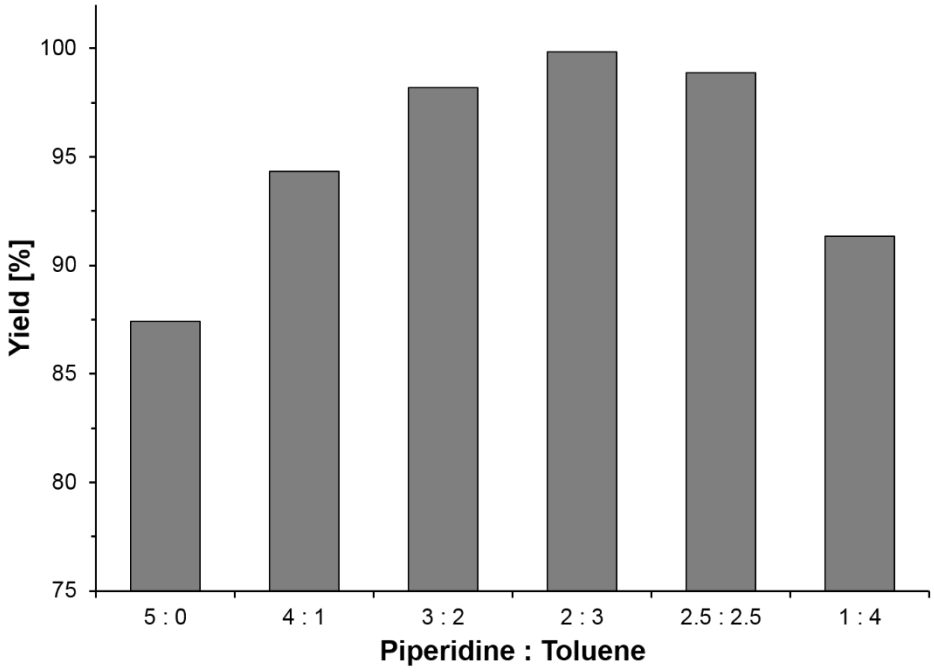
Yield [%]
Piperidine : Toluene
5 : 0
4 : 1
3 : 2
2 : 3
2.5 : 2.5
1 : 4

Optimization of the amount of substrate with 1 mol% Pd (Catalyst 4 or $PdCl_2(PPh_3)_2$), 0.5 mol% CuI, and a 1:1 ratio of Piperidine : Toluene

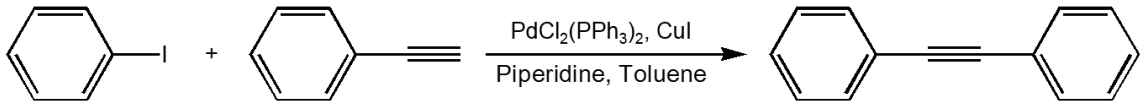

$PdCl_2(PPh_3)_2$	CuI	Phenylacetylene	Iodobenzene	Toluene	Piperidine
1 mol%	0.5 mol%	120 mol%	100 mol%		
0.0161 mmol	0.0079 mmol	1.73 mmol	1.44 mmol		
0.0113 g	0.0015 g	0.19 ml	0.16 ml	5 ml	5 ml

Time [h]	Substrate [%] Iodobenzene	Product [%] Diphenylacetylene
0.0	100.00	0.00
0.25	0.00	100.00
0.50	0.00	100.00
0.75	0.00	100.00
1.00	0.00	100.00
2.00	0.00	100.00
3.0	0.00	100.00
4.0	0.00	100.00
5.0	0.00	100.00
6.0	0.00	100.00

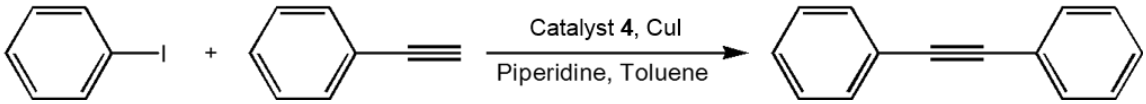

Catalyst 4	CuI	Phenylacetylene	Iodobenzene	Toluene	Piperidine
1.0 mol%	0.5 mol%	120 mol%	100 mol%		
0.0164 mmol	0.0084 mmol	1.91 mmol	1.62 mmol		
0.0130 g	0.0016 g	0.21 ml	0.18 ml	2.5 ml	2.5 ml

Time [h]	Substrate [%] Iodobenzene	Product [%] Diphenylacetylene
0.0	100.00	0.00
0.25	64.30	35.70
0.50	36.51	63.49
0.75	18.28	81.72
1.00	8.78	91.22
2.00	0.17	99.83
3.0	0.0	100.0
4.0	0.0	100.0
5.0	0.0	100.0
6.0	0.0	100.0

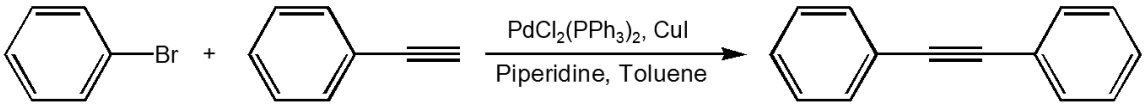

$PdCl_2(PPh_3)_2$	CuI	Phenylacetylene	Bromobenzene	Toluene	Piperidine
1.0 mol%	0.5 mol%	120 mol%	100 mol%		
0.0182 mmol	0.0091 mmol	2.19 mmol	1.81 mmol		
0.0113 g	0.0015 g	0.24 ml	0.19 ml	5 ml	5 ml

Time [h]	Substrate [%] Bromobenzene	Product [%] Diphenylacetylene
0.0	100.00	0.00
0.25	100.00	0.00
0.50	100.00	0.00
0.75	100.00	0.00
1.00	100.00	0.00
2.00	100.00	0.00
3.0	100.00	0.00
4.0	100.00	0.00
5.0	100.00	0.00
6.0	100.00	0.00

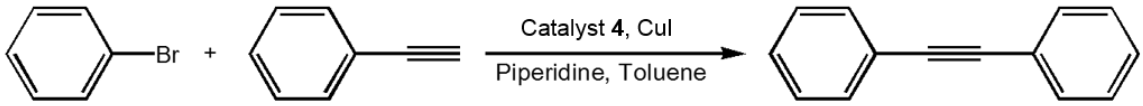

Catalyst 4	CuI	Phenylacetylene	Bromobenzene	Toluene	Piperidine
1.0 mol%	0.5 mol%	120 mol%	100 mol%		
0.0109 mmol	0.0053 mmol	1.27 mmol	1.05 mmol		
0.0087 g	0.0010 g	0.14 ml	0.11 ml	5 ml	5 ml

Time [h]	Substrate [%] Bromobenzene	Product [%] Diphenylacetylene
0.0	100.00	0.00
0.25	100.00	0.00
0.50	100.00	0.00
0.75	100.00	0.00
1.00	100.00	0.00
2.00	100.00	0.00
3.0	100.00	0.00
4.0	100.00	0.00
5.0	100.00	0.00
6.0	100.00	0.00

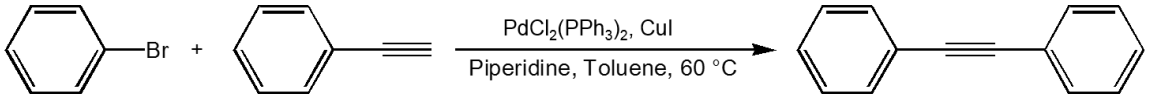

$PdCl_2(PPh_3)_2$	CuI	Phenylacetylene	Bromobenzene	Toluene	Piperidine
1.0 mol%	0.5 mol%	120 mol%	100 mol%		
0.0150 mmol	0.0074 mmol	1.82 mmol	1.52 mmol		
0.0105 g	0.0014 g	0.20 ml	0.16 ml	5 ml	5 ml

Time [h]	Substrate [%] Iodobenzene	Product [%] Diphenylacetylene
0	0	0
0.25	95.66	4.34
0.50	94.44	5.56
0.75	93.85	6.15
1.00	93.31	6.69
2.00	90.11	9.89
3.00	86.44	13.56
4.00	82.30	17.70
5.00	77.26	22.74
6.00	71.31	28.69

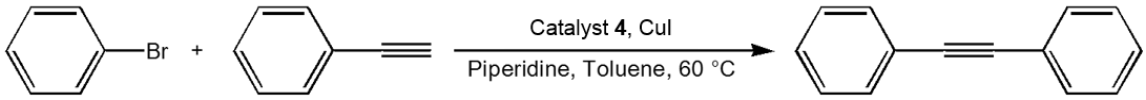

Catalyst 4	CuI	Phenylacetylene	Iodobenzene	Toluene	Piperidine
1.0 mol%	0.5 mol%	120 mol%	100 mol%		
0.0114 mmol	0.0058 mmol	1.37 mmol	1.14 mmol		
0.0091 g	0.0011 g	0.15 ml	0.12 ml	5 ml	5 ml

Time [h]	Substrate [%] Iodobenzene	Product [%] Diphenylacetylene
0.00	100.00	0.00
0.25	98.51	1.49
0.50	98.39	1.61
0.75	98.34	1.66
1.00	98.23	1.77
2.00	97.78	2.22
3.00	97.53	2.47
4.00	97.09	2.91
5.00	96.44	3.56
6.00	95.91	4.09

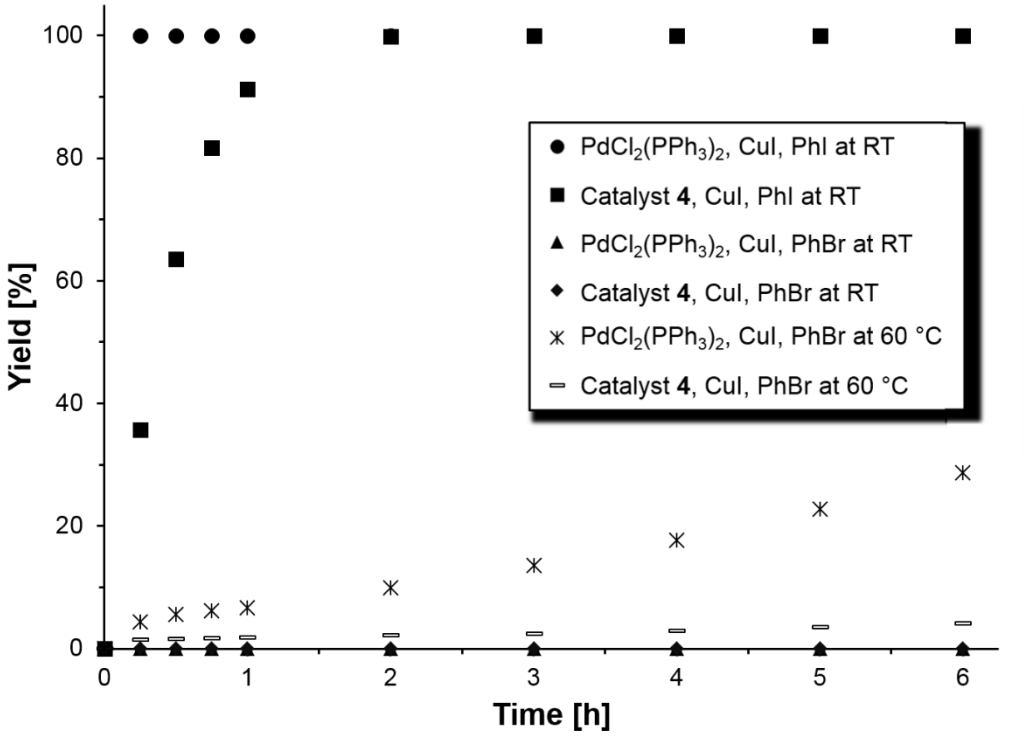
100
80
60
40
20
0
Yield [%]
0
1
2
3
4
5
6
Time [h]
PdCl2(PPh3)2, CuI, PhI at RT
Catalyst 4, CuI, PhI at RT
PdCl2(PPh3)2, CuI, PhBr at RT
Catalyst 4, CuI, PhBr at RT
PdCl2(PPh3)2, CuI, PhBr at 60 °C
Catalyst 4, CuI, PhBr at 60 °C

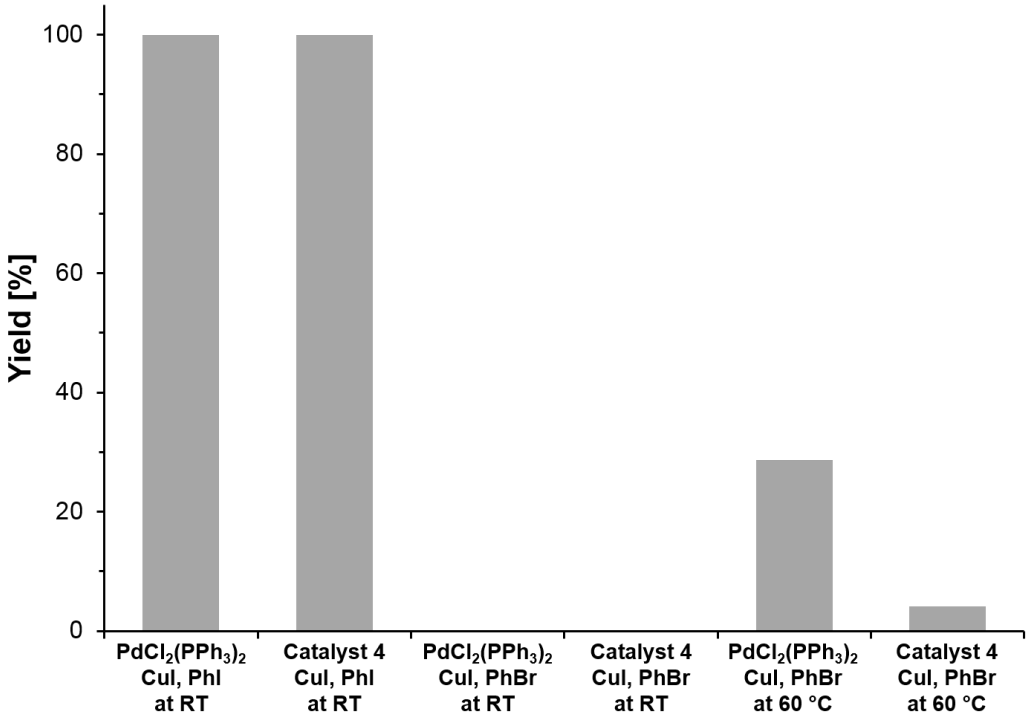
100
80
60
40
20
0
Yield [%]
PdCl2(PPh3)2 CuI, PhI at RT
Catalyst 4 CuI, PhI at RT
PdCl2(PPh3)2 CuI, PhBr at RT
Catalyst 4 CuI, PhBr at RT
PdCl2(PPh3)2 CuI, PhBr at 60 °C
Catalyst 4 CuI, PhBr at 60 °C

Catalysis under optimized conditions with immobilized Pd complex 4i and CuI

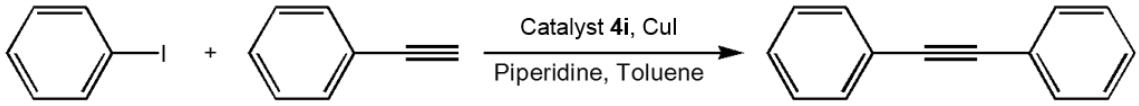

Catalyst 4i	CuI	Phenylacetylene	Iodobenzene	Toluene	Piperidine
1 mol%	0.5 mol%	120 mol%	100 mol%		
0.123 mmol	0.0063 mmol	1.53 mmol	1.27 mmol		
0.0895 g	1.2 mg	0.17 mL	0.14 mL	2.5 mL	2.5 mL

Cycle #1		
Time [h]	**Substrate [%] Iodobenzene**	**Product [%] Diphenylacetylene**
0.00	100.00	0.00
0.25	92.41	7.59
0.50	85.92	14.08
0.75	78.71	21.29
1.00	66.42	33.58
2.00	54.60	45.40
3.00	18.73	81.27
4.00	4.94	95.06
5.00	0.44	99.56
6.00	0.07	99.93

Cycle #2		
Time [h]	**Substrate [%] Iodobenzene**	**Product [%] Diphenylacetylene**
0.00	100.00	0.00
0.25	99.58	0.42
0.50	98.26	1.74
0.75	96.74	3.26
1.00	94.54	5.46
2.00	90.35	9.65
3.00	87.31	12.69
4.00	85.92	14.08
5.00	83.61	16.39
6.00	81.53	18.47

Cycle #3		
Time [h]	**Substrate [%] Iodobenzene**	**Product [%] Diphenylacetylene**
0.00	100.00	0.00
0.25	99.77	0.23
0.50	98.97	1.03
0.75	98.96	1.04
1.00	98.95	1.05

2.00	97.49	2.51
3.00	96.35	3.65
4.00	95.49	4.51
5.00	95.29	4.71
6.00	93.08	6.92

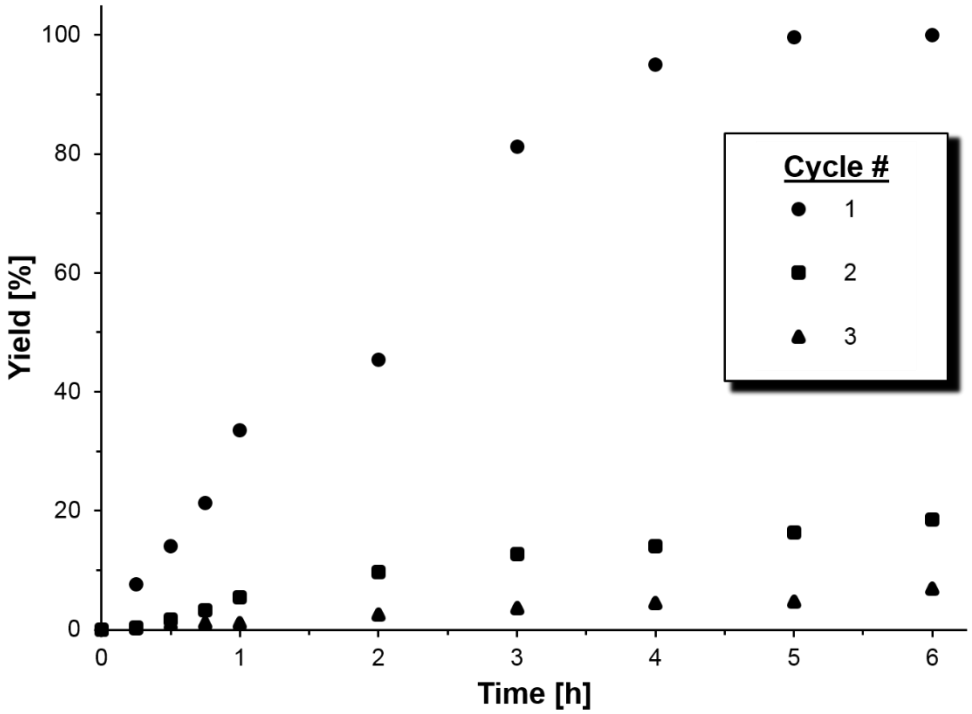
Yield [%]
Time [h]
Cycle #
1
2
3

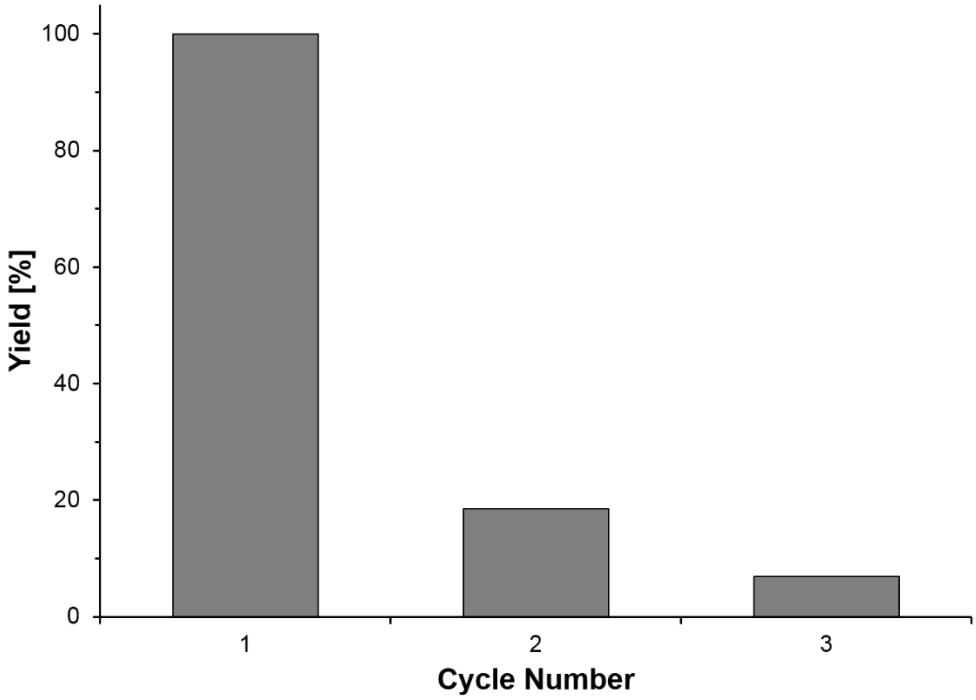
Yield [%]
Cycle Number

Catalysis under optimized conditions with Pd complex $PdCl_2(PPh_3)_2$ and immobilized Cu complex 7i

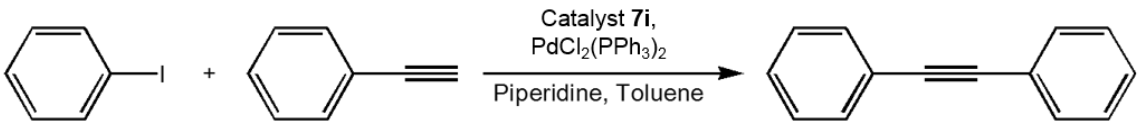

$PdCl_2(PPh_3)_2$	Catalyst 7i	Phenylacetylene	Iodobenzene	Toluene	Piperidine
1 mol%	4 mol%	120 mol%	100 mol%		
0.0043 mmol	0.0216 mmol	0.64 mmol	0.54 mmol		
3.1 mg	0.1830 g	0.07 mL	0.06 mL	5.0 mL	5.0 mL

Cycle #1		
Time [h]	**Substrate [%] Iodobenzene**	**Product [%] Diphenylacetylene**
0.0	100.00	0.00
0.25	74.77	25.23
0.50	50.62	49.38
0.75	28.09	71.91
1.0	15.01	84.99
2.0	0.91	99.09
3.0	0.00	100.00
4.0	0.00	100.00
5.0	0.00	100.00
6.0	0.00	100.00

Cycle #2		
Time [h]	**Substrate [%] Iodobenzene**	**Product [%] Diphenylacetylene**
0.0	100.00	0.00
0.25	76.73	23.27
0.50	47.41	52.59
0.75	22.67	77.33
1.0	12.46	87.54
2.0	0.00	100.00
3.0	0.00	100.00
4.0	0.00	100.00
5.0	0.00	100.00
6.0	0.00	100.00

Cycle #3		
Time [h]	**Substrate [%] Iodobenzene**	**Product [%] Diphenylacetylene**
0.0	100.00	0.00
0.25	73.90	26.10
0.50	53.28	46.72
0.75	33.78	66.22
1.00	19.35	80.65

2.00	0.00	100.00
3.0	0.00	100.00
4.0	0.00	100.00
5.0	0.00	100.00
6.0	0.00	100.00

Cycle #4		
Time [h]	**Substrate [%] Iodobenzene**	**Product [%] Diphenylacetylene**
0.0	100.00	0.00
0.25	91.49	8.51
0.50	86.25	13.75
0.75	75.40	24.60
1.00	73.04	26.96
2.00	42.85	57.15
3.0	18.67	81.33
4.0	4.84	95.16
5.0	0.00	100.00
6.0	0.00	100.00

Cycle #5		
Time [h]	**Substrate [%] Iodobenzene**	**Product [%] Diphenylacetylene**

0.0	100.00	0.00
0.25	93.32	6.68
0.50	90.38	9.62
0.75	85.15	14.85
1.00	78.87	21.13
2.00	54.79	45.21
3.0	28.27	71.73
4.0	17.46	82.54
5.0	78.82	92.18
6.0	2.18	97.83

Cycle #6		
Time [h]	**Substrate [%] Iodobenzene**	**Product [%] Diphenylacetylene**
0.0	100.00	0.00
0.25	60.73	39.27
0.50	60.21	39.79
0.75	59.50	40.50
1.00	59.39	40.61
2.00	47.20	52.80
3.0	38.87	61.13

4.0	28.97	71.03
5.0	19.34	80.66
6.0	13.54	86.46

Cycle #7		
Time [h]	**Substrate [%] Iodobenzene**	**Product [%] Diphenylacetylene**
0.0	100.00	0.00
0.25	56.84	43.16
0.50	56.78	43.82
0.75	53.37	46.63
1.00	52.90	47.10
2.00	46.14	53.86
3.0	38.36	61.64
4.0	30.00	70.00
5.0	23.76	76.24
6.0	23.03	76.97

Cycle #8		
Time [h]	**Substrate [%] Iodobenzene**	**Product [%] Diphenylacetylene**
0.0	100.00	0.00

0.25	94.88	5.12
0.50	91.33	8.67
0.75	88.93	11.07
1.00	88.14	11.86
2.00	79.10	20.90
3.0	67.52	32.48
4.0	56.17	43.83
5.0	45.18	55.82
6.0	33.55	66.45

Cycle #9		
Time [h]	**Substrate [%] Iodobenzene**	**Product [%] Diphenylacetylene**
0.0	100.00	0.00
0.25	93.31	6.69
0.50	91.05	8.95
0.75	90.00	10.00
1.00	87.99	12.01
2.00	74.20	25.80
3.0	65.44	34.56
4.0	55.43	44.57

5.0	46.72	53.28
6.0	35.83	64.17

Cycle #10		
Time [h]	**Substrate [%] Iodobenzene**	**Product [%] Diphenylacetylene**
0.0	100.00	0.00
0.25	92.97	7.03
0.50	91.88	8.12
0.75	90.00	10.00
1.00	87.59	12.41
2.00	78.59	21.58
3.0	67.21	32.79
4.0	60.40	39.60
5.0	51.67	48.33
6.0	41.37	58.63

Cycle #11		
Time [h]	**Substrate [%] Iodobenzene**	**Product [%] Diphenylacetylene**
0.0	100.00	0.00
0.25	96.36	3.64

0.50	93.93	6.07
0.75	93.26	6.74
1.00	90.71	9.29
2.00	83.46	16.54
3.0	76.40	23.60
4.0	69.34	30.66
5.0	62.21	37.79
6.0	53.85	46.15

Cycle #12		
Time [h]	**Substrate [%] Iodobenzene**	**Product [%] Diphenylacetylene**
0.0	100.00	0.00
0.25	94.88	5.12
0.50	91.94	8.06
0.75	90.09	9.91
1.00	87.13	12.87
2.00	76.72	23.28
3.0	66.34	33.66
4.0	55.72	44.28
5.0	42.88	57.12

6.0	38.53	61.47

Cycle #13		
Time [h]	**Substrate [%] Iodobenzene**	**Product [%] Diphenylacetylene**
0.0	100.00	0.00
0.25	95.84	4.16
0.50	95.64	4.36
0.75	94.04	5.96
1.00	94.62	6.38
2.00	87.81	12.19
3.0	82.28	17.72
4.0	77.12	22.88
5.0	70.57	29.43
6.0	65.49	34.51

Cycle #14		
Time [h]	**Substrate [%] Iodobenzene**	**Product [%] Diphenylacetylene**
0.0	100.00	0.00
0.25	98.04	1.96
0.50	95.76	4.24

0.75	04.03	5.97
1.00	93.98	6.02
2.00	88.89	11.11
3.0	80.47	19.53
4.0	76.90	23.10
5.0	72.73	27.27
6.0	68.94	31.06

Cycle #15		
Time [h]	**Substrate [%] Iodobenzene**	**Product [%] Diphenylacetylene**
0.0	100.00	0.00
0.25	100.00	0.00
0.50	98.04	1.96
0.75	96.31	3.69
1.00	95.05	4.95
2.00	89.69	10.31
3.0	84.25	15.75
4.0	79.47	20.53
5.0	74.22	25.78
6.0	69.12	30.88

Cycle #16		
Time [h]	**Substrate [%] Iodobenzene**	**Product [%] Diphenylacetylene**
0.0	100.00	0.00
0.25	97.99	2.01
0.50	97.49	2.51
0.75	96.50	3.49
1.00	94.55	5.45
2.00	88.38	11.61
3.0	82.01	17.99
4.0	76.40	23.59
5.0	71.67	28.33
6.0	66.90	33.1

Cycle #17		
Time [h]	**Substrate [%] Iodobenzene**	**Product [%] Diphenylacetylene**
0.0	100.00	0.00
0.25	98.93	1.07
0.50	98.56	1.44
0.75	97.31	2.69
1.00	96.52	3.48

2.00	92.90	7.10
3.0	89.90	10.10
4.0	86.75	13.25
5.0	84.20	15.80
6.0	79.75	20.25

Cycle #18		
Time [h]	**Substrate [%] Iodobenzene**	**Product [%] Diphenylacetylene**
0.0	100.00	0.00
0.25	98.46	1.54
0.50	97.33	2.67
0.75	95.80	4.20
1.00	95.71	4.29
2.00	90.16	9.84
3.0	87.38	12.62
4.0	83.78	16.22
5.0	79.82	20.18
6.0	75.89	24.11

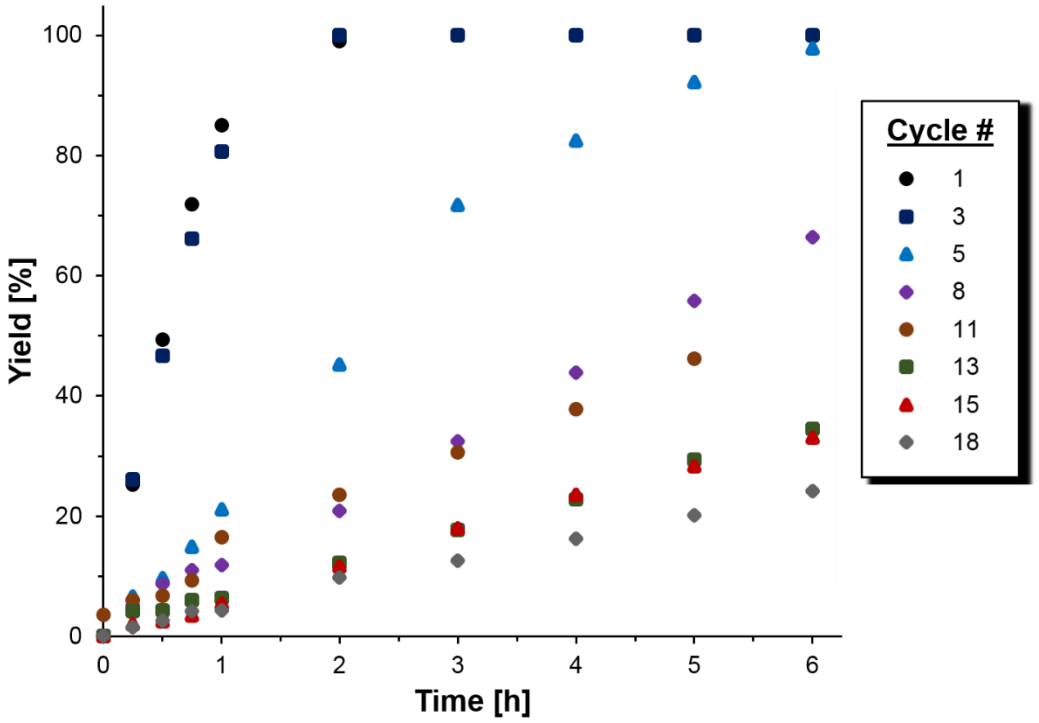
Yield [%]
Time [h]
Cycle #
1
3
5
8
11
13
15
18

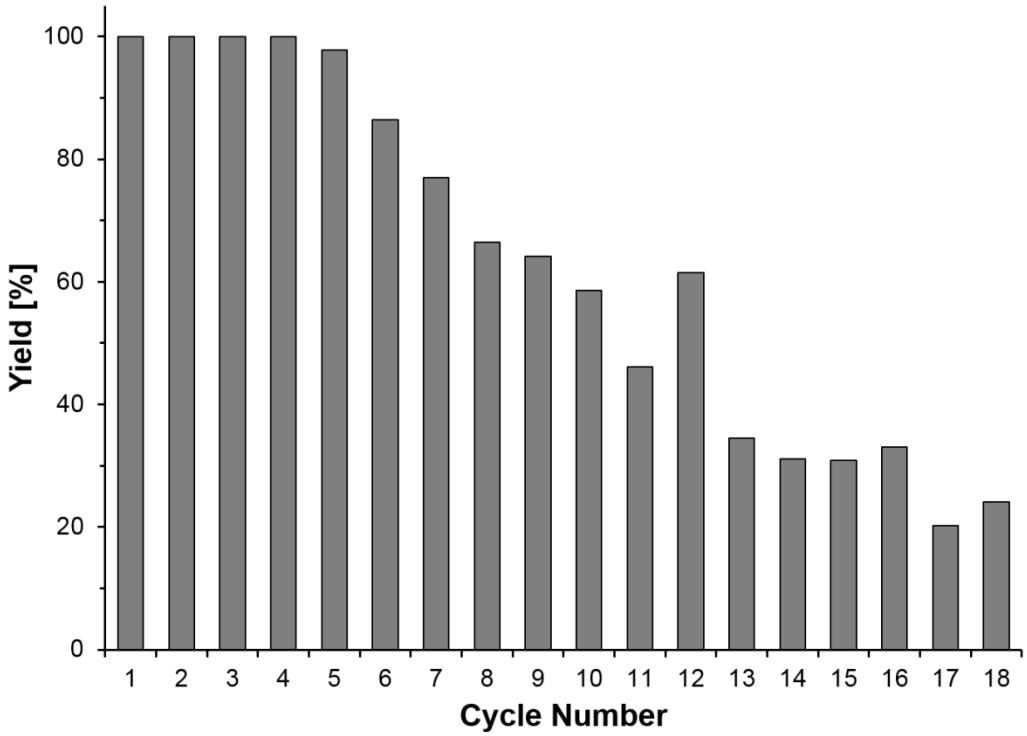
Yield [%]
Cycle Number

Catalysis under optimized conditions with immobilized Pd complex 5i and CuI

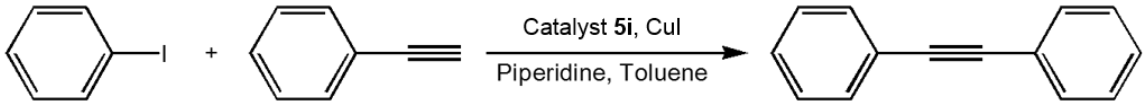

Catalyst 5i	CuI	Phenylacetylene	Iodobenzene	Toluene	Piperidine
1.0 mol%	0.5 mol%	120 mol%	100 mol%		
0.0196 mmol	0.0089 mmol	1.97 mmol	2.37 mmol		
0.140 g	0.0017 g	0.22 ml	0.26 ml	5.0 ml	5.0 ml

Cycle #1		
Time [h]	**Substrate [%] Iodobenzene**	**Product [%] Diphenylacetylene**
0	100.00	0.00
0.25	99.06	0.94
0.50	98.64	1.36
0.75	97.89	2.11
1.00	97.61	2.39
2.00	96.18	3.82
3.00	94.32	5.68
4.00	91.62	8.38
5.00	88.10	11.90
6.00	86.81	13.19

Cycle #2		
Time [h]	**Substrate [%] Iodobenzene**	**Product [%] Diphenylacetylene**
0	100.00	0.00
0.25	99.92	0.08
0.50	99.90	0.10
0.75	99.88	0.12
1.00	99.85	0.15
2.00	99.82	0.18
3.00	99.70	0.30
4.00	99.65	0.35
5.00	99.59	0.41
6.00	99.53	0.47

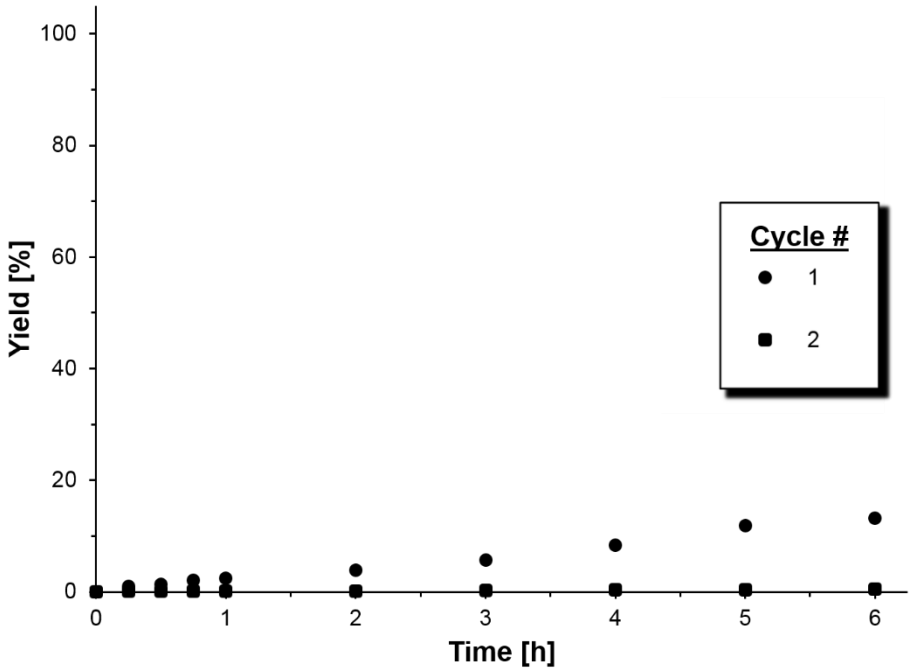
100
80
60
40
20
0
Yield [%]
0
1
2
3
4
5
6
Time [h]
Cycle #
1
2

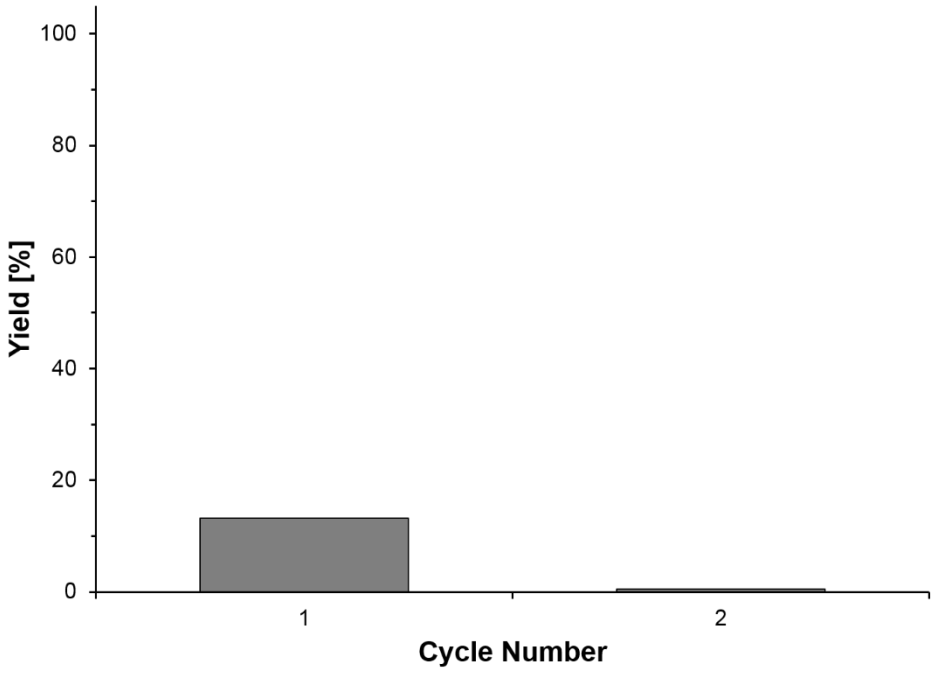
100
80
60
40
20
0
Yield [%]
1
2
Cycle Number

Homogeneous catalysis under optimized conditions with Pd complex 5 and CuI

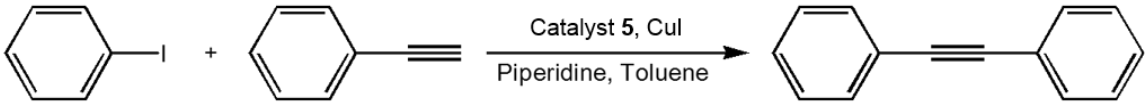

Catalyst 5	CuI	Phenylacetylene	Iodobenzene	Toluene	Piperidine
1.0 mol%	0.5 mol%	100 mol%	120 mol%		
0.0353 mmol	0.0173 mmol	3.50 mmol	4.19 mmol		
0.0289 g	0.0033 g	0.39 ml	0.46 ml	2.5 ml	2.5 ml

Time [h]	Substrate [%] Iodobenzene	Product [%] Diphenylacetylene
0	100	0
0.25	97.70	2.30
0.50	97.15	2.85
0.75	96.44	3.56
1.00	95.20	4.80
2.00	93.69	6.31
3.00	91.02	8.98
4.00	88.90	11.10
5.00	87.11	12.89
6.00	85.53	14.47

Homogeneous catalysis with chelate ligand 2, $PdCl_2(NCPh)_2$, and CuI under optimized conditions

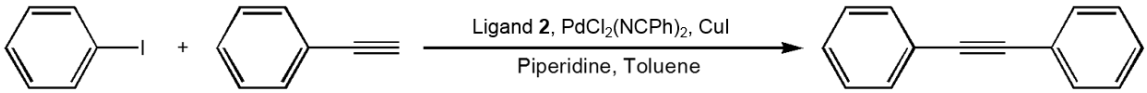

Ligand 2	$PdCl_2(NCPh)_2$	CuI	Phenylacetylene	Iodobenzene	Toluene	Piperidine
1.0 mol%	1.0 mol%	0.5 mol%	120 mol%	100 mol%		
0.0383 mmol	0.0383 mmol	0.0194 mmol	4.64 mmol	3.86 mmol		
0.0246 g	0.0147 g	0.0037 g	0.51 ml	0.43 ml	7.5 ml	7.5 ml

Time [h]	Substrate [%] Iodobenzene	Product [%] Diphenylacetylene
0	100	0
0.25	100	0
0.50	99.67	0.33
0.75	99.62	0.38
1.00	99.32	0.68
2.00	97.62	2.38
3.00	95.40	4.60
4.00	91.93	8.07
5.00	88.26	11.74
6.00	85.20	14.80

Homogeneous Catalysis with Catalyst 6 and CuI under optimized conditions

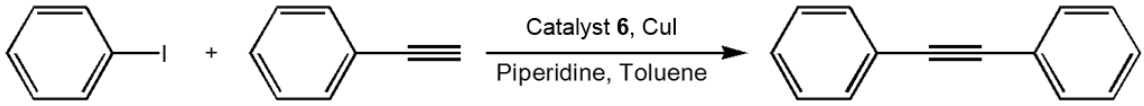

Catalyst 6	CuI	Phenylacetylene	Iodobenzene	Toluene	Piperidine
1.0 mol%	0.5 mol%	120 mol%	100 mol%		
0.0148 mmol	0.0074 mmol	1.73 mmol	1.44 mmol		
0.0142 g	0.0014 g	0.19 ml	0.16 ml	5.0 ml	5.0 ml

Time [h]	Substrate [%] Iodobenzene	Product [%] Diphenylacetylene
0	100.00	0
0.25	98.11	1.8928
0.50	97.17	2.83
0.75	96.07	3.93
1.00	94.95	5.05
2.00	88.28	11.72
3.00	82.59	17.41
4.00	74.53	25.47
5.00	65.36	34.64
6.00	56.06	43.94

Homogeneous catalysis with PCy_3, $PdCl_2(NCPh)_2$, and CuI under optimized conditions

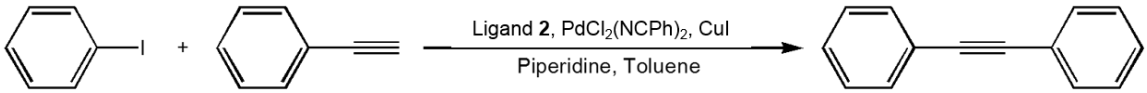

PCy_3	$PdCl_2(NCPh)_2$	CuI	Phenylacetylene	Iodobenzene	Toluene	Piperidine
2.0 mol%	1.0 mol%	0.5 mol%	120 mol%	100 mol%		
0.0678 mmol	0.0339 mmol	0.0168 mmol	4.10 mmol	3.41 mmol		
0.0190 g	0.0130 g	0.0032 g	0.45 ml	0.38 ml	5.0 ml	5.0 ml

Time [h]	Substrate [%] Iodobenzene	Product [%] Diphenylacetylene
0.0	100.00	0
0.25	99.70	0.2976
0.50	98.39	1.61
0.75	97.47	2.53
1.00	96.84	3.16
2.00	96.22	3.78
3.0	96.18	3.82
4.0	96.17	3.83
5.0	96.16	3.84
6.0	96.02	3.98

Homogeneous catalysis with PBu_3, $PdCl_2(NCPh)_2$, and CuI under optimized conditions

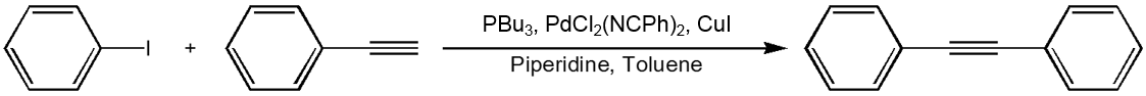

PBu_3	$PdCl_2(NCPh)_2$	CuI	Phenylacetylene	Iodobenzene	Toluene	Piperidine
2.0 mol%	1.0 mol%	0.5 mol%	120 mol%	100 mol%		
0.0544 mmol	0.0383 mmol	0.0137 mmol	3.19 mmol	2.69 mmol		
0.0110 g	0.0105 g	0.0026 g	0.35 ml	0.30 ml	7.5 ml	7.5 ml

Time [h]	Substrate [%] Iodobenzene	Product [%] Diphenylacetylene
0	100	0
0.25	100	0
0.50	100	0
0.75	100	0
1.00	100	0
2.00	100	0
3.00	100	0
4.00	100	0
5.00	100	0
6.00	100	0

Homogeneous catalysis with $PdCl_2(NCPh)_2$ and CuI under optimized conditions

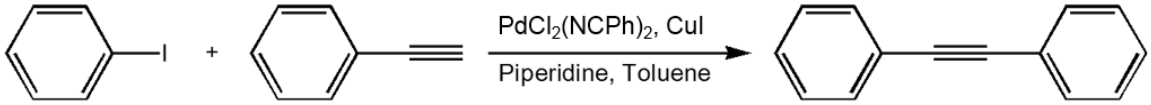

$PdCl_2(NCPh)_2$	CuI	Phenylacetylene	Iodobenzene	Toluene	Piperidine
1.0 mol%	0.5 mol%	120 mol%	100 mol%		
0.0383 mmol	0.0137 mmol	3.19 mmol	2.69 mmol		
0.0105 g	0.0026 g	0.35 ml	0.30 ml	5 ml	5 ml

Time [h]	Substrate [%] Iodobenzene	Product [%] Diphenylacetylene
0	100	0
0.25	97.70	2.30
0.50	93.81	6.19
0.75	91.04	8.96
1.00	89.00	11.00
2.00	87.85	12.15
3.00	87.67	12.33
4.00	87.55	12.45
5.00	87.51	12.49
6.00	87.50	12.50

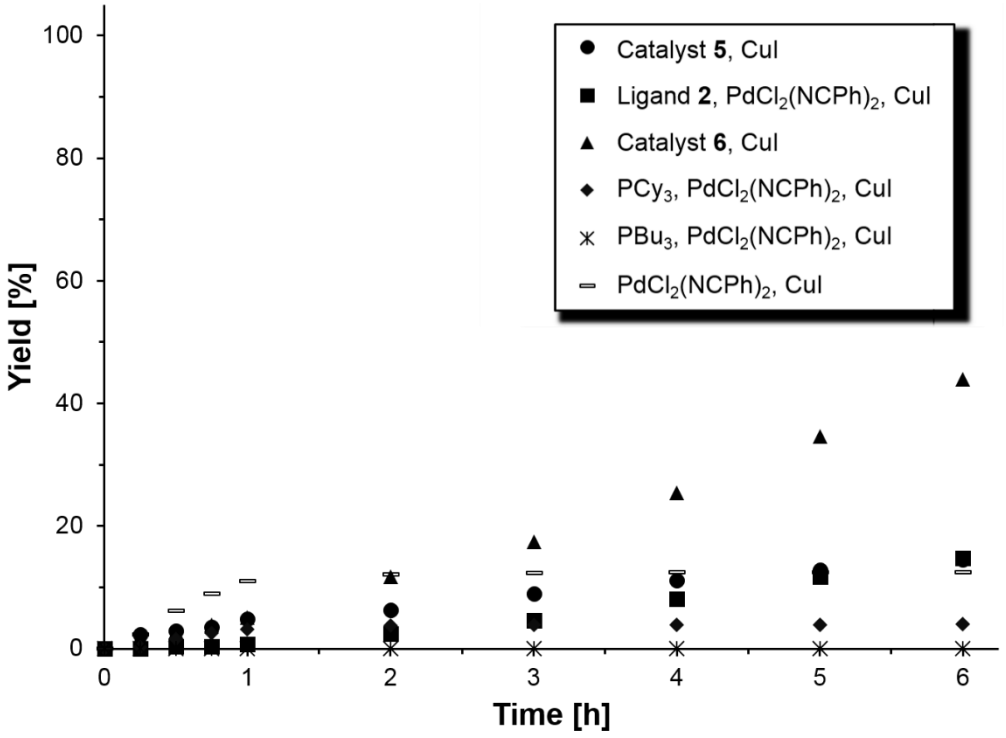
Catalyst 5, CuI
Ligand 2, PdCl2(NCPh)2, CuI
Catalyst 6, CuI
PCy3, PdCl2(NCPh)2, CuI
PBu3, PdCl2(NCPh)2, CuI
PdCl2(NCPh)2, CuI
Yield [%]
Time [h]
0
20
40
60
80
100
0
1
2
3
4
5
6

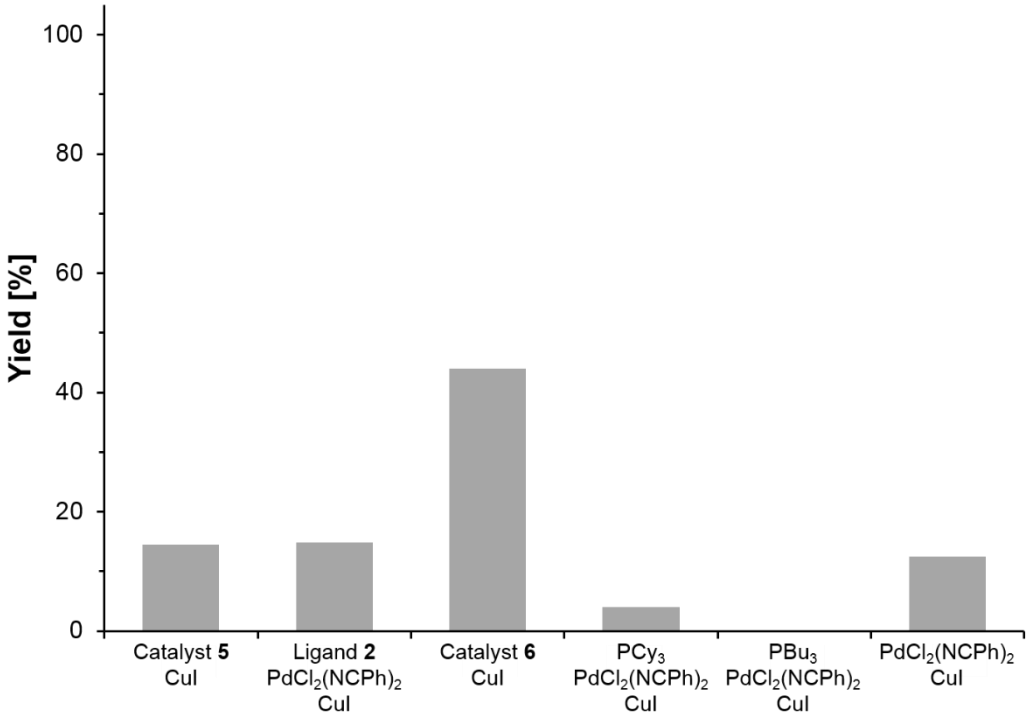
Yield [%]
0
20
40
60
80
100
Catalyst 5 CuI
Ligand 2 PdCl2(NCPh)2 CuI
Catalyst 6 CuI
PCy3 PdCl2(NCPh)2 CuI
PBu3 PdCl2(NCPh)2 CuI
PdCl2(NCPh)2 CuI

APPENDIX D

PALLADIUM MIGRATION AND COMPETITION RESULTS

Immobilized Ligands and Palladium Complexes

^{31}P HRMAS NMR (Acetone)

(**1i**: 0.131 mmol/g, 10.5 particles/100 nm^2)

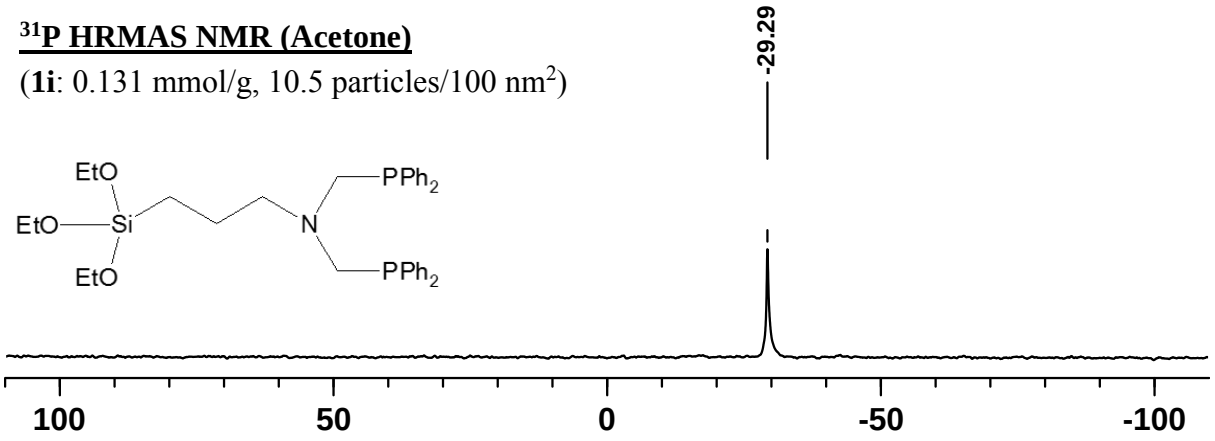

^{31}P HRMAS NMR (Acetone)

(**4i**: 0.131 mmol/g, 10.5 particles/100 nm^2)

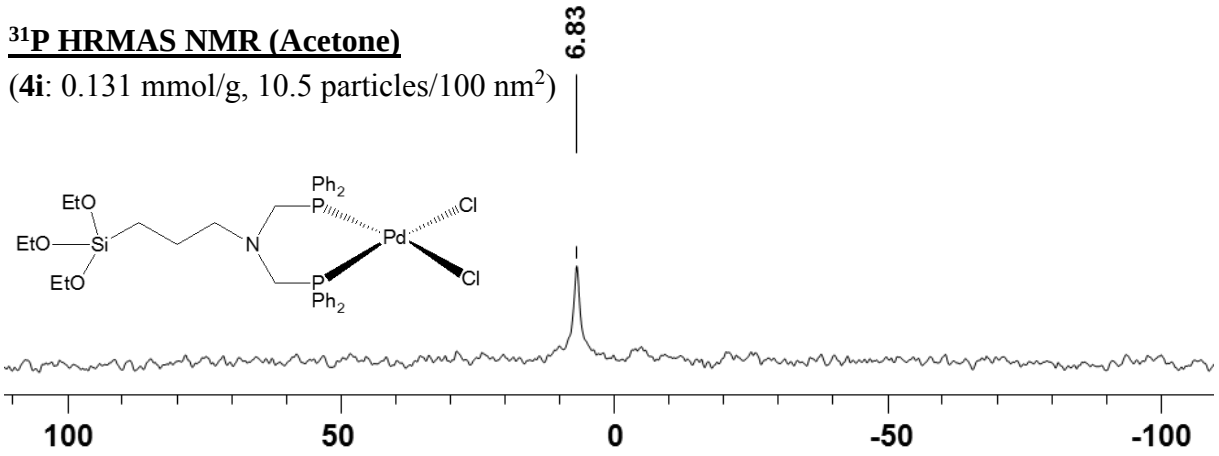

^{31}P HRMAS NMR (Acetone)

(**2i**: 0.147 mmol/g, 11.8 particles/100 nm^2)

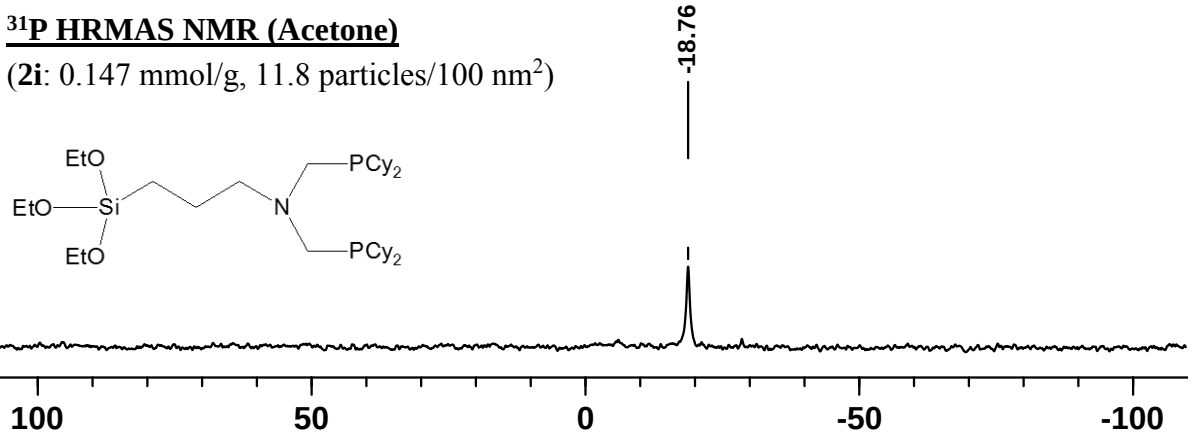

^{31}P HRMAS NMR (Acetone)

(**5i**: 0.140 mmol/g, 11.2 particles/100 nm^2)

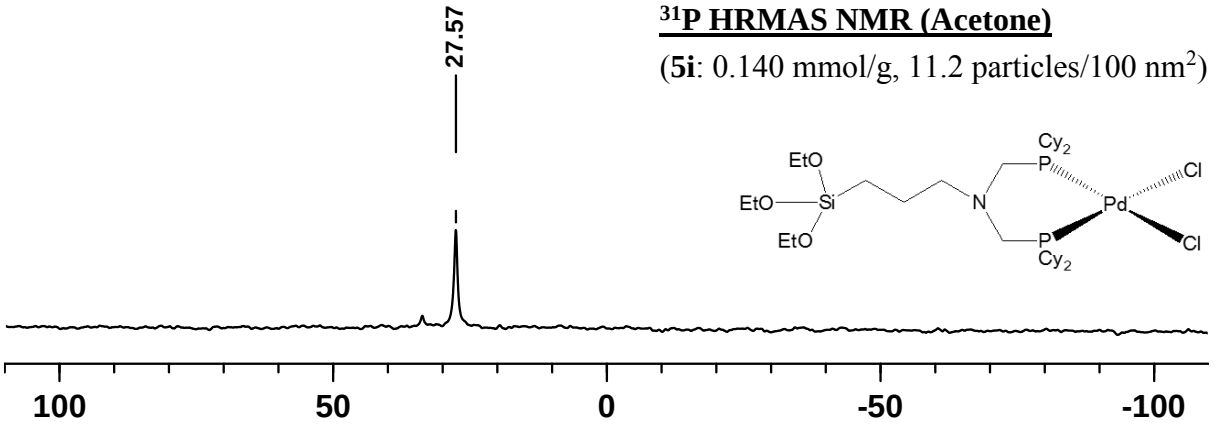

^{31}P HRMAS NMR (Acetone)

(**3i**, 100% surface coverage: 0.131 mmol/g, 10.5 particles/100 nm^2)

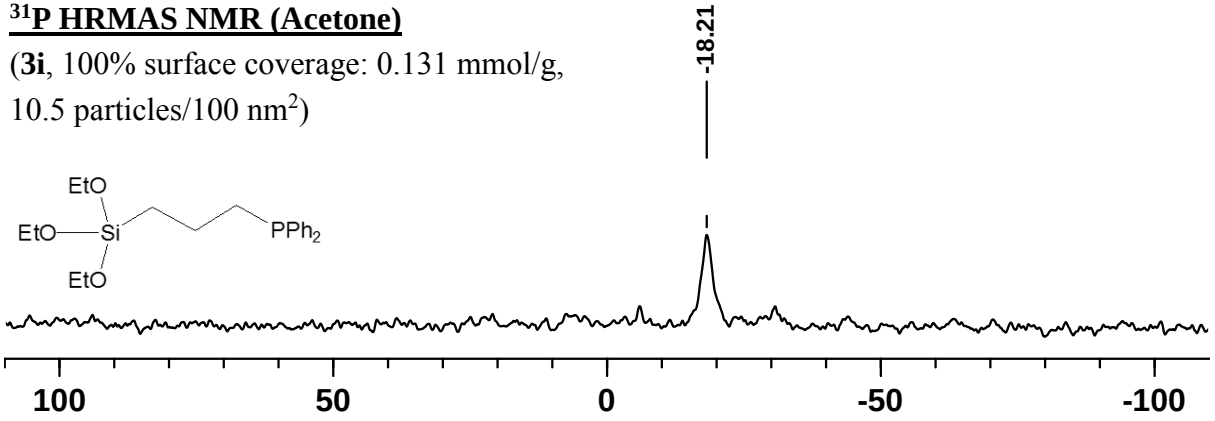

^{31}P HRMAS NMR (Acetone)

(**6i,** 100% surface coverage: 0.0699 mmol/g, 5.6 particles/100 nm^2)

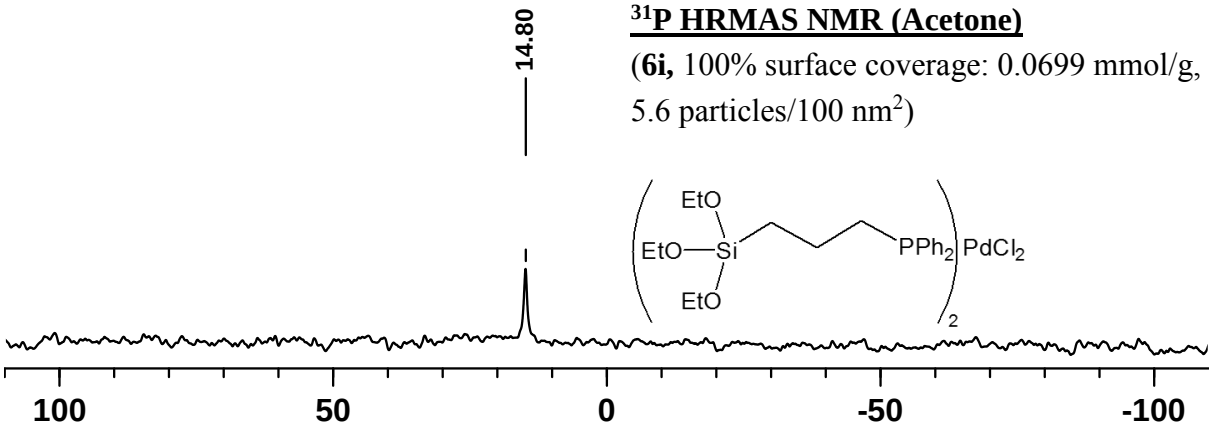

Batches with Immobilized Ligands and Their Pd Complexes

4i mixed in a 1:1 ratio with **1i** (1024 scans)

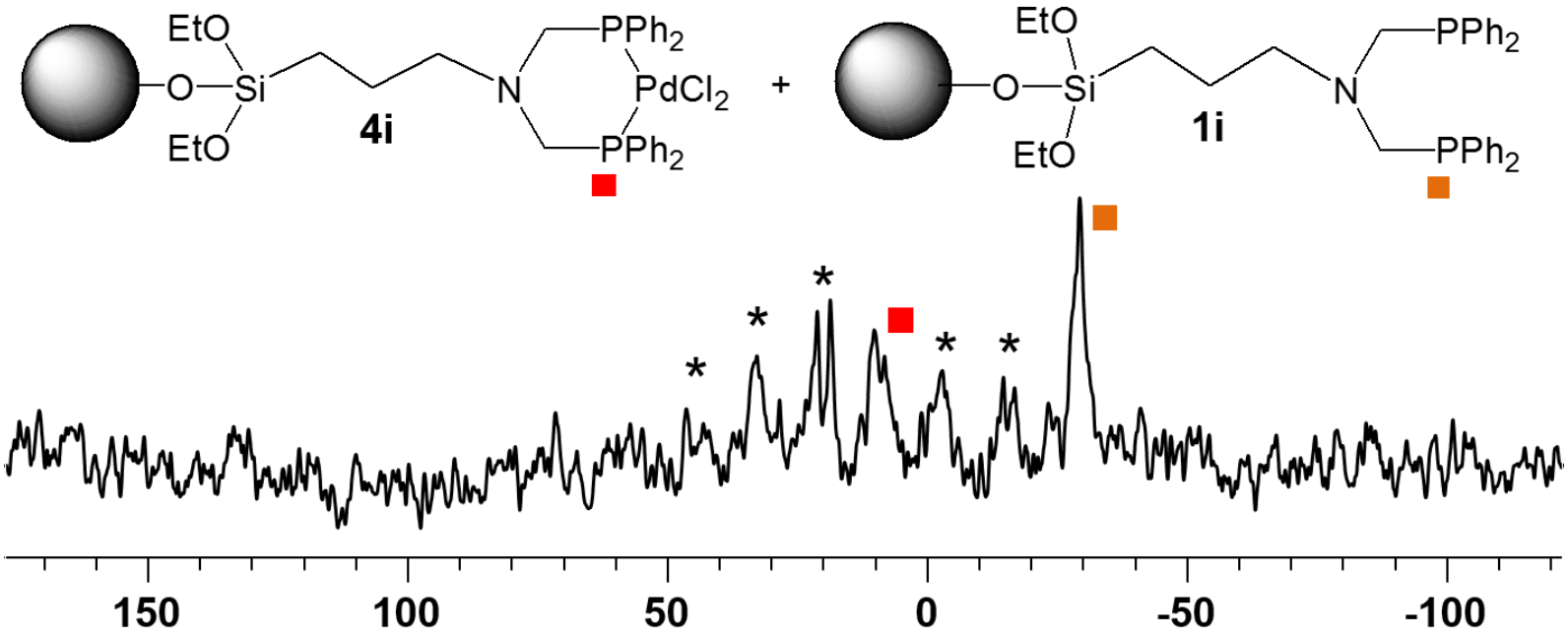

4i mixed in a 1:1 ratio with **1i** (re-measured, 1024 scans)

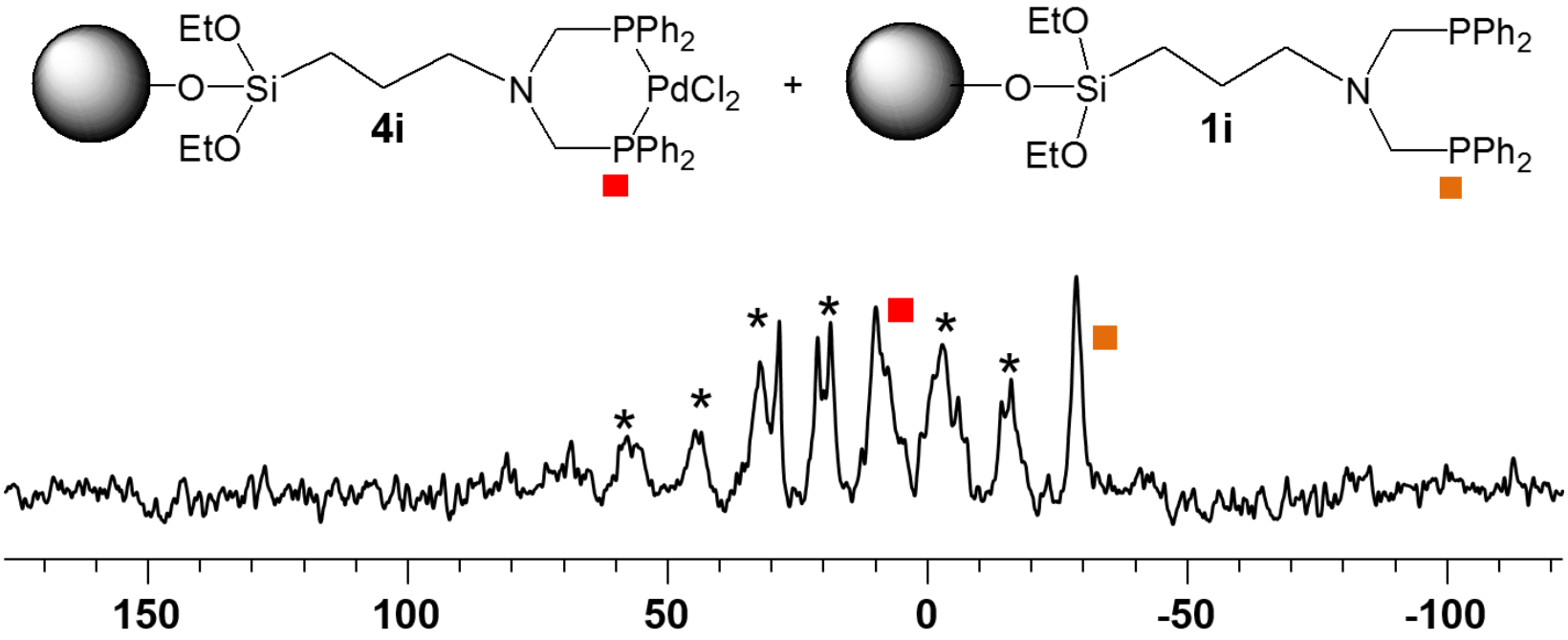

Ligand **1i** (**7**% surface coverage) added to the same silica support with complex **4i** (**7%**) (8,000 scans)

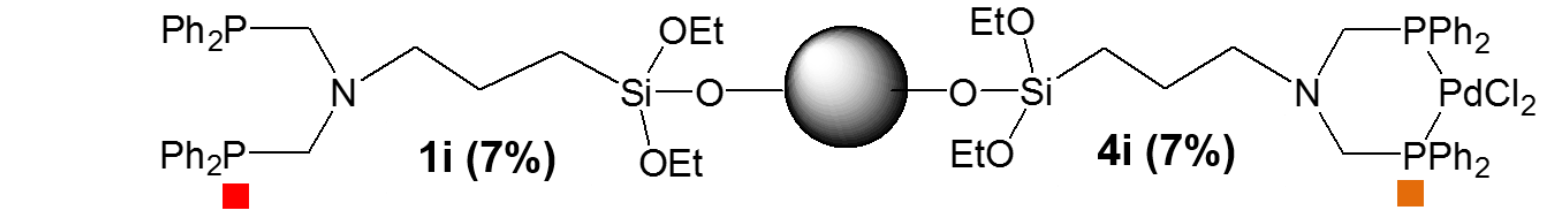

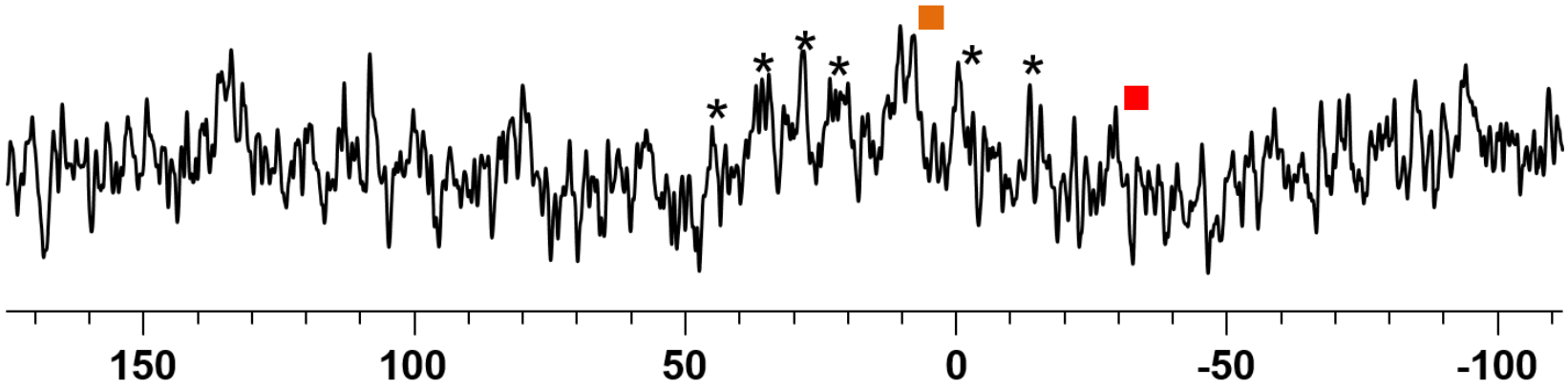

Ligand **1i** (**7%** surface coverage) added to the same silica support with complex **4i** (**7%**) (40,000 scans)

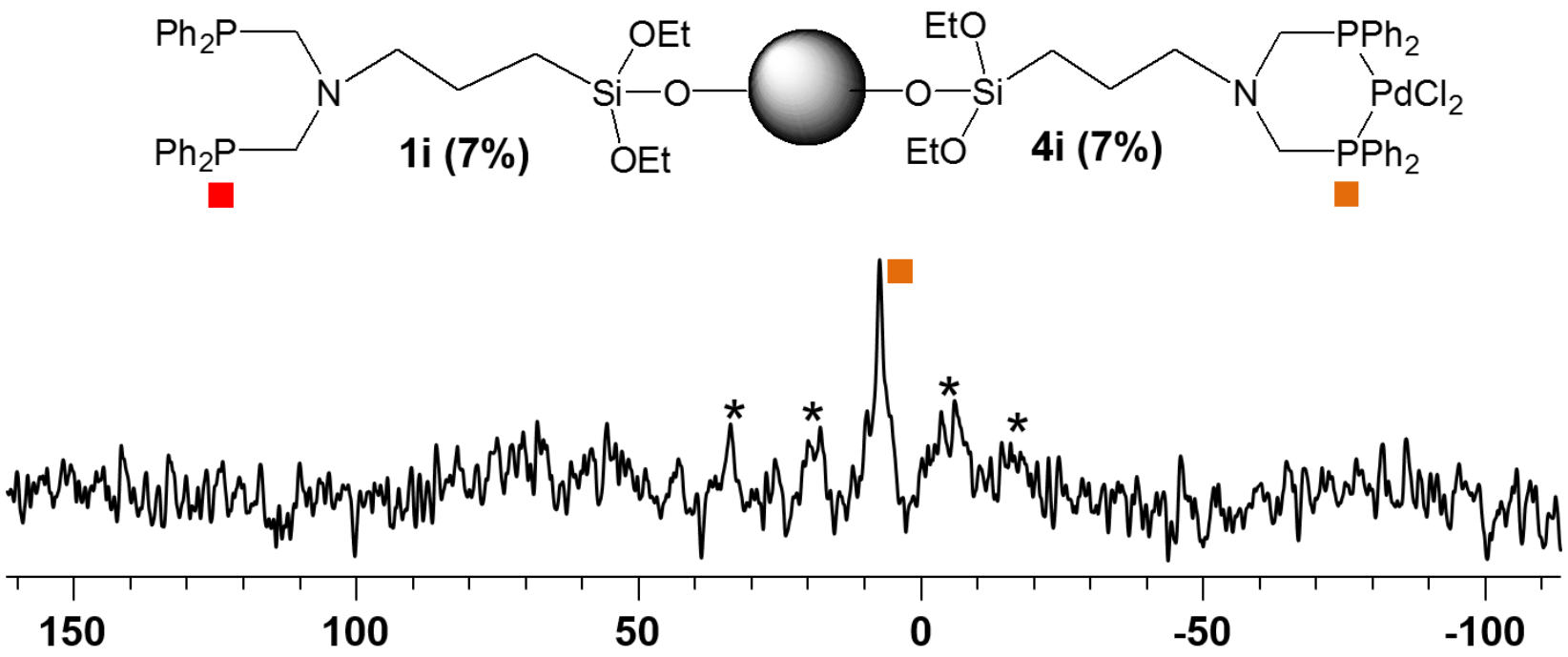

Complex **5i** mixed in a 1:1 ratio with ligand **2i** (512 scans)

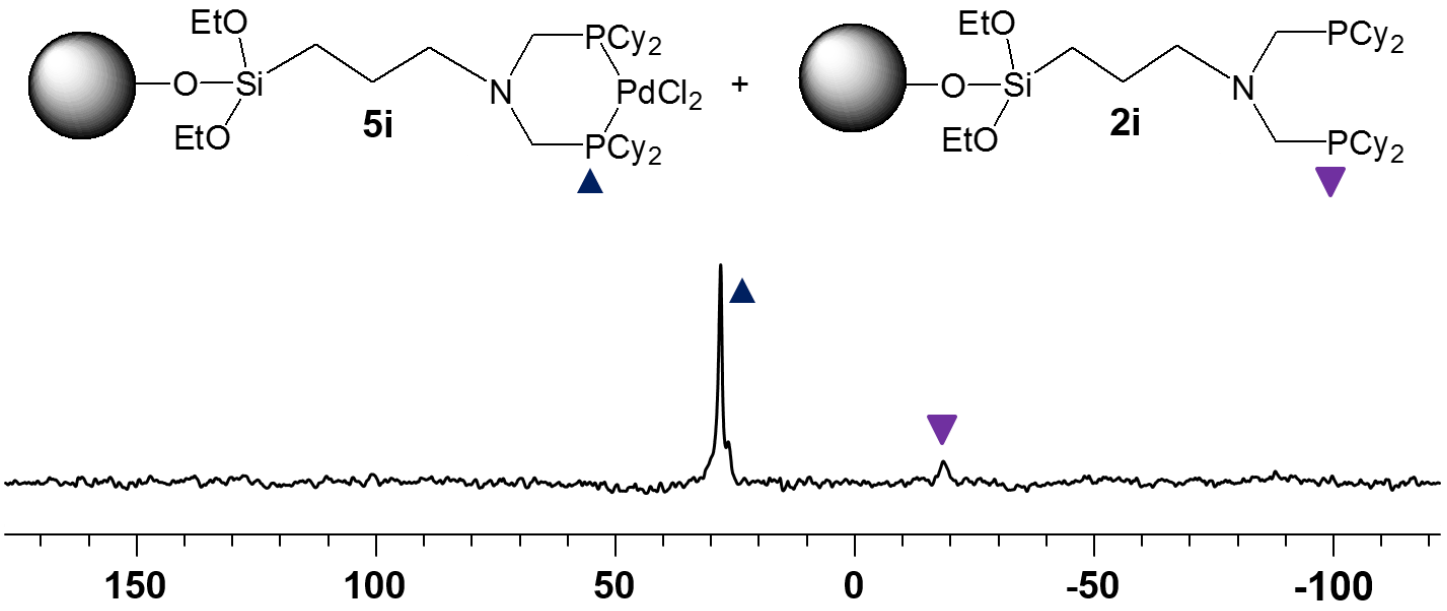

Complex **6i** mixed in a 1:1 ratio with ligand **3i** (512 scans)

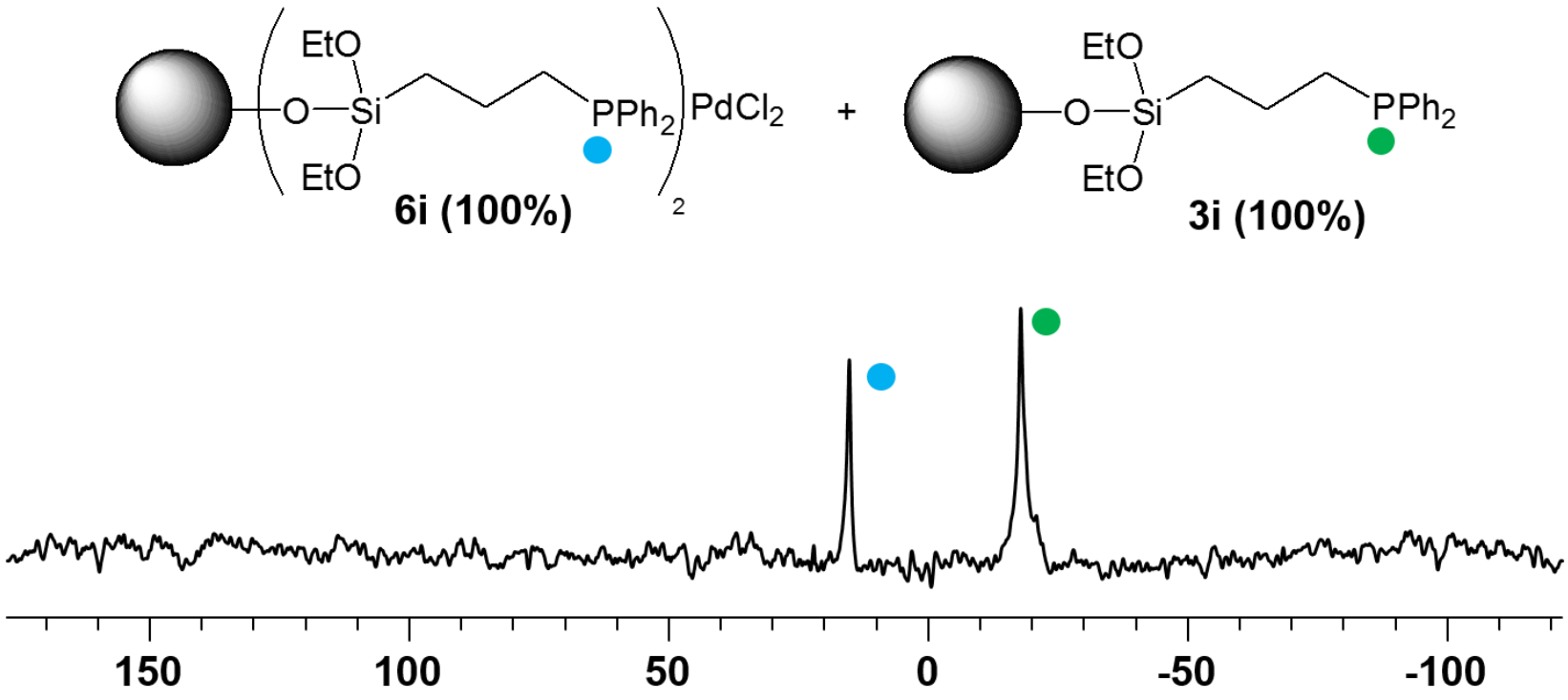

Immobilized 4i Combinations

Complex **4i** mixed in a 1:1 ratio with ligand **2i**

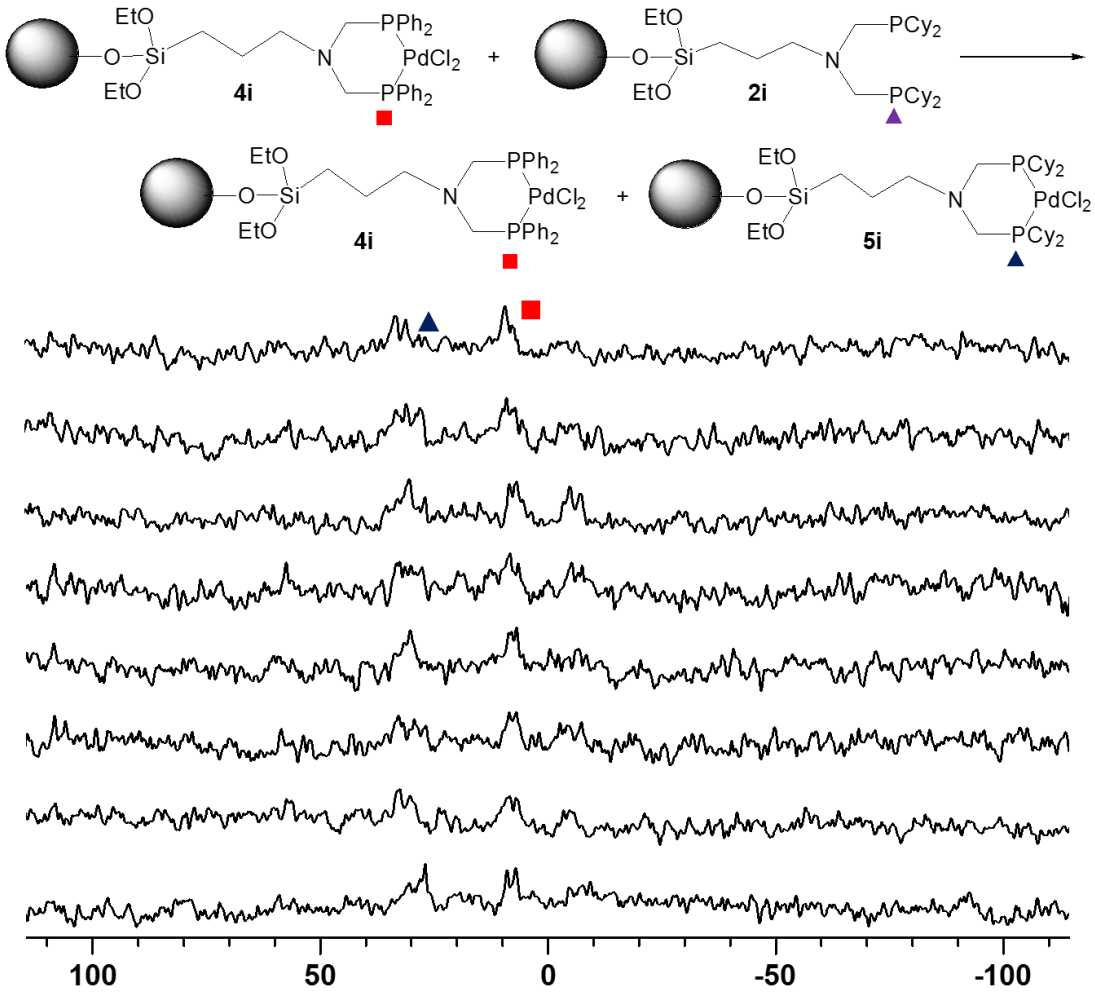

Complex **4i** mixed in a 1:1 ratio with ligand **2i** after stirring for 12 h in acetone (5000 scans)

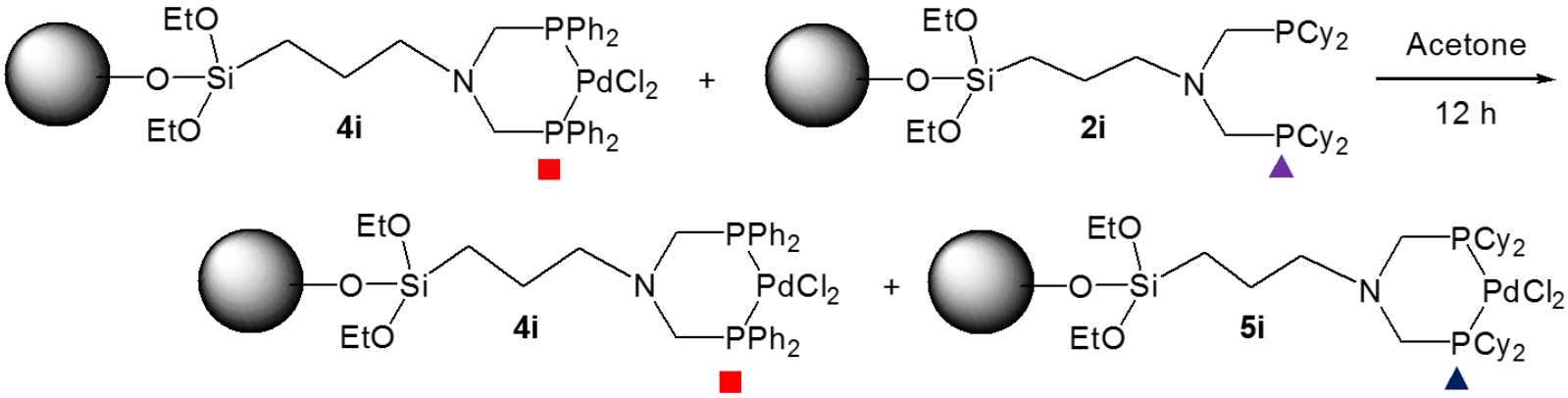

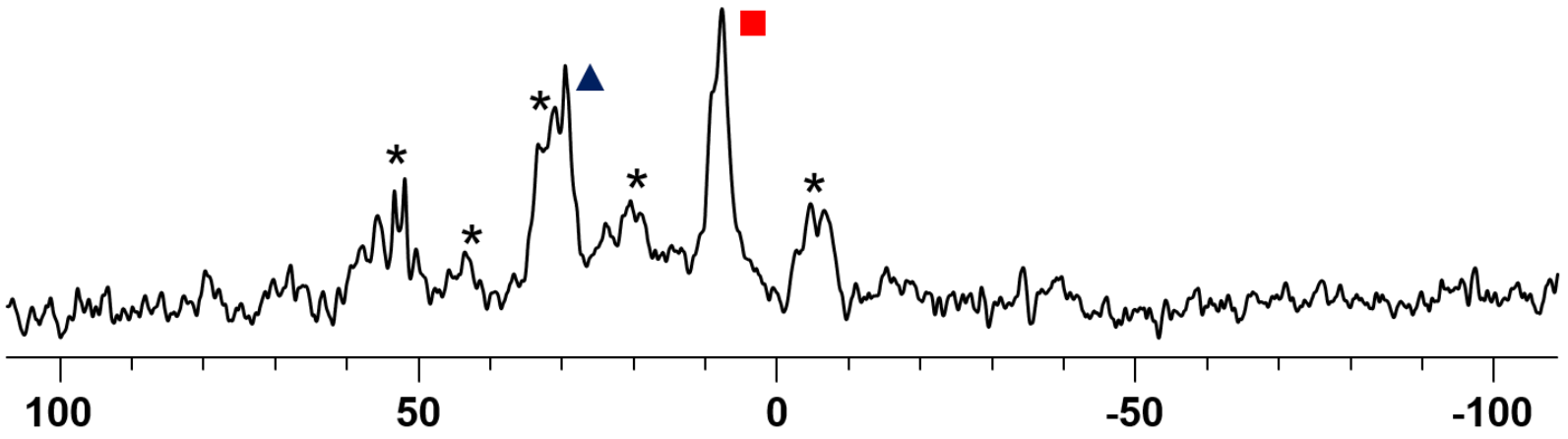

Complex **4i** mixed in a 1:1 ratio with ligand **3i** (100%)

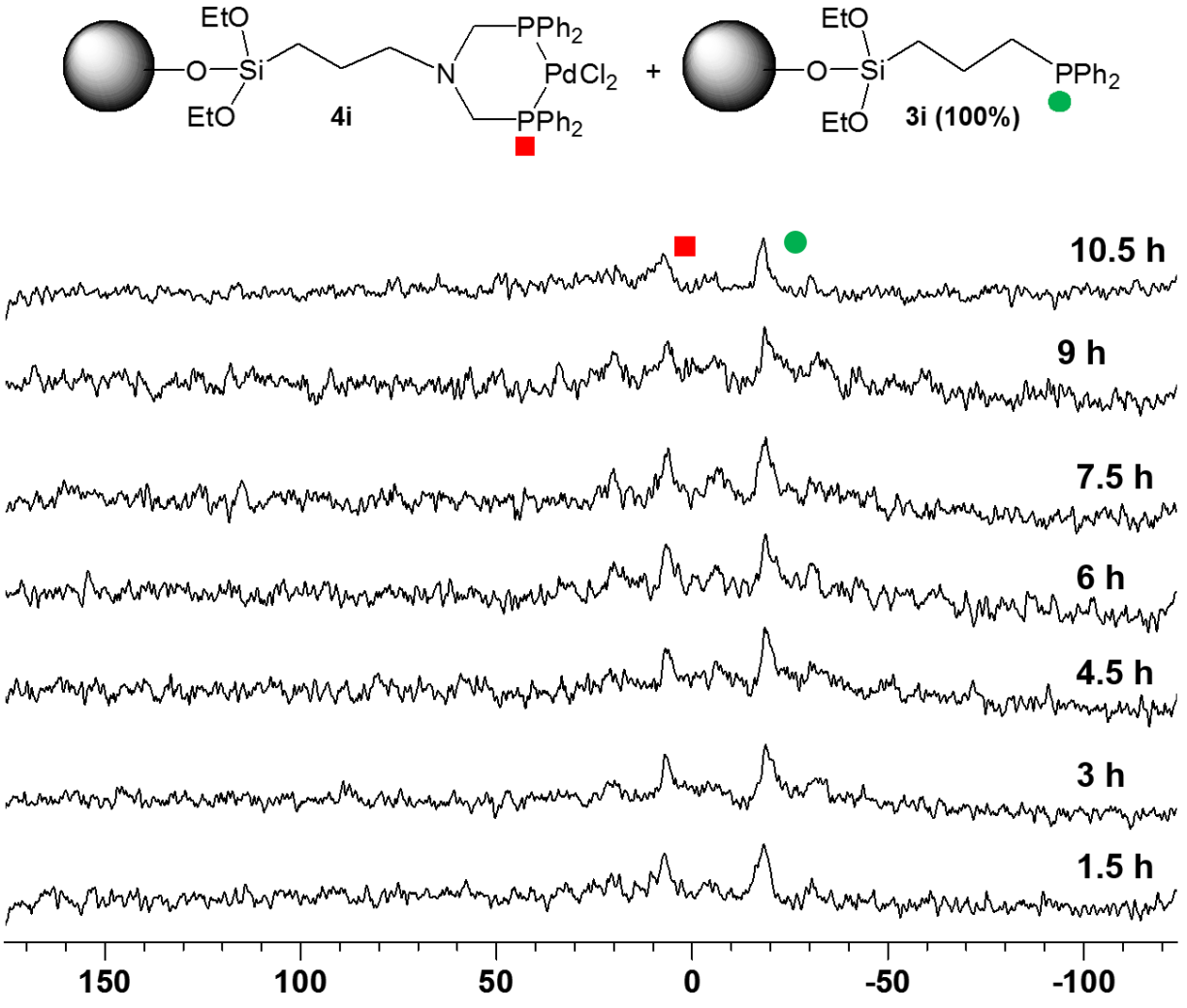

Complex **4i** mixed in a 1:1 ratio with ligand **3i** (100%) with 1 equivalent of added $PdCl_2(NCPh)_2$

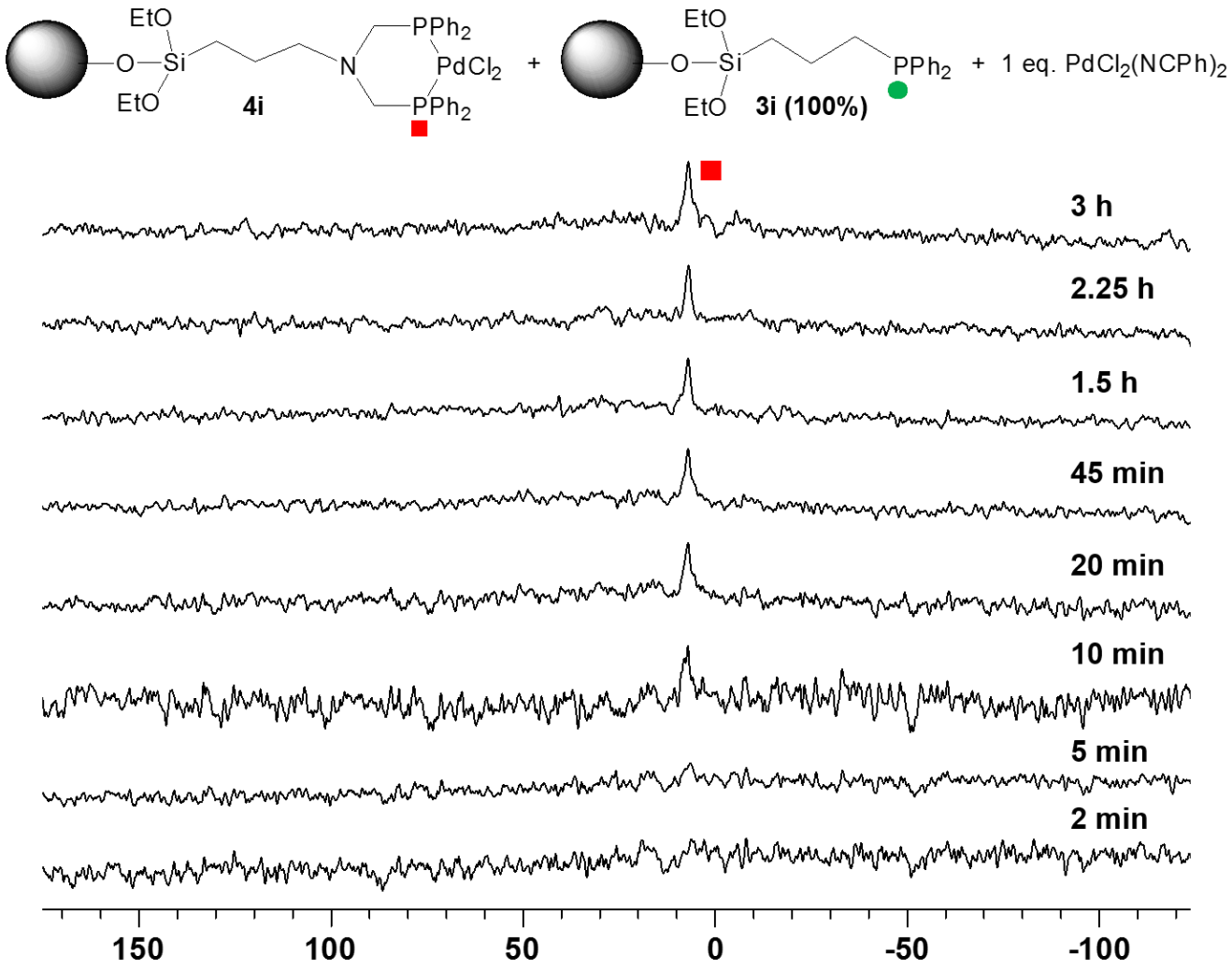

Complex **4i** mixed in a 1:1 ratio with ligand **3i** (100%) with 1.5 equivalents of added BH_3·THF.

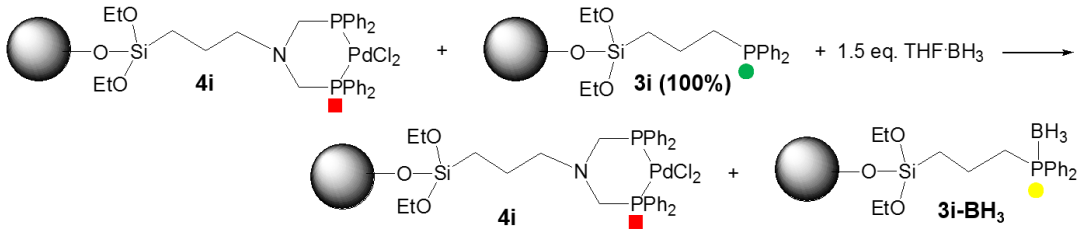

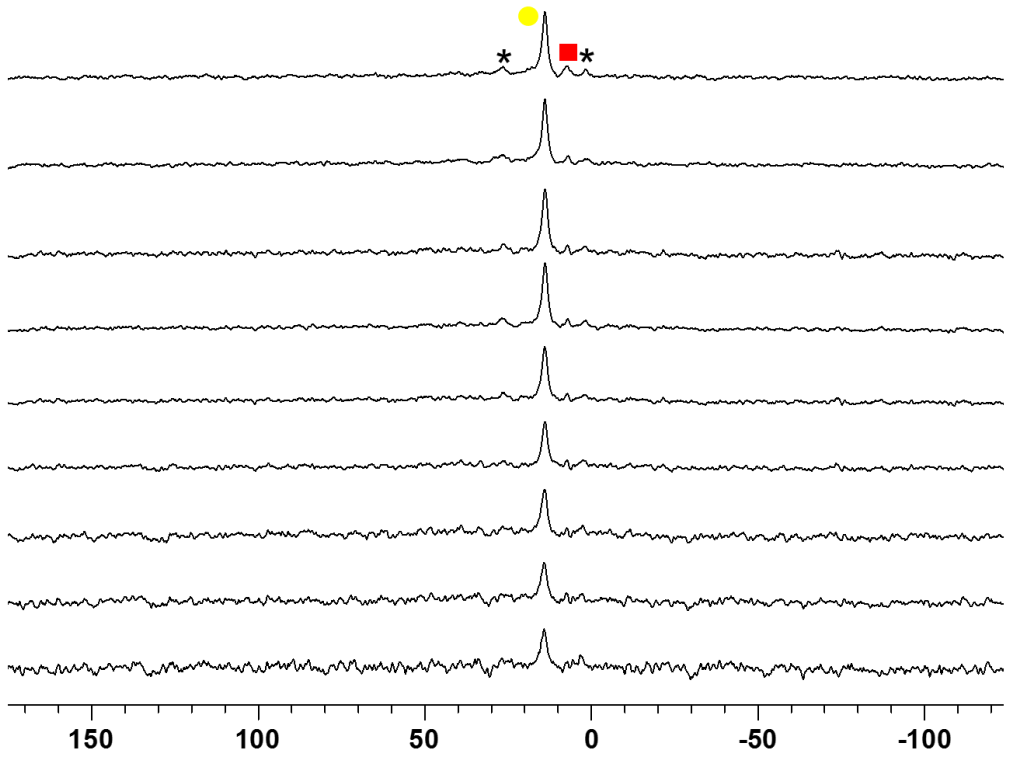

Complex **4i** mixed in a 1:1 ratio with ligand **3i** (50%)

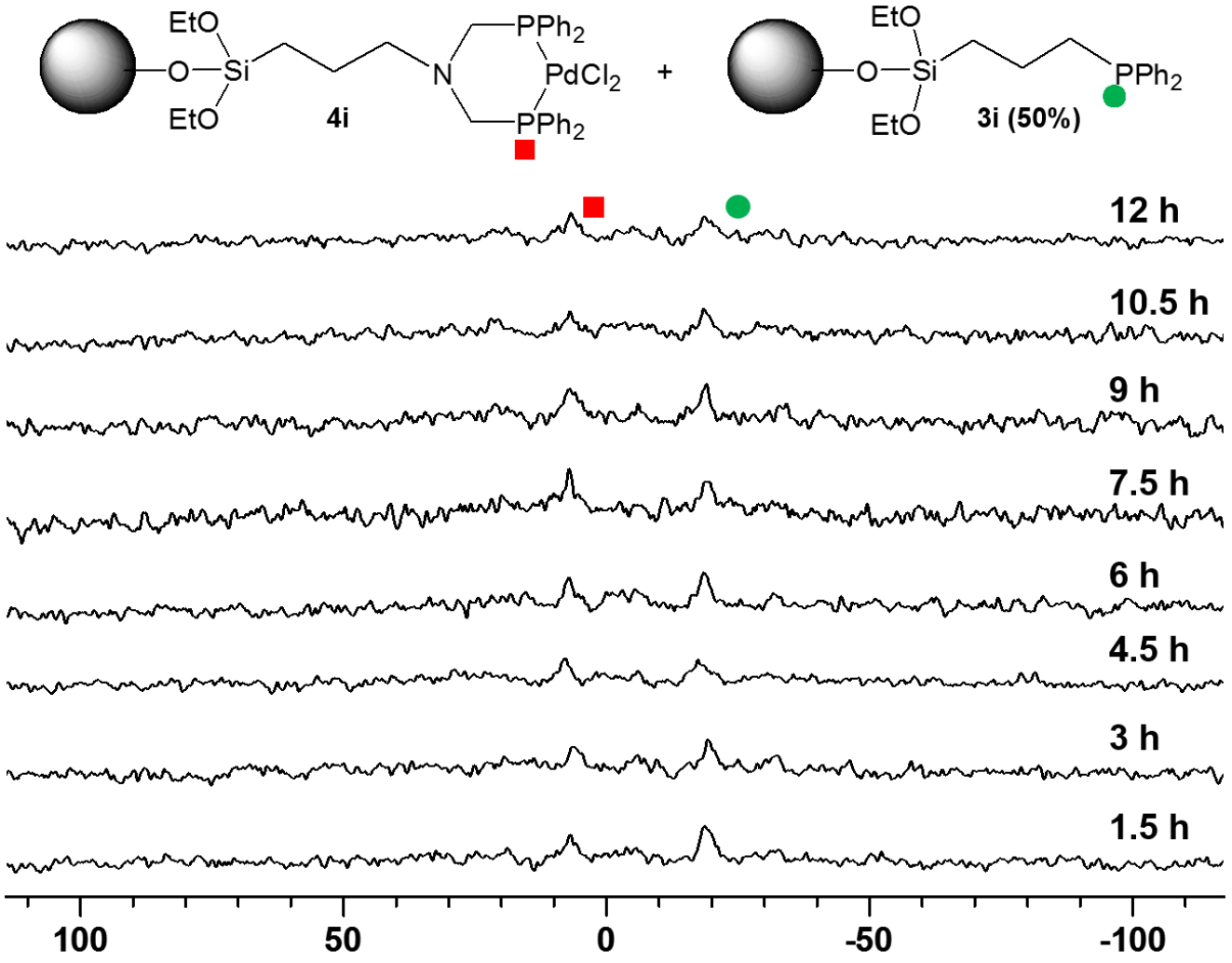

Immobilized 5i Combinations

Complex **5i** mixed in a 1:1 ratio with ligand **1i**

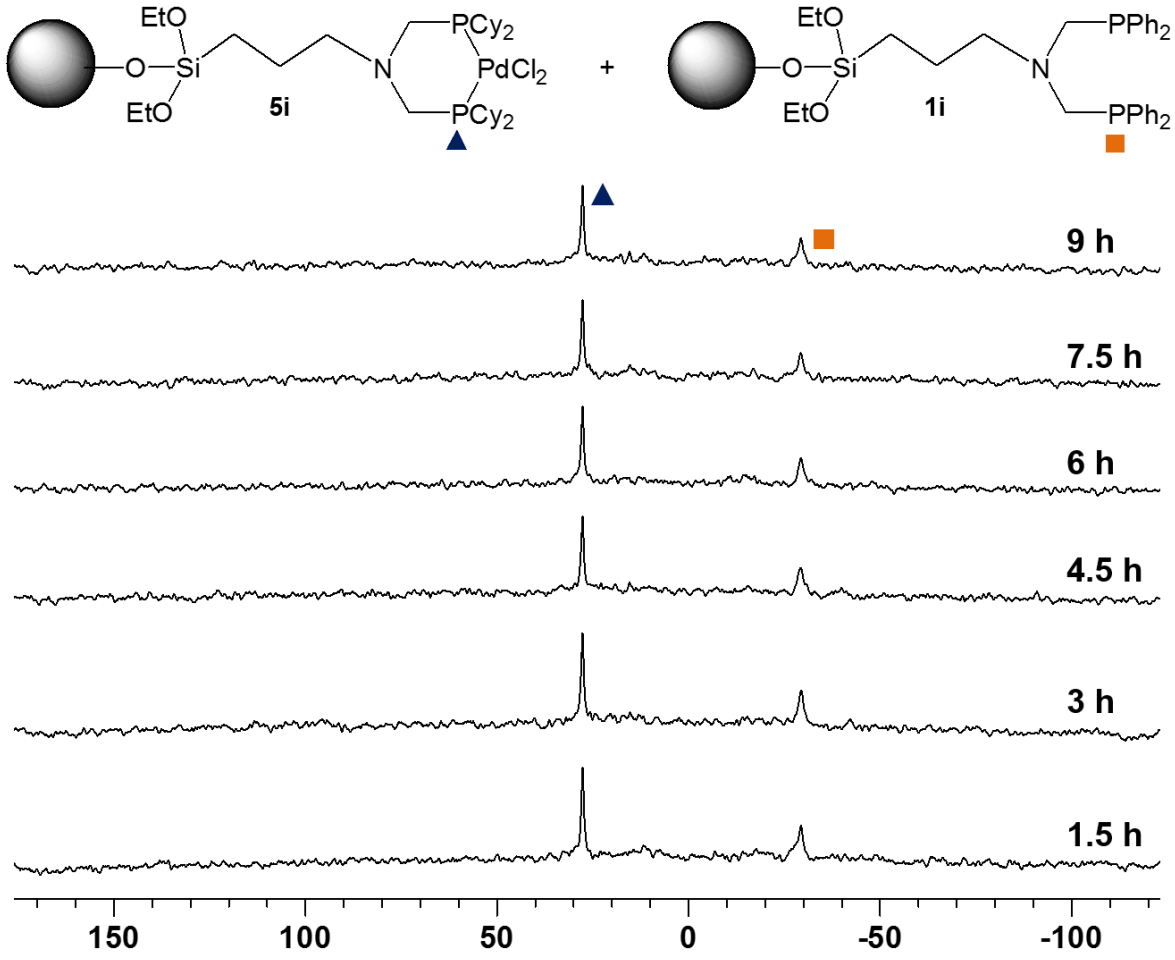

Complex **5i** was mixed in a 1:1 ratio with ligand **3i** (100%)

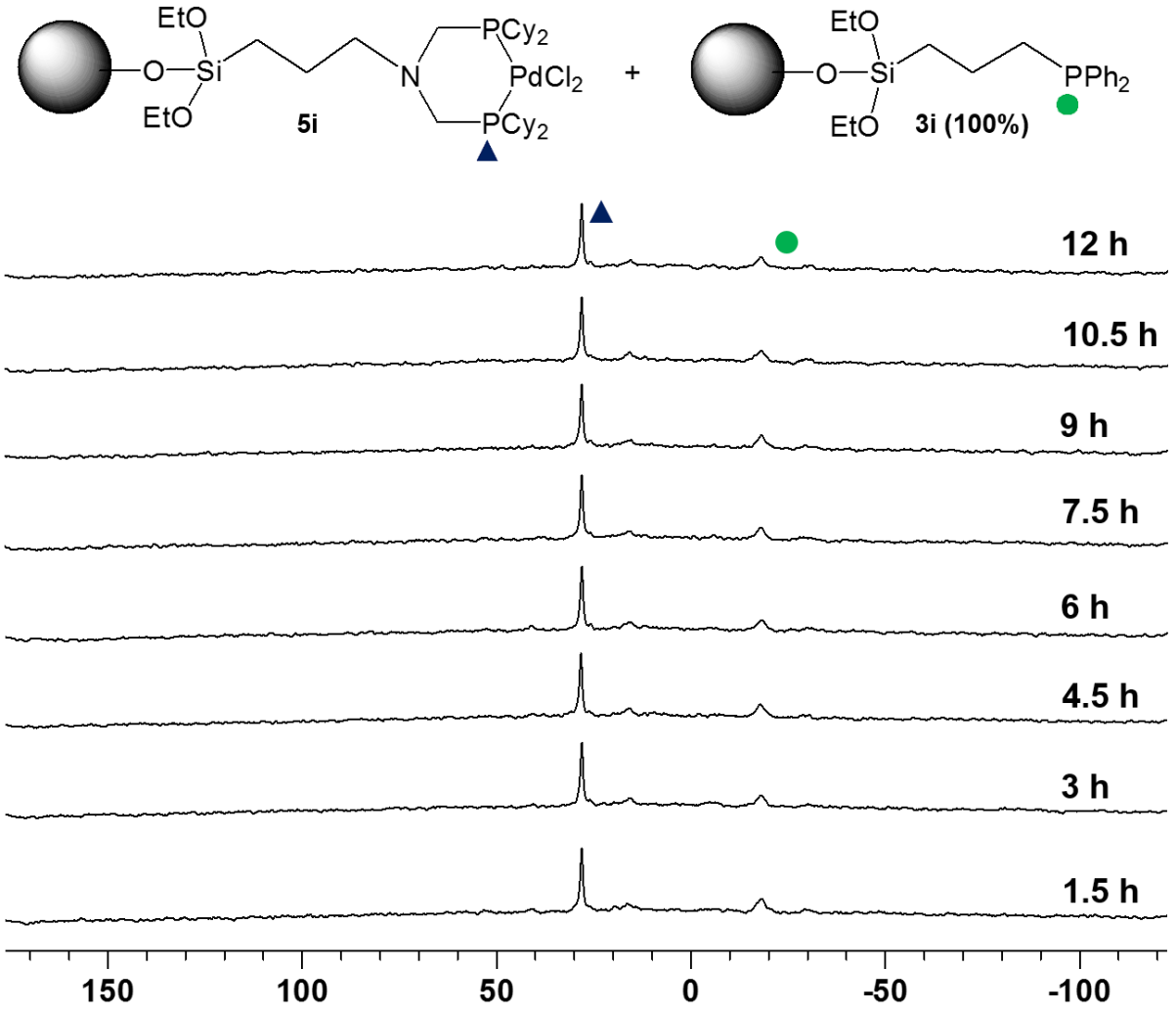

Complex **5i** mixed in a 1:1 ratio with ligand **3i** (50%)

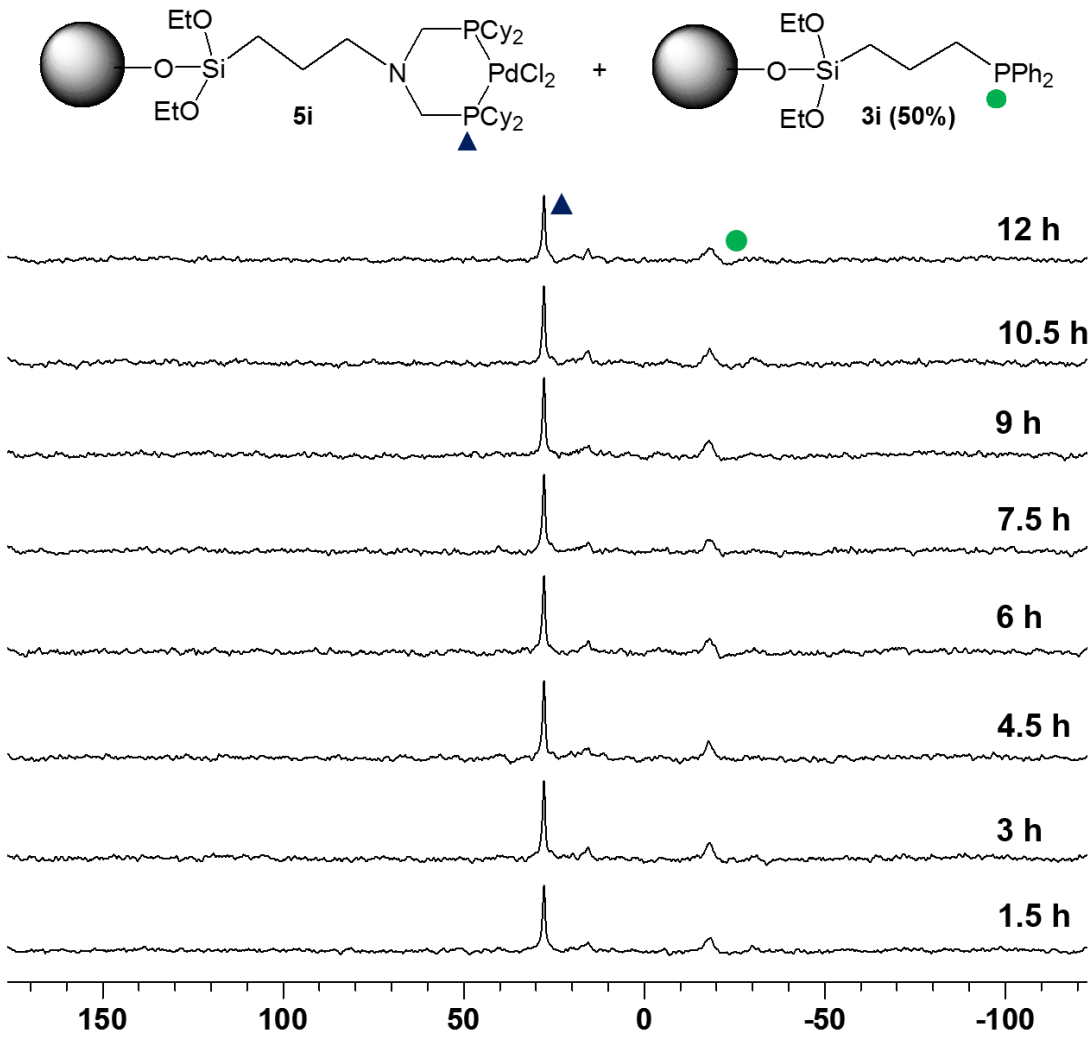

Immobilized 6i Combinations

Complex **6i** (100%) mixed in a 1:1 ratio with ligand **1i**

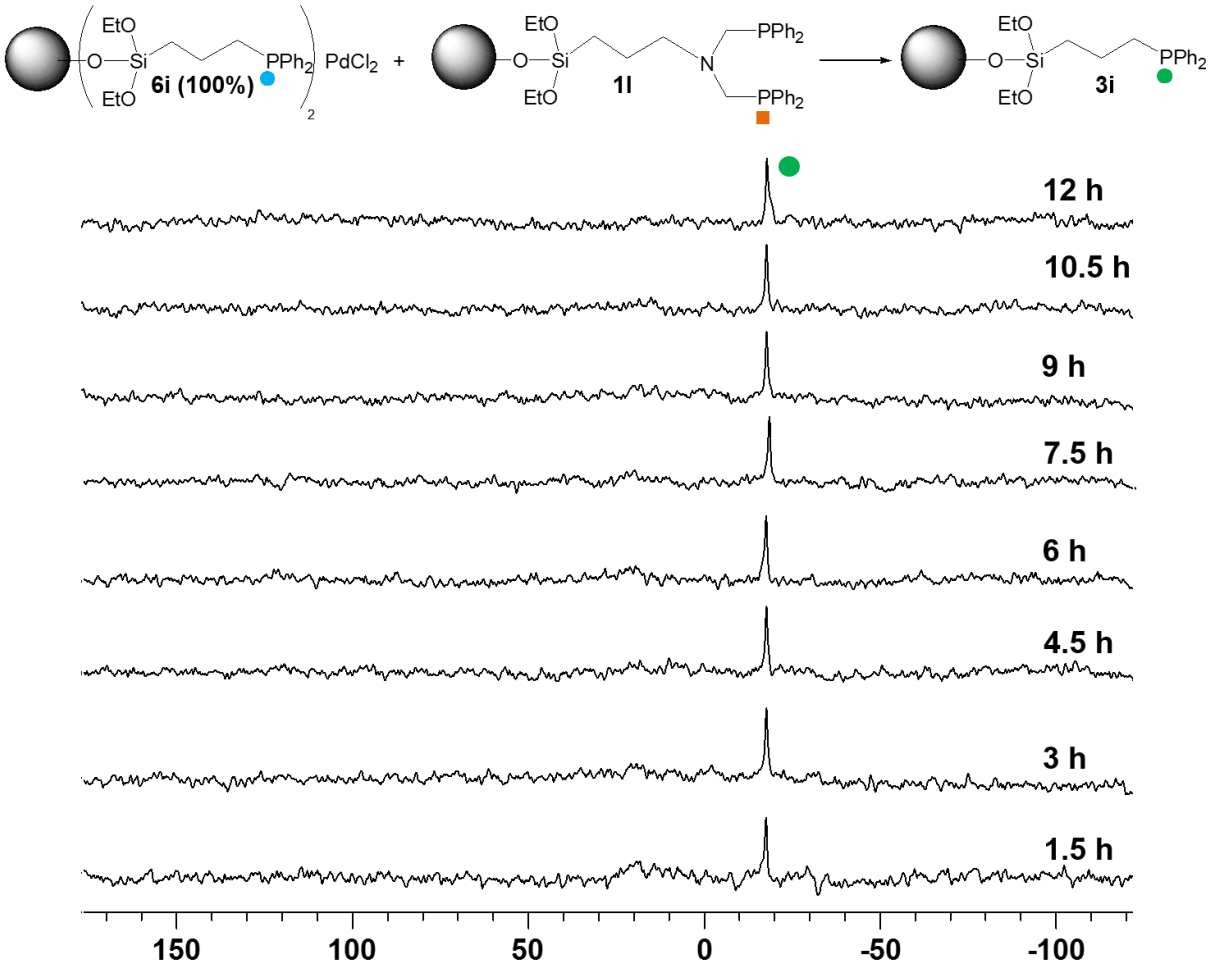

Complex **6i** (100%) mixed in a 2:1 ratio with ligand **1i**

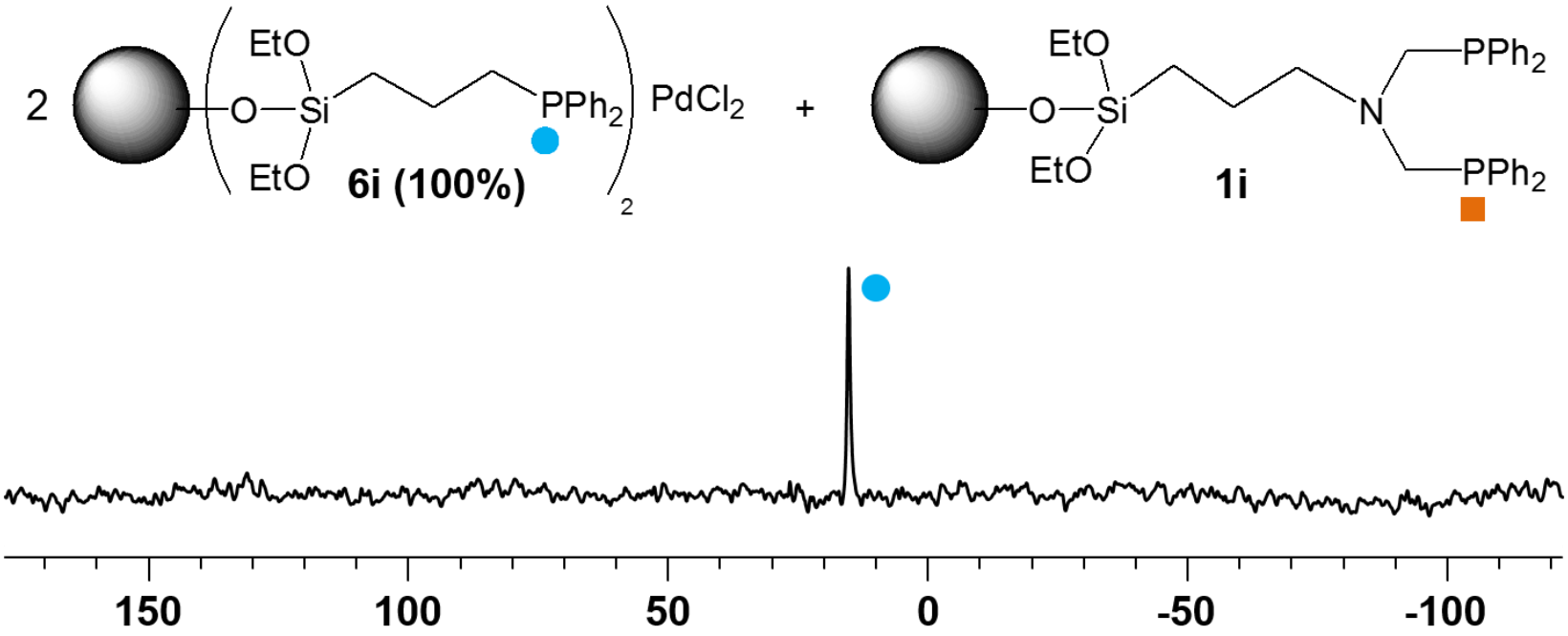

Complex **6i** (100%) was mixed in a 1:1 ratio with ligand **2i**

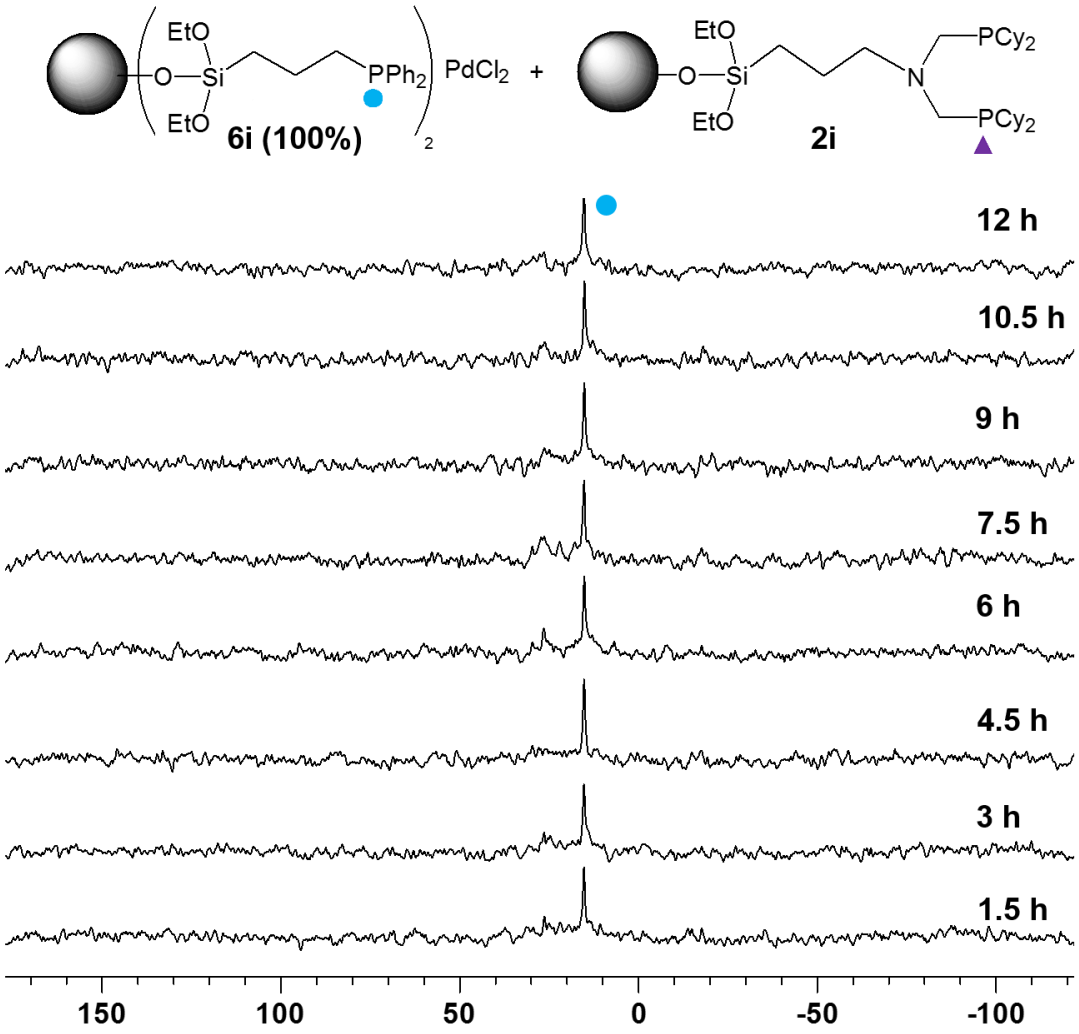

Complex **6i** (100%) mixed in a 1:1 ratio with ligand **2i**

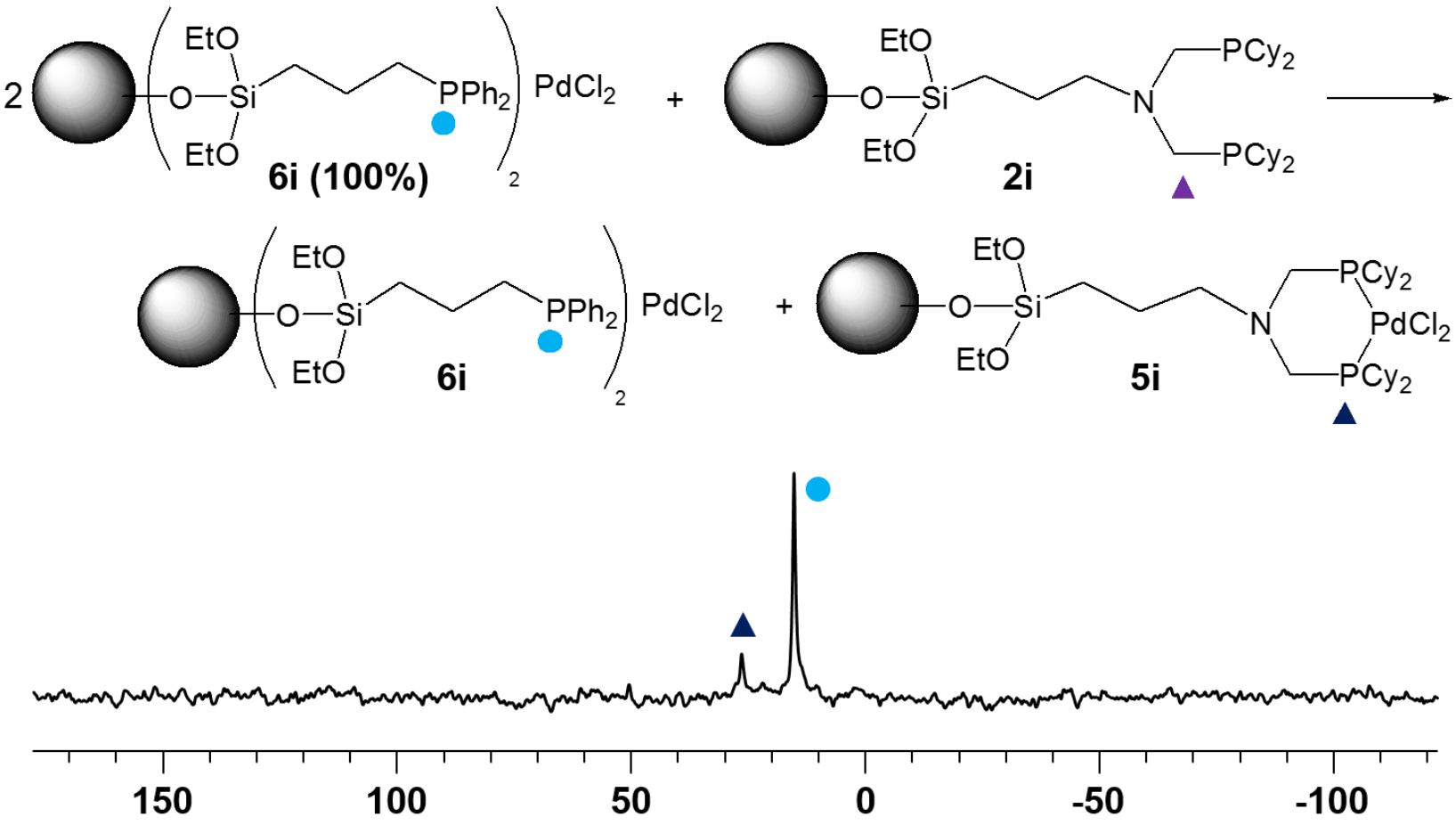

Complex **6i** (100%) mixed in a 1:1 ratio with ligand **3i** with 3 equivalents of $THF{\cdot}BH_3$ added

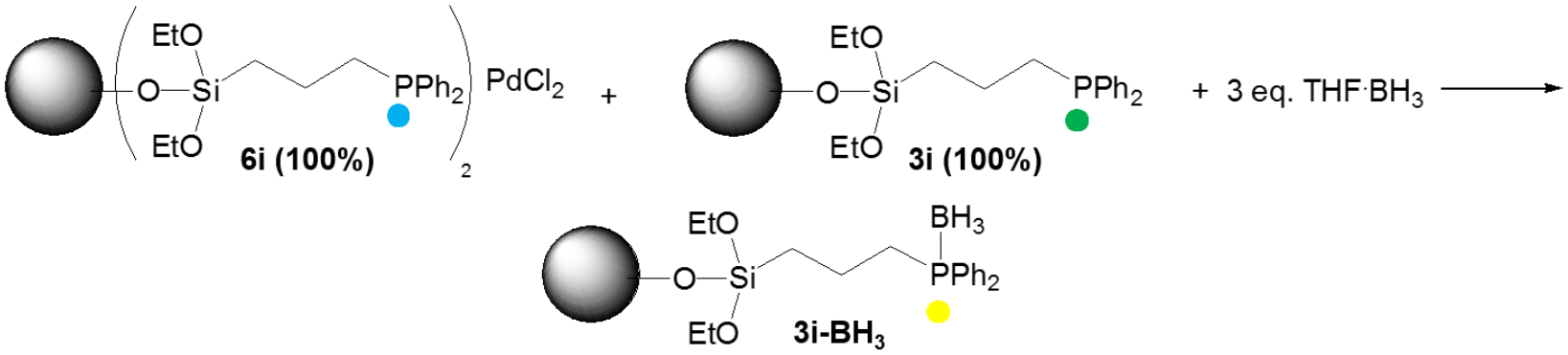

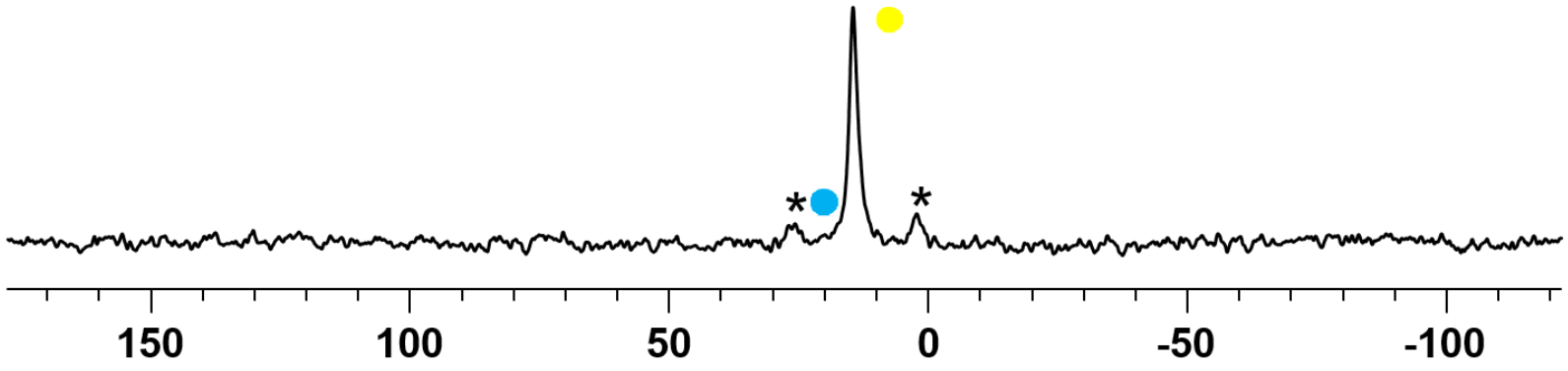

Additional Experiments

Starting material $(EtO)_3Si(CH_2)_3NH_2$ (top 2 spectra) vs $[(EtO)_3Si(CH_2)_3NH_2]_2PdCl_2$ complex (bottom 2 spectra)

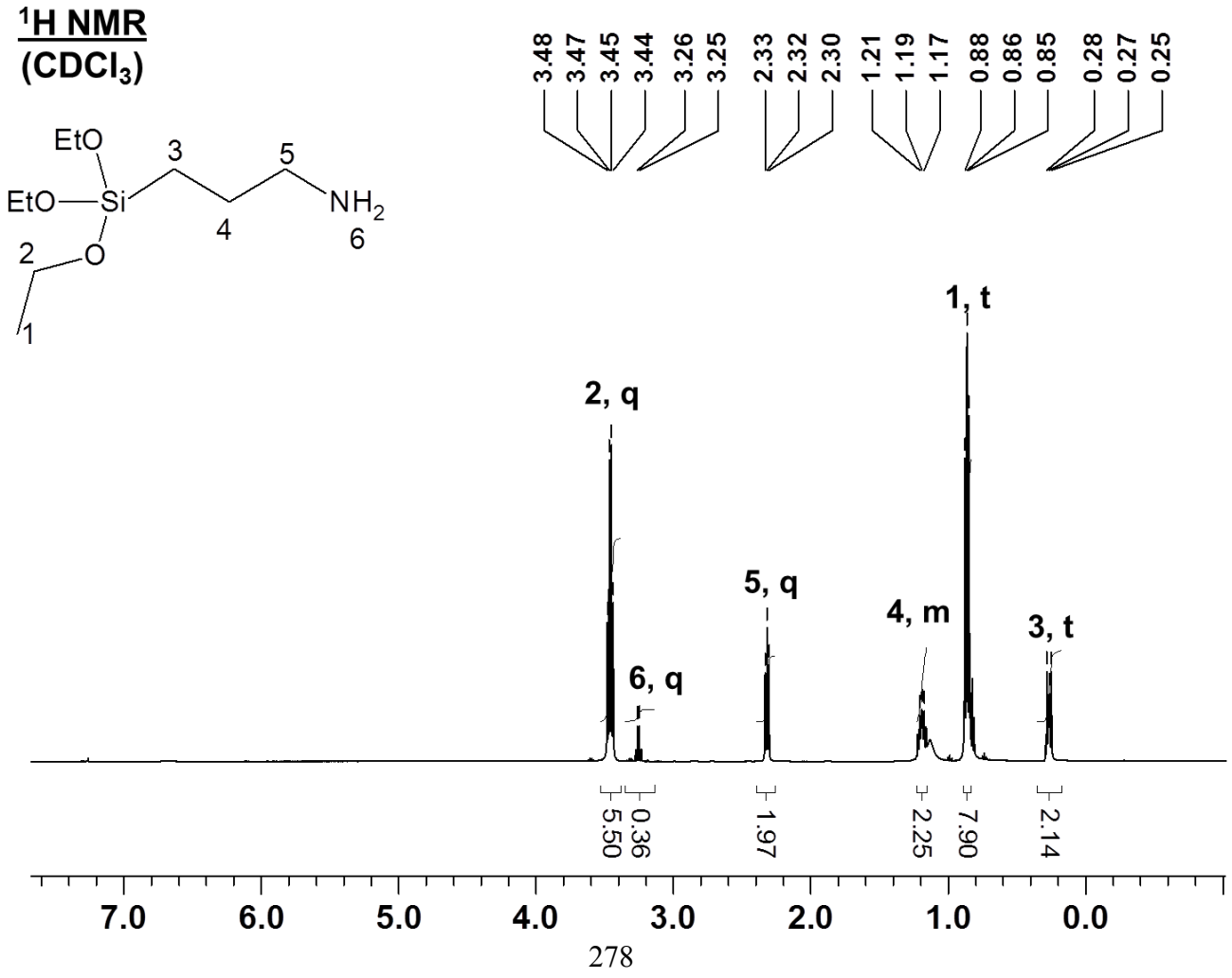

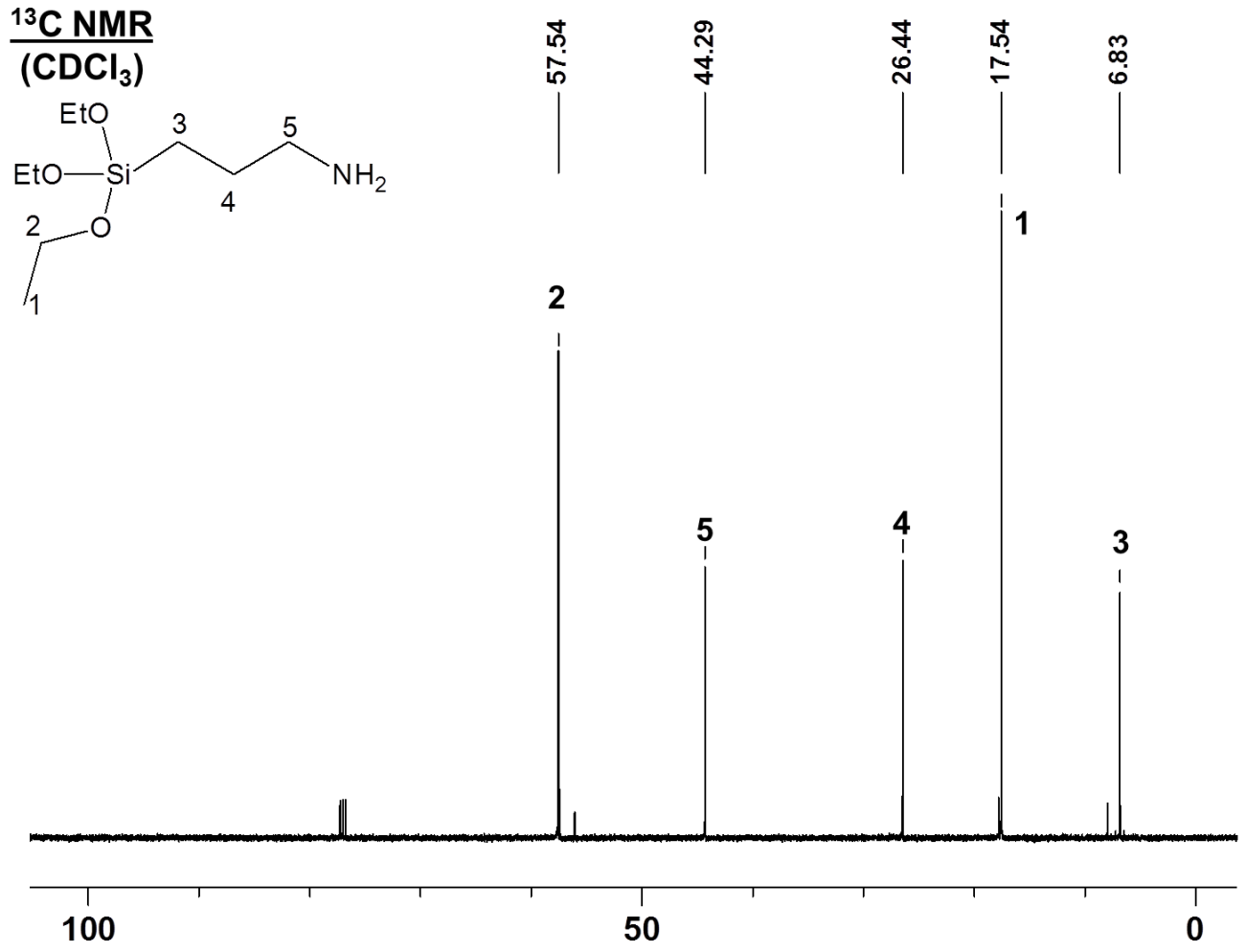
13C NMR
(CDCl3)
EtO
EtO
Si
O
1
2
3
4
5
NH2
57.54
44.29
26.44
17.54
6.83
1
2
3
4
5
100
50
0

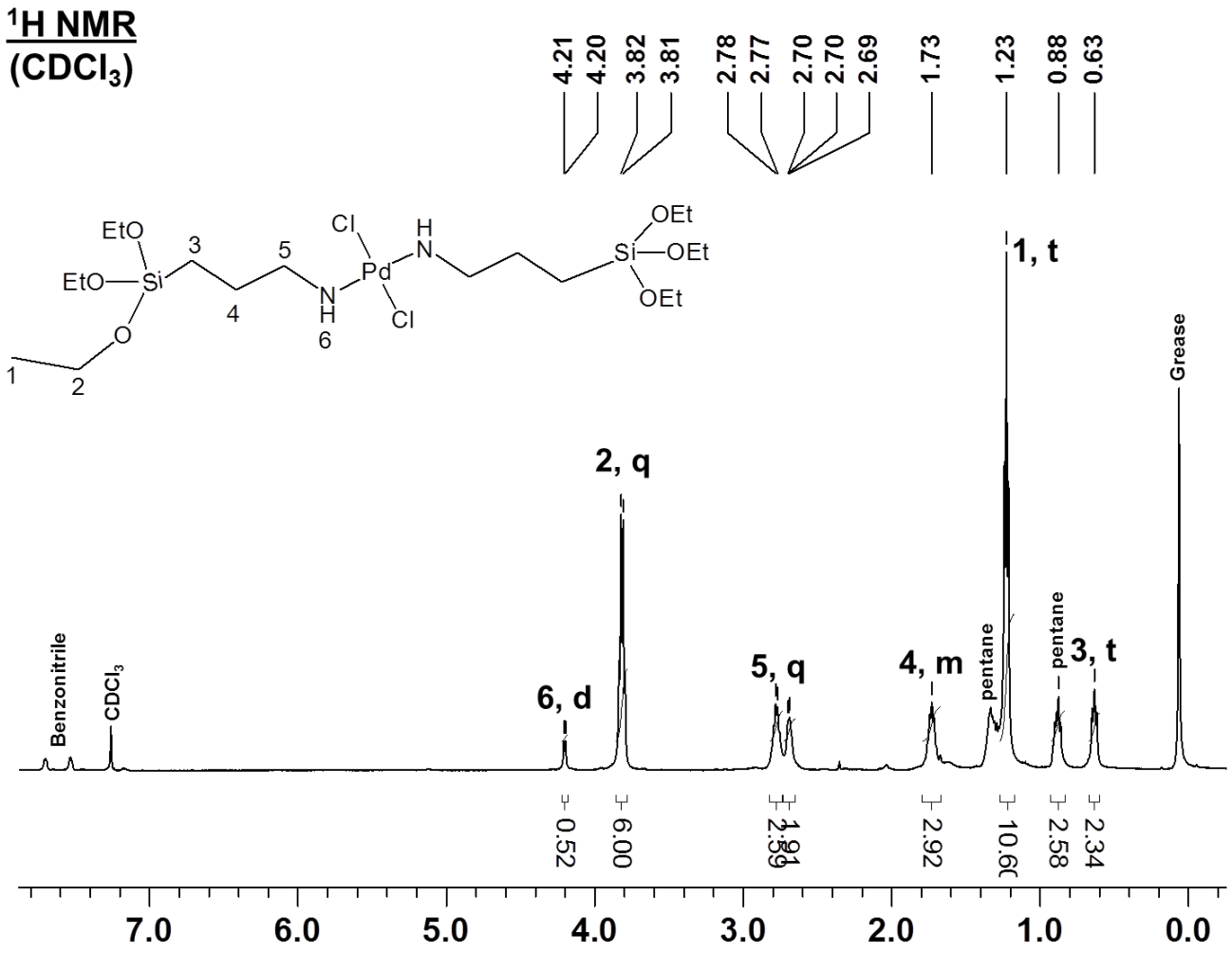
1H NMR
(CDCl3)
4.21
4.20
3.82
3.81
2.78
2.77
2.70
2.70
2.69
1.73
1.23
0.88
0.63
EtO
EtO
Si
O
Cl
Pd
Cl
H
N
N
H
OEt
Si
OEt
OEt
1
2
3
4
5
6
1, t
Grease
2, q
Benzonitrile
CDCl3
6, d
5, q
4, m
pentane
pentane
3, t
0.52
6.00
2.39
1.91
2.92
10.60
2.58
2.34
7.0
6.0
5.0
4.0
3.0
2.0
1.0
0.0

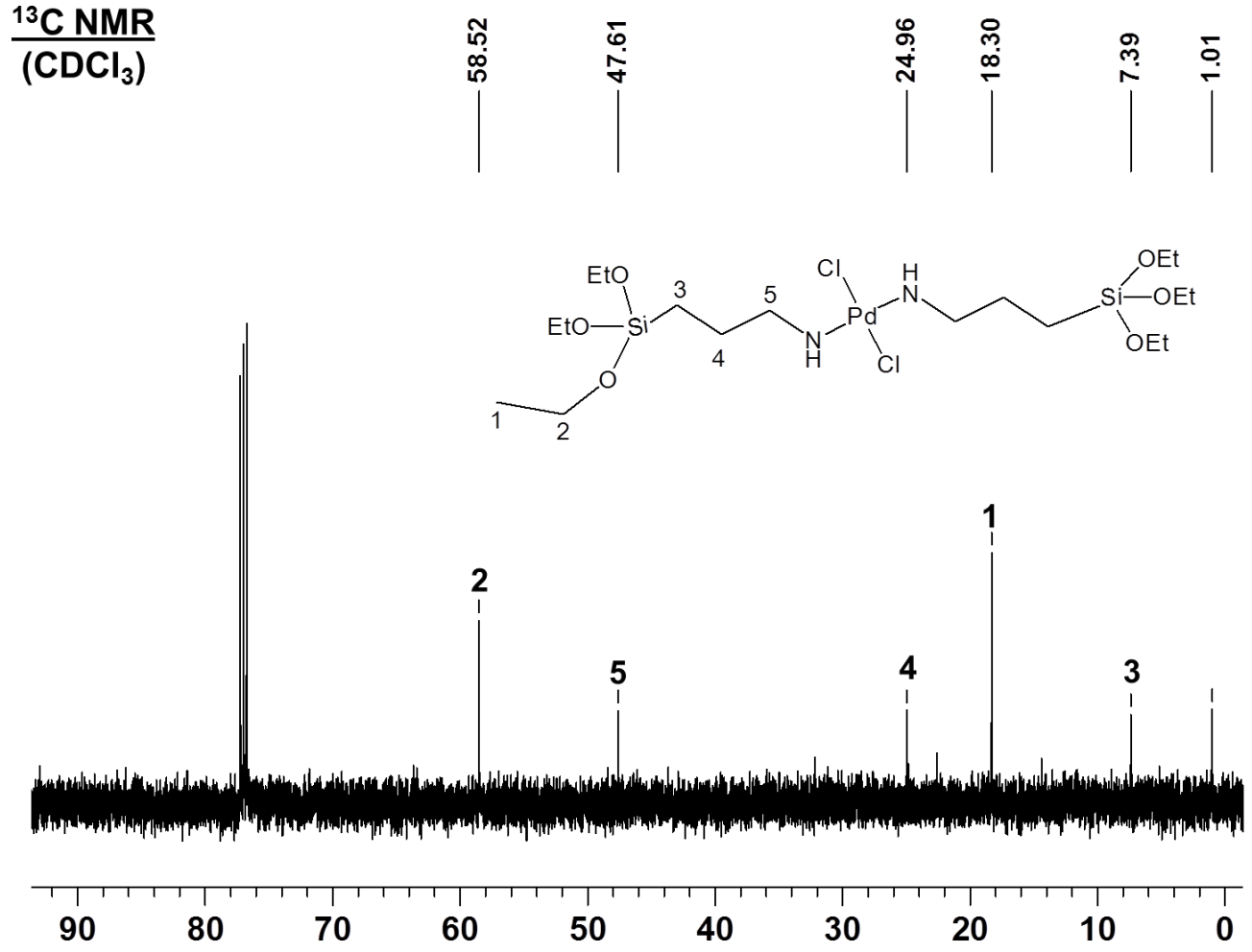
13C NMR
(CDCl3)
58.52
47.61
24.96
18.30
7.39
1.01
EtO
EtO
Si
O
1
2
3
4
5
N
H
Cl
Pd
Cl
H
N
OEt
Si
OEt
OEt
1
2
3
4
5
90
80
70
60
50
40
30
20
10
0

Complex **6i** mixed in a 1:1 ratio with the immobilized amine ligand **8i** (0.095 mmol/g)

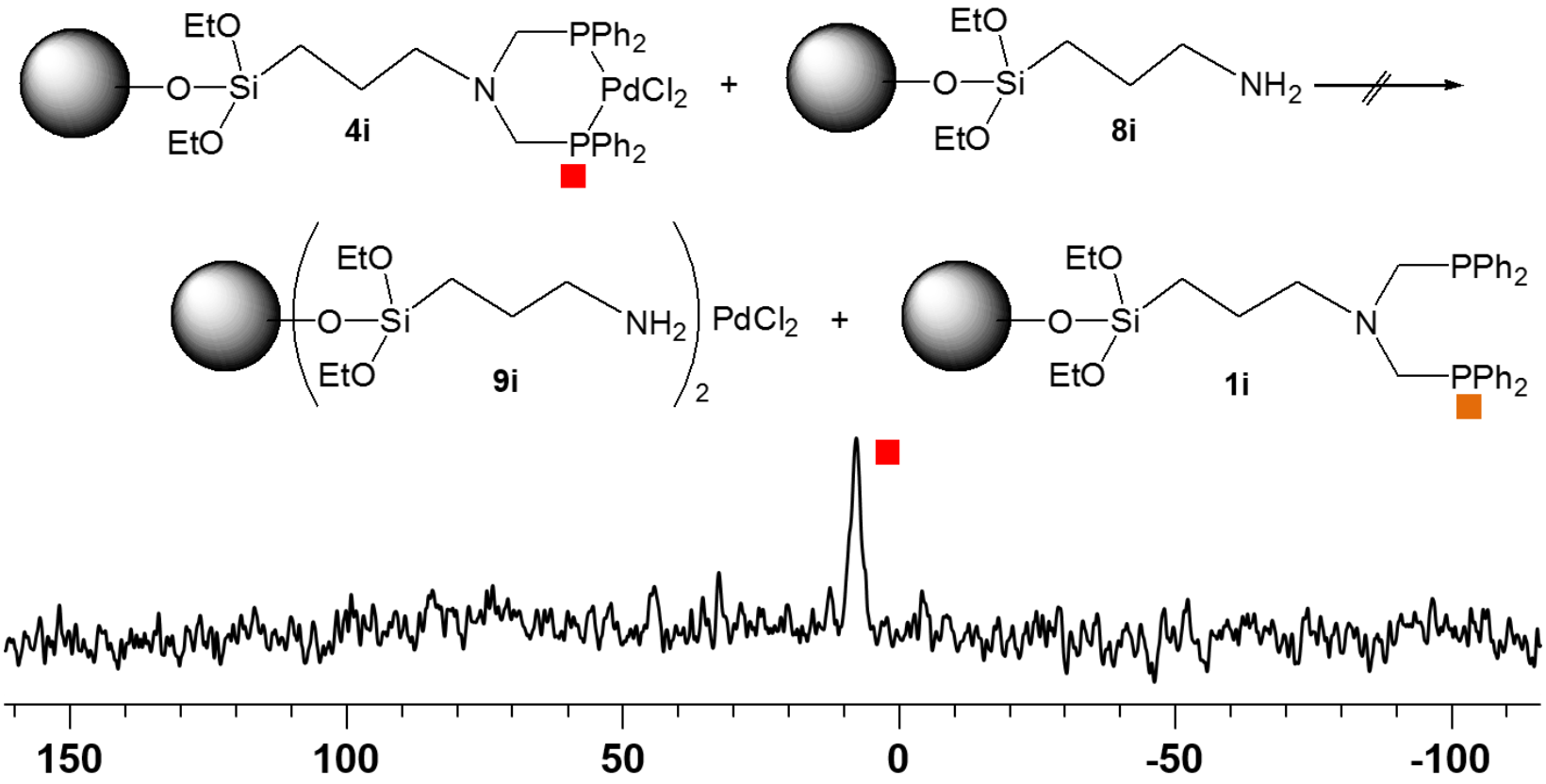

Ligand **1i** mixed in a 1:1 ratio with the immobilized amine Pd complex **9i** (0.095 mmol/g)

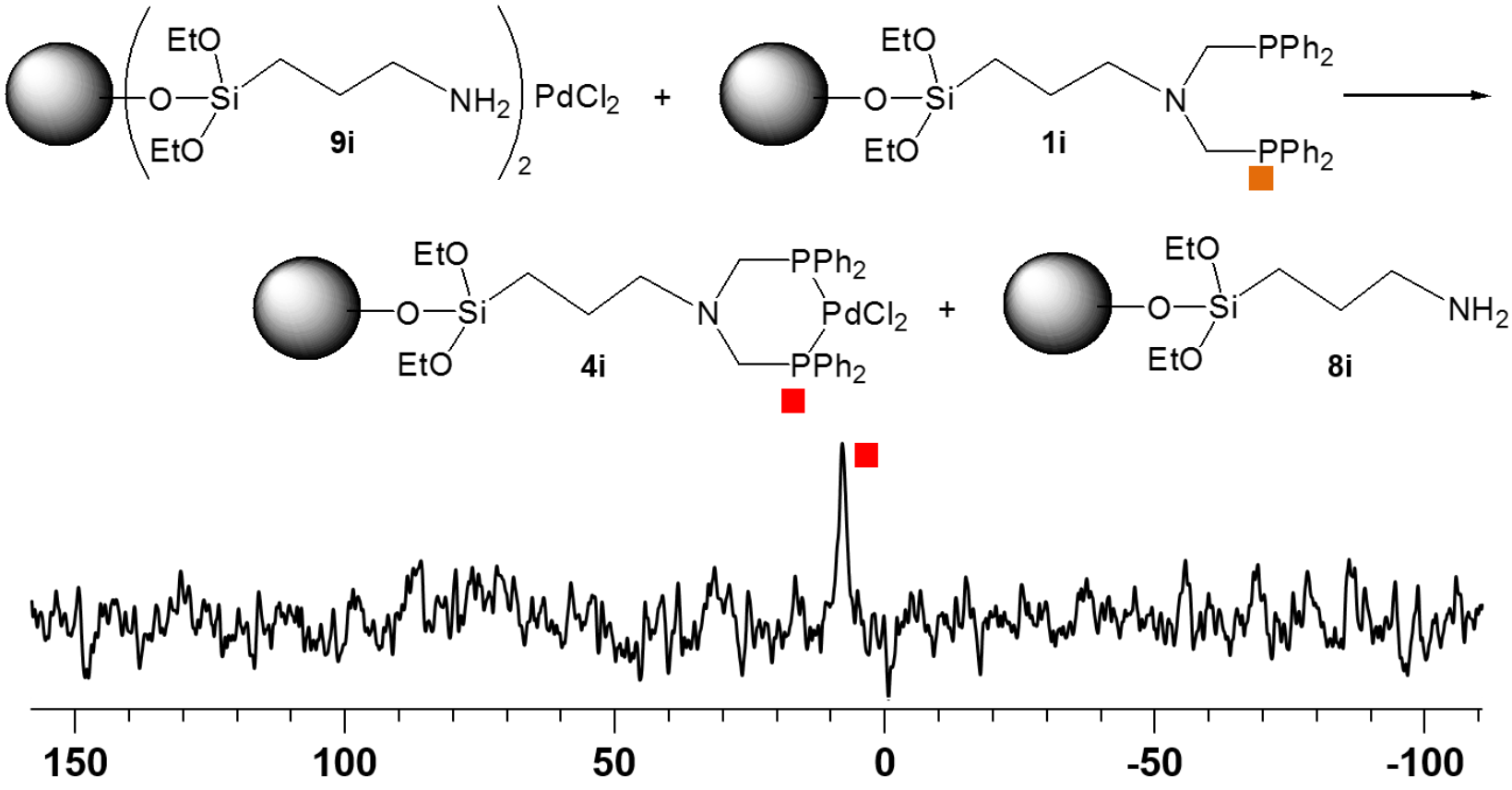

APPENDIX E

COMPOUND CATALOG

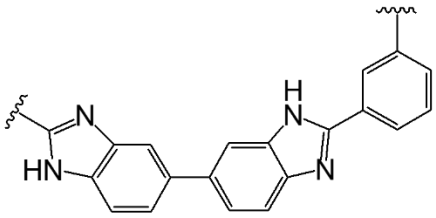

Poly**b**enz**i**midazole (PBI)

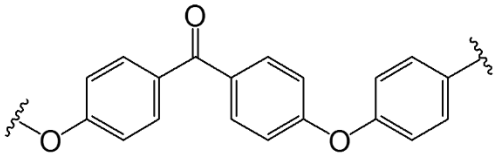

Poly**e**ther**e**ther**k**etone (PEEK)

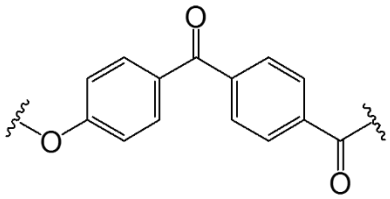

Poly**e**ther**k**etone**k**etone (PEKK)

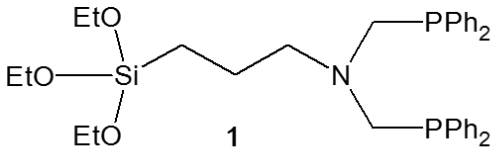

1

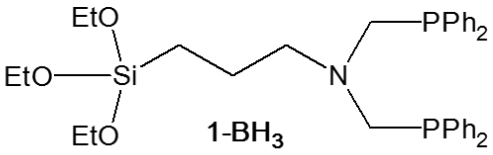

1-BH$_3$

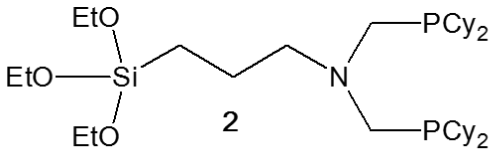

2

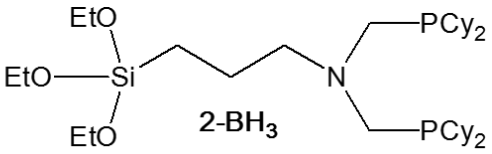

2-BH$_3$

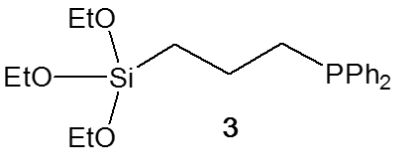

3

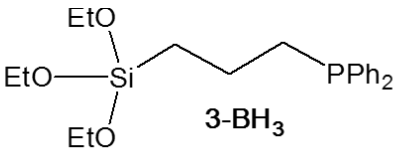

3-BH$_3$

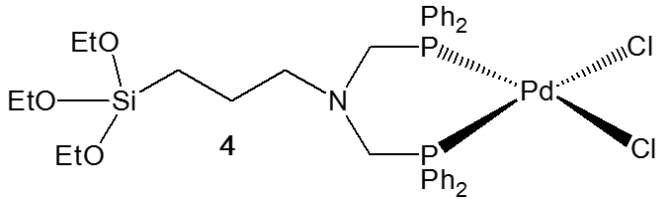
EtO
EtO
Si
EtO
Ph2
P
Cl
N
Pd
P
Ph2
Cl

4

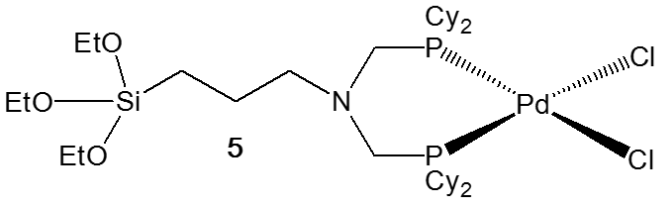
EtO
EtO
Si
EtO
Cy2
P
Cl
N
Pd
P
Cy2
Cl

5

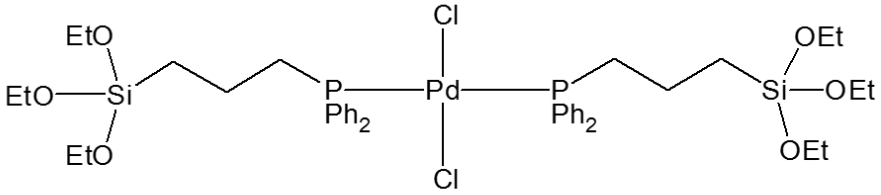
EtO
EtO
Si
EtO
P
Ph2
Cl
Pd
Cl
P
Ph2
OEt
Si
OEt
OEt

6

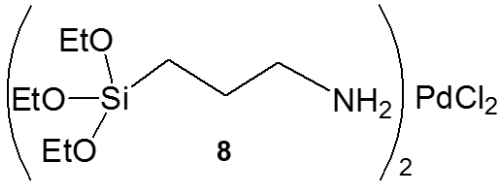
EtO
EtO
Si
EtO
NH2
2
PdCl2

8

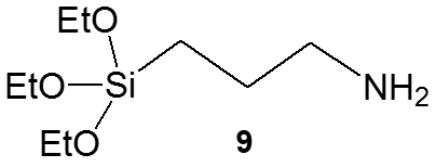
EtO
EtO
Si
EtO
NH2

9